



# VCU

Virginia Commonwealth University  
VCU Scholars Compass

---

Theses and Dissertations

Graduate School

---

2012

## A Novel Method For Determining Acetabular Orientation

Sean Higgins

*Virginia Commonwealth University*

Follow this and additional works at: <https://scholarscompass.vcu.edu/etd>



Part of the [Biomedical Engineering and Bioengineering Commons](#)

© The Author

---

Downloaded from

<https://scholarscompass.vcu.edu/etd/398>

This Thesis is brought to you for free and open access by the Graduate School at VCU Scholars Compass. It has been accepted for inclusion in Theses and Dissertations by an authorized administrator of VCU Scholars Compass. For more information, please contact [libcompass@vcu.edu](mailto:libcompass@vcu.edu).

© Sean W. Higgins 2012

All Rights Reserved

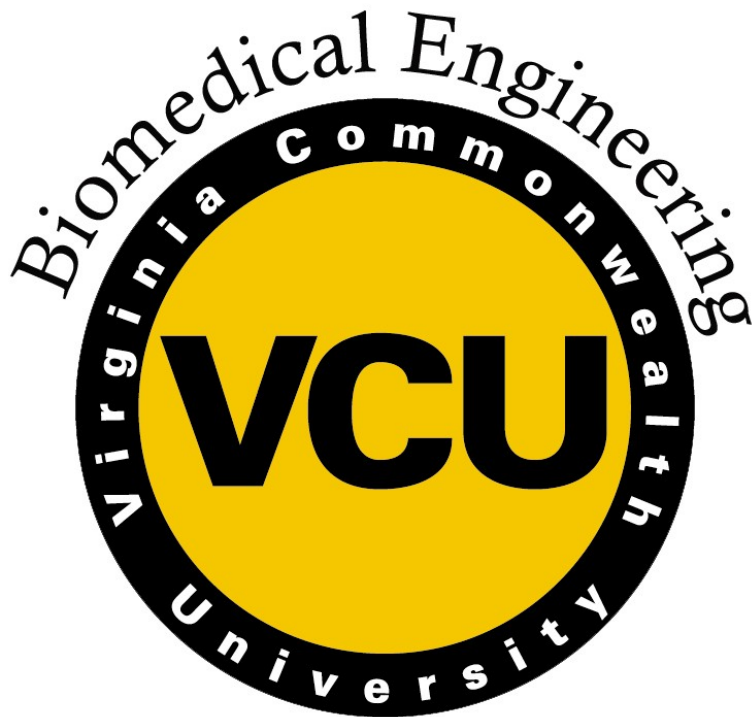
# **A Novel Method For Determining Acetabular Orientation**

A Thesis submitted in partial fulfillment of the requirements for the degree of Master of Science in Biomedical Engineering at Virginia Commonwealth University

by

SEAN WILLIAM HIGGINS  
B.S., Virginia Polytechnic Institute and State University, 2004

Director: Jennifer S. Wayne, Ph.D.  
Departments of Biomedical Engineering & Orthopaedic Surgery



© Virginia Commonwealth University  
Richmond, Virginia  
August 2012

## **Acknowledgement**

There are many people who have helped me along the way during my time at VCU that deserve recognition. I would like to thank my advisor Dr. Jennifer Wayne for providing me the opportunity to work in the Orthopaedic Research Laboratory. Her time, patience, and expert input have provided both educational and professional experiences that exceeded expectation. I would also like to recognize all of the members of the Orthopaedic Research Laboratory, both past and present, for making it a collaborative and fun environment to work in. For their contributions to this research, I would like to specifically thank Dr. William Jiranek from the Department of Orthopaedic Surgery, Dr. Curtis Hayes and Dr. Kevin Hoover from the Department of Radiology, Meade Spratley, and Richie Boe.

The good times I have had with both my old and new friends over the past few years have provided welcome, and much needed distractions. Thank you all for the laughs and for tolerating my bohemian humor. I am very grateful for the ongoing support and love of my family. Most importantly, I would like to give an special thanks to my wife Brooke. I can never thank you enough for your unwavering support, understanding, and encouragement in all of my endeavors. You are amazing. I love you.

# Table of Contents

Acknowledgement .....	ii
Table of Contents .....	iii
List of Tables .....	vi
List of Figures .....	viii
List of Abbreviations .....	xiii
Abstract .....	xv
1 INTRODUCTION .....	- 1 -
Preface .....	- 1 -
1.1 ANATOMY, DEVELOPMENT & BIOMECHANICS OF THE HIP .....	- 2 -
1.2 QUANTITATIVE TWO-DIMENSIONAL CLINICAL EVALUATIONS.....	- 9 -
1.2.1 Qualitative Signs.....	- 10 -
1.2.2 Plain Radiographic Indices .....	- 11 -
1.2.3 Two-Dimensional Axial Measures .....	- 23 -
1.2.4 Measurement of the Proximal Femoral Component.....	- 27 -
1.3 ERROR ASSOCIATED WITH TWO-DIMENSIONAL MEASURES.....	- 33 -
1.3.1 AP Radiography Sources of Error .....	- 34 -

1.3.2 Controls for AP Radiography .....	- 39 -
1.3.3 2-D Computed Tomography Sources of Error.....	- 44 -
1.4 MODERN THREE-DIMENSIONAL STUDIES OF THE ACETABULUM .....	- 49 -
1.5 PELVIC ASSYMETRY RELATED TO THE INNOMINATE BONE.....	- 54 -
1.6 PREMISE FOR ADVANCED RESEARCH.....	- 58 -
2 MATERIALS AND METHODS.....	- 60 -
2.1 MATERIALS .....	- 60 -
2.2 METHODS.....	- 60 -
2.2.1 Three-Dimensional Surface Generation & Data Extraction .....	- 61 -
2.2.2 Acetabular Rim Point Selection.....	- 69 -
2.3 PROGRAMMATIC METHODS .....	- 73 -
2.3.1 Automatic Detection of APP Coordinate System.....	- 77 -
2.3.2 Hemi-Pelvis Coordinate System .....	- 80 -
2.3.3 AR Point Selection & Plane Fitting.....	- 84 -
2.3.4 True & False Pelvic Regions .....	- 92 -
2.4 CALCULATED OUTPUTS.....	- 97 -
2.4.1 Full Pelvis Measures .....	- 97 -
2.4.2 Hemi-Pelvis Measures .....	- 98 -
2.5 STATISTICAL METHODS .....	- 100 -
2.5.1 Reliability Analysis.....	- 100 -

2.5.2 Population Data Testing.....	- 109 -
3 RESULTS .....	- 110 -
3.1 RELIABILITY STUDY RESULTS .....	- 110 -
3.1.1 Full Pelvis .....	- 110 -
3.1.2 Hemi-Pelvis.....	- 112 -
3.2 FULL PELVIS ANALYSIS RESULTS .....	- 114 -
3.3 HEMI-PELVIS ANALYSIS RESULTS.....	- 128 -
4 DISCUSSION .....	- 141 -
4.1 Hemi-Pelvis.....	- 141 -
4.2 Full Pelvis.....	- 145 -
4.3 Future Research.....	- 155 -
Literature Cited.....	- 159 -
Appendix A: Acetabulator- Detailed Flow Chart .....	- 178 -
Appendix B: Acetabulator- Graphical Flow Montage.....	- 181 -
Vita.....	- 190 -

## List of Tables

Table 1.1- Normal Values of Weight-Bearing Zone Index (Tönnis Angle) .....	- 15 -
Table 1.2- Normal Values of Center-Edge Angle (CE Angle) .....	- 17 -
Table 1.3- Normal Values of Sharp's Angle (Acetabular Angle) .....	- 20 -
Table 1.4- Normal Values of Acetabular Anteversion Angle (AcAV Angle) .....	- 25 -
Table 1.5- Normal Values of Anterior Acetabular Sector Angle (AASA) .....	- 27 -
Table 1.6- Normal Values of Posterior Acetabular Sector Angle (PASA) .....	- 27 -
Table 1.7- Various Estimates of Interobserver Measurement Variability .....	- 37 -
Table 1.8- Various Estimates of Intraobserver Measurement Variability .....	- 37 -
Table 2.1- Definitions of Full Pelvis Acetabular Measures .....	- 98 -
Table 2.2- Definitions of Hemi-Pelvis Acetabular Measures .....	- 99 -
Table 2.3- Definitions of Hemi-Pelvis Innominate Measures .....	- 100 -
Table 3.1- Full Pelvis Interobserver Reliability .....	- 111 -
Table 3.2- Full Pelvis Intraobserver Reliability .....	- 111 -
Table 3.3- Full Pelvis Interobserver Minimum Detectable Difference .....	- 112 -
Table 3.4- Full Pelvis Intraobserver Minimum Detectable Difference .....	- 112 -
Table 3.5- Hemi-Pelvis Interobserver Reliability .....	- 113 -
Table 3.6- Hemi-Pelvis Intraobserver Reliability .....	- 113 -
Table 3.7- Hemi-Pelvis Interobserver Minimum Detectable Difference .....	- 114 -
Table 3.8- Hemi-Pelvis Intraobserver Minimum Detectable Difference .....	- 114 -
Table 3.9- Results For Full Pelvis Measures .....	- 114 -
Table 3.10- Results For Hemi-Pelvis Measures .....	- 129 -



Table 4.1- Normal Values Reported For 3-D Anteversion ..... - 148 -

Table 4.2- Normal Values Reported For 3-D Inclination ..... - 149 -

Table B.1- Acetabulator Code Summary (v3.0) ..... - 181 -

Table B.2- Point Clouds & Located Points ..... - 189 -

## List of Figures

Figure 1.1- Major structures and ligaments of the hip joint.....	- 3 -
Figure 1.2- Typical hip joint range of motion.....	- 4 -
Figure 1.3- Epiphyseal growth of the innominate bone.....	- 6 -
Figure 1.4- Normal curvature of the acetabular rim .....	- 7 -
Figure 1.5- Stress distributions in the acetabular roof- the sclerotic sourcil.....	- 8 -
Figure 1.6- Depiction of intact and broken Shenton's line.....	- 10 -
Figure 1.7- Depiction of Perkins's horizontal and vertical lines .....	- 11 -
Figure 1.8- Depiction of horizontal Y-Line (Hilgenriener's Line).....	- 12 -
Figure 1.9- Commonly used linear distances measured on AP radiographs for children and adults.....	- 13 -
Figure 1.10- Depiction of weight-bearing zone index .....	- 14 -
Figure 1.11- Depiction of CE angle.....	- 17 -
Figure 1.12- Craniocaudal view of patient positioning for attaining <i>faux profil</i> radiograph .....	- 18 -
Figure 1.13- Pelvis with structures forming the pelvic teardrop.....	- 20 -
Figure 1.14- Depiction of the acetabular angle .....	- 20 -
Figure 1.15- Depiction of the ACM angle .....	- 21 -
Figure 1.16- The M-Z distance .....	- 22 -
Figure 1.17- Hip joint at the axial center of the femoral head & LeDamany's incompatibility index...	- 24 -
Figure 1.18- Depiction of the sector angles .....	- 26 -
Figure 1.19- Normal and abnormal neck-to-shaft angles.....	- 28 -
Figure 1.20- Depiction of the correction of coxa valga and vara using femoral osteotomies.....	- 29 -
Figure 1.21- Depiction of normal femoral neck anteversion measurements .....	- 30 -

Figure 1.22- Differences in femoral development between excessive and inadequate coverage .....	- 32 -
Figure 1.23- Depiction of cam and pincer-type FAI.....	- 32 -
Figure 1.24- Standard definitions for 3-D pelvic rotations .....	- 33 -
Figure 1.25- Fixation device and anatomic landmarks used for attaining AP radiographs. ....	- 34 -
Figure 1.26- AP radiograph of pelvis showing rotation towards the right side .....	- 40 -
Figure 1.27- Pelvic rotation controlled by aligning the sacrococcygeal joint (SCJ).....	- 43 -
Figure 1.28- Nagao et al.'s method of attaining acetabular orientation .....	- 44 -
Figure 1.29- Variation in AASA and PASA at levels cranial and caudal to the center .....	- 45 -
Figure 1.30- 2-D study from McKibbin compared to 3-D study from Nagao et al .....	- 51 -
Figure 1.31- Typical views for performing measures that compare bilateral differences .....	- 55 -
Figure 2.1- Procedure for setting patient specific threshold levels.....	- 62 -
Figure 2.2- 3-D representation of spheres fit around the femoral heads- segmentation .....	- 63 -
Figure 2.3- Axial view at the equatorial plane of proximal femur- segmentation .....	- 64 -
Figure 2.4- Obvious ossification that was not considered part of the AR .....	- 64 -
Figure 2.5- Depiction of the manual selection of the AR surface performed in 3-matic.....	- 66 -
Figure 2.6- Innominate bones showing both prominent and absent AR ridges at the anterior column. -	67 -
Figure 2.7- Left innominate bone showing features used for the full pelvis analysis.....	- 68 -
Figure 2.8- Left innominate bone showing features needed for the hemi-pelvis analysis.....	- 68 -
Figure 2.9- Left innominate bone displaying the three estimate points selected on each AR .....	- 70 -
Figure 2.10- Hemispherical cup points of intersection on anterior and posterior aspects of the notch .	- 71 -
Figure 2.11- Representation of an AR unfolded as if it were flattened onto a 2-D surface.....	- 71 -
Figure 2.12- The curvature of the AR used as a secondary guide to locate acceptable points. ....	- 72 -
Figure 2.13- Highlighted appearance of the raised, crescent shaped articular cartilage .....	- 73 -
Figure 2.14- GUI of the Acetabulator used to locate file sources and set parameters for analysis.....	- 74 -

Figure 2.15- Top level process flow for data collection and programmatic analysis. ....	- 75 -
Figure 2.16- Usage and convention of the direction cosine matrix. ....	- 76 -
Figure 2.17- Acetabulator output plots of automatically generated C.S. ....	- 79 -
Figure 2.18- Ventral most points automatically located on the bilateral ASIS and PT .....	- 80 -
Figure 2.19- Hemi-pelvis C.S. shown on left innominate bone.....	- 82 -
Figure 2.20- Variable orientation of the hemi-pelvis sagittal plane.....	- 84 -
Figure 2.21- Depiction of tomograms slicing the surface of the AR. ....	- 85 -
Figure 2.22- Plot displaying the average change in orientation of the plane fit to the acetabulum .....	- 87 -
Figure 2.23- C.S. orientation for initial point selection routine on the AR.....	- 89 -
Figure 2.24- Minimum separation and search windows determined from estimated AR diameter.....	- 89 -
Figure 2.25- Empirically derived relationship determining out-of-bounds points.....	- 91 -
Figure 2.26- Acetabulator output plots showing out-of-bounds point.....	- 91 -
Figure 2.27- Left innominate bone showing converged points automatically selected on AR.....	- 92 -
Figure 2.28- The normal vectors of the true and false pelvic regions.....	- 93 -
Figure 2.29- Plane that is approximately parallel to the aperture of the obturator. ....	- 94 -
Figure 2.30- Points of the posterior AR and PT used to form the cutoff vector .....	- 96 -
Figure 2.31- The obturator point cloud projected onto the estimate plane .....	- 96 -
Figure 2.32- Left innominate bone showing standard measures of inclination and anteversion .....	- 98 -
Figure 2.33- Measures of acetabular inclination and version used for the hemi-pelvis analysis.....	- 99 -
Figure 2.34- Hemi-pelvis measures relating acetabular orientation to true and false pelvic regions ..	- 100 -
Figure 3.1- Mean anatomic inclination depicted on left acetabulum for entire population .....	- 115 -
Figure 3.2- Mean anatomic anteversion depicted on left acetabulum for entire population.....	- 115 -
Figure 3.3- Population results for radiographic inclination .....	- 117 -
Figure 3.4- Population results for radiographic anteversion.....	- 117 -

Figure 3.5- Population results for anatomic inclination.....	- 118 -
Figure 3.6- Population results for anatomic anteversion .....	- 118 -
Figure 3.7- Population results for operative inclination.....	- 119 -
Figure 3.8- Population results for operative anteversion .....	- 119 -
Figure 3.9- Subject of interest observed to have the most radiographic inclination .....	- 121 -
Figure 3.10- Subject of interest observed to have the least radiographic inclination .....	- 122 -
Figure 3.11- Subject of interest observed to have the least anatomic anteversion.....	- 123 -
Figure 3.12- Subject of interest observed to have the most anatomic anteversion .....	- 124 -
Figure 3.13- Bilateral differences in radiographic inclination .....	- 125 -
Figure 3.14- Bilateral differences in radiographic anteversion.....	- 126 -
Figure 3.15- Bilateral differences in anatomic inclination.....	- 126 -
Figure 3.16- Bilateral differences in anatomic anteversion .....	- 127 -
Figure 3.17- Bilateral differences in operative inclination .....	- 127 -
Figure 3.18- Bilateral differences in operative anteversion .....	- 128 -
Figure 3.19- Population results for hemi-pelvic inclination .....	- 130 -
Figure 3.20- Population results for hemi-pelvic version.....	- 130 -
Figure 3.21- Subject of interest observed to have the least AX-to-FPP inclination .....	- 131 -
Figure 3.22- Population results for acetabulum-to-true pelvis inclination.....	- 132 -
Figure 3.23- Distributions of male and female acetabulum-to-true pelvis inclination .....	- 132 -
Figure 3.24- Population results for acetabulum-to-false pelvis inclination .....	- 134 -
Figure 3.25- Population results for acetabulum-to-true pelvis version.....	- 135 -
Figure 3.26- Population results for acetabulum-to-false pelvis version.....	- 135 -
Figure 3.27- Bilateral differences in global hemi inclination .....	- 137 -
Figure 3.28- Bilateral differences in global hemi version.....	- 138 -

Figure 3.29- Bilateral differences in AX-to-TPP inclination..... - 138 -

Figure 3.30- Bilateral differences in AX-to-TPP version ..... - 139 -

Figure 3.31- Bilateral differences in AX-to-FPP inclination ..... - 139 -

Figure 3.32- Bilateral differences in AX-to-FPP version ..... - 140 -

Figure 4.1- Comparisons of 3-D acetabular orientation to the safe zone of Lewinnek et al..... - 151 -

## List of Abbreviations

<b>General Abbreviations</b>	
2-D	Two-dimensional
3-D	Three-dimensional
THA	Total hip arthroplasty
AP	Anteroposterior
DDH	Developmental Dysplasia of the Hip
FAI	Femoroacetabular Impingement
OA	Osteoarthritis
CT	Computed Tomography
MRI	Magnetic Resonance Imaging
ICC	Intraclass Correlation Coefficient
MDD	Minimum Detectable Difference
SD	Standard Deviation
GUI	Graphical User Interface
<b>Previous Studies</b>	
AC Angle	Hilgenreiner's Acetabular Index [1]
Y-line	Horizontal line connecting the gaps of triradiate cartilage [1]
HTE angle	Horizontal Toit Externe Angle [2]
AHI	Acetabular Head Index [3]
FHEI	Femoral Head Extrusion Index [3]
CE Angle	Center-Edge Angle [4]
LCE Angle	Lateral Center-Edge Angle = CE Angle [5]
VCA angle	Vertical-Center-Anterior = Angle Anterior Acetabular Index [6]
AcAV	Acetabular Anteversion Angle [7]
AASA	Anterior Acetabular Sector Angle [8]
PASA	Posterior Acetabular Sector Angle [8]
HASA	Horizontal Acetabular Sector Angle [8]
CCD angle	Caput Collum Diaphysis Angle = Neck-to-Shaft Angle [9]
AV angle	Femoral Neck Anteversion Angle [9]
FeAV angle	Femoral Neck Anteversion Angle [10]
SCJ	sacrococcygeal joint
<b>Current Study</b>	
AX	Acetabular Axis (opening direction)
APP	Anterior Pelvic Plane
SPP	Superior Pelvic Plane
C.S.	Coordinate System
TPP	True Pelvic Plane
FPP	False Pelvic Plane
AR	Acetabular Rim
ASIS	Anterior Superior Iliac Spine
AIIS	Anterior Inferior Iliac Spine
PSIS	Posterior Superior Iliac Spine
PT	Pubic Tubercle





# **Abstract**

## A NOVEL METHOD FOR DETERMINING ACETABULAR ORIENTATION

By Sean William Higgins, B.S.

A Thesis submitted in partial fulfillment of the requirements for the degree of Master of Science in Biomedical Engineering at Virginia Commonwealth University.

Virginia Commonwealth University, 2012

Major Director: Jennifer S. Wayne, Ph.D., Professor  
Biomedical Engineering & Orthopaedic Surgery & Director, Orthopaedic Research Laboratory

Enhanced knowledge of the acetabulum is of paramount importance in the diagnostic, planning, and execution stages of procedures and treatments targeting the hip joint. The convoluted and highly variable morphology of the structures comprising the bony pelvis make ascertaining measures of the acetabulum challenging. Furthermore, current methods for determining acetabular orientation assume symmetry between the separate halves of the pelvis by utilizing a coordinate system based on bilateral landmarks. The purpose of this study was to determine the three-dimensional orientation of the entire acetabulum. For this research, an improved programmatic method was developed for determining acetabular orientation using three-dimensional data. Accurate measures of commonly used acetabular orientation were ascertained from a large population of normal subjects. In addition, unilateral-based measures were performed using a new “hemi-pelvis coordinate system”. Significant differences between genders were observed in both the overall orientation of the acetabulum and the structural arrangement of the innominate bone.

# 1 INTRODUCTION

## Preface

Studies and observations of the hip joint and its afflictions are known to date back as far as Hippocrates.[11,12] The more recent radiographic studies of the hip joint have been performed for over 100 years now. There is also an expansive amount of surgical techniques and procedures that have evolved over many years which are of great interest and importance. With such an extended timeline of relevant research, there is an overwhelming amount of literature available on matters pertaining to the hip joint. At the time of writing this, a limited PubMed search of the combined terms: "hip arthroplasty", "hip arthritis", and "hip dysplasia" yielded over 40,000 results. With such a large body of literature available, it is inevitable that the works of some pertinent contributions will be overlooked. To focus the background information, the following introduction is comprised from a selection of works found in the literature and is intended to provide a clear picture of how our quantitative understanding of the hip joint has evolved within the limits of available imaging technology.

In addition to general background information on the hip, a summary of common quantitative measures is provided. Measures performed using plain radiograms are presented first, followed by the more recent indices developed for axial imaging modalities. Because x-ray technology has been in use for over 100 years now, there have been numerous indices developed that use plain radiograms. The summary provided herein is intended to provide an outline of some of the more commonly utilized non-invasive techniques for evaluating the bony structures of the hip joint. It is not intended to be a comprehensive listing, but rather to provide a picture of current diagnostic indices. In addition, the shortcomings of these indices will be discussed to

highlight where areas for improvement exist. The newest techniques of evaluating the hip have utilized recent advancements in software to generate three-dimensional (3-D) renderings. Towards the end of this section, the most recent studies which use these new capabilities will be examined. The findings of this study will be compared to the few studies that have used comparable methods later on in the discussion section. The above List of Abbreviations is provided below to serve as a guide for the many abbreviations that have been used in the literature as well as in this study. While the femoral component is critical to a full understanding of the hip joint, the research presented herein is focused on the normal acetabular component and therefore, discussion will primarily be limited to aspects pertaining to the acetabulum.

## **1.1 ANATOMY, DEVELOPMENT & BIOMECHANICS OF THE HIP**

The human hip joint is a major element of the musculoskeletal system which provides the ability to perform activities of daily living. Our fluidic and upright mobility is achieved through the considerable range of motion permitted by the hip. The hip is a diarthrodial synovial joint that connects the bones of the lower limb to the trunk of the body through the pelvis. The biomechanics of the hip joint have classically been compared to a simple ball-and-socket. Analogously, the ball end is formed by the femoral head which is received by the cup-shaped acetabulum (Figure 1.1a). Just underneath the insertion point of the joint capsule there is a fibrocartilagenous labrum (also called the limbus or cotyloid ligament) connected to the bony margin that surrounds the periphery of the acetabulum which functionally deepens, seals, and further stabilizes it.[4,13–17] The other major ligaments constraining the femur in the acetabulum are the ligament of head of femur, iliofemoral ligament, ischiofemoral ligament, zona obicularis and the transverse acetabular ligament (Figure 1.1b & Figure 1.1c).[16,18,19]

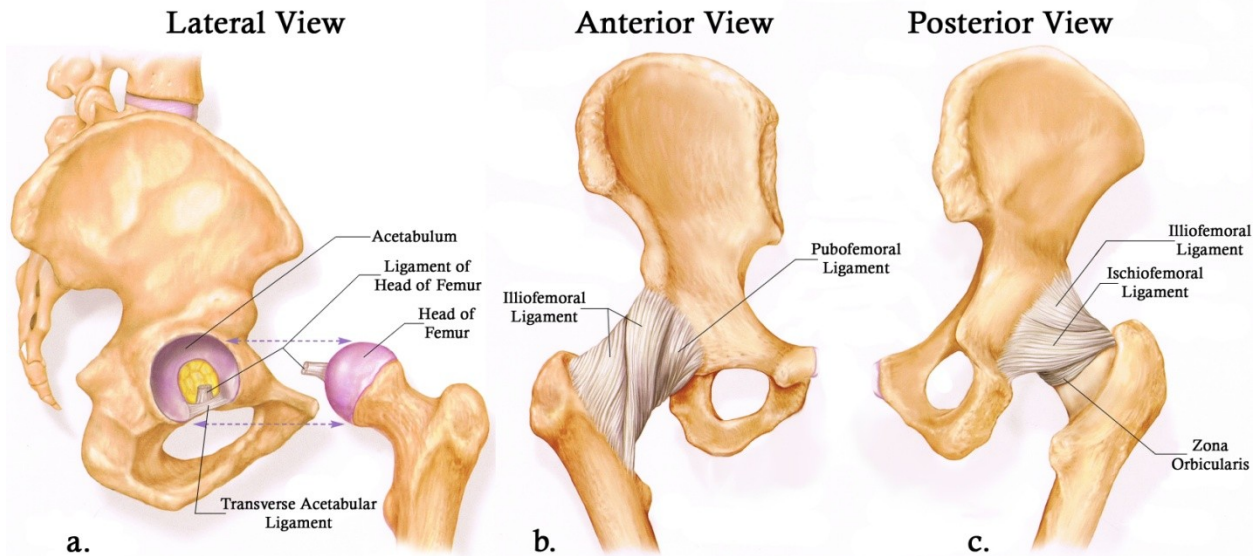
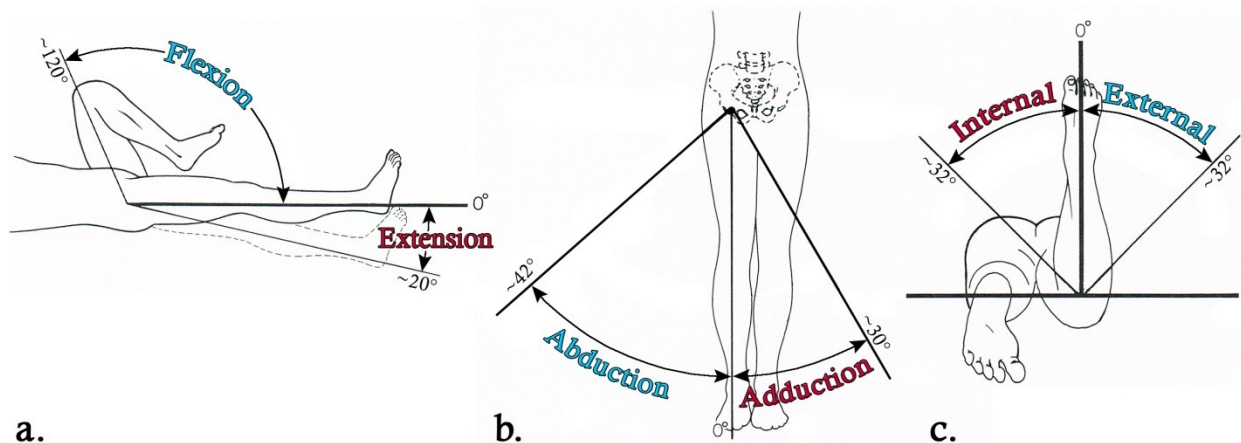


**Figure 1.1-** Major structures and ligaments of the hip joint. *Adapted from [19]*

The hip joint supports the loads required to keep our bodies stable through a large range of motion. In addition to supporting the weight of the body, the normal hip joint experiences loads during normal gait cycle ranging around three times body weight immediately after heel strike with forces increasing to four times body weight before toe-off. During more strenuous activities such as running or stumbling these forces can reach as high as eight times our body weight.[16,20–22] These large forces are transmitted through the articulating cartilage of the horseshoe shaped, lunate surface covering the superior and lateral aspects of the acetabulum and through the femoral head. Articulation is allowed for in all three anatomic planes with corresponding movements of flexion and extension in the sagittal plane, abduction and adduction in the frontal plane and internal and external rotations in the transverse plane. It is the compound morphology of both the acetabular and femoral components that controls the range of motion. We are allowed the largest range of motion in flexion with an approximate range of zero to 120-125 degrees, limited primarily by the hamstring muscle group, while the reciprocal extension has the least ranging from zero to 10-20 degrees and is limited by the thickening of the joint capsule and the iliofemoral ligament (Figure 1.2a). Typical abduction ranges from zero to 42-50

degrees, limited by the adductor muscles. Adduction typically ranges from zero to 25 or 30 degrees, limited by the tensor muscle and fascia of the abductor muscles (Figure 1.2b). Ranges of zero to 32 degrees are typical for external (lateral) as well as for internal (medial) rotation, both limited by the fibrous capsular constraints (Figure 1.2c).[16,17,20,23–25]



**a.** Flexion tested in supine position and extension tested in prone position. **b.** Abduction and Adduction tested in supine position. **c.** Internal and external rotation tested in either the prone or seated position. Adapted from [23,26]

Normally, the articulating surfaces of the acetabulum and femoral head are congruent with one another allowing for even stress distribution over the contacting areas. Deformities of the femur and/ or acetabulum can limit the range of motion and cause uneven stress distributions on the bony structures. In humans, abnormalities of the femur and acetabulum are often both present as the coupled structures are known to influence each other during development. It is understood that the presence of the spherical proximal femur and its mechanical interaction with the acetabulum is necessary for normal development of the hip joint.[1,13–15,27–31] Once structural development has progressed it is impossible to determine whether femoral head morphology is a result of acetabular shape or vice versa.[27] While developmental causality is still not fully understood, most studies suggest that acetabular deformities are due to primary femoral abnormality. It is believed that the acetabulum uses the spherical femoral head as a template for proper development.[14,15] For example, Legg-Calvé-Perthes' disease (or just

Perthes' disease) is a pathologic condition of the immature hip with a pathway known to arise in the femoral component. Perthes' disease is believed to be triggered by the occlusion of the circumflex artery which supplies blood to the capital femoral epiphysis. The bone tissue of the femoral epiphysis becomes necrotic and collapses under the mechanical load. During remodeling, the damaged aspherical femoral head reossifies and subsequently causes secondary deformation of the acetabulum.[14,32–36]

During development, the separate bilateral halves of the pelvis are divided into three individual sections. These three bones; the ilium, ischium and pubis are separated by the triradiate cartilage which forms a y-shaped union at the center of the acetabulum that allows for even interstitial, physal growth of the bone (Figure 1.3a). There are also three secondary centers of bone growth that appear around 8 to 9 years of age. Epiphyseal growth from these secondary sites originates from the cartilage complex surrounding the acetabulum which contributes to appositional growth and increased depth. The largest of these is known as the os acetabuli, located on the pubis which helps form the anterior wall of the acetabulum. The acetabular epiphysis forms on the ilium and contributes to the development of the acetabulum's superior margin. There is also a small epiphysis on the ischium which increases the posterior coverage (Figure 1.3b).[14,15,31,37] While the pelvis is developing, the acetabulum becomes more anteverted and superolateral coverage increases until around the age of 15. [28,30,38–46] The hip joint shows rapid development up to the age of 8-10 years and can be considered completely developed by radiological standards at the age of 15 years [40,41]. Typically, the three bones become completely ossified and fuse together to form the innominate (or coxal) bone by 18 years of age.[13,14,37,45]

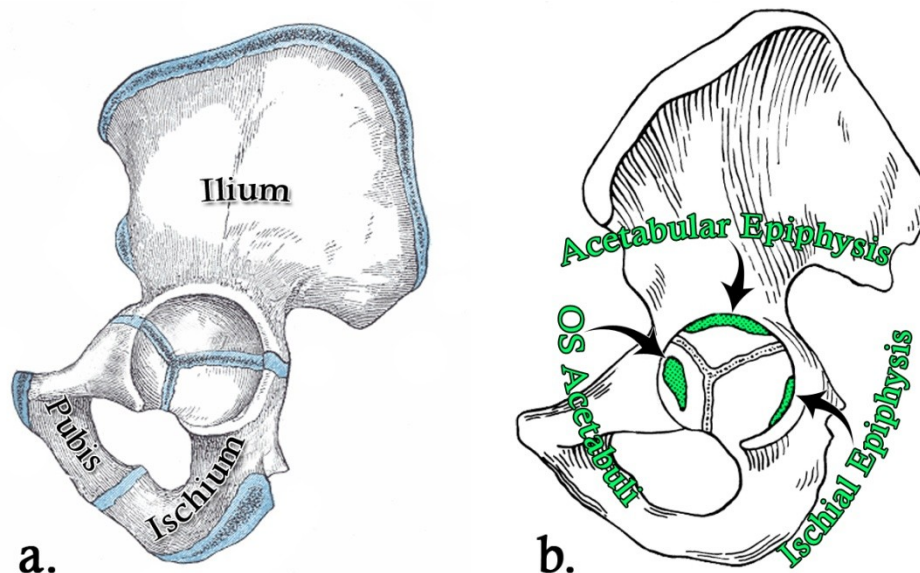


**Figure 1.3-** Epiphyseal growth of the innominate bone. **a.**-The ilium, ischium and pubis bones comprise the innominate bone separated by the y-shaped triradiate cartilage highlighted in blue. **b.**- Secondary appositional growth centers on the periphery of the acetabulum increase depth. *Adapted from [15,47]*

In general, the normal opening of a fully developed acetabulum is directed forward, outward and downward.[4] The final state of the three secondary growth centers forms an irregular succession of three peaks and valleys around the osseous border of the acetabulum. The peaks are roughly separated by the y-shape of the triradiate cartilage. The acetabular notch forms the most inferior valley, also known as the incisura acetabuli or cotyloid notch. The posterior valley is referred to as the "posterosuperior depression". The curvature on the anterior margin is known as the "psoas valley" because it allows for passage of the soft tissues that form the iliopsoas muscle (Figure 1.4).[48–51] The appearance of these valleys varies greatly, forming everything from irregular shapes to almost absent, appearing as straight lines. The adult pelvis is divided into two separate regions, one superior and one inferior. The ilium forms the superior region, known as the "greater" or "false pelvis", and the inferior region comprised of the pubis and ischium is the "lesser" or "true pelvis".[47,52] It is unknown if any relation exists between the morphology/orientation of the acetabulum and the final regions occupied by the true and false pelvis.

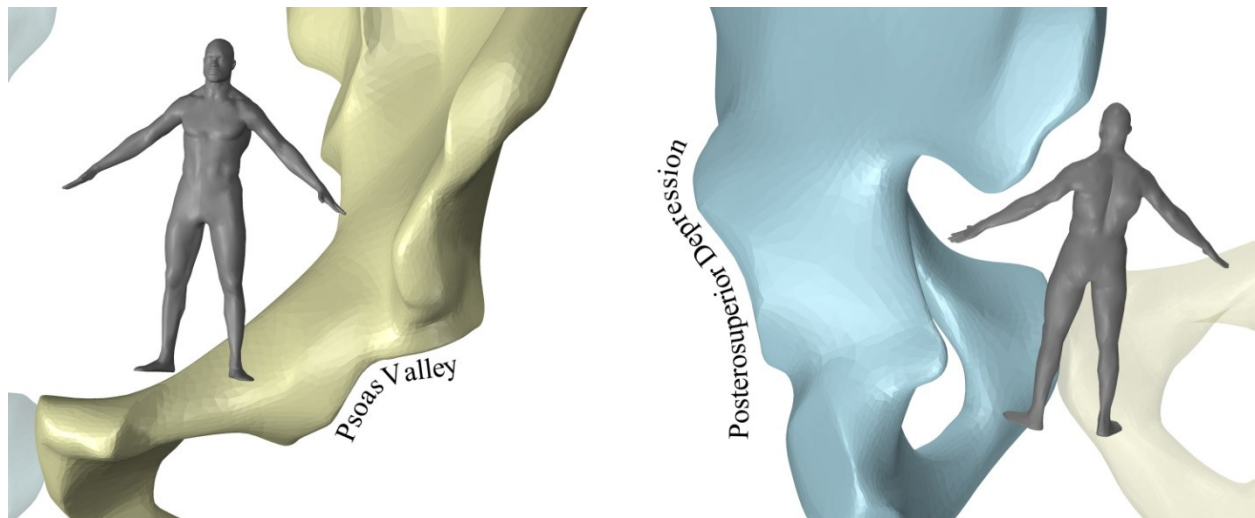


**Figure 1.4-** Normal curvature of the acetabular rim. The anterior and posterior margins respectively form the psoas valley (*left*) and posterosuperior depression (*right*).

At any given time the, femoral head is only covered by approximately two-fifths of the acetabulum.[26] Compressive forces transmitted through the femur are supported by the superior margin (or roof) of the acetabulum. Abnormalities of the acetabulum, which are generally referred to as “dysplasia(s)”, range from inadequate to excessive coverage.[27,53] The term hip dysplasia is typically associated with inadequate coverage along the superior margin of the acetabulum and shallow depth.[13,31,54–63] A lack of coverage and containment can result in displacement of the proximal femur from the acetabulum, which is clinically referred to as a subluxated hip. Subluxation is used to describe varying degrees of partial dislocation caused by abnormal morphology of the femur, acetabulum, or a combination of both.[28] Interestingly, hip dysplasia is notably more prevalent and severe in females. [11,14,28,55,57,60,62,64–67] While genetic and ethnic factors are known to be involved, the etiology of hip dysplasia is still largely unexplained and may begin during *in utero* development.[11,28,31,44,65]

The relationship between the femoral head and the acetabulum has a direct biomechanical effect on how forces are transmitted between the two bony structures and subsequently how resulting stresses are distributed.[55,68–70] The lack of coverage and possible



subluxation in dysplastic hips results in decreased surface area available for load distribution, resulting in higher stress concentrations (Figure 1.5). In accordance with Wolff's law, the bone of the acetabular roof is continuously remodeled to support the loading it experiences. [26,68,71–73] In 1932, Waldenström first reported the observation of denser, sclerotic, subchondral bone that corresponds to the weight-bearing site of the acetabular roof which is now known as the sourcil.[4,68] Plain radiographs can be used as a visual aid for identifying abnormalities of the hip joint by characterizing the geometrical appearance of the sourcil. Normal hip joints display an eyebrow shaped sourcil with an even and uniform thickness. Dysplastic hips with inadequate superolateral coverage present an uneven sourcil thickness that appears wedge shaped (Figure 1.5).[29,38,68] As the subchondral bone strengthens itself and becomes stiffer, its ability to absorb transmitted forces is reduced. Consequently, a reciprocal increase in energy dissipation is required within the relatively thin layer of articular cartilage. This increase in compressive loading (stress) experienced by the cartilage is a known pathogenesis for secondary osteoarthritis. [16,26,39,53,54,61,66–68,74–80]

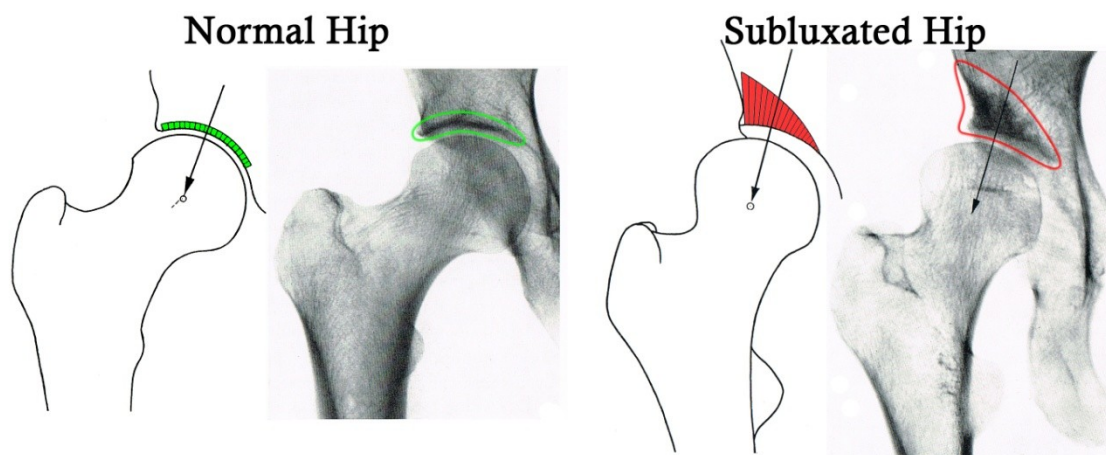


**Figure 1.5-** Stress distributions in subchondral bone of the acetabular roof resulting radiographic presentation of sclerotic sourcil for both normal (*green*) and subluxed (*red*) hip joints. *Adapted from [68]*

## 1.2 QUANTITATIVE TWO-DIMENSIONAL CLINICAL EVALUATIONS

The invention of roentgenography enabled development of the first non-invasive methods for quantifying morphometric features of the hip joint. The earliest indices appeared almost a century ago using anteroposterior (AP) radiographs. Many of the techniques that have been developed for plain radiography, both qualitative and quantitative, are still commonly used in both medicine and related research.[4,39] The impetus to characterize and quantify the acetabulum has been driven by the need to establish parameters for determining morphology separating normal from aberrant hip joints. Plain AP radiography is still considered the gold standard for preliminary diagnosis and evaluation treatment for hip abnormalities after the first three months of life and into adulthood.[29,38,39,55,81–88] Various indices are often confused with one another and sometimes the same terminology is used to designate entirely different measures.[9,39,45,89,90] In some cases, various measures are combined along with other indicators to form a more reliable method of diagnosis.[30,46,62–64,91–93]

Most indices developed for evaluating the acetabulum, and their corresponding studies, are concerned with exploring dysplastic and/or abnormal morphology. While measurement and identification of abnormal acetabular geometries is of significant importance, establishing normal values for any measure is the first critical step in understanding the native morphology. It is also worth noting that studies focusing on abnormal populations often work with slightly different methods as well as varying degrees of severity and criteria to select their subjects, making direct comparisons between investigations difficult. [8,9,30,39,40,44,46,59,74,76,89,94–98] The research presented herein is focused on establishing normal values for adult pelvic and acetabular morphology. Therefore, only normal values of the more pertinent and established measures for adults will be presented.

### 1.2.1 Qualitative Signs

While the primary interest of this research is focused on quantitative measures, the first radiographic means to evaluate the hip were qualitative signs. The classic signs used to diagnose developmental issues resulting in subluxation of the hip are that of Shenton and Perkins.[39,65,82,99–102] In 1911, Dr. Edward Shenton described a continuous arc created by the osseous borders of the obturator foramen's upper margin and the inner margin of the femoral neck.[99,103] The radiographic silhouette created by these structures is now commonly referred to as "Shenton's line". Normally Shenton's line should form a smooth and uninterrupted curve when drawn from the under surface of the superior ramus (obturator) to inferior surface of the proximal femoral metaphysis. When the curvature of Shenton's line appears broken, the proximal femur has become subluxated or otherwise dislocated from the acetabulum, which is indicative of severe dysplasia (Figure 1.6).[4,31,39,43,66,82,99,103]

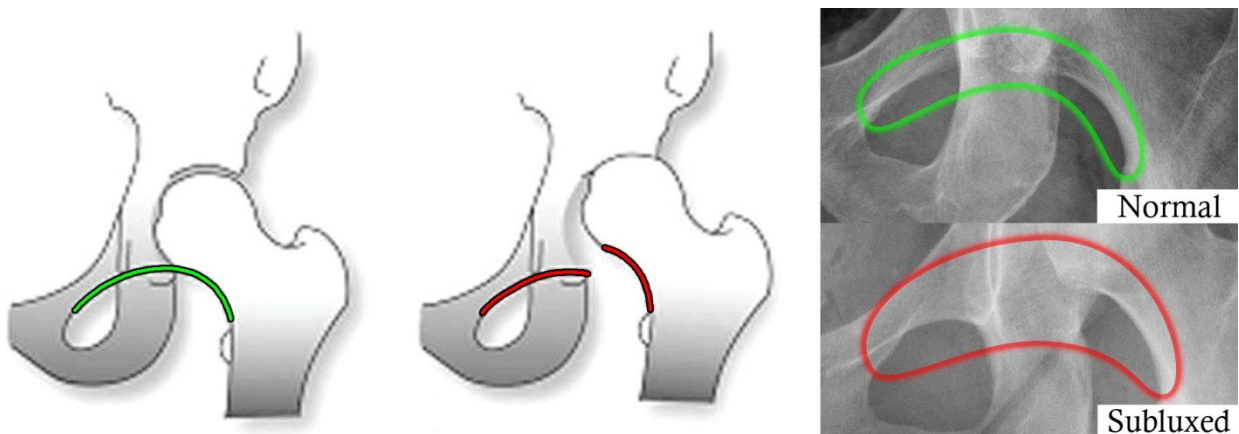


**Figure 1.6-** Depiction of intact/normal (*green*) and broken (*red*) Shenton's line. *Adapted from [104,105]*

Doctor George Perkins published a brief communication in 1928 that established two lines on the pelvic AP radiographs to locate the ossification center of the developing femoral head.[100] A horizontal line was established that connected the two medial most points of the

ilia in the gap of the triradiate cartilage. The vertical line, commonly known as the "Perkins line", is drawn perpendicular to the horizontal line through the most lateral edges of the acetabulums. In normally developing hips, the metaphysis of the femoral head should be below the horizontal line and medial to the vertical line (Figure 1.7). Ossification centers falling outside of this quadrant in the first few years of life are considered abnormal and will almost certainly need intervention. [1,28,39,65,82,100]

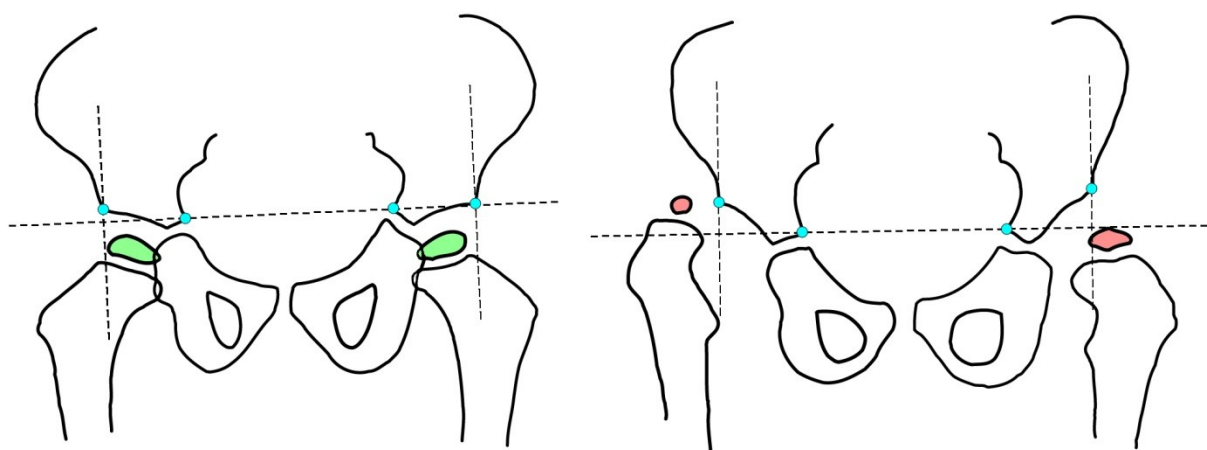


Figure 1.7- Depiction of Perkins's horizontal and vertical lines locating the femoral head ossific nuclei on normal (*left*) and abnormal (*right*) pelvises. Adapted from [100]

### 1.2.2 Plain Radiographic Indices

Of the many indices that utilize plain two-dimensional (2-D) radiographs, there are some which are more practically and reliably employed for evaluating the acetabulum.

[33,40,44,46,62,63,76,84,92] The following highlights some of the more pertinent measures which provided the foundation for the quantitative understanding of the hip joint. One of the first quantitative methods for evaluating the acetabulum was presented in 1925 by professor and medical doctor Heinrich Hilgenreiner. His angular measure is sometimes referred to as the acetabular angle, acetabular index, AC angle, acetabular roof angle or acetabular slope in the literature.[40,43,92] His measures provided a way to radiographically diagnose "congenital" dislocation in the hip (now preferably referred to as "developmental" dysplasia of the hip

[28,87,102]) of newborns and infants. Hilgenreiner, along with others, believed that developmental dysplasia of the hip (DDH) should be treated earlier than what was the current standard at the time. Subsequent research supported these theories and proved that early, conservative, treatment of DDH does result in more favorable outcomes if not complete resolution of the defect.[1,13,14,28,43,77,101,106]

Hilgenreiner's measures are commonly used during the early stages of life. During this time the developing hip joint is mainly comprised of cartilaginous nonossified bone, which appears radiolucent, making contours impossible to identify using plain radiography.[1,4,28,38] To address this, Hilgenreiner established the a horizontal axis, commonly referred to as the "Y-line" or "Hilgenreiner's line", which was drawn through the two y-shaped gaps in the triradiate cartilage. If the cartilaginous gap is broad, this line is usually drawn contacting the most inferior lateral point on the visible ossified margin of the ilium, which corresponds to the deepest point of the acetabulum.[28,1,4,39,40,63] A line representing the inclination of the acetabular roof is drawn from the previously established deepest point of the acetabulum to the most lateral bony edge of the acetabulum. The acetabular angle is formed between the horizontal line and inclined line of the acetabulum (Figure 1.8).[1,4,39,40,63] In his original works, Hilgenreiner reported normal values for infants should be approximately 20°.[1]

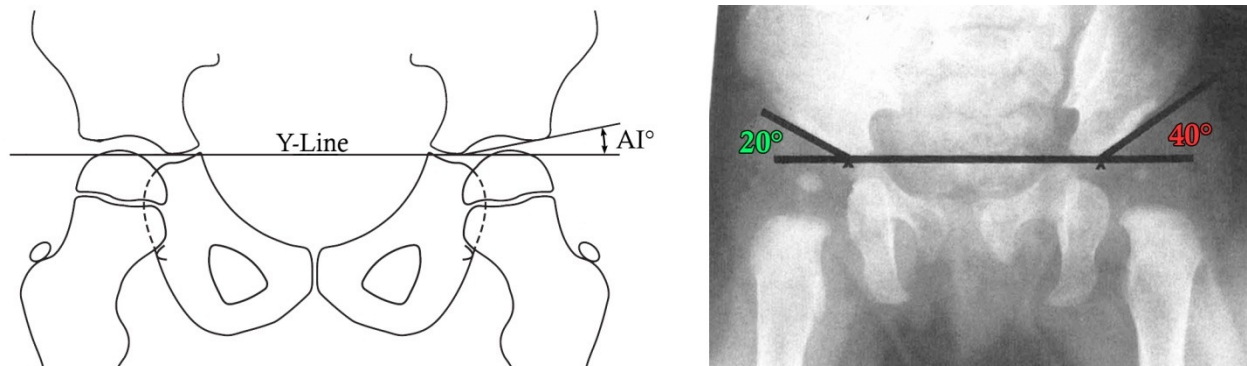


**Figure 1.8-** Depiction of horizontal Y-Line (Hilgenreiner's Line) drawn through the gaps of the triradiate cartilage, the line of acetabular inclination and the acetabular index (AI°) angle formed from their intersection (*left*). Bilateral measurement of AI° in AP radiogram of 6-month old female with known dysplasia of the left hip (*right*). Adapted from [39,63]

Hilgenreiner also defined two distances to be used as diagnostic measures that locate the proximal end of the femur. To start, the ossification at the central most superior point of the proximal femoral diaphysis is located. The length of a line drawn perpendicularly from the Y-line to the point on the proximal femur is known as the H-distance (height). The D-distance (depth) is measured along the Y-line from the point where it is intersected by H-distance line to the deepest point of the acetabulum, previously used for establishing the line representing acetabular inclination (Figure 1.9a).[1,4,28,39] In some cases, the more caudal Y-line is used in place of Perkins' horizontal line for a more stringent qualitative assessment the femoral head's location (Figure 1.7 & Figure 1.8).[1,28,65,102] While the location of the femoral head is of importance, the H and D-distances have shown to be of limited diagnostic significance making the acetabular angle the primary measure of interest.[39,40,42,65,107] The acetabular angle is still a widely used indice for assessing acetabular morphology during the early developmental stages of life.[38–40,107] For example, in 1934 Putti presented a detailed method of diagnostic scoring to assign the affected hip a functional grade using the patient's symptoms and physical signs combined with Hilgenreiner's measures.[30,108]

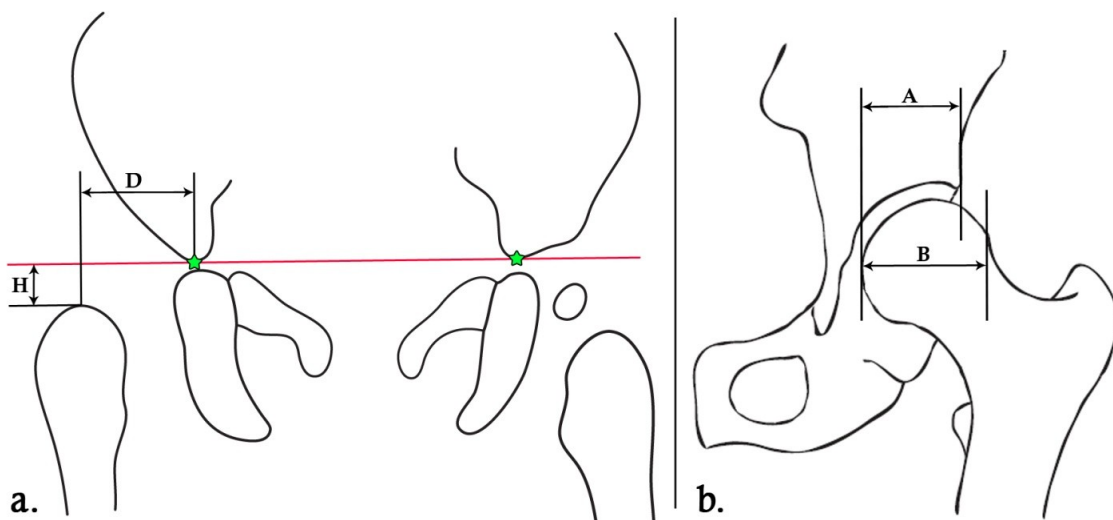


**Figure 1.9-** Commonly used linear distances measured on AP radiographs for children and adults. **a.-** Hilgenreiner's H and D distances shown on a representation of dysplastic right hip with Y-line (red). **b.-** Heyman & Herndon's measures used to form a ratio of femoral diameter (A) to coverage (B). *Fig b Adapted from [96]*

Hilgenreiner's measurements have shown to be difficult to reliably perform, especially after ossification of the triradiate cartilage or in children over the age of 10 to 12 years. [30,38,39,46,64,92,107] While it would seem that Hilgenreiner's measures have little bearing on assessing the adult acetabulum, subsequent indices were developed directly from his work making it relevant to this discussion. The most notable is Dietrich Tönnis's comparable loading/weight-bearing zone index (sometimes called Tönnis angle or acetabular roof obliquity) for adults, which was developed using Hilgenreiner's concepts [92,109,110]. The loading zone index is sometimes referred to as the synonymous "horizontal toit externe" angle (HTE angle) presented by Lequesne one year after Tönnis in 1963.[2,29,92,110–112] Because the triradiate cartilage is fused in adults, the loading zone index uses a line between the most inferior medial edge of the bilateral sourcils to set a horizontal baseline, or another acceptable horizontal pelvic axis is used. The angle subtended between the horizontal axis and a line from medial edge to the most lateral edge of the sourcil is used to represent the inclination of the acetabular roof (Figure 1.10).[5,63,79,92,104,109,112–115] Angles exceeding 10°, or less than 0°, are considered to be abnormal in adults.[5,29,83,104,112,116]

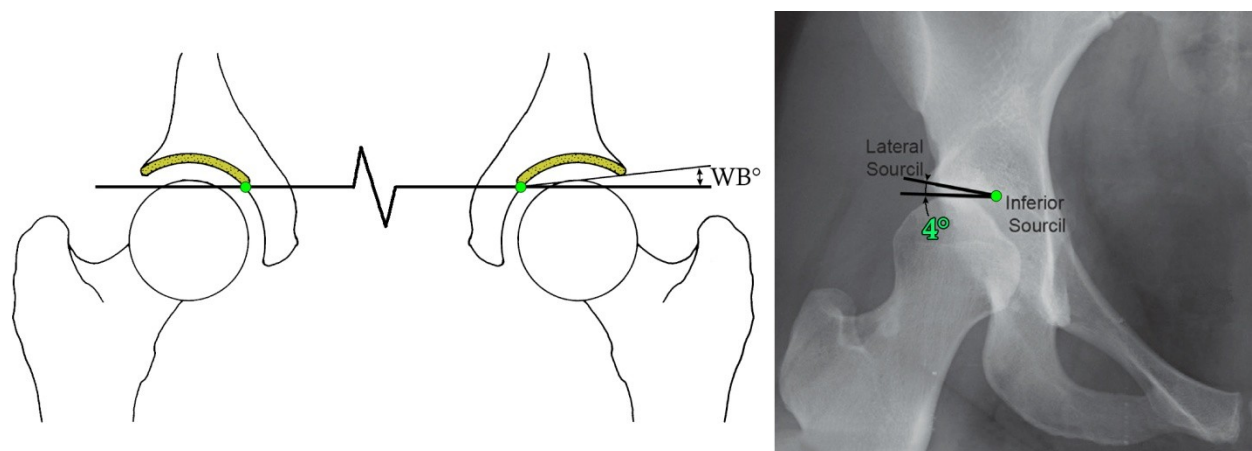


**Figure 1.10-** Depiction of weight-bearing zone index ( $WB^\circ$ ) subtended by horizontal pelvic axis formed by inferior medial sourcils (*green points*) and a line connecting the inferior and lateral sourcil margins (*left*). Right side measurement of  $WB^\circ$  in AP radiogram of a normal adult (*right*). Adapted from [29,117]

**Table 1.1- Normal Values of Weight-Bearing Zone Index (Tönnis Angle)**

Study	Werner et al. (2012)	Stubbs et al. (2011)	Lequesne et al. (2004)	Özçelik et al. (2002)	Nakamura et al. (1989)	Weighted Mean
Mean Angle	4.4°±6.8°*	4.8°±3.8°	3.6°±4.5°	3.3°±4.7°	4.4°±5.1°	4.1°±5.9°
n (hips)	2452	60	446	1162	254	4374

\* Standard Deviation back-calculated from 95% CI

While not directly related to Hilgenreiner's concepts, Heyman and Herndon presented a ratio of linear measures that has shown to be more applicable than the H and D distances in adults.[3] The acetabular head index (AHI), or femoral head extrusion index (FHEI), was originally used to in conjunction with a comprehensive set of measurement ratios, or "quotients", to evaluate the deformities associated with Perthes' disease.[3,92] Two horizontal distances are measured, one for the diameter of the femoral head and the other spanning from the most medial edge of the femoral head to Perkins's line. The AHI is a ratio of these measures which describes the acetabulum's coverage of the femoral head (Figure 1.9b). In subsequent investigation of Perthes', Dickens and Menelaus just used the distance from Perkins's line to the lateral edge of the femoral head to describe the amount of femoral head that was not covered by the acetabulum.[118] This measure is somewhat more subjective as it is solely dependent on the size of the subject's anatomy and not normalized by using a ratio as done in the AHI. It was originally reported that a normal acetabulum should provide around 70% to 90% coverage.[3] Since their initial study, the AHI has been selected from Heyman and Herndon's array of quotients to investigate various hip related issues on a wide range of human populations. [35,44,46,66,75,79,84,95,96,116,119–122]

In 1939, Gunnar Wiberg presented what would become one of the most commonly used and important indices of assessing acetabular morphology.[4,10,29,33,40,87,95] The center-edge angle of Wiberg, commonly known as the CE angle, or less frequently referred to as the lateral center-edge angle (LCE angle), is an effective 2-D measure of superolateral femoral head



coverage.[5,27,53,112,114] Having felt that measures for assessing the acetabulum in the developing human pelvis in the previous works of Hilgenreiner were sufficient, Wiberg developed his angular measure for further developed bone structures.[4] Specifically, it has been determined that the measurement of the CE angle is most useful in children 5-years of age and older once the appearance of the femur's capital epiphysis is radiographically evident.[30,39,64,81,123] The superolateral coverage of the femoral head provided by the acetabulum is considered one of the most critical aspects of normal hip morphology. [4,40,124,125] Measures of superolateral coverage are important because they convey the ability of hip joint to transmit vertical loads.[64] Because a lack of superolateral coverage is the primary morphological characteristic linked to DDH [13,54–61], the CE angle is commonly used as a diagnostic indicator.[4,10,29,38,63,126]

Wiberg's measure, like Hilgenreiner's, begins by establishing a transverse axis in the form of a horizontal line on an AP radiograph. Ossification of femoral head centers typically becomes visible on radiographs between the second and ninth months of life, which allowed Wiberg to devise an axis connecting the two femoral heads.[1,4,28,39] The center of the femoral head was originally (and still is) located using a template with concentric rings for mature bone structures, or by locating the center of ossification on the proximal femur for developing bone structures.[4,30,39,41,46,127] The CE angle is subtended between vertical (perpendicular to the horizontal axis) and a line extending from the center of the femoral head to the lateral edge of the acetabulum's bony margin (Figure 1.11). Using this scheme, the proximal femoral component is directly related to acetabulum in a single indice. In his original works, Wiberg suggested that CE angle values larger than  $25^\circ$  should be considered normal and that angles between  $20^\circ$  and  $25^\circ$  are borderline.[4] These values has been confirmed in subsequent studies and are now widely

accepted standards for cutoff values to delineate between normal and pathological hips.[8,10,28–30,41,44,62,64,74,96,97,114,128]

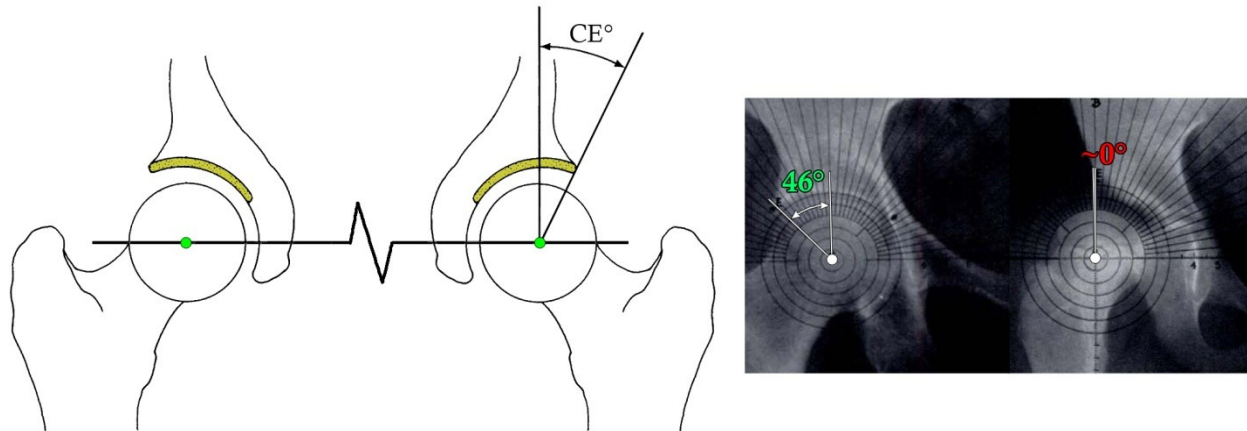


**Figure 1.11-** Depiction of CE angle (CE°) subtended between vertical and a line from the center of the femoral head (*green points*) to the lateral edge of the acetabulum (*left*). Right side measurements of CE° in AP radiograms of a normal (46°) and dysplastic (~0°) adults (*right*). Adapted from [29,30]

**Table 1.2- Normal Values of Center-Edge Angle (CE Angle)**

Study	Werner et al. (2012)	Park & Im (2011)	Jacobsen et al. (2004)	Lequesne et al. (2004)	Nakamura et al. (1989)	Weighted Mean
<b>Mean Angle</b>	33.6°±10.1°*	37.9°±5.6°	34.8°±7.6°	32.3°±6.5°	32.2°±6.4°	34.6°±7.9°
<b>n (hips)</b>	2452	856	8302	446	254	12310

\* Standard Deviation back-calculated from 95% CI

Measurement of the CE angle is not as subjective to the position of the femur as noted for the acetabular or weight-bearing index because the center of the spherical femoral head does not change location when rotated. Errors caused by imaging performed with the hip in abduction, adduction, external and internal rotations have shown to be as small as  $\pm 1^\circ$ . [30] Even though these errors are relatively small, the progression of OA is difficult to predict from any single radiographic indice or set of indices. [66,76] As had been done by Putti with Hilgenreiner’s measures, several comprehensive systems were developed for evaluating hips with suspected pathological defects using Wiberg’s CE angle. Some of the more notable classification systems that utilize the CE angle in conjunction with other symptoms were developed by Severin (1941) [91], Massie and Howorth (1950) [30], and Tönnis. [92]

Lequesne and de Séze observed that some dysplasias are not solely isolated to the superolateral portion of the acetabular roof and could also affect the anterior region. In 1961, they introduced their "anterior acetabular index"[6], more commonly known as the vertical-center-anterior angle (VCA angle).[2,29,92,129] To appreciate anterolateral coverage, they acquired radiographs in standing position from a quasi-lateral view (65°-25°) know as the *faux profil* ("false profile") view (Figure 1.12).[61,92,122,130] Lequesne and de Séze adopted Wiberg's angular scheme by using two lines originating from femoral head center, one vertical, and one extending to the anterior acetabular margin to form the VCA angle (Figure 1.12). Normal values for the VCA angle are equivalent that of the CE angle.[6,29,92,116,131] One shortcoming of performing measurements using the *faux profil* view is that anterior acetabular margin can be difficult to identify because the radiopaque line of the acetabular roof tends to fade anteriorly.[92]

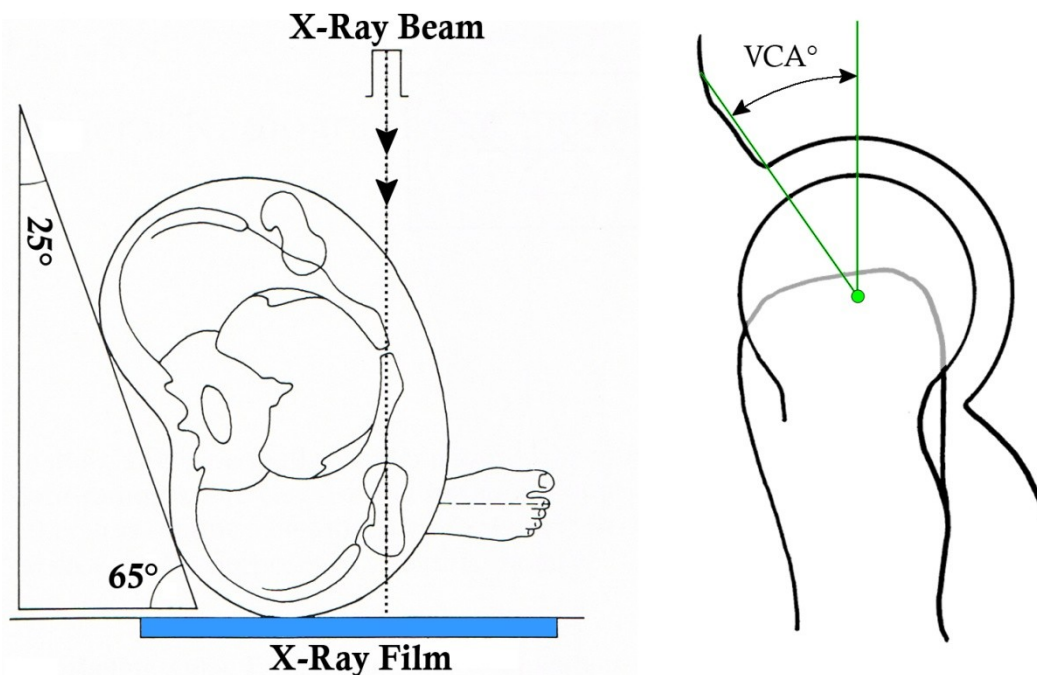


**Figure 1.12-** Craniocaudal view of patient positioning for attaining *faux profil* radiograph (left). Depiction of VCA angle (VCA°) subtended between vertical and a line from the center of the femoral head (green points) to the anterolateral edge of the acetabulum (right). Adapted from [29,92]

Before Tönnis presented his weight-bearing zone index, there was no indice that allowed for measurement of the adult acetabulum exclusive from the femoral head(s). Deformities of the either proximal femur, or even slight subluxation, will directly affect readings when using the femoral heads to establish a horizontal reference. In such cases, the readings of the CE angle may not be representative of the actual condition of the acetabulum(s).[62,132,133] Ian Sharp recognized this deficiency and devised a way to quantify the acetabulum without using the femoral component. Sharp presented his "acetabular angle" in 1961 which became popular in the English literature[132], however the same measurement technique was independently presented in the German literature by Ullmann in 1939.[134,135] Both Sharp and Ullmann used the inferior margin of the bilateral pelvic teardrops to establish a horizontal reference line. The pelvic teardrop, or U-figure, is formed in the AP view by the radiographic projection of cortical bone in the true pelvic region. The lateral aspect of the teardrop begins along the lunate surface of the acetabulum and continues inferiorly into the fossa, wrapping around the cotyloid notch (the "U" turn) in the obturator foramen to form the inferior aspect. The medial aspect is formed moving superiorly along the medial cortex of the pelvic wall and terminating at the arcuate line just posterior to the iliopectineal eminence (Figure 1.13).[132,136–139] The acetabular angle is subtended between the interteardrop line, and a line extending from the inferior tip of the pelvic teardrop to the superolateral most edge of the acetabulum (Figure 1.14). Sharp reported a range of 33°-38° for normal hips using radiographs from 100 non-symptomatic patients. [132] The upper limit for what should still be considered a normal hip varies slightly with values reported by Ullmann as 45° [134], 42° by Sharp [132], and 43° by Stulberg and Harris[62].[92]

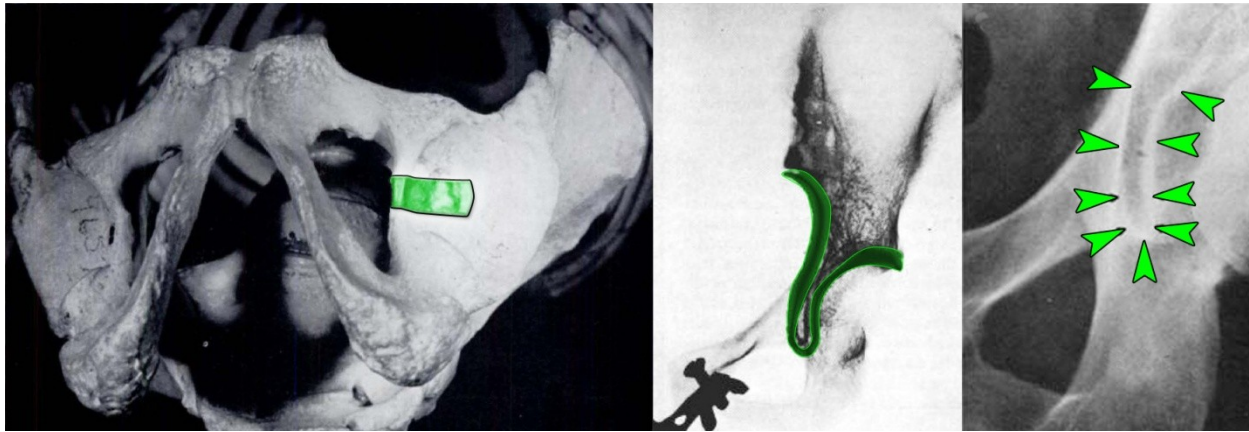


**Figure 1.13-** Caudocranial view of pelvis with lead strip (*green*) placed on structures forming the pelvic teardrop (*left*). AP radiographic view of left side teardrop with lead strip (*center*) and without (*right*). Adapted from [136,137]

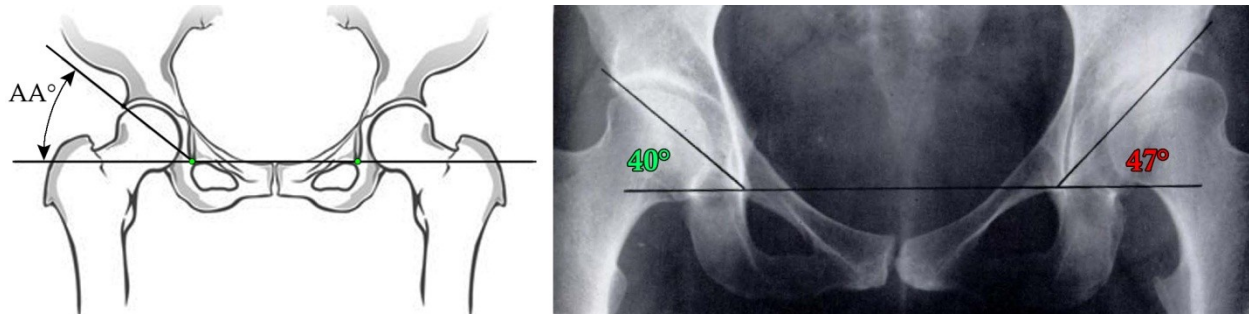


**Figure 1.14-** Depiction of the acetabular angle ( $AA^\circ$ ) subtended between the interteardrop line (*green points*) and a line from the inferior margin of the teardrop to the superolateral edge of the acetabulum (*left*). Bilateral measurement of  $AA^\circ$  in AP radiogram of an adult female with visible dysplasia and subluxation of the left hip (*right*). Adapted from [132,140]

**Table 1.3- Normal Values of Sharp's Angle (Acetabular Angle)**

Study	Park & Im (2011)	Jacobsen et al. (2004)	Özçelik et al. (2002)	Schwend et al. (1999)	Nakamura et al. (1989)	Weighted Mean
Mean Angle	38.1°±4.2°	37.9°±3.7°	39.2°±4.6°	37.0°±3.6°	38.0°±3.6°	38.0°±3.8°
n (hips)	856	8302	1162	400	254	10974

The final important indice to be highlighted that utilizes plain radiographs is the ACM angle, presented by Idelberger and Frank in 1952.[141] The term "ACM" arises from the point used in the construction of the angle on AP radiographs. Like most AP measures, the superolateral edge of the acetabulum is used to establish point A. Point B is located on the most inferior margin of the acetabulum, identified by the bright spot created by the acetabular notch. The line A-B defines the entrance of the acetabulum with the midpoint designated as point M.

Point C is located where a line perpendicular to A-B that originates from M intersects the bony edge of the acetabulum. If point C lands in the acetabular fossa, the correct placement should be on the continuation of the sourcil's curved sclerotic line. The angle subtended between the lines C-A and C-M form the ACM angle (Figure 1.15).[40,63,92] Heyman & Herndon (1950) [3], as well as Stulberg & Harris (1974) [62], proposed similar configurations which utilized the inferior margin of the teardrop as point B to establish the equivalent of segment M-C for measuring the depth of the acetabulum. Murray (1965) also used a similar configuration that located the upper corner of the symphysis pubis for point B for measuring the depth of the acetabulum.[128] Idelberger and Frank reported normal values of the ACM angle in adults to range between 40° and 50°.[92,141] Tönnis also reported that hips should be considered dysplastic if their angle exceeded 49°.[64]

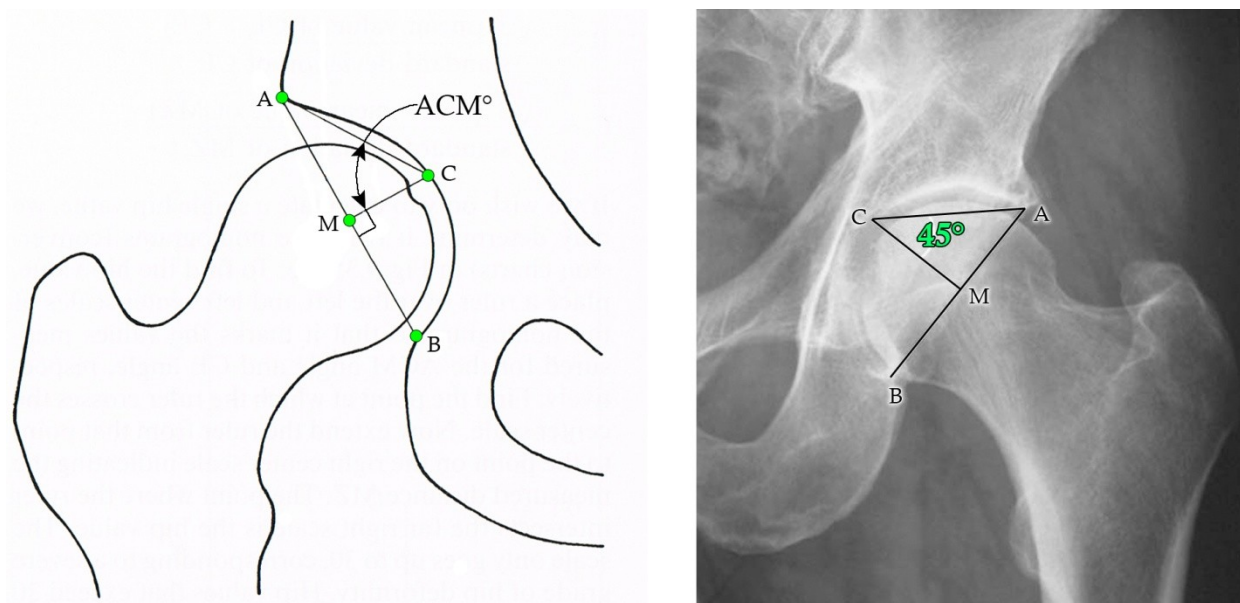


**Figure 1.15-** Depiction of the ACM angle ( $ACM^\circ$ ) subtended between the line segments CA and CM (*left*). Radiographic measurement of a left side ACM angle= $45^\circ$  representing a perfectly hemispherical acetabulum (*right*). Adapted from [92,142]

The ACM angle is also important because it provides an appreciation of the acetabulum's depth. [64,92] When the CE and ACM angles are simultaneously measured on a hip, the center of the femoral head can be related to the functional depth of the acetabulum. In normal hips, the

acetabulum is close to a complete hemisphere, thus the corresponding ACM angle should be about  $45^\circ$ . If the femoral head was perfectly concentric with a hemispherical acetabulum there centers would coincide.[40,44,64,77,81] Tönnis used this concept to create his comprehensive "Hip Value" where he used both the CE and ACM angles and called the distance between the two centers the "M-Z distance", where Z corresponds to the center of the femoral head and M to the center of the acetabulum (Figure 1.16). The Hip Value combines the CE and ACM angles along with the M-Z distance to create a single diagnostic score.[64,92]

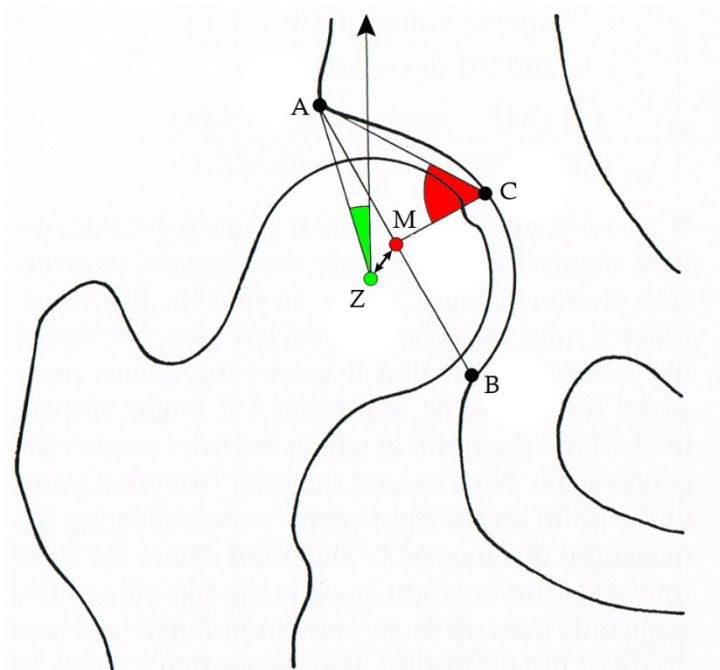


**Figure 1.16-** The center of the acetabulum as located by the ACM angle (*red*) and femoral head center located by the CE angle (*green*). The M-Z distance is measured between the two centers. *Adapted from [92]*

The indices outlined above have served as the foundation for quantitative clinical evaluation and research of the hip joint. With the minimal cost and ease of attaining images using plain radiography, it is expected that they will continue to serve as the basis for diagnostic indicators for years to come. While some modern techniques are becoming more readily available and economical, simple measurements made on AP radiographs will most likely remain the gold standard for initial diagnostic screening.[81,82,85,86,88] These and other early

radiographic indices changed how and when various abnormalities of the hip are viewed, diagnosed, and subsequently treated. [1,30,42,64,74,91,101,128]

### **1.2.3 Two-Dimensional Axial Measures**

With the advent of modern axial imaging technologies came enhanced visualization of complex morphology found in the hip joint. Axial based imaging such as computed tomography (CT) and magnetic resonance imaging (MRI) have provided the ability to view internal anatomic structures in the axial plane, and other interpolated planes, with a great level of detail.

Surprisingly, only a few measures have been developed for evaluating acetabular morphology that utilize CT or MRI imaging. Of the various indices that have been devised, there are two which are most commonly used to describe the geometry of the acetabulum. These two measures are known the "acetabular anteversion angle", developed by Visser and Jonkers, and the "sector angles" by Anda and his colleagues.[7,8]

In 1980, Visser and Jonkers utilized axial tomograms provided by CT imaging to present a method of measuring the orientation of both the acetabulum and femoral neck.[7,58,143] The angles they measured had actually been developed three-quarters of a century earlier by LeDamany's in his works on congenital hip dislocation, and prior to the recent advent of CT, had only been attainable on anatomical specimens.[7,45,143,144] LeDamany had an early understanding and appreciation of the compounding effect created by the geometric relationship between femoral neck and acetabulum and its effect on hip joint mechanics. The compounding relationship between the torsion of the femoral neck and anteversion of the acetabulum was expressed in a single measure known as the "incompatibility index" , which is the sum of the two angles (Figure 1.17).[7,143,144]. Visser et al. rekindled the interest in the dated measures with the use of modern radiological methods in their work on DDH.[7,143] The method devised by



Visser et al. for measuring acetabular anteversion has since been widely applied in studies of the acetabulum.[8,10,51,54,56,57,60,67,78,82,97,98,145,146] The various measurement techniques that have been developed for quantifying the complementary geometry of the femoral neck are explained briefly in the following section.

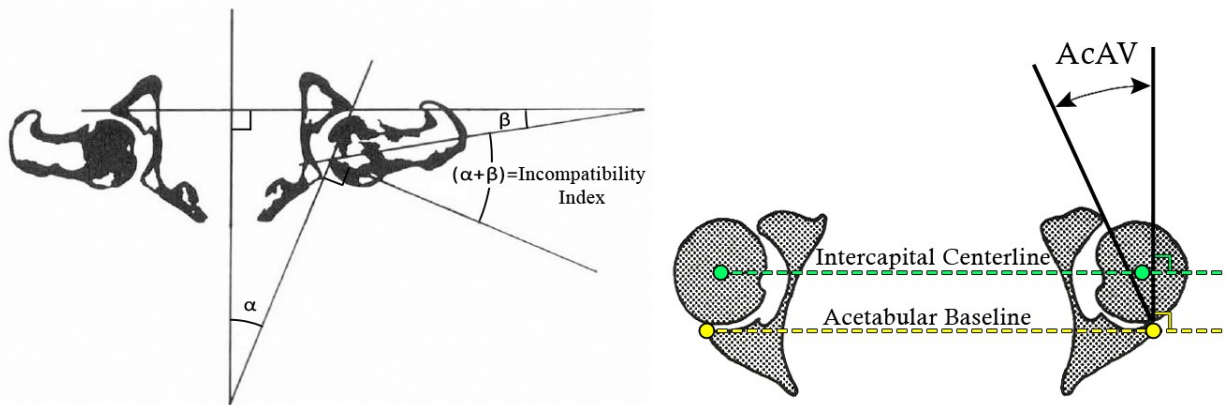


**Figure 1.17-** Axial view of hip joint at the center of the femoral head. Depiction of LeDamany's incompatibility index (*left*). Commonly used horizontal reference lines and AcAV borrowed from the incompatibility index. *Adapted from [8,10]*

The acetabular anteversion angle (AcAV), also commonly abbreviated as the AVA, AAV or AA angle, is measured from a tomogram at a level closest to the center of the femoral head (ideally at the exact center) (Figure 1.17).[7,8,60,67,78,143,146] A baseline is established that connects the posterior borders of the acetabular cup which, with proper patient positioning, is ideally parallel to the femoral transcondylar axis and perpendicular to the anatomic sagittal plane.[7,143,147] Some other researchers have chosen to use the intercapital centerline connecting the centers of the femoral heads as an equivalent baseline.[8,10,146,148] AcAV is measured between the sagittal plane, established by the baseline, and a line connecting the anterior and posterior margins of the acetabulum (Figure 1.17).[7,143,147] In a sense, AcAV could be viewed as an analog to Sharp's angle translated to the axial plane in that it describes the orientation of the acetabulum based only on its intrinsic features (i.e.- without using the femoral head). Visser and Jonkers initially reported the normal AcAV to be 16.5° for adults [7,143],

subsequent studies have shown that this value is probably slightly larger than originally reported (Table 1.4). While AcAV measured in conjunction with FeAV efficiently describes the relationship between the femur and the acetabulum in the axial plane, its value as a diagnostic indicator in assessing patients with hip dysplasia still remains unclear.

[8,10,54,56,57,59,60,67,78,82,97,98,145,146,148]

**Table 1.4- Normal Values of Acetabular Anteversion Angle (AcAV Angle)**

Study	Fujii et al. (2010)*	Jacobsen et al. (2005)	Hoiseth et al. (1989)	Anda et al. (1986)	Reikerås et al. (1983)	Weighted Mean
<b>Mean Angle</b>	20.7°±6.4°	20.3°±7.1°	19.4°±5.2°	20.0°±4.8°	16.9°±5.4°	19.3°±5.7°
<b>n (hips)</b>	50	78	80	82	94	384

\* Fujii et al. used a corrected axial plane perpendicular to the APP for measurements.

In 1986, Anda et. al used CT imaging to develop a new method of describing acetabular coverage in the axial view.[8] Using their new "sector angles" in conjunction with the CE angle, they provided the most complete 3-D characterization of the hip joint at the time. The sector angles utilize a transverse reference line much like the CE angle that connects the centers of the bilateral femoral heads, called the intercapital centerline (Figure 1.17). The sector angles quantify the amount of anterior and posterior coverage of the femoral head provided by the acetabulum at the equatorial plane of the femoral head (or closest transaxial slice) (Figure 1.18). Because the sector angles relate the location of the acetabular margins to the center of the femoral head they are considered complimentary axial measures to the CE angle. The anterior acetabular sector angle (AASA) is formed at center of the femoral head between the intercapital centerline and a line extending to the anterior margin of the acetabulum. The posterior acetabular sector angle (PASA) is measured in a similar fashion by using the posterior margin of the acetabulum. The entire angle of coverage in the axial plane is called the horizontal acetabular sector angle (HASA), which is equivalent to the summation of the AASA and PASA (Figure

1.18).[8,10] It is worth noting that Murphy et al. developed equivalent measures, after Anda et al. presented their work, which he called the posterior and anterior CE angles.[8,77,94]

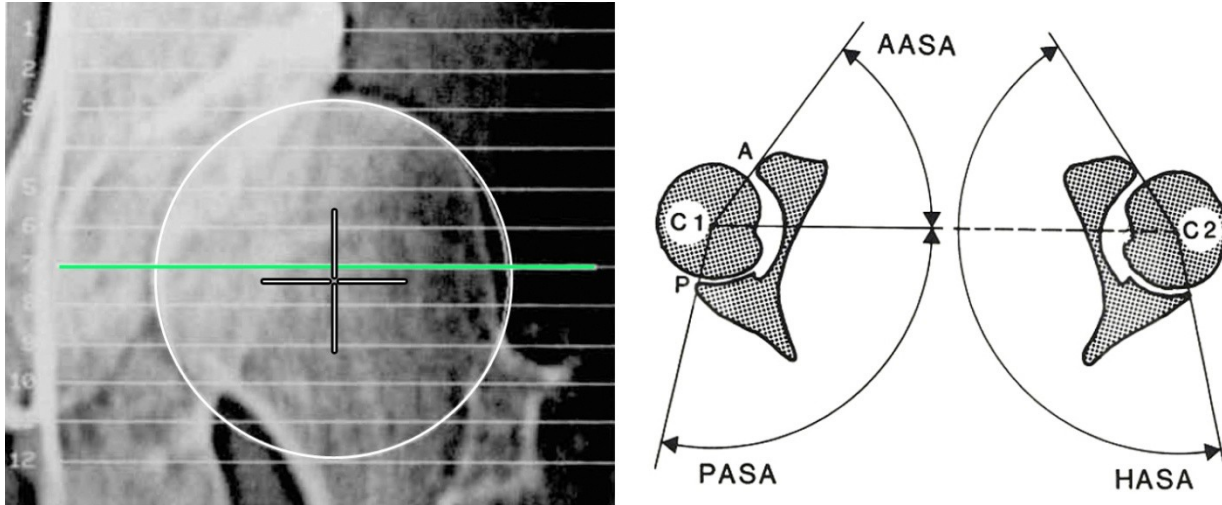


**Figure 1.18-** Depiction of the sector angles (*right*), ideally measured at the equatorial plane of the femoral head (*green*) or at the closest slice (*left*). Adapted from [8,10]

In their original study, Anda et. al used 41 patients to determine normal values for AASA, PASA and HASA. With no significant difference found between females and males or left and right sides, the calculated mean value for AASA to be  $63.5^{\circ} \pm 6.0^{\circ}$  and PASA was  $103.5^{\circ} \pm 8.1^{\circ}$ . [8] Follow-up studies for normal hips that used CE angles  $> 20^{\circ}$  for subject inclusion are compiled in Table 1.5 and Table 1.6. By using a CE angle  $< 20^{\circ}$  as an indicator for abnormal acetabulums, Anda and his colleagues measured the sector angles in dysplastic hips of women. They reported average AASA, PASA and HASA as all significantly lower than normal acetabulums. Out of 33 dysplastic hips, 24 (73%) had AASA below the normal limit and 12 (36%) had PASA below the normal limit, with 11 included in the group with insufficient AASA. This study clearly showed that acetabulums lacking superior coverage typically demonstrate lack of coverage in the posterior and/or anterior margins as well, with insufficient anterior coverage being more common. [10] Follow-up studies have further reinforced the findings of Anda et al., confirming that dysplastic hips typically display a global lack of coverage. [54,56,77,97,98]

**Table 1.5- Normal Values of Anterior Acetabular Sector Angle (AASA)**

Study	Fujii et al. (2010)*	Jacobsen et al. (2006)	Murphy et al. (1990)	Hoiseith et al. (1989)	Anda et al. (1986)	Weighted Mean
<b>Mean Angle</b>	63.1°±8.3°	60.8°±10.8°	62.6°±7.9°	65.9°±9.9°	63.5°±6.0°	63.6°±8.4°
<b>n (hips)</b>	50	41	49	80	82	302

\* Fujii et al. used a corrected axial plane perpendicular to the APP for measurements.

**Table 1.6- Normal Values of Posterior Acetabular Sector Angle (PASA)**

Study	Fujii et al. (2010)*	Jacobsen et al. (2006)	Murphy et al. (1990)	Hoiseith et al. (1989)	Anda et al. (1986)	Weighted Mean
<b>Mean Angle</b>	103.4°±8.8°	94.3°±7.9°	104.5°±7.3°	107.0°±11.7°	103.5°±8.1°	103.3°±9.0°
<b>n (hips)</b>	50	41	49	80	82	302

\* Fujii et al. used a corrected axial plane perpendicular to the APP for measurements.

## 1.2.4 Measurement of the Proximal Femoral Component

As mentioned previously, it is the compound relationship of the femoral component and acetabulum that dictate the range of motion and efficacy of the hip joint. While this research focuses on measurements of the acetabulum, it is important to note the two most common measurements used to describe the complimentary proximal femoral component. The first parameter discussed is the angle of inclination formed in the coronal plane between the femoral neck and long axis of the femoral shaft (Figure 1.19). Anatomically, this feature laterally offsets the femoral shaft from the pelvis, allowing the leg to move through a relatively large range of motion.[20] This angular measure is referred to by many names such as the neck-to-shaft angle, neck-shaft angle, head-neck-shaft angle, angle of inclination or more formally as the caput collum diaphysis or centrum collum-diaphyseal angle (CCD angle). [9,17,20,68,92,149,150] Much like the 2-D measures discussed for the acetabular component, the standard method of attaining the neck-to-shaft angle utilizes an AP radiograph. Ideally the plane formed by the femoral neck and its shaft are positioned parallel to the film.[150]

## Neck-to-Shaft Angle

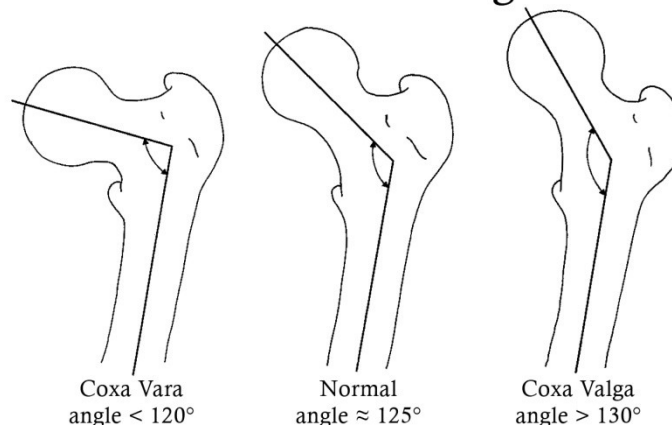


**Figure 1.19-** Normal and abnormal neck-to-shaft angles measured in the coronal plane. *Adapted from [20]*

During normal development the neck-to-shaft angle gradually decreases from as high as 150° and settles to values of around 120° to 132° once skeletal maturity is reached. [9,16,17,20,64,92,149–151] While the neck-shaft angle has a dominant relationship to the stressing of the femoral neck, it only has a limited influence on the stresses exerted on the acetabulum due to the mechanical arrangement of the joint. However, abnormalities affecting the neck-shaft angle can cause incongruence between the acetabulum and femoral head resulting in concentrated pressure distributions. If allowed to persist, these elevated pressures can cause the cartilage to prematurely degenerate or become damaged.[68,74] Deformities of femur, with respect to the neck-shaft angle, range from excessively large angles to those that are abnormally small. While there are no specific values that designate what is considered abnormal, angles that exceed 130° result in a condition referred to as coxa valga and those that are below 120° result in coxa vara (Figure 1.19).[17,20,68,92] If deemed necessary, both coxa valga and coxa vara can be corrected with various osteotomies of the femoral neck (Figure 1.20).[17,32,68,70,92,152]

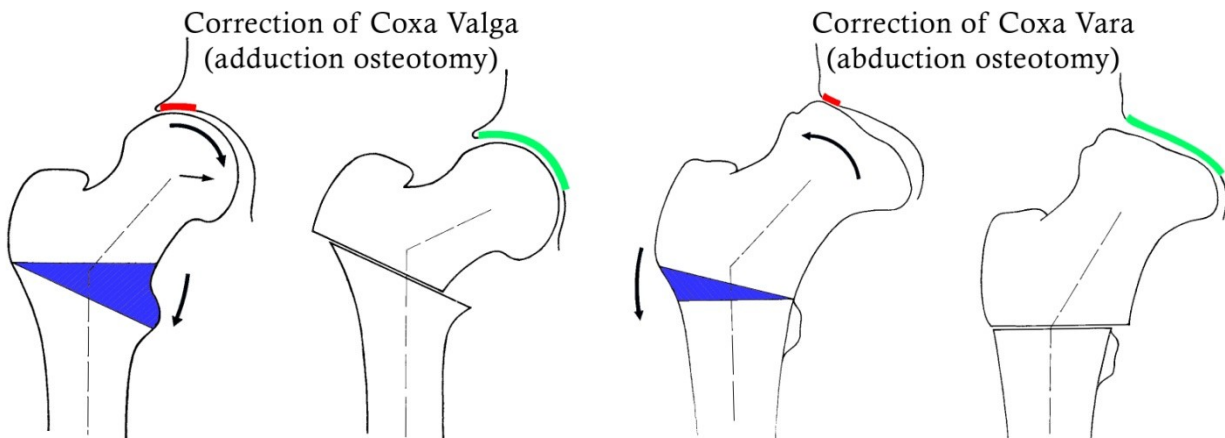


**Figure 1.20-** Depiction of the correction of coxa valga and vara using femoral osteotomies. *Adapted from [68]*

In the transverse view, the axis of the femoral neck is normally anteverted with respect to a coronal plane of the femur formed by the transverse transcondylar or knee axis (a line tangent to the dorsal aspect of the femoral condyles) and the long axis of the shaft. The angular relationship used to describe the version of the femoral neck is called the angle of anteversion or antetorsion (AV or FeAV angle).[9,10,20,64,92,98,150,153] The FeAV angle is measured between the posterior transcondylar axis and a line drawn from the center of the femoral head to the center of the femoral neck at its most narrow point (neck axis), both projected onto a plane normal to long axis of the femur (Figure 1.21).[9,10,20,149,150,153] Various standard radiographic methods can be used to attain this angle, in general they require two images and combine measurements with geometrical calculations.[78,92,150,153] FeAV can be easily and more accurately measured utilizing modern CT imaging by superimposing a series of tomograms. Typically one or two images containing the axial center of the dorsal femoral condyles is required, along with one from the center of the femoral head and one through the origin of the femoral neck.[29,60,78,97,143,148,153] The angle of anteversion is also known to decrease during skeletal development, beginning at angles ranging from 31° to 40° and settling to values around 10° to 14° in adulthood.[9,17,67,78,92,149–151] The angle of femoral

anteversion displays a large range of values, which can be considered pathologic when the neck is retroverted (negative anteversion angle) or excessively anteverted.[17,92,143,149,150]

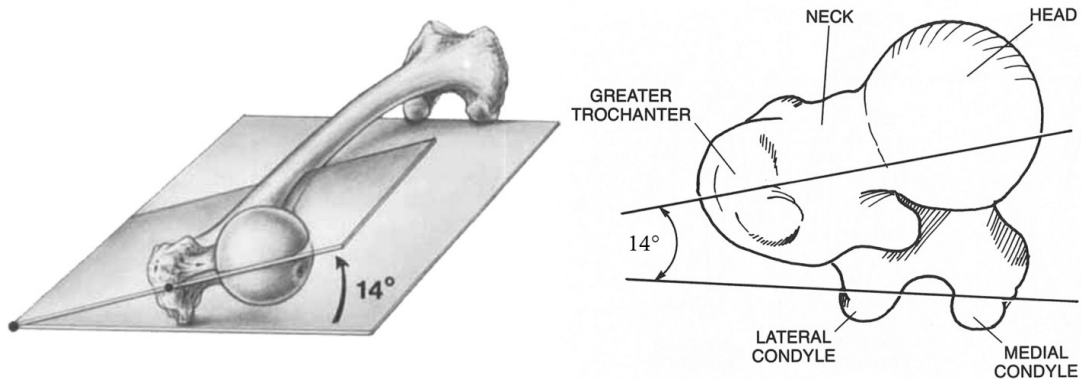


**Figure 1.21-** Depiction of normal femoral neck anteversion measurements. *Adapted from [20,150]*

As noted previously, the development of a normal hip joint requires the mutual presence of both an acetabulum that provides sufficient coverage and a spherical femoral head. While primary femoral afflictions like Perthes' are known to have a secondary affect on the acetabulum, various deformities of the femoral neck are thought to be secondary to abnormal acetabular development.[30,57,82,92] For example, a significantly higher occurrence of coxa valga has been shown to develop in hips that have decreased superolateral coverage. This correlation is believed to be “definitely” secondary to the acetabular deficiency which has also shown to significantly contribute in the development of coxarthrosis.[30,57,97] These findings further stress the importance of having a properly developed acetabulum.

In hips that have abnormally anteverted femoral necks, a corresponding and complimentary reduction of acetabular anteversion is required for stable joint mechanics. [67,78,143] Studies investigating femoral torsion in hips with normal acetabular morphometry have shown no significant correlation between FeAV and acetabular coverage or orientation. [10,45,67,148] Similarly, in developing hips that are known to have acetabular dysplasia

(primarily indicated by lack of superior coverage), studies again found no correlation between acetabular and femoral anteversion angles except for in severe cases.[10,60,78,82] Conversely, in older patients with persisting dysplastic hips that have shallow articulating cavities, the femoral neck has shown significantly more anteversion. This has shown to be more prevalent in acetabulums that lack both superior and anterior coverage, which further compounds joint instability and its deleterious effects.[10,57,97,98] It is important to note that when measuring the anteversion of the acetabulum independent from the femoral head, the angle may appear within normal limits when the cavity is globally deficient (superolateral, posterior and anterior regions).[8,145,146] Interestingly, all studies that have employed measurements of anteversion using the acetabulum only (e.g.- AcAV angle) did not find any correlation between femoral and acetabular anteversion, regardless of whether or not the hip was normal or dysplastic. [10,60,67,78,82,148] Studies that applied a method which incorporated the femoral head(s) and measured the posterior and anterior sections separately (e.g.- sector angles), did find a significant relationship between acetabular orientation and femoral anteversion.[10,57,97,98] Even with modern imaging and measurement techniques, the anatomic relationship between acetabular and proximal femoral orientation in dysplastic hips remains poorly understood.[57]

In a dysplastic hip with inadequate acetabular coverage, a more elliptical femoral head with decreased epiphyseal height and a thickened valgus neck tend to develop. Conversely, an acetabulum that provides excessive coverage will develop a femoral component with a spherical head, increased epiphyseal height and a varus neck of decreased thickness.[27,154] (Figure 1.22) Even subtle presentations of these deformities causes a condition commonly known as femoroacetabular impingement (FAI). In some cases, the development of an aspherical femoral head-neck junction that is usually both shorter and thickened is referred to as a "pistol grip"



deformity because of shape formed by the proximal femur.[34,122,155–160] The literal name of "cam" impingement is given to the cases where the thickening and asphericity femoral component creates incongruity, resulting in unwanted contact or jamming against the acetabulum. In the case of excess acetabular coverage or retroversion, the labrum is pinched via linear contact between the acetabular rim and the proximal femur, hence the name "pincer" impingement (Figure 1.23).[34,122,156–159] Cam-type impingement is more common in men whereas pincer is more prevalent in women, but a varying combination of both types is typically present.[34,122,159] Investigations of FAI's degrading effects have recently garnered more attention as they been directly linked to secondary arthritis of the hip joint.[27,74,86,122,155–159,161–163]

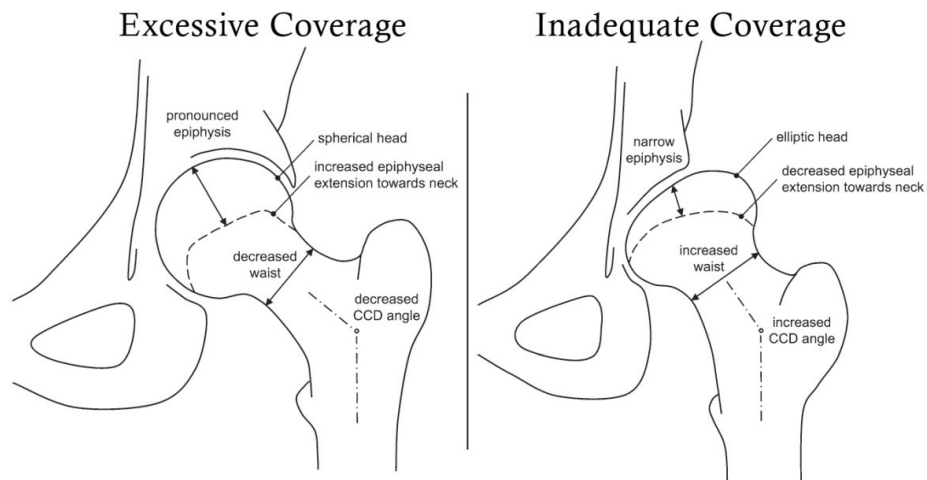


**Figure 1.22-** Differences in femoral development seen between acetabulums that provide excessive (*left*) and inadequate coverage (*right*). Adapted from [27]

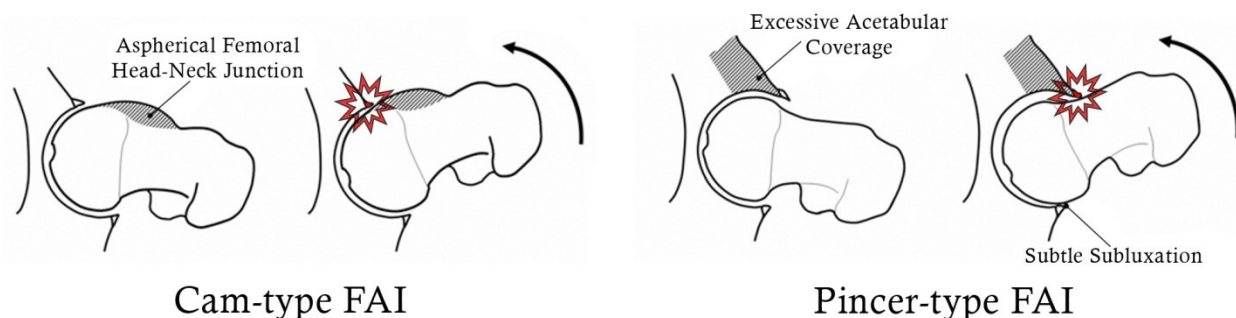


**Figure 1.23-** Depiction of cam (*left*) and pincer-type (*right*) FAI and the point of impingement (*red*). Adapted from [122]

### 1.3 ERROR ASSOCIATED WITH TWO-DIMENSIONAL MEASURES

Irrespective of the modality used to attain images, all 2-D measurements have certain inherent and unavoidable sources of error. Obviously when any manual measurement is performed there will be variation amongst different observers (interobserver) and also within the same observer (intraobserver) when measures are repeated. Regardless of how much effort is made to minimize this source of error by use of templates, overlays, goniometers, or software, there is always some measurable amount of error that will inevitably occur.

[28,30,38,46,83,84,107,117,123,127,164–167] While it is not the focus of this study, notable levels of error due to both patient malpositioning and observer variability have been found in proper identification of qualitative indicators such as Shenton's line and the interpretation of the acetabular teardrop's appearance [12,54,83,119,151,164,166,168]. To remain consistent with the literature, the terms pelvic tilt, rotation, and obliquity are used to respectively describe the rotation of the pelvis around the transverse, longitudinal, anteroposterior axes of the body (Figure 1.24).[169,170]

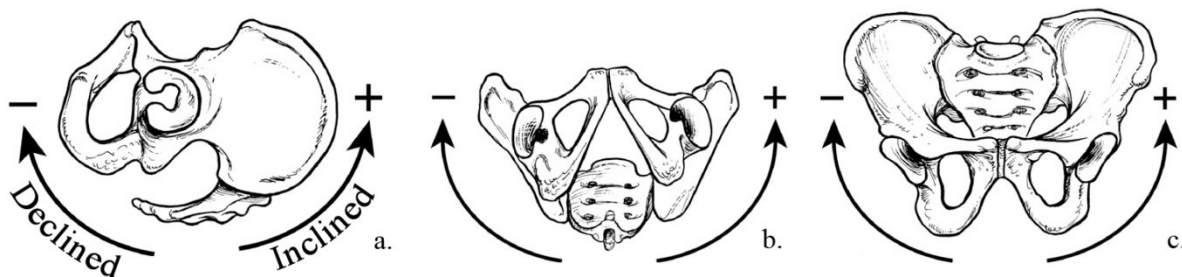


**Figure 1.24-** Standard definitions for 3-D pelvic rotations. **a.** Pelvic tilt (inclination and declination). **b.** Pelvic rotation (body left/right). **c.** Pelvic obliquity (body left/right). *Adapted from [170]*

The primary source of error that is universally inherent to all 2-D based measures, arises from the variability in patient positioning during imaging. This source of error is frequently noted to have an adverse affect on the accuracy of measures performed on both AP radiographs

[12,28,30,40,42,64,65,74,78,85,89,97,104,125,139,151,153,168,171], and axial images.[78,126,143,148,151,171,172] Fixation devices have been employed for holding patients in the intended position in an attempt to minimize positional sources of error (Figure 1.25). However, problems controlling the rotational position of the pelvis have shown to persist.[39,92,173] The effect of patient positioning and pelvic alignment on 2-D measures of the hip joint has been thoroughly studied and reported. [12,38,55,64,83,84,95,107,112,119,123,126,127,139,143,164–166,168,171,174]

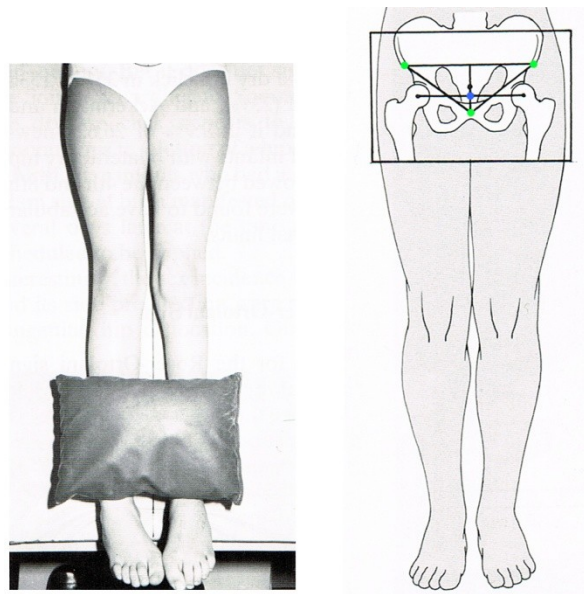


**Figure 1.25-** Example use of a fixation device and anatomic landmarks used for attaining AP radiographs. Depiction of a simple sand bag used secure the position of the legs (*left*). Reference points of the bilateral anterior superior iliac spines and pubic symphysis (*green*) used to form a triangle for properly centering the x-ray tube (*right*). *Adapted from [92]*

### 1.3.1 AP Radiography Sources of Error

When measuring parameters associated with the hip joint, preference varies between having subjects standing anatomically upright or in the supine position at the time of imaging. It has been shown that there is very little difference in pelvic tilt between standing and supine positions (besides weight-bearing factors).[95,126] The standard method for attaining AP radiographs of the pelvis uses a film-focus distance of around 100-120cm with the beam centered

between the femoral heads and projecting perpendicular to the standing frontal plane, defined by the bilateral anterior iliac spines and pubic symphysis (Figure 1.25). [4,28,29,54,85,92,151,171] Specific to all standard radiography views, improper positioning of the x-ray emitting tube in a position not normal to the view of interest and/or at an improper distance, will cause divergence (or convergence) of the beams projection onto the film. This results in distortion of the resulting 2-D image and thus contributes to measurement error when attaining angles.

[8,30,42,54,55,85,89,95,104,151,153,168,175]. Wiberg was one of the first to be aware of the potential introduction of error from patient malpositioning, so he examined its effects on his CE angle by taking two separate images in his entire series of 100 patients. The first image was taken in the supine position with the patellae facing directly upwards and the second was taken in the Lauenstein position which places the knee and hip in flexion enough to cause the pelvis to tilt/decline about 15°. [4,176] Wiberg noted that the change in pelvic inclination caused an approximated decrease in his angular measurement of 2 to 4 degrees. [4]

Using a large number of subjects, Broughton et al. thoroughly examined the variability inherent to commonly used 2-D measures in *children* from 5 to 15 years of age. [123] They statistically analyzed measurements repeatedly made by different observers (or raters) on the same radiographs, as well as on two separately attained radiographs of the same patient. Therefore, the interobserver and intraobserver variations estimated error arising from both measurement technique and image acquisition. This study showed that the CE angle realized the largest amount of error for measures of the acetabulum with 95% prediction intervals of  $\pm 9.3^\circ$  for intraobserver and  $\pm 9.1^\circ$  interobserver. The intraobserver prediction interval tells us that if a single CE angle measurement from a single observer was recorded at  $30^\circ$  we could be 95% confident that the true value was between  $39.3^\circ$  and  $20.7^\circ$ . The interobserver interval shows that

if true value was indeed  $30^\circ$  we can be 95% confident that measurements provided from two separate observers and/or two separate radiographs of the same patient will fall between  $20.9^\circ$  and  $39.1^\circ$ . As a point of interest, the variability of the readings was shown to be independent of the magnitude of the reading or degree of abnormality.[123] Their results for other key measures are shown in Table 1.7 and Table 1.8. Nelitz et al. performed a study using many of the same measures on radiographs of 100 dysplastic *adult* hips.[84] The authors noted that there are different problems associated with performing measures on skeletally mature adults when compared to developing skeletal structures. Another important variation of this study is that they used the same radiographer for all films and only used one film for each subject. This eliminates major sources of variability, which subsequently makes their results appear more favorable than would be expected in typical clinical settings. Because all of the subjects were skeletally mature, they applied the acetabular index of the weight-bearing zone. For the purposes of comparing reliability, the two measures can be viewed as comparable on the basis that they use similar or the same bony landmarks in a related manner. Nelitz et al. reported standard deviations (SD) of the variability in measurements from using different raters (interobserver) and within the same rater (intraobserver), along with corresponding intraclass correlation coefficients. Their findings of measurement variability in dysplastic adults also showed a large amount of error resulting from *only* observer error (Table 1.7 & Table 1.8).

**Table 1.7- Various Estimates of Interobserver Measurement Variability**

Reliability Measure	Study	n films/ hips measured	raters	trials	CE Angle	Acetabular/ Weight-Bearing Index	Sharp's Angle	ACM Angle	Neck-Shaft Angle	FHEI
<b>95% Prediction Intervals</b>	Broughton et al. (1989)	63/126	2	2	±9.1°	±5.5°	-	±4.5°	±12.6°	±3.8mm*
<b>Standard Deviation</b>	Nelitz et al. (1999) <sup>†</sup>	100/50	3	2	±13.9°	±11.6°	±7.2°	±10.8°	±17.1°	±11.9%**
<b>ICC</b>	Nelitz et al. (1999) <sup>†</sup>	100/50	3	2	0.87	0.85	0.76	0.58	0.79	0.84
<b>ICC</b>	Mast et al. (2010) <sup>††</sup>	39/78	2	2	0.73	0.45	0.63	-	0.58	0.9
<b>MDC</b>	Mast et al. (2010) <sup>††</sup>	39/78	2	2	8.3°	9.3°	5.0°	-	12.2°	5.0mm

<sup>†</sup> Goniometer used to perform measures

<sup>††</sup> Imaging software used to perform measures/ templating

\* Used femoral head uncovering (perkins's line to lateral femoral head)

\*\* Quotient used- reported in % coverage

**Table 1.8- Various Estimates of Intraobserver Measurement Variability**

Reliability Measure	Study	n films/ hips measured	raters	trials	CE Angle	Acetabular/ Weight-Bearing Index	Sharp's Angle	ACM Angle	Neck-Shaft Angle	FHEI
<b>95% Prediction Intervals</b>	Broughton et al. (1989)	50/100 (30/60) <sup>‡</sup>	1	2 (1) <sup>‡</sup>	±9.3°	±6.1°	-	±4.7°	±10.4°	±3.5mm*
<b>Standard Deviation</b>	Nelitz et al. (1999) <sup>†</sup>	100/50	2	2	±11.8°	±0.1°	±3.6°	±1.5°	±2.5°	±9.2%**
<b>ICC</b>	Nelitz et al. (1999) <sup>†</sup>	100/50	2	2	0.90	0.88	0.76	0.65	0.83	0.8
<b>ICC</b>	Mast et al. (2010) <sup>††</sup>	39/78	2	2	0.92	0.92	0.70	-	0.95	0.88
<b>MDC</b>	Mast et al. (2010) <sup>††</sup>	39/78	2	2	3.0-6.0°	2.0-5.5°	3.4-4.3°	-	4.8-15.9°	4.0mm

<sup>†</sup> Goniometer used to perform measures

<sup>††</sup> Imaging software used to perform measures/ templating

\* Used femoral head uncovering (perkins's line to lateral femoral head)

\*\* Quotient used- reported in % coverage

<sup>‡</sup> Used 60 subjects to attain two radiographs on the same day both rated by 1 observer

The intraclass correlation coefficient (ICC) is widely accepted as a universal reliability index and its application has shown to be an effective statistical method for measuring the amount of variability between and amongst observers (see section 2.5.1).[112,177–184] However, to gain a better appreciation of reliability it is helpful to describe it using the units of the measurements themselves (e.g.- degrees, lengths, etc.).[185–187] One excellent statistical tool for doing just that, is known as the minimum detectable change/difference (MDD). The MDD describes the amount of difference needed between observed measurements to be confident that a "true" change exists that is not a result of measurement error (95% confidence is typically used). Mast et al. used AP radiographs of 39 adults with mildly dysplastic hips that were diagnosed with FAI to determine the ICC and MDD of commonly used measures.[112] For the CE angle, they found MDD values ranging from three to six degrees due to intraobserver variability and a value of 8.3° for interobserver variability.[112,116] The rest of their results are shown along with the other studies previously outlined to give a general appreciation of the variability associated with measures performed using AP radiography (Table 1.7 & Table 1.8).

By using different methods to describe variability (i.e.- ICC, MDD, confidence intervals and SD), a clearer picture of measurement inaccuracy related to plain radiographic indices emerges. It is important to understand that in a realistic clinical or research setting the performance of any single measure is limited by its *least* accurate estimate of reliability. The studies detailed above were chosen for their substantial number of subjects, robust design, and in the case of Broughton et al., the use of two independently acquired radiographs of the same subject.[84,112,123] Numerous other studies have been performed to assess the reliability and repeatability of various measures that were not directly mentioned.

[12,55,83,85,107,112,117,119,120,127,129,140,151,165,167,174,188] Mast et al. provides a

recent compilation of various reliability measures for the indices described herein.[112] Many of these studies show results that appear more favorable due to a lack of appropriate controls, or conversely, one or more factors being overly controlled. It is important to note that most studies use raters of differing skill levels as well as different controls and patient populations, which results in a wide range of reported values. For these reasons it is both impractical and of little value to make direct comparisons across the wide range reliability studies.

### **1.3.2 Controls for AP Radiography**

German orthopedist and professor Dietrich Tönnis was responsible for pioneering and popularizing the concept of controlling for patient positioning using bilateral measures of symmetry on AP radiographs in the 1960's and 70's.[64,92,109] The indices known as the "quotient of pelvic rotation" and "symphysis-os ischium angle" (or symphyseal-ischial angle), were originally developed to control measures of Hilgenreiner's acetabular index in developing children. It was known that rotations of the pelvis could cause significant distortion of the projected geometry of the acetabular roof, thus altering any subsequent measures. Tönnis used the symmetry of the pelvis to develop bilateral measures of the obturator foramina and ischial bones. His concepts have been widely applied to other measures attained from AP radiography. Many studies now apply selection criteria for the proper positioning of patients by observing the symmetric appearance of the bilateral obturator foramina.

[29,39,54,55,64,74,75,83,95,96,138,139]

Rotation about the longitudinal axis of the body causes a decrease in the acetabular index on the side to which it is rotated, and an increase on the contralateral side. The amount of rotation is accounted for by calculating the quotient of pelvic rotation. As rotation occurs, the perspective of the projected view changes and the transverse diameter of the obturator on the



side to which the pelvis is being rotated appears smaller and the contralateral side appears larger. The quotient of pelvic rotation is ratio of the foramina's horizontal diameters, which should equal 1 in neutral rotation (assuming the pelvis *is* perfectly symmetric) (Figure 1.26). Quotient values between 1.8 and 0.56 were recommended by Tönnis to keep any bilateral differences in measurement of the acetabular index around  $\pm 2^\circ$ . [64,92] Jacobsen et al. performed a well designed follow-up study to develop controls for his own radiographic materials using cadaveric pelvises mounted in a specially designed frame. Using controlled rotation through a range of  $42^\circ$ , they found that quotient values of 0.7-1.8 and 0.5-1.8 should be maintained to keep measurement variation within  $\pm 2^\circ$  for CE angle and Sharp's angle, respectively. [95] Because these control measures are also made by different observers and at different times, they too are subject to error. The amount of error has shown to be quite small, with an intraobserver variance reported of  $\pm 0.19^\circ$  and an interobserver variance of  $\pm 0.13^\circ$ . [107]

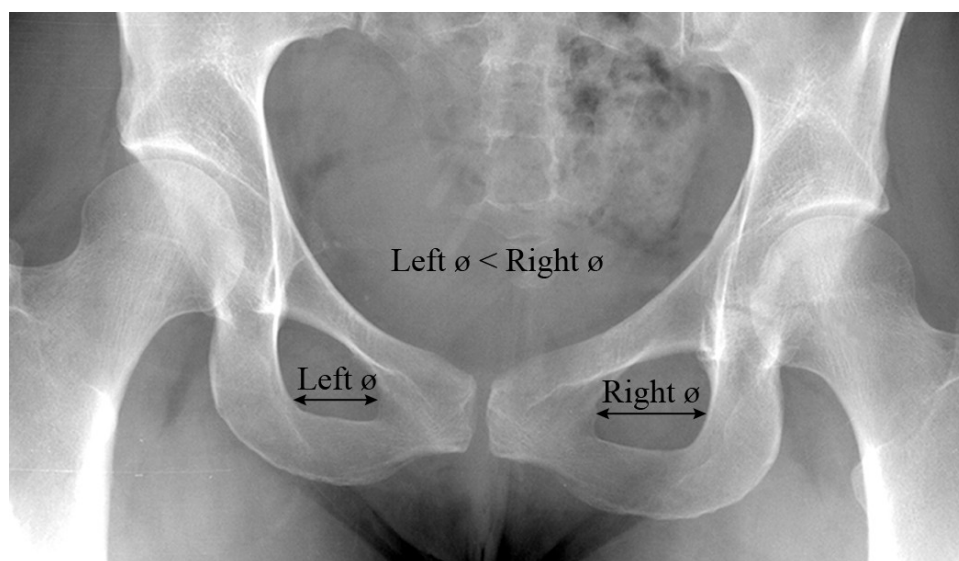


**Figure 1.26-** AP radiograph of pelvis showing rotation towards the right side about longitudinal axis of the body.

Pelvic tilt in the AP view also causes measurement errors related to indices that utilize the acetabular roof. With decreased lumbar lordosis, the pelvis tilts backward and any angle will inversely show an apparent increase. Conversely, with increased lumbar lordosis and pelvic

inclination, the angle measured will appear to decrease. Tönnis accounted for pelvic tilt in the developing pelvis with the use of his symphysis-os ischium angle. This angle is formed between bilateral lines tangent to both the superior border of the pubis and the superior margin of the ischium, connecting centrally at aperture of the pubic symphysis. Normal ranges specified by Tönnis for this angle were derived from 1,582 x-rays and ranged from 85° to 135° depending on the age of the patient. Within the specified range of symphysis-os ischium angles for a given age group, measurement error of the acetabular index was controlled to within three degrees. If pelvic rotation and tilt are both outside of the recommended limits then bilateral measurements can vary as much as eight degrees.[64,92,107] The variance associated with measuring symphysis-os ischium angles is much larger than that of quotient of pelvic rotation, with a reported intraobserver variance of  $\pm 6.4^\circ$  and interobserver variance of  $\pm 4.7^\circ$ . [107] The variability associated with this control is of little consequence for adults pelvises because its measurement is unattainable as the ischium is no longer appears as a discrete figure.

Ball and Kommenda also developed a method to assess pelvic inclination called the *pelvic tilt index*. [168] This indice uses a ratio of the obturator foramen's vertical diameter-to-the distance from the upper brim of the pubis to the Y-line. The concept works much like the quotient of pelvic rotation; with the projected distances of the two vertical lines changing relative to one another as pelvis is tilted forwards or backwards. With the pelvis in acceptable limits of inclination the index should be between values of 0.75 and 1.2. [92,107,168,189] The pelvic tilt index has shown to be more reliable than the symphysis-os ischium angle with reported intraobserver and interobserver variances similar to that of the of pelvic rotation at  $\pm 0.14^\circ$  and  $\pm 0.12^\circ$ , respectively. [107]

In more recent efforts, Tannast et al. presented a method that corrects for both pelvic tilt and rotation using standard radiography.[85] Malpositioning was corrected for by geometrically correlating the vertical distance between sacrococcygeal joint and the superior border of the mid-symphysis pubis, acquired on both a standard AP view and a lateral radiograph. Neutral pelvic tilt was defined as an inclination angle of  $60^\circ$  measured between a horizontal reference created by the interteardrop line, and line connecting the sacral promontory to the foremost point of the symphysis pubis. Pelvic rotation is corrected for by vertically aligning the point of the mid-symphysis pubis with center of the sacrococcygeal joint (Figure 1.27). By using the known conical projection of the x-ray beam and its focus distance from the target, along with the assumption that the acetabulum is spherical, a 3-D representation of the hip joint can be calculated. Tannast, Zheng, and their colleagues at the University of Bern in Switzerland have developed this concept into a software package called Hip<sup>2</sup>Norm<sup>©</sup>. After the manual selection of specific landmarks on the digitized radiographs, the software can calculate many of the commonly used radiographic measures. The concept and software have shown to be reliable for performing standard measures with the added advantage of correcting for patient malpositioning.[85,88,167] This other techniques that utilize 2-D projections to measure interpolated features of the 3-D acetabulum require some assumptions to perform calculations, such as a perfectly spherical acetabular cavity.[51,88,167,190,191] As previously explained, the underlying cause for many hip joint problems are either an aspherical acetabulum and/or femoral head which limits the diagnostic utility of such methods.

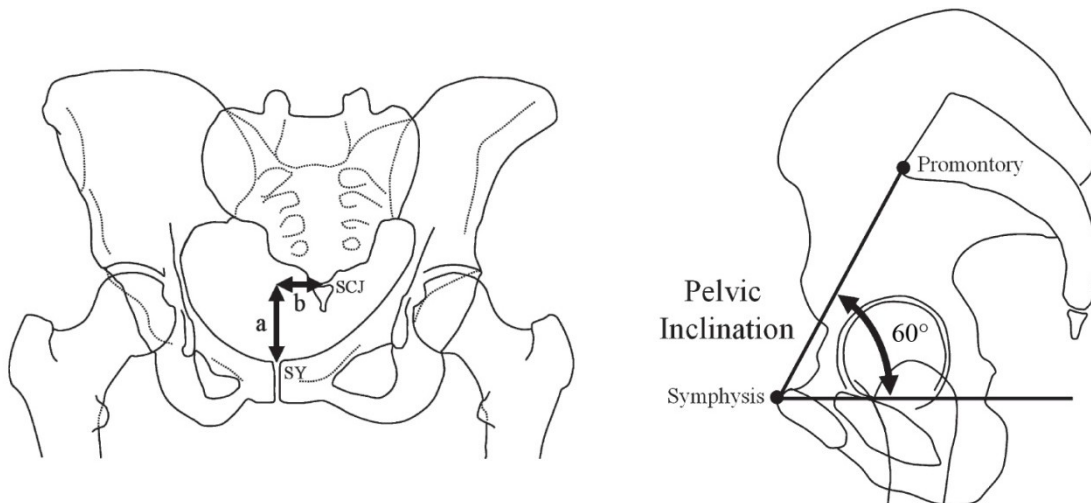


**Figure 1.27-** Pelvic rotation controlled by aligning the sacrococcygeal joint (SCJ) with the upper margin of the mid-symphysis pubis (SY) (*left*). Pelvic tilt controlled by setting a line from sacral promontory to the foremost point of the symphysis pubis at 60° relative to horizontal (*right*). Adapted from [85]

Nagao et al., also developed a method that utilized multiple radiographic projections to correct for pelvic malposition.[111] Using aligned landmarks on posteroanterior and lateral views, a complex geometric relationship was derived to orient the pelvis with a frontal plane defined by the anterior points of the bilateral anterior superior iliac spines (ASIS) and pubic tubercles (i.e.- the anterior pelvic plane). Their method utilized three points to directly define the plane of the acetabular rim so that angular measures could be used to describe its orientation (Figure 1.28). Radiolucent metallic markers were placed on the most anterior, posterior and superior points of the acetabular rim of 55 cadaveric specimens. X-rays were taken of the specimens and the geometrically derived calculations were then performed to determine the orientation of the acetabulum's opening plane. While the complex shape of the acetabular rim would have an impact on any method that directly defines a plane from three points, their method does not require the assumption of a perfectly hemispherical cup. Their geometric method was validated by showing that measurements of both the lateral and anterior “opening angles”, performed directly on the specimens, had respectively high correlations of 0.803 and 0.822 to the calculated measures attained from the radiographs.[111] In a follow-up study, they

also showed their radiographic method to have very good inter-and intraobserver agreement between two observers, with respective ICC values of 0.937 and 0.948.[57]

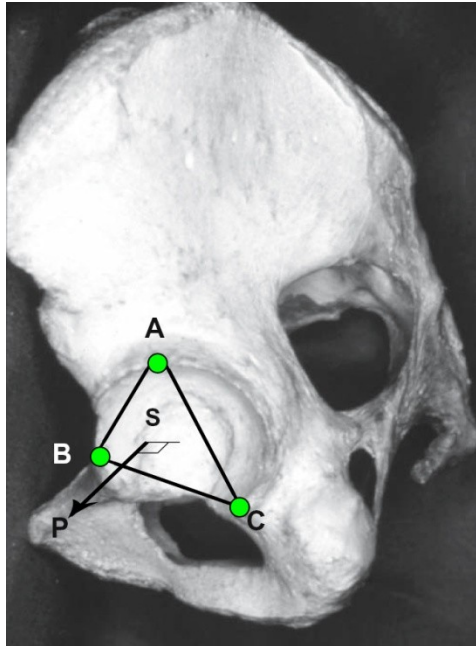


**Figure 1.28-** Nagao et al.'s method of attaining acetabular orientation used three points (A,B, & C- *green*) to form the opening plane of the acetabulum. *Adapted from [111]*

### 1.3.3 2-D Computed Tomography Sources of Error

Because measures of the hip made using axial imaging have only existed for a small fraction of the time compared to that of plain film, considerably less information is known pertaining to sources of error. As found with AP radiographs, CT measures are also subject to problems related to patient positioning.[78,126,143,148,151,170–172,192] The standard method for positioning the patient for CT imaging of the pelvis ideally locates the roofs of both acetabuli at the same level by horizontally aligning the bilateral ASIS. Additionally, the points of the ASIS should reside in the same plane as the ventral prominences of the pubic tubercles (PT) with the patient either in a supine or prone position.[7,8,45,67,78,92,143,148] Reikerås et al. measured acetabular anteversion with images taken in both the supine and prone positions and found no significant difference between the attained measures.[67]

Measures of the acetabulum made using 2-D tomograms are less susceptible to positional error compared to plain AP radiography, in that they are not sensitive to rotation about the longitudinal axis of the body.[126,143,170] Little information is available in regard to the proper slice thickness recommended for measuring angles of the acetabulum using CT. While slice thickness varies between studies, it has been shown that axial measures of the acetabulum vary somewhat around levels near the center ( $\pm 10\text{mm}$ ) of the femoral head (Figure 1.29).

[8,54,59,143] Because both AcAV and the sector angles are measured from the tomogram slice closest to the center of the femoral head, there is some measureable amount of error realized from utilizing a slice slightly more caudal or cranial than the actual center. Anda et al. estimated that if an improper slice was selected 5mm cranial or caudal to the center slice the error in measurement of the sector angles would be approximately  $5^\circ$ . [8]

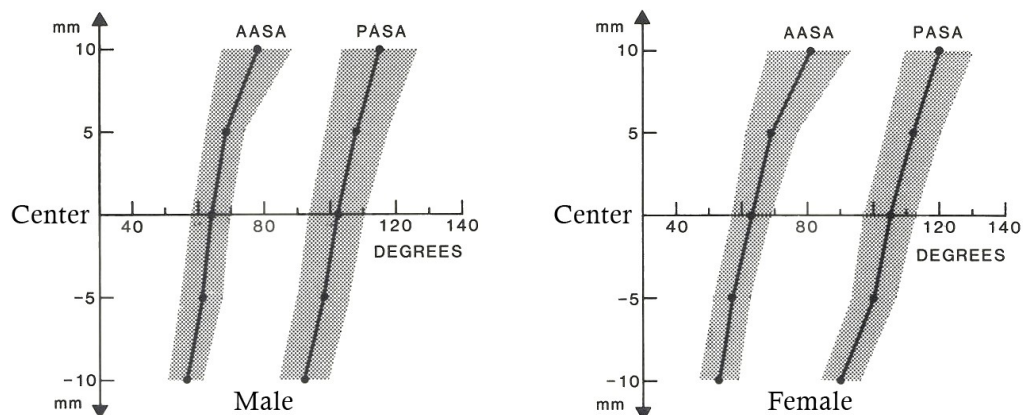


**Figure 1.29-** Variation in AASA and PASA at levels cranial and caudal to the center in both males (*left*) and females (*right*).  
Adapted from [8]

It is known that the perceived orientation of the acetabulum in the transverse plane is primarily dependant on the inclination of the pelvis at the time of imaging.

[8,67,78,126,143,148,170,192,193] As the pelvis becomes more inclined (tilts anteriorly), the acetabulum appears more retroverted, causing an angular decrease in AcAV.[143,192] Changes in pelvic inclination also affect the sector angles, with an increase in tilt resulting in a perceived

increase of AASA and a decrease of PASA (the opposite is true for decreased pelvic tilt). Anda et al. noted a mean inpatient difference of sector angles that varied between  $2.5^{\circ}$  and  $4.2^{\circ}$ , which they attributed to slight variations in pelvic tilt.[8] In a follow-up study, they quantified the effect of pelvic tilt on sector angles and AcAV by using a specially designed inclinometer that controlled the tilt of the frontal plane as defined by the bilateral points of the ASIS and PT. It was determined that within physiological ranges of pelvic tilt, for every  $1^{\circ}$  change in pelvic inclination there will be a commensurate change of  $0.5^{\circ}$  in measured AcAV, and a  $0.7^{\circ}$  change in sector angles. They also showed that there is negligible difference in the inclination of the pelvis in the standing or supine position.[126] Abel et al. measured acetabular anteversion through a range of controlled pelvic tilt of  $15^{\circ}$  of posterior (declined) to  $35^{\circ}$  anterior (inclined). For their single cadaveric specimen, they found that the right side AcAV decreased from  $41^{\circ}$  at the declined position to  $11^{\circ}$  at the inclined position and likewise the left side changed from  $38^{\circ}$  to  $10^{\circ}$ . [192] The average change of  $29^{\circ}$  observed by Abel et al. in AcAV through a corresponding range of  $50^{\circ}$  in pelvic tilt by is similar to the  $25^{\circ}$  change predicted by Anda et al. and others.[126,192–194]

A comprehensive study by van Bosse et al. recently investigated the compounding effects of both pelvic tilt and obliquity.[170] They discovered that pelvic obliquity had a notable contribution to measurement error in both AcAV and the sector angles. They rotated a pelvic model through a combined range of  $\pm 20^{\circ}$  in both tilt and obliquity. The result was an enormous range of observed measures in the same pelvis, with respective ranges of AcAV, AASA, PASA, and HASA at  $\sim 50^{\circ}$ ,  $95^{\circ}$ ,  $55^{\circ}$ , and  $132^{\circ}$ . This showed that even small changes in both pelvic obliquity and tilt can have large effects on axial measures. For instance, a combined  $10^{\circ}$  of tilt and  $5^{\circ}$  of obliquity was shown to cause a commensurate change of  $10^{\circ}$  in AASA, PASA and

AcAV. The effects of pelvic tilt, observer variability, and selection of axial tomogram level are additive, while not as severe as plain radiography, they also give rise to the possibility of large amounts of measurement error.

The natural curvature of the acetabulum's border is partially responsible for the underlying causes of axial misreadings taken at slightly different levels and/or rotational positions. [51,54,126,146,170,172,193] Recent studies of the acetabular rim (AR) have provided detailed insight into its complex shape, and discovered that it seems to have no apparent correlation with other factors in normal subjects.[48–51,195,196] The curvature of the normal psoas valley is approximately 5mm in depth and the posterior depression is 6mm, with respective upper ranges reported to be as large as 10 and 14mm.[49,50,196] This would obviously cause large variations in 2-D measures taken at a single level on acetabulums that may actually have the same overall 3-D orientation. By performing a simple trigonometric calculation on an acetabulum with a 50mm diameter, the average depths of the psoas valley and posterior depression result in separate respective changes of approximately 6 and 7 degrees in AcAV measurement. The validity of this assumed calculation is confirmed by Maruyama et al., by their direct measurement of anteversion on 100 of anatomic specimens ( $n=200$  hips).[48] They measured AcAV on the natural curved profile and then normalized it using a straight edge spanning the psoas valley. The average difference in anteversion was reported to be approximately  $6.2^\circ$ . Combining the  $\sim 6^\circ$  of error contributed by the curvature of the acetabulum with the variation of  $\sim 5^\circ$  resulting from observer error [192], it can be reasonably expected that any 2-D measurement scheme will be subject to about  $10^\circ$  of error even the position of the pelvis is perfectly controlled.



The review of the commonly utilized 2-D measures described in the previous sections provides a rather interesting insight into the general nature of quantitative hip joint analysis. A high level view of the normal values provided for all the angular measures reveals an undeniable trend. Analyses that couple the femoral head to the acetabulum have considerably more variability introduced into the measures. While this holds true using any of the measures, comparison of the more common classical measures can be made between the CE angle and Sharp's acetabular angle (Table 1.2 & Table 1.3), and in axial measures between the sector angles and AcAV (Table 1.4, Table 1.5, and Table 1.6). This trend emerges when observing the SD reported for each of the measures. Standard deviation values for angles with the femoral head integrated into their scheme are approximately double those that evaluated the acetabulum in isolation. In some cases the differences are more than double where the same subjects were used to perform both measures. It is somewhat intuitive that linking two variable anatomic structures together would increase the variability of any compound measurement. Much of this variability could be attributed to the geometry of the acetabulum, being that it is considerably more complex and difficult to measure than the proximal femoral component. In accord with the thoughts of Sharp [132]; while it is strictly correct to evaluate the entire hip joint as an interconnected system, the acetabulum needs to be studied discretely to gain an accurate understanding of its true nature.

#### **1.4 MODERN THREE-DIMENSIONAL STUDIES OF THE ACETABULUM**

Recent advances in software have enabled digital reconstruction of osseous structures, which allows for spatial manipulations to be made post-imaging. The ability to control the position of these structures allows for their alignment to identifiable bony landmarks. Modern studies of the hip joint have utilized this new rendering capability to control, or otherwise manipulate, patient positioning. [49,50,54,56,90,125,140,155,169,172,192,193,197,198] First utilized by McKibbin in his study of anatomic specimens, a frontal plane known as the anterior pelvic plane (APP) has become the accepted gold standard for aligning pelvis in a wide range of studies and surgical procedures.[45,77,126,170,175,199] Only a few studies have ascertained 2-D measurements using CT data after aligning the pelvis to the APP.[51,54,56,125,126,172,192] Drastic improvements in measurement reliability have been observed when using software to correct for patient positioning.[192] These improvements have pushed the interpretation of the ICC for inter-and intraobserver scores into a new realm, with a few recent reports of scores exceeding 0.9.[56,57,60,125,129,170,172] By eliminating the variability introduced by patient malpositioning, these techniques show a significant advancement from their earlier predecessors.

Obviously, measurement techniques using anatomic specimens are not applicable for clinical use on living patients. However, their results are comparable and useful in building a better understanding of natural acetabular orientation. The previously mentioned radiographic techniques of Nagao et al. [111] and Tannast et al. [85] were not a direct 3-D measure of acetabular orientation, but rather an interpolation of its estimated orientation from multiple 2-D projections. However, the validation study performed by Nagao et al. directly measured the opening plane of the acetabulum using a fixture and specially designed goniometer that contacted three points on the acetabulum. The authors made a valid and important critique of

traditional measures, noting that angles used to describe the "opening" of the acetabulum using points projected onto a 2-D film do not truly represent the *actual* 3-D morphology of the structure.[111] While it is not specifically stated or depicted, it is assumed that a separate study by Köhnlein et al. used a similar method to measure the acetabular orientation of 33 pelvises.[51] According to their methods, a "goniometer" was used to measure the orientation of the acetabulum's opening plane by contacting the "tripod of the anterosuperior, anteroinferior, and the posteroinferior rim prominences". The concept of acetabular orientation being described using an opening plane, within a 3-D realm, is critical to understanding the hip joint and pertinent to the research presented herein. Therefore, it is important to clarify the difference between an anatomic study that performs 2-D measures from one that attains 3-D measures. The studies from McKibbin [45], Maryuama et al. [48], Köhnlein et al. [51], and Nagao et al. [111] all use an osteometric board to align the pelvis to the APP. However, McKibbin and Maryuama et al. use a measurement technique that only contacts two points spanning the acetabulum to form a single angular measure in a 2-D plane. The latter two studies form a plane of the acetabulum by contacting three points where two angular measures are needed to fully describe its orientation in 3-D space (Figure 1.30). This same concept can be used to delineate between studies that may render a 3-D representation of the pelvis, but perform a measurement that is essentially only in 2-D.[5,60,160,172,191,192]

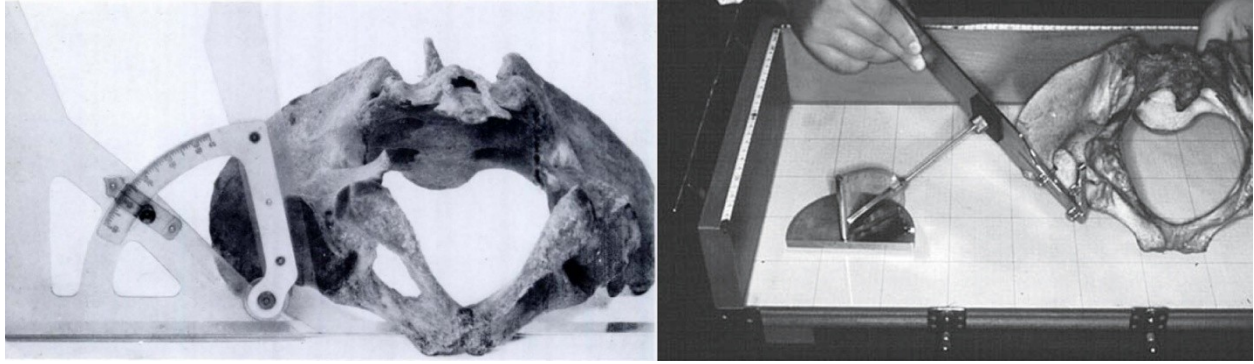


**Figure 1.30-** Study from McKibbin performing a 2-D measure of anteversion (*left*). Study from Nagao et al. performing a 3-D measure using a special goniometer (*right*). Adapted from [45,111]

Although using the APP to consistently align the pelvis alleviates a considerable amount of measurement error, 2-D measures of the acetabulum taken at a single axial level or frontal projection only account for a fraction of the complete morphology involved. As previously explained, these 2-D snapshots are only indicative of the hip's anatomy at the level of the equatorial plane (or other level of interest), or from a frontal projection. The inconsistent configuration of the acetabulum's highly irregular border prevents accurate determination of its comprehensive 3-D orientation using plain radiography and axial tomography. Furthermore, planes directly defined using exactly three points will also be subject to some amount of error arising from the curvature of the acetabulum. Only a few studies have attempted to construct a plane representing the 3-D opening of the acetabulum to measure its orientation.[49–51,77,90,111,125,198,200] An even fewer number have done this using enough points selected on the AR to create a best-fit plane using 3-D reconstructions of CT data.[50,77,90,125,198,200] The complex acetabular ridge has proved to be difficult to locate, making accurate detection of its complete profile challenging.[10,48–50,111,146,161,175] To-date, all studies performing 3-D measures on renderings of actual patient data have had to manually select points on the acetabular rim. Two studies have selected points on partial sections of the AR to form an opening plane.[125,200] One of which reported significant changes in orientation when

accounting for the entire AR using the same subjects; with anteversion almost tripling that of the measures using only the posterior and superior portions of the acetabulum.[200] Therefore, if the *true* 3-D orientation of the acetabulum is to be described with a high level of reliability, it is critical to incorporate the entire AR.

The first *true* 3-D analyses of the hip joint investigated the congruency and coverage of both normal and dysplastic acetabulums.[77,130,201] These early works pioneered the concept of using 3-D models to visually optimize acetabular coverage in preoperative planning for joint-preserving osteotomies. Studies performed by SB Murphy and MB Millis et al. were one of the first to report the functional 3-D orientation of the acetabulum, utilizing rendered 3-D models and the APP to correct for patient positioning. Little is known about how many points or what methods were used to fit planes to the acetabuli. The authors loosely describe the creation of the plane used to define the orientation of the acetabulum, "...by calculating a plane that best described all the points on the acetabular rim using a computer optimization algorithm".[77] Interestingly, Murphy et al. found that dysplastic acetabuli were globally deficient, forming approximately one-third of a sphere as compared with the almost perfectly hemispherical normal acetabulum. Along with the absence of qualifying methods with statistical based reliability studies, the few early 3-D based studies had limited sample sizes. This was most likely due to the cost of the imaging, required hardware, software and skilled operators, all of which have since been exponentially reduced making such studies more feasible.[77,130,175,201,202]

Since the early efforts described above, a surprisingly small number of studies have fit a plane to the acetabulum and resolved it into *true* 3-D measures while controlling for pelvic positioning. Several of these studies have performed direct measurements on anatomic or cadaveric specimens [49,51,111], and others have leveraged the benefits of computer generated

renderings.[50,77,90,198,200] The results for the 3-D inclination of the acetabulum between genders have been mixed, showing no definitive or significant differences. Conversely, all of the 3-D studies have suggested a trend of females having acetabuli that are more anteverted than males. A few have showed this difference to be statistically significant [50,90,200], one of which noted the need for more subjects/statistical power to be confident in the difference.[200] Most interestingly, a separate anatomic study from Köhnlein et al. showed the difference between male and female acetabular version as significant when using a 2-D measure, but not different when using a 3-D opening plane in the same population.[51] Thus, the understanding of differences between genders in normal 3-D acetabular orientation is still very much in question.

As mentioned previously, all current 3-D studies of the acetabulum have used manually selected points located on computer based renderings or directly probed on a physical specimen. There have been two programmatic methods recently proposed for automatically detecting the profile of the acetabular rim.[203,204] While these methods could potentially be applied to make relevant measures of the acetabulum, they are yet to report values from any patient populations. A curvature based method using geodesic active contours with evolving level sets, originally developed to find edges on 3-D surfaces of vertebral bodies, was adapted by Tan et al. to detect the AR.[203,205] Their method was applied to simplified cup shapes that were representative of shallow acetabuli. No estimates of accuracy or reliability were reported, and they noted the need for manual adjustments of various parameters to detect the edges of cups with differing curvatures. Thus, the current status of their method remains as only a programmatic concept for detecting edges on rendered 3-D surfaces.

Most recently, Puls et al. presented a computational method for detecting the AR of modified artificial anatomical models using 3-D surfaces attained directly from a hand-held laser

scanner.[204] This experimental method is also yet to be applied on surfaces rendered from 3-D medical imaging data. They tested their method's accuracy by physically probing points on the same AR detected using their algorithm and comparing the orientation of their respective opening planes. It was reported that they were 95% confident that the inclination of the physically probed plane was within  $-2.99^{\circ}$  to  $2.67^{\circ}$  to the automatically determined plane. Similarly, the reported accuracy of anteversion was within a 95% confidence interval of  $-2.02^{\circ}$  to  $1.99^{\circ}$ . The ICC of the manually probed plane was determined, but the reliability and possible sources of error of the automatically detected plane was not reported. While it is not directly comparable to the programmatically determined orientation of the acetabulum, the manually established plane had reported 95% confidence intervals for intraobserver ICCs ranging from 0.82 to 0.99 and interobserver ICCs from 0.79 to 0.99. Other than the methods presented from Tan et al. and Puls et al., no methods for automatically detecting the acetabulum have been seen in the literature.[203,204] Furthermore, there is yet to be a method purposed for locating the APP in 3-D renderings of pelvis.

### **1.5 PELVIC ASSYMETRY RELATED TO THE INNOMINATE BONE**

Knowledge of overall pelvic morphology and gender specific differences has existed for many years.[47,52] As briefly mentioned, there is no knowledge pertaining to the relationship between the true and false pelvic regions of the innominate bone once the triradiate cartilage has fused. Studies of adult pelvic bones are typically limited to simple coxometric measures of linear distances, spans, and projected 2-D angles.[55,206–208] Most measures describing the anatomic characteristics exclusive to the innominate structure are performed in a undefined lateral view that is more-or-less parallel to the inlet of the acetabulum.[206,209] The remaining studies that compare bilateral differences between coxal bones are dependent upon standard 2-D AP views

(Figure 1.31).[55,207] The scarce number of studies performing measures intrinsic to the innominate bone rarely provide quantitative information that relates to acetabular orientation.[209]

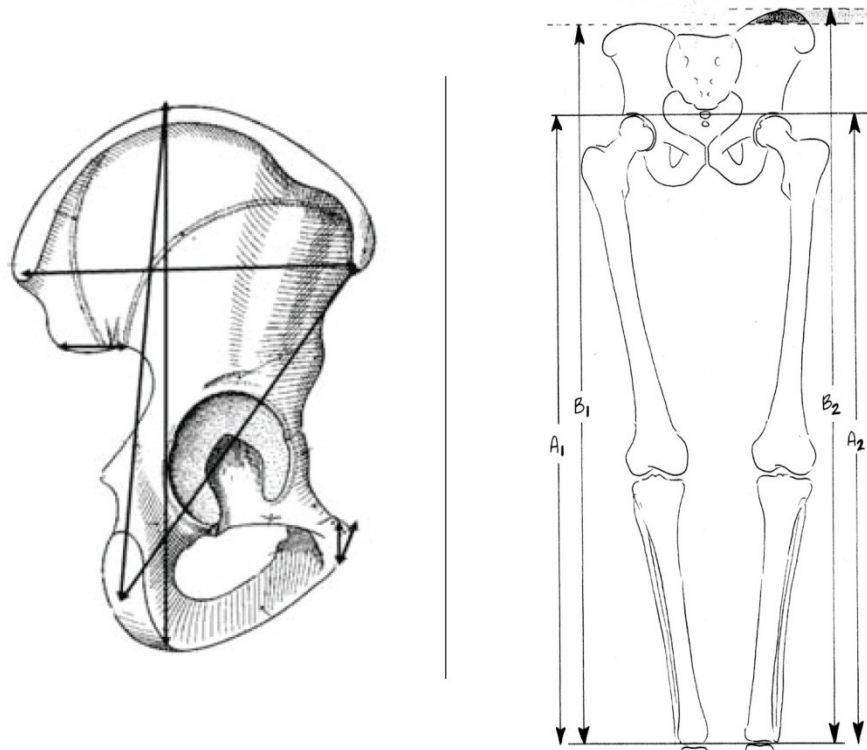


**Figure 1.31-** Typical views for performing measures that compare bilateral differences of the pelvis. Example lateral view of the innominate bone used for basic anthropometric measures (*left*). AP view of the pelvis and legs used by Badii et al. to measure the heights of the ilia relative to the acetabulums. *Adapted from [206,207]*

Albiñana et al. performed a detailed study relating the arrangements of the ilium, ischium and pubis on AP radiographs of *babies* with unilateral DDH showed significant bilateral differences between the structures of the innominate bones.[55] This study's findings suggested that growth disturbances not only effect the acetabulum, but the entire pelvis. A comparable study was performed by Boulay et al. using *adult* anatomic specimens with no pathological history that displayed massive bilateral differences in superolateral coverage within the same specimens indicating that unilateral DDH was almost certainly present.[206] This study also showed bilateral differences between innominate bones as significant. Interestingly, both studies



showed significant bilateral differences in the size of the obturator foramen (larger in DDH) which would directly affect the structure of the true pelvis, and thus the location of the pubic tubercle.[55,206] A study performed by Badii et al. measured the height of the ilium in a large population of normal adults ( $n=323$ ).[207] They found that a significant portion of the subjects had a measurable difference in ilium height, and that the left ilium that was significantly shorter than the right (Figure 1.31). Thus, it is suspected that both normal and abnormal populations of adults will have some amount of measurable bilateral discrepancy in height of the false pelvis related to the acetabulum. Although this value is relatively small ( $\sim 1-2\text{mm}$ ), any bilateral discrepancy in the height or position of the ilia could affect the foremost location the ASIS.[206,207] Some of the observed bilateral differences persisting in normal populations may be explained by the higher prevalence of right-handed dominance.[206,207] Regardless of the reason, the significant bilateral differences observed in the innominate bone could affect the locations of both the ASIS and PT. Changes in the locations of these bony landmarks would in turn have a direct impact on the orientation of the any reference geometry using them to evaluate the orientation of the pelvis (e.g.- the APP).

Both studies highlighted from Boulay et al. and Badii et al. used bilateral features to align the pelvis and establish a reference for performing measures.[206,207] Albiñana et al. utilized a vertical line of symmetry on the sacrum for alignment and measurements, which is still not intrinsic to only the innominate bone.[55] One study performed by Fujii et al. used CT imaging to measure axial torsion of the innominate bone in normal females and those with DDH at levels of the ASIS, anterior inferior iliac spine (AIIS), and PT.[56] While this study is subject to all of the shortcomings of performing manual measurements on axial images, it did correct for patient positioning using bilateral features of the ASIS and PT. However, as a result of correcting for

positioning, it too was dependent on bilateral features which were also used to establish references for performing measures. Regardless of these issues, they found a highly significant and interrelated torsional relationship about the long axis of the body between the acetabulum and both true and false pelvic regions. This relationship was previously unknown and undetectable using measures on lateral and/or AP views. These findings provide valuable insight into the complex relationship between the acetabulum and coxal bone. Currently, there is no way to intrinsically assess the inherently 3-D relationship between the acetabulum and innominate bone in which it resides.

The significant levels of asymmetry observed in both normal and abnormal pelvises may affect measurements that utilize a reference frame based on the bilateral features.[55,206,207] From the previous discussion, it should be easily understood that when using a reference datum established from the femoral heads to perform measures of the acetabulum, the individual anatomic variation in both the acetabulum and femur are additive; thus increasing the variability of resulting measures. This added measurement variability makes it difficult to interpret how the resulting readings are affected by the contributions of the individual structures. This same logical argument can be made for using the bilateral halves of the pelvis. As shown, each halve (hemipelvis) has its own structural variability which will affect any bilaterally based reference used for subsequent measurements. The innominate bones are separated anteriorly at the pubic symphysis by the fibrocartilaginous interpubic disk which is static, and posteriorly by the sacrum which forms the dynamic sacroiliac joints.[18,47,52] Therefore, not only do the individual innominate bones contribute to the additive variability of any bilateral reference, but also the structure of the sacrum which links them together.

## 1.6 PREMISE FOR ADVANCED RESEARCH

As stressed in the latter parts of this chapter, the errors realized from patient malpositioning, inter-and intraobserver variations, the normal curvature of the acetabulum, as well as the asymmetry of the pelvis, are unavoidable in *all* 2-D imaging modalities. Because there is a significant amount of variability inherent to all 2-D measurements, there is no firm consensus for accepted values delineating between normal and dysplastic hips. The error that inevitably persists in the measures, broadens the range of what Wiberg called “borderline values” that can be considered “no man’s land,” making it difficult to discriminate between normal and pathologic hip joints.[4,45] Despite these persisting issues, commonly ascertained 2-D measures and qualitative signs have provided insight into the etiology of secondary OA due to grossly unbalanced arrangements of the femoroacetabular components.

[4,28,35,43,57,61,74,76,79,91,96,128,131,132,159]. One of today’s challenges is found in the many cases of primary OA that are still considered “idiopathic”, which have been recently suspected to be secondary to more subtle underlying deformities.

[33,34,61,74,79,98,131,158,159] To prove if such subtle anatomic deformities have a significant impact on the hip joint, a method performing measurements would have to be accurate enough to detect them. These enigmatic deformities have, for the most part, gone unnoticed using any of the commonly employed 2-D measures.[5]

Detailed knowledge of the subtleties associated with complex 3-D maladies of the hip joint is critical to understanding their pathology and improving treatments. The value of this enhanced understanding would extend to many areas such as total hip arthroplasties (THA), FAI, and acetabular reorientation osteotomies. [51,56,61,77,130,159,160,170,175,201,209] Current knowledge and comprehension of the hip joint is limited by the methods used to evaluate it. The

use of CT imaging, and the even more recent ability to generate 3-D reconstructions from CT data, has already been widely acknowledged as a far better way to evaluate the hip joint. [10,29,56,58,59,61,74,81,82,130,143,160,161,171,175,197,201,210] Even though the use of computers and modern imaging have become more commonplace in orthopaedics, it has been noted that the development of software needed for performing useful diagnostic measures is still lagging behind.[165,175,202] To the point, the research presented herein was focused on addressing many of the issues previously outlined, for evaluating the more challenging geometry of the acetabulum.

The primary focus of this research was to develop a method for performing measures of the acetabulum that leveraged the benefits of 3-D rendering to both correct for patient positioning and remove sources of human error. To do this, a unique and purpose specific software program was developed called the "Acetabulator™". This programmatic tool calculated commonly used measures of acetabular orientation within a reference frame based on the APP. In addition, a new coordinate system (C.S.) was devised to calculate unique measures relating acetabular orientation exclusively to the innominate bone in which it is embedded. It was also important to statistically qualify these new methods as a reliable and accurate tool used for making such measurements. Normal morphology must be understood before suspected pathological deviations can be evaluated.[51] Therefore, the Acetabulator was used to establish baseline measurements, explore gender specific differences, and prevalence of bilateral asymmetry using a large population of normal subjects.

## **2 MATERIALS AND METHODS**

### **2.1 MATERIALS**

After receiving Institutional Review Board approval, 200 pelvic CT studies were obtained from our institution's extensive database of individuals undergoing abdominal imaging for suspected renal colic or other non-musculoskeletal conditions. The high resolution scans required to locate small objects (i.e.- kidney stones), provided excellent detail of the surrounding bony structures. CT images were acquired using Siemens SOMATOM Sensation<sup>®</sup> 16 or 64 scanners (Siemens Medical Solutions USA, Inc. Malvern, PA) at a slice thickness of 1mm, average x-y resolution of 0.72 pixels, and a high spatial resolution pixel matrix of 512x512. The population consisted of 88 males with a mean age of 39 years (*range- 19 to 88 years*) and 112 females with a mean age of 43 years (*range- 20 to 83 years*). All hip joints were absent of any visible abnormalities, previous corrective surgeries, or injury related procedures. Digital Imaging and Communications in Medicine format (DICOM<sup>®</sup>; NEMA<sup>®</sup> [National Electrical Manufacturers Association], Rosslyn, VA) standardized images for each study were exported for further analysis.

### **2.2 METHODS**

The Acetabulator was developed to provide a programmatic "tool" for calculating 3-D measures of the acetabulum. The primary intent was to improve reliability and save time by removing the need to manually select the numerous points required to perform such measures. It was also intended that anyone with moderate training and instruction could perform an analysis. In general, the Acetabulator refines manually selected estimate data into accurate calculated measures. The exact locations of bony landmarks were automatically detected to establish the

reference frames for performing measures. These landmarks were programmatically identified from manually selected surfaces covering the general regions where points of interest reside. The orientation of the acetabulum was calculated using an initial estimate formed by three manually selected points on its periphery. This estimate was improved using the data describing the entire surface of the acetabulum. The estimate based approach used by the Acetabulator generates 3-D datums needed to perform subsequent calculations that describe the orientation of the acetabulum relative to various anatomical planes.

Three individuals carried out the surface generation and data collection from the 200 CT studies. The majority of subjects were processed by myself (SH), an experienced 3-D CAD user. The remainder was carried out by a doctoral student (ES) well versed in human anatomy, and a second year medical student (RB). All data for the general population was reviewed and processed using the Acetabulator exclusively by myself. The same three individuals participated in a thorough reliability study for the purposes of assessing inter-and intraobserver variability.

### **2.2.1 Three-Dimensional Surface Generation & Data Extraction**

The Acetabulator required a few specific data sets for performing an analysis that needed to be manually extracted for each subject. The data was extracted from 3-D models of the pelvises rendered from the DICOM scan data using a commercially available software package called Mimics<sup>®</sup> with version 14 or higher (Materialise NV, Leuven, Belgium). The first step in generating the 3-D models was importing the DICOM images into a Mimics project file where a lossless compression was applied to assure no data was lost in the conversion process. To reduce file size, the range of axial images was cropped just cranial to the iliac crests and caudal to the inferior ramus of ischium to capture the entire pelvis. Next, the pelvis needed to be isolated from the surrounding soft tissues by specifying a brightness level (threshold) that corresponded to the

bony tissue. The voxel intensity or brightness was expressed in Hounsfield units, which describes the radiodensity relative to water (zero value) that would appear as completely black. While there are predefined radiodensities pertaining to bone available, bone density varies between each person which required slightly different threshold values. To ascertain subject specific values, a profile line was drawn at the level of the acetabulum from trabecular bone, crossing the cortical wall, and out into soft tissue. The profile line displayed the grey values along its length in a set of interactive plots which were used to set the threshold level. The proper level was set so that trabecular bone was selected and the less radiodense tissues were excluded (Figure 2.1).

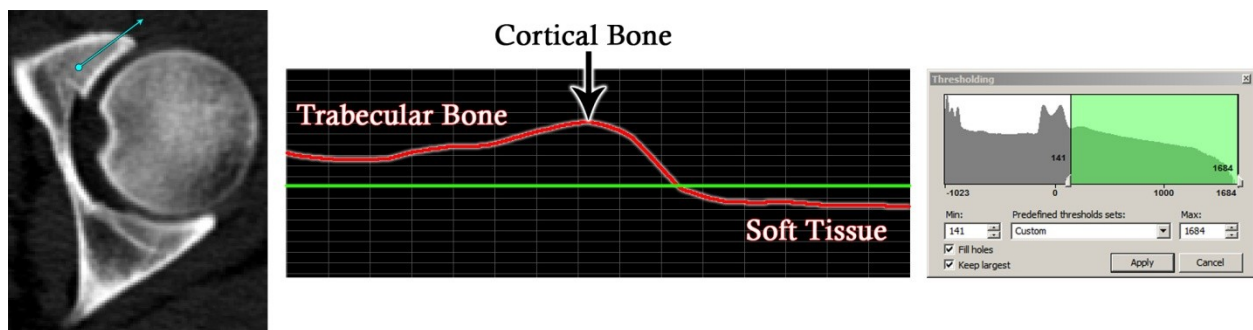


**Figure 2.1-** Procedure for setting patient specific threshold levels. Profile line is drawn (*cyan*) spanning the cortical wall (*left*). Grey values along the profile line are displayed (*red*) which shows trabecular bone as slightly more intense than soft tissue (*center*). The threshold value is set at a level so that only bony tissue is selected (*green line-center/ green area-right*).

An editable mask was created which filled the voxels with Hounsfield values above the threshold level. Mimics provides the settings "fill holes" and "keep largest" which were respectively used to fill voids isolated in the mask, and retain the single largest contiguous volume. Because the articulating surfaces of the acetabulum and femur are in contact (or very close), the femoral components were included in the initial mask. To isolate the pelvis, spheres covering the femoral heads were approximated using the MedCAD<sup>®</sup> module (Figure 2.2). A separate mask was created from the spheres which was used in a Boolean operation to create a new mask that excluded the femoral heads (Figure 2.3). The Boolean subtraction deselected the

majority of voxels filling the proximal femur, however some remained around the periphery which needed to be manually removed. Once the proximal femurs were fully segmented from the pelvis, a 3-D body was rendered from the selected voxels for inspection. Mimics volumetrically renders 3-D bodies (as opposed to surface rendering) [210], however only surface data was required for this analysis. Therefore, the 3-D bodies were inspected for discontinuous surfaces (holes) around the areas of interest (e.g.- the acetabulum) which were manually closed if necessary. Any obvious osteophytes or ossified portions of labrum were removed to exclude them from the ARs (Figure 2.4).

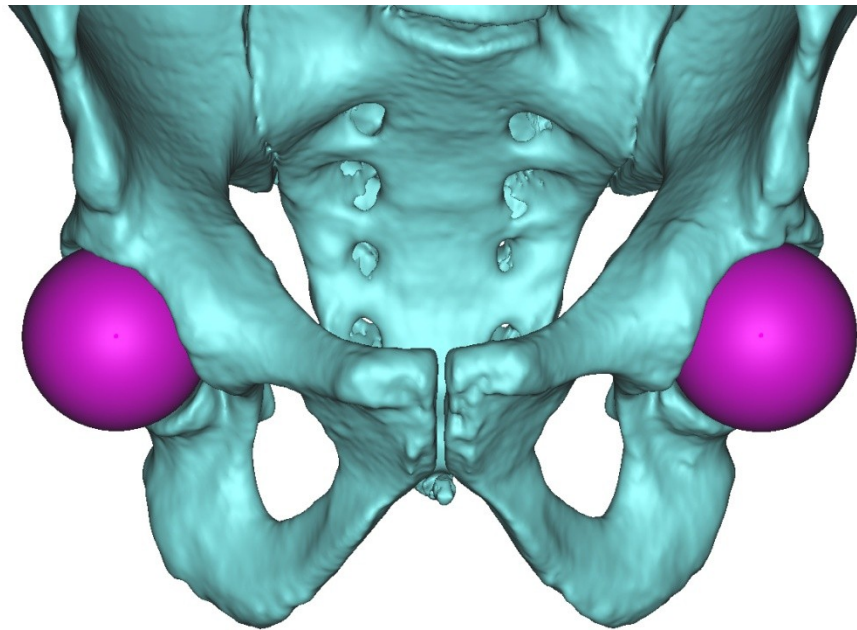


**Figure 2.2-** 3-D representation of spheres fit around the femoral heads used to segment them from the pelvis.



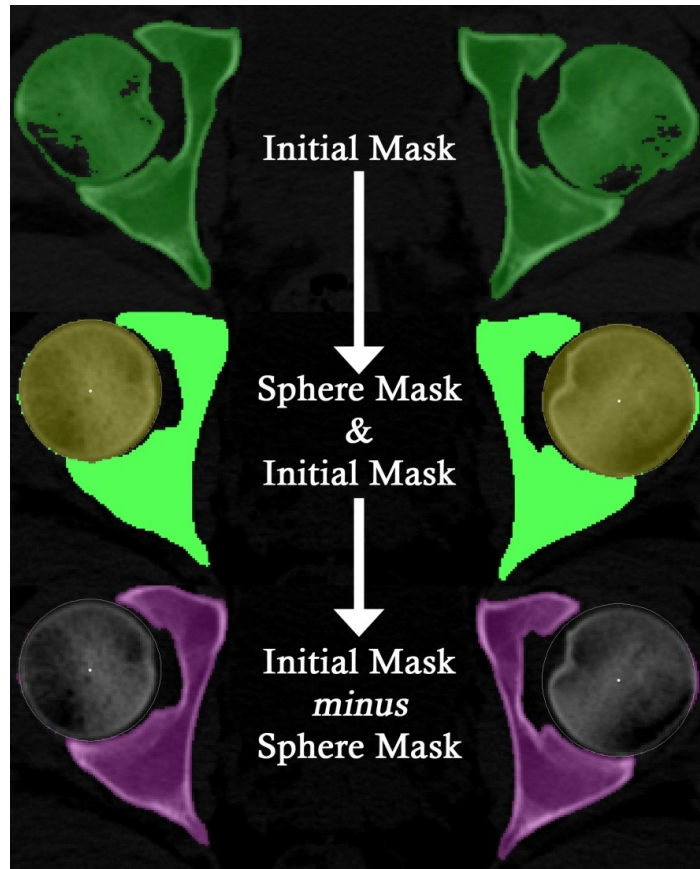


**Figure 2.3-** Axial view at the equatorial plane of proximal femur. Primary segmentation performed using multiple masks and Boolean operations to remove femoral head.

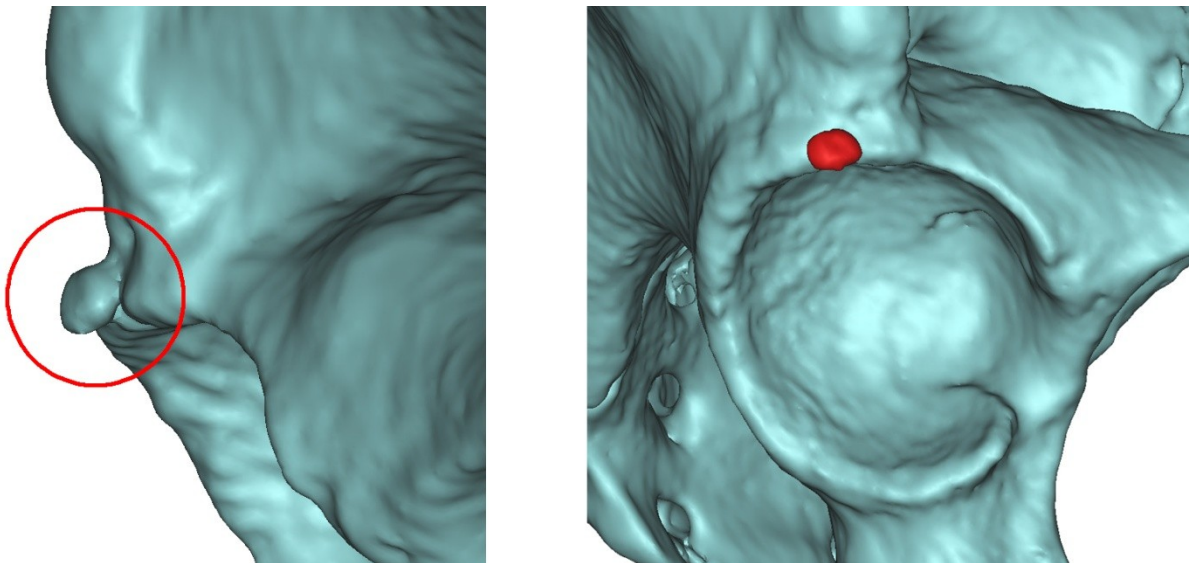


**Figure 2.4-** Obvious ossification that was not considered part of the AR. Frontal view showing fragment separation from the continuous AR (*left*). Lateral view highlighting the excluded fragment body in red (*right*).

Once a satisfactory mask was created with no surface holes or osteophytes, a final 3-D body was generated. Consistent settings were used to assure the rendered models best represented the actual bony structures. Accuracy driven algorithms (as opposed to continuity), with no reduction of triangles, were used in creating the surface mesh. In Mimics dialog, this corresponded to "grey value" interpolation with a preference for "accuracy" and matrix reduction in all directions set to 1, with triangle reduction turned off. Using accuracy based algorithms accounted for all of the selected voxels which resulted in small artifacts on the surface of the model (usually appearing as small spikes). To remove these artifacts, a conservative amount of Laplacian smoothing was applied using algorithms that compensate for the effects of shrinkage. Mimics was used to perform volumetric analyses on a subset of six pelvises (3 male & 3 female), observing the effects of smoothing on the models. Settings were empirically determined by comparing models before and after smoothing until no visibly detectable change in volume was observed. It was determined that performing 4 iterations using a smoothing factor of 1 assured the volume of the final model closely matched that of the unsmoothed model.

The surfaces of the models were represented using a tessellated triangular mesh in a file format known as stereolithography (\*.stl), commonly referred to as simply an "STL file". The final models were imported into 3-matic<sup>®</sup> (an extension of Mimics) to the extract surface data needed for the Acetabulator. Specific regions of interest on the faceted surface of the pelvis were manually selected for export (Figure 2.5). With the exception of the acetabulum, the amount of surface selected on any structure was not critical as long as the selection sufficiently covered the region. If an insufficient amount of surface was selected, it typically resulted in an error cancelling the subsequent analysis. If not, a series of output plots were generated to visually assure the proper amount of surface was selected. In the case of the acetabulum, only one caveat

applied for a small portion of the AR. In some individuals the acetabulum does not form a prominent ridge where it passes the anterior column at the margin between the AR and AIIS (Figure 2.6). For these subjects, care was taken so that selection did not stray up the anterior column away from the AR. As an added precaution, an error checking algorithm was created in the Acetabulator to check for such a scenario which is described in section 2.3.3.

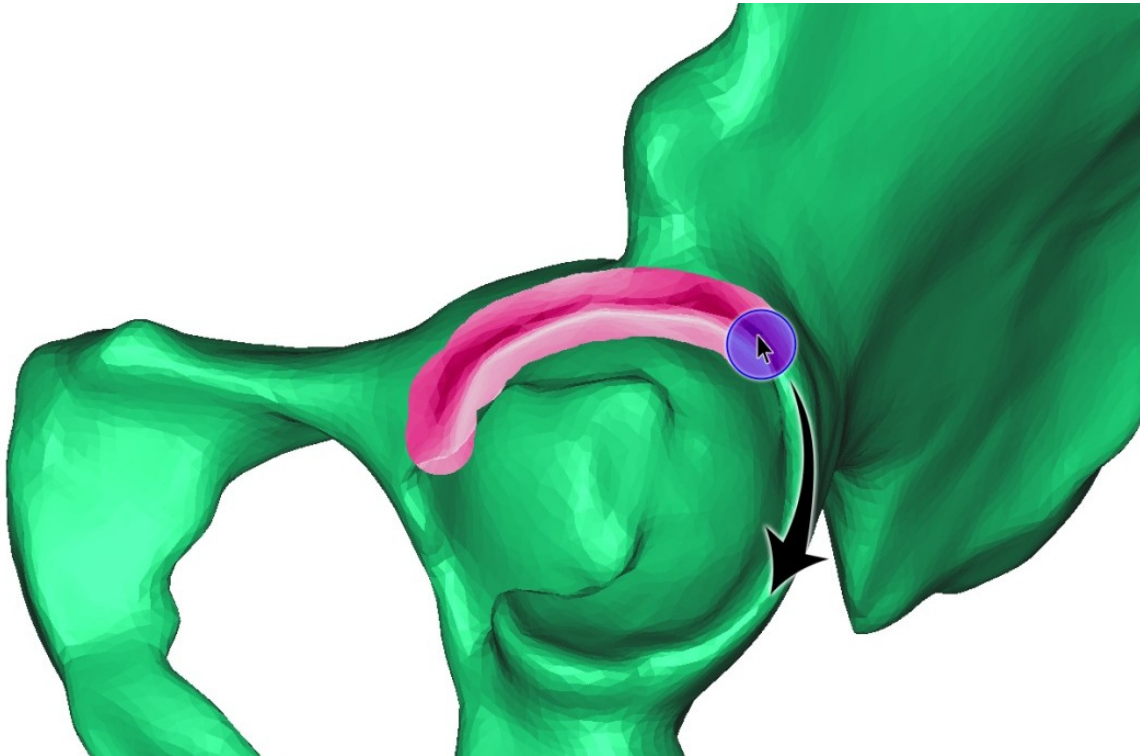


**Figure 2.5-** Depiction of the manual selection of the AR surface (*pink*) performed in 3-matic.

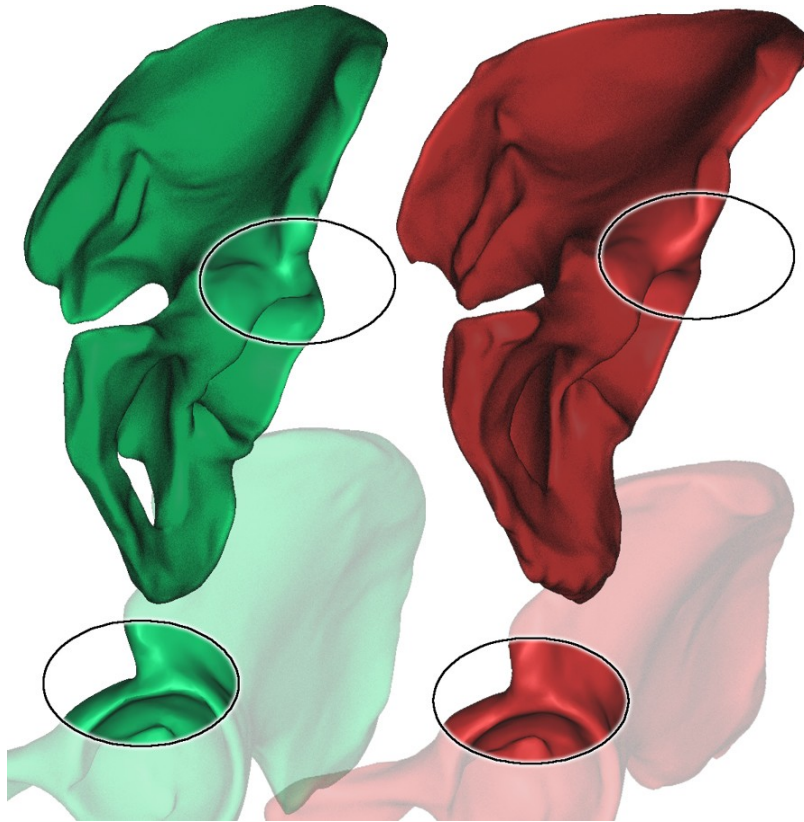


**Figure 2.6-** Left male innominate bones of comparable size showing both prominent (*left-green*) and absent (*right-red*) AR ridges at the anterior column.

Point clouds were exported in text files (\*.txt) containing the 3-D Cartesian coordinates of the nodes (vertices of the triangular facets) on each discrete STL surface. A macro was created to expedite the process of extracting the surface sets by performing some of the repetitive operations. This macro automatically separated the surfaces of interest and exported them as discrete point clouds. For the full pelvis analysis (based on the APP), the surfaces covering the general regions of the bilateral AR, ASIS, and PT were selected (Figure 2.7). Additional selections were needed for the hemi-pelvis analysis, including the posterior superior iliac spine (PSIS), anterior inferior iliac spine (AIIS), ischial spine, and interior perimeter of the obturator foramen (Figure 2.8).

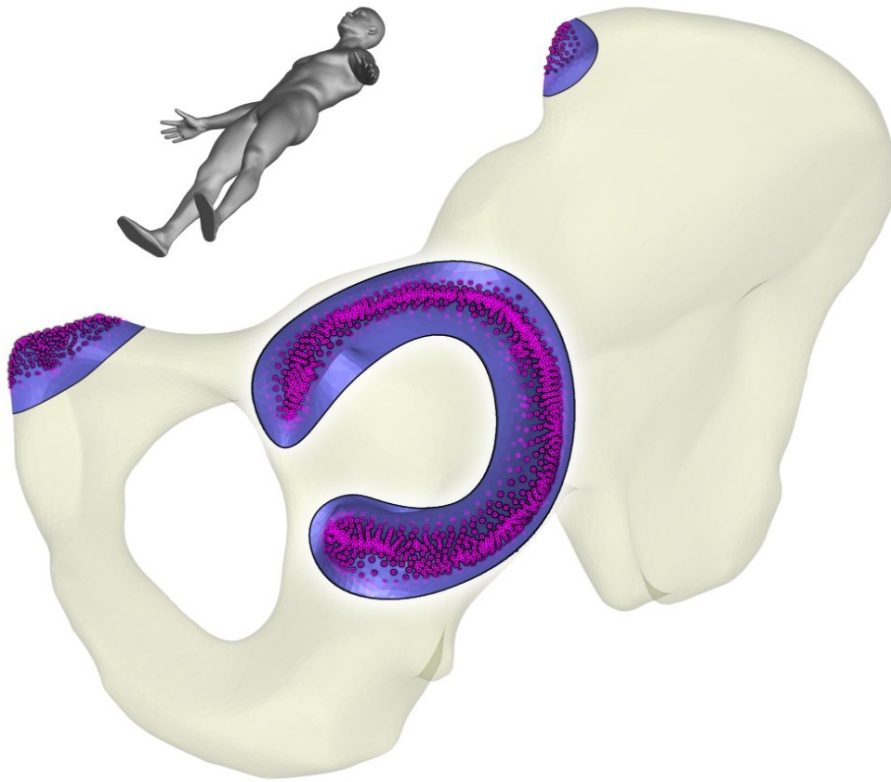


**Figure 2.7-** Left innominate bone showing features used for the full pelvis analysis. Nodes (*pink*) covering the surfaces (*blue*) of the ASIS, PT, and AR are exported as point clouds.

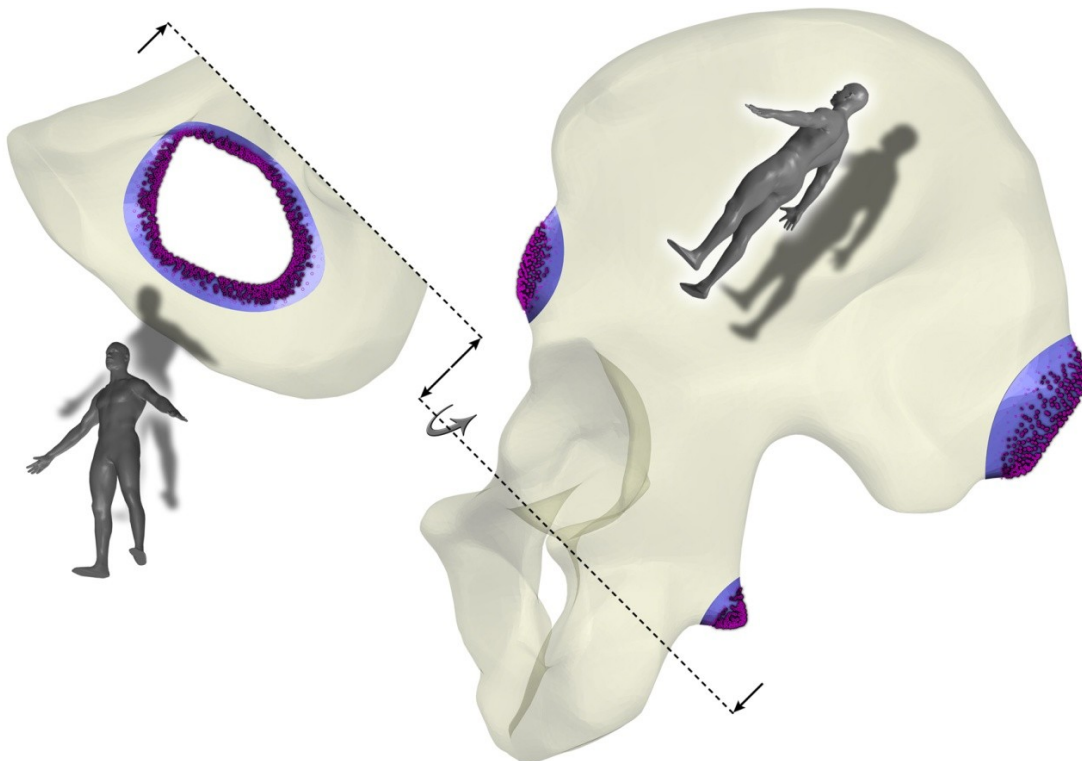


**Figure 2.8-** Left innominate bone showing features needed for the hemi-pelvis analysis. Nodes (*pink*) covering the surfaces (*blue*) of the PSIS, AIIS, ischial spine, and interior frame of the obturator foramen are exported as point clouds.

### 2.2.2 Acetabular Rim Point Selection

Three points needed to be manually selected on each AR to provide initial estimates of various acetabular features. Using the MedCAD<sup>®</sup> module, points on each side of the acetabular notch, and one point on the superior margin of the acetabular rim were located (Figure 2.9). The space between the points flanking the acetabular notch specified the region occupied by its cleft. This region was *excluded* from the Acetabulator's automatic point selection routine. Or conversely, these points specified the range of AR that was *included* as part of the selection routine. Therefore, relatively more importance was placed on selecting the location of these points than the one on the superior margin. If selection these points was achieved within ~1cm (about the width of a fingerprint), the same region on the AR would be utilized, yielding similar results from the programmatic analysis. Similar to Nagao et al. [111], the three points were used together to form a plane that served as an initial estimate of the acetabulum's orientation (Figure 1.28). Conveniently, the points excluding the notch formed a close approximation of the aperture's opening plane with the loosely selected point on the superior aspect of the rim. Thus, any point along the superior margin of the AR that formed a "best guess" estimate of orientation sufficed for the third point. This estimate plane consistently formed a reasonable approximation, regardless of varying or even irregular acetabular morphology.

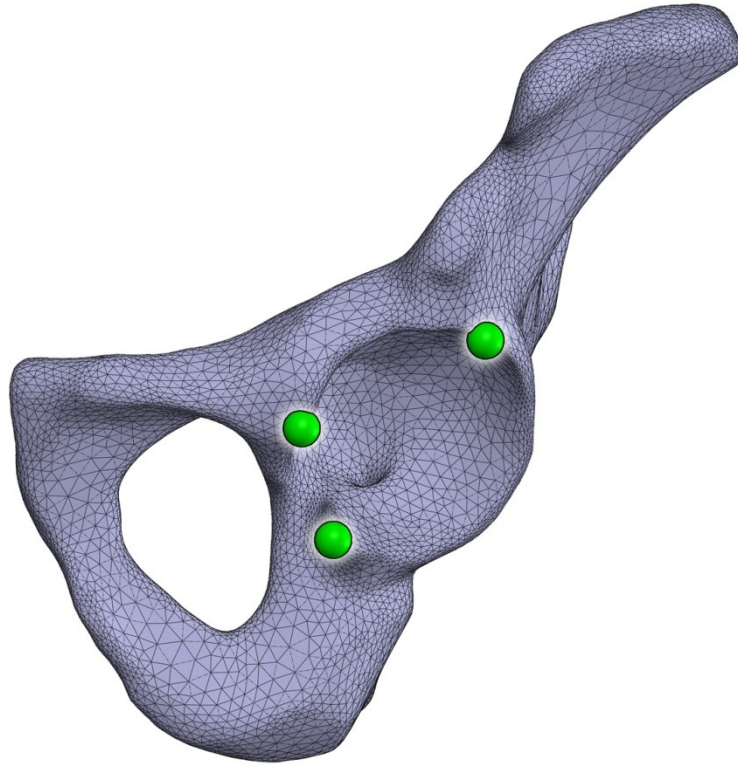


**Figure 2.9-** Left innominate bone displaying the three estimate points selected on each AR (*green*).

To produce the most consistent results possible, some visual and conceptual guides were developed to aid in selection of the AR estimate points. To promote agreement on the location of landmarks, the following guidelines were used by the three individuals whom performed the data collection for this research (SH, ES, & RB). For a primary guide, the curvaceous profile of the rim was mentally visualized as if it were replaced by a perfectly hemispherical cup with a straight edge (similar to a standard prosthetic cup used in THA). The size of this imaginary cup was at a depth that split the differences/normalized the peaks and valleys of the rim. Ideally, if the diameter of the cup matched that of the rim's crest (slightly reamed THA cup), the anterior and posterior points flanking the notch would be placed at the intersection of the hemisphere's edge and the acetabulum (Figure 2.10). As mentioned, the point location on the superior aspect was not as critical as the other two. Keeping in mind that its sole purpose was to provide a third

point for forming an estimate of the acetabulum's aperture, any deficiencies or notable prominences were avoided (Figure 2.11).

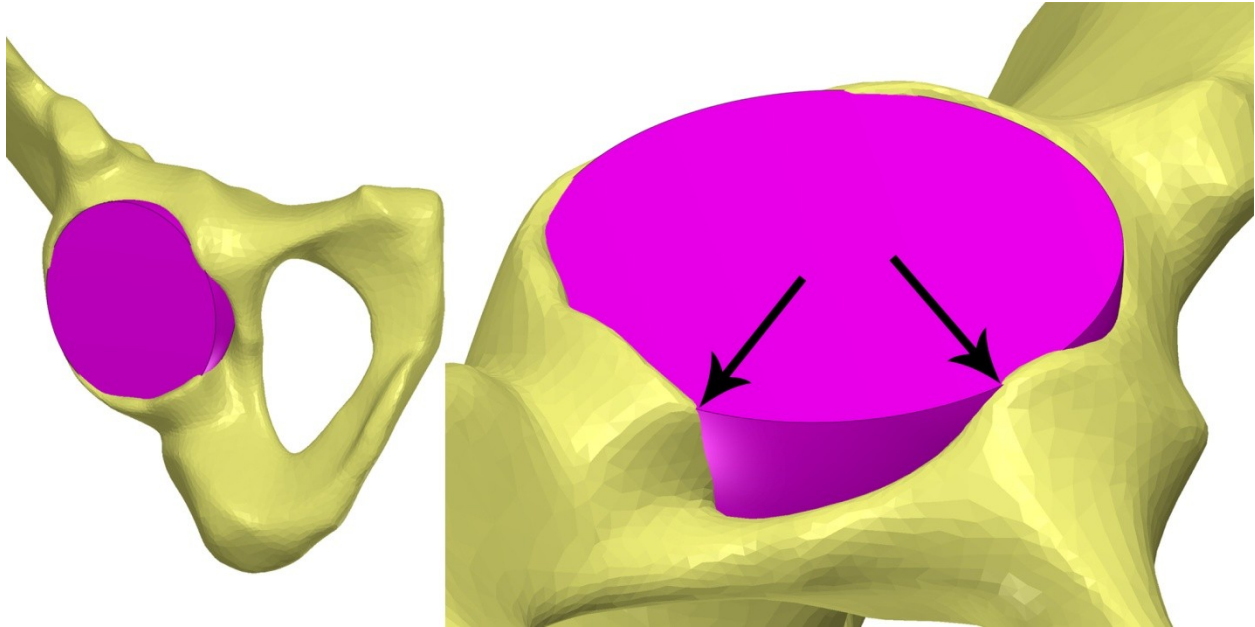


**Figure 2.10-** Imagined hemispherical cup (*pink*) superimposed in an acetabular cup with its flat face bisecting peaks and valleys of the AR's curvature. Points of intersection on anterior and posterior aspects of the notch (*black arrows*).

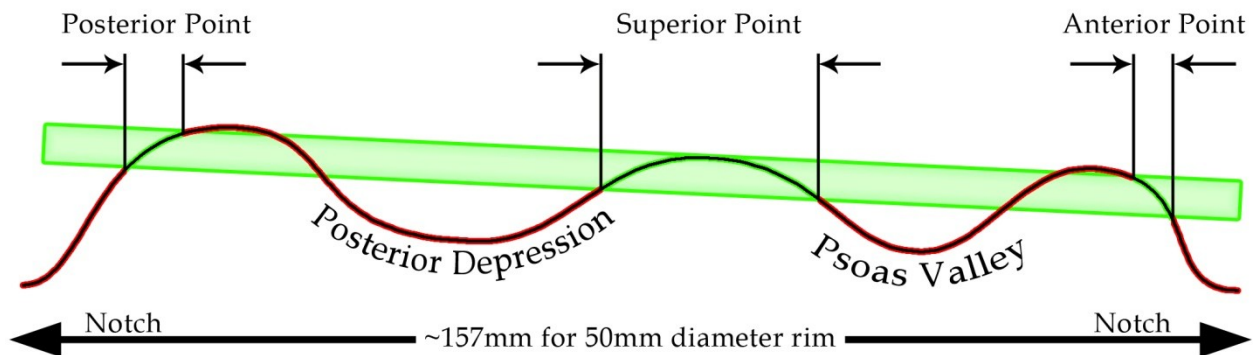


**Figure 2.11-** Representation of an AR unfolded as if it were flattened onto a 2-D surface. The general areas for acceptable (*green*) and unacceptable (*red*) point selection shown along the distal lateral ridge. Selection of points in the acceptable areas results in a range of possible estimate planes (*green box*).

During the course of this investigation, a wide range of acetabular morphologies were observed. In some cases, the anteroinferior and posteroinferior horns on each side of the acetabular notch were deficient, making visualization of the primary guide difficult. A secondary guide was developed to address this type of morphological presentation. Instruction was given to



visualize as if one was traveling along the periphery of the acetabulum on its crest such that their view was always tangent to the curvature of the rim (similar to a rollercoaster ride). As they approached the acetabular notch from either side, the posterior/anterior points should have been placed around the area where their view's perspective would have shifted into the notch (where you would put your hands up in excitement). Traveling along the regions from the deepest point of either the posterosuperior depression or psoas valley, heading towards the acetabular notch, would have placed their perspective more laterally with the field of view away from the body. This indicated that point placement would have been too far away from the acetabular notch, thus excluding meaningful portion(s) of the AR. If one continued along the AR, their perspective would shift until eventually they would be looking medially at the floor of notch. This would indicate that point placement was too far inside acetabular notch, thus including non-meaningful portion(s) of the acetabulum. The region between these two areas, where the perspective begins to shift sharply from lateral to medial, was an acceptable region for point selection (Figure 2.12).

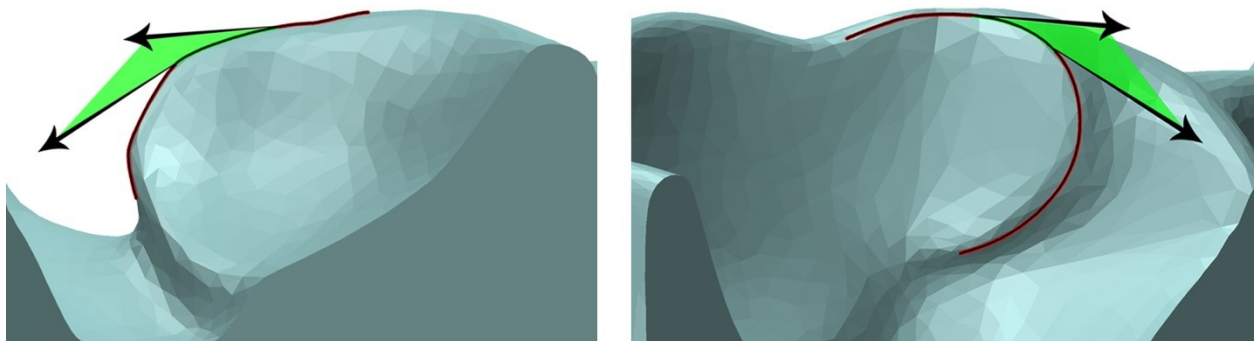


**Figure 2.12-** The curvature of the AR used as a secondary guide to locate acceptable points (*green areas*) on the posterior (*left*) and anterior (*right*) side of the acetabular notch.

Typically, the point on the posterior aspect of the acetabulum can be easily located using this curvature based method. In some instances, the morphology around the anterior point can be less distinct, becoming convoluted where the superior pubic ramus melds into the acetabulum. Regenerated 3-D structures appear as monochrome triangulated surfaces which can make

identifying more subtle landmarks difficult. If visible, the raised portion of the crescent shaped articular cartilage served as an aid for identifying the anterior point and prevented selecting a point that may have inadvertently strayed medially along the pubic ramus (Figure 2.13).

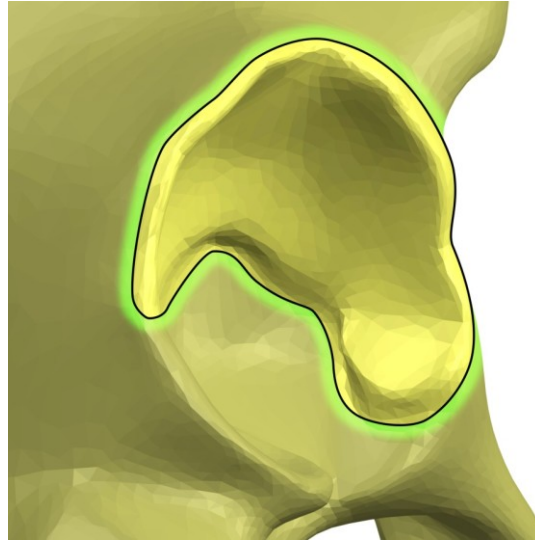


**Figure 2.13-** Highlighted appearance of the raised, crescent shaped articular cartilage used to identify the anterior AR point.

Any combination of the methods outlined above could have been used to select the three appropriate points on the AR. In general, it was more important to select points that best represented the range of AR to be *included*, rather than ones that formed an accurate orientation plane. This is because the Acetabulator's iterative approach would eventually converge on the plane that best described all of the included AR (Section 2.3.3). After all six points (three on each acetabulum) were selected for each subject, their 3-D Cartesian coordinates were exported in a single text (\*.txt) file.

## **2.3 PROGRAMMATIC METHODS**

The Acetabulator program was developed using a technical computing language called MATLAB<sup>®</sup> version 2010b (MathWorks<sup>®</sup>, Inc., Natick, MA). New ideas and improved programming were incorporated over a two year period contributing to the program's evolution. The results presented herein were attained using the latest version (v3.0). Therefore, this

discussion will be limited to only the current state of the program. A graphical user interface (GUI) was designed to load the collected data into the program, input scan parameters, control plotting options, and execute an analysis (Figure 2.14). The Acetabulator performed the two seemingly disparate analyses of the full and hemi-pelvis via this single interface. This resulted in a somewhat lengthy body of code that switched between operations performed for the full pelvis analysis and ones for the hemi-pelvis. To present this in a coherent manner, a top level flow chart is provided to give an overall picture of method, including the data collection and programmatic approach (Figure 2.15). This section only outlines the critical operations performed by the Acetabulator. A more detailed flow chart and sequential montage of graphics with accompanying descriptions are provided in Appendix A: Acetabulator- Detailed Flow Chart and Appendix B: Acetabulator- Graphical Flow Montage.

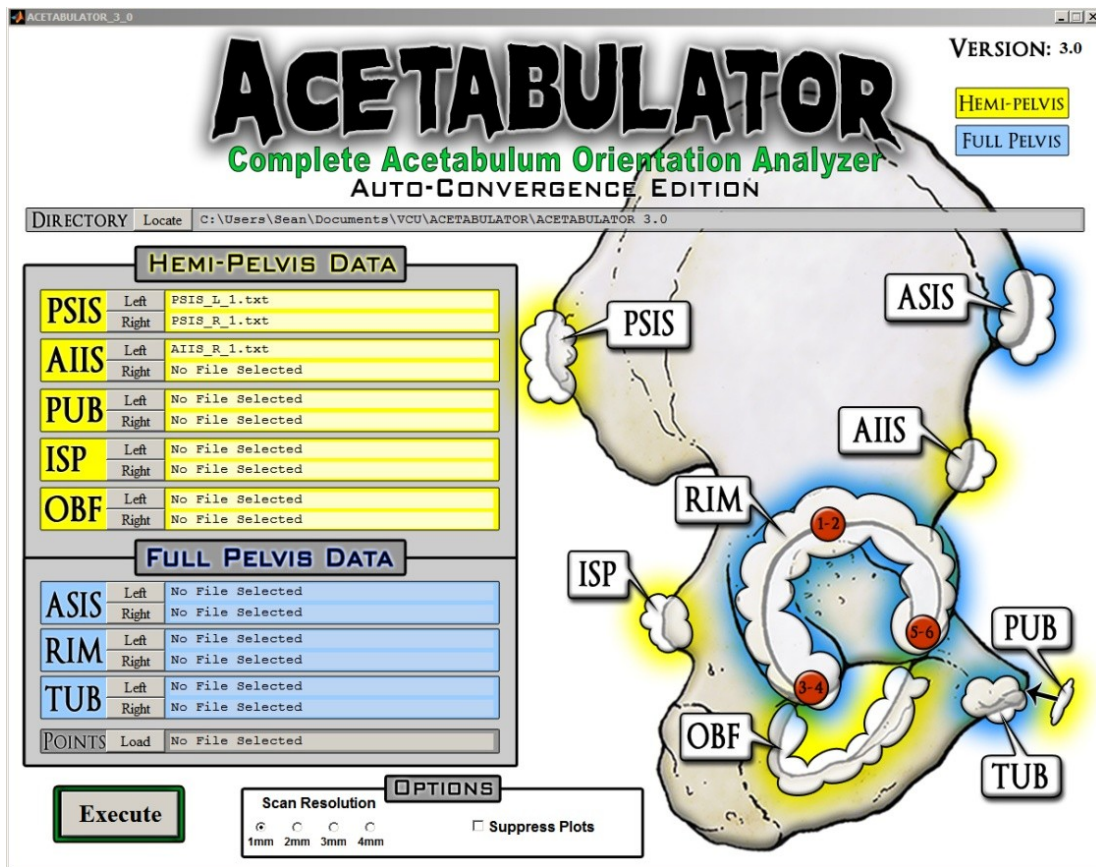


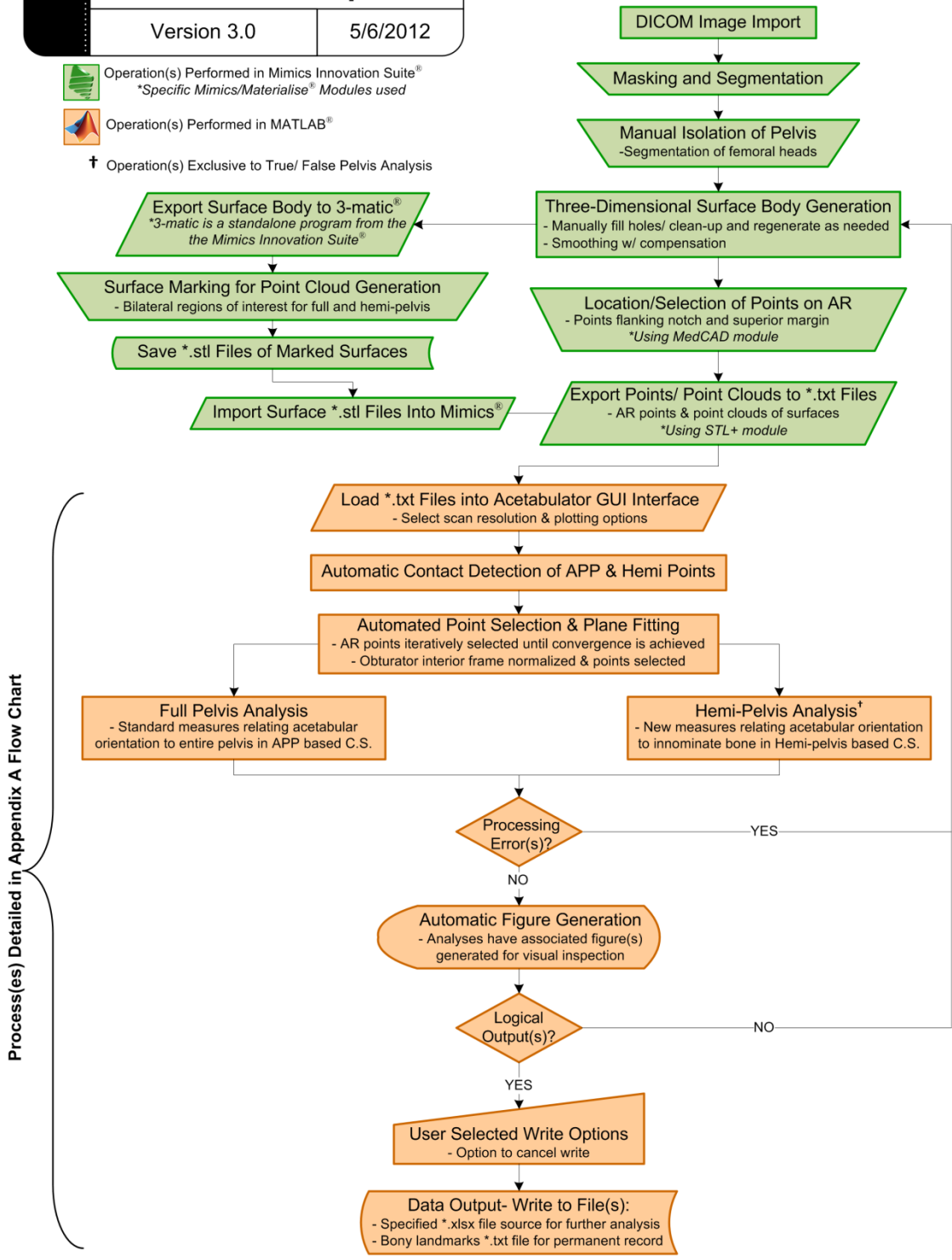


Figure 2.14- GUI of the Acetabulator used to locate file sources and set parameters for analysis.

# Acetabulator- Top Level

Version 3.0      5/6/2012

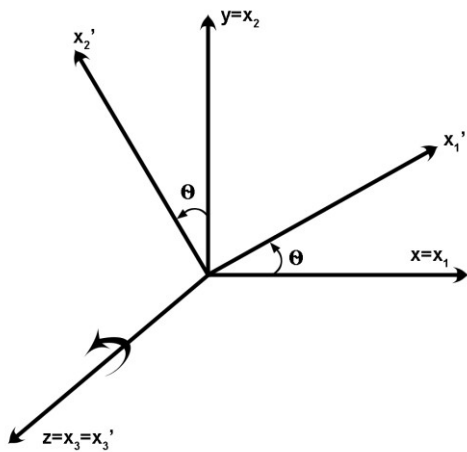
-  Operation(s) Performed in Mimics Innovation Suite®  
\*Specific Mimics/Materialise® Modules used
-  Operation(s) Performed in MATLAB®
- † Operation(s) Exclusive to True/ False Pelvis Analysis



Process(es) Detailed in Appendix A Flow Chart

Figure 2.15- Top level process flow for data collection and programmatic analysis.

In general, the programmatic strategy of the Acetabulator rotated the C.S. to align axes with estimated datums. Rotations were achieved using direction cosine matrices that related the current C.S. to the orientation of the desired C.S. or datum (Figure 2.16). Matrices containing the Cartesian coordinate point locations were simply multiplied by direction cosine matrices to perform the rotation(s). Once the coordinate axes were aligned in the desired direction(s), various operations were performed to select points of interest. For example, if a C.S. were to be aligned with the long axis of a conical surface (e.g.- a bony prominence), the node at the tip of the cone would have a maximum coordinate value along the aligned axis. Whenever mention of "rotation" or "alignment" is made, simple trigonometric relations were used to determine the angle of rotation, and direction cosine matrices were used to perform the subsequent transformation. Plots were incorporated into the MATLAB code after every series of rotations to visually confirm that the desired alignment was achieved.



**Convention:** The cosine moving between the "old" ( $x_i$ ) to the "new" ( $x_i'$ ) axis is the *direction cosine matrix*  $[\beta]$

$$[\beta] = \begin{bmatrix} \cos(x_1 \& x_1') & \cos(x_2 \& x_1') & \cos(x_3 \& x_1') \\ \cos(x_1 \& x_2') & \cos(x_2 \& x_2') & \cos(x_3 \& x_2') \\ \cos(x_1 \& x_3') & \cos(x_2 \& x_3') & \cos(x_3 \& x_3') \end{bmatrix}$$

For axes shown: 
$$[\beta] = \begin{bmatrix} \cos(\theta) & \sin(\theta) & 0 \\ -\sin(\theta) & \cos(\theta) & 0 \\ 0 & 0 & 1 \end{bmatrix}$$

\*Note:  $\cos(90^\circ + \theta) = -\sin(\theta)$  and  $\cos(90^\circ - \theta) = \sin(\theta)$

**Figure 2.16-** Usage and convention of the direction cosine matrix.

### **2.3.1 Automatic Detection of APP Coordinate System**

To eliminate a major source of potential human error, the APP based C.S. was automatically determined by the Acetabulator. The programmatic scheme for selecting the bilateral ASIS and PT points was relatively simple in concept. Two basic governing principles were applied to perform the point selection. The first and most important principle was that the APP is created by mechanical contact of the bilateral ASIS and PT with a planar surface. [45,48,169,211] This consistently forms a reliable frontal plane of the pelvis that can be reproduced in studies that use anatomic specimens with osteometric boards [45,48,51,209], those who use devices to position the pelvis during radiographic imaging [126,212], as well as for guided surgical procedures.[49,169,199,200,213] The second principle used the simple fact that a plane is directly defined by three (and only three) unique points in 3-D space. Therefore, only one possible combination of anterior most points on the bilateral ASIS and PT would satisfy both of these conditions.

Initially, the point clouds of the PT were combined to form a single array of nodes. The centroids of the combined PT and bilateral ASIS were calculated from the average of all the points within each cloud. These three points formed a plane that served as an initial estimate of the APP's orientation. The C.S. was translated to the geometric center of these three points and the y-axis was aligned to the estimate plane's vector normal. The node with a maximum y-value was selected from each of the three point clouds. These points formed a new plane which the y-axis was realigned to. This process was repeated until the algorithm converged upon the three most anterior points, which would be the points of mechanical contact with a planar surface. In reality, the pelvis could physically "rock" back and forth between the two foremost points of the PT depending on how the pelvis was placed on the surface, or the from differing mass in each

bilateral halve. Therefore, the midpoint between the two foremost points of the PTs was used to establish the third point to form the APP (Figure 2.17). The combined PT points clouds were separated to locate the contralateral foremost point. This point was simply the vertex with the maximal y-coordinate in the side that was not previously selected. The points of the bilateral ASIS and midpoint of the PT established the APP which served as a coronal plane. A vector that resided in the APP was calculated as perpendicular to a line connecting the bilateral ASIS points. The sagittal plane was parallel to this vector and normal to the APP plane. Naturally, the axial plane was defined as perpendicular to both the coronal and sagittal planes (Figure 2.18).

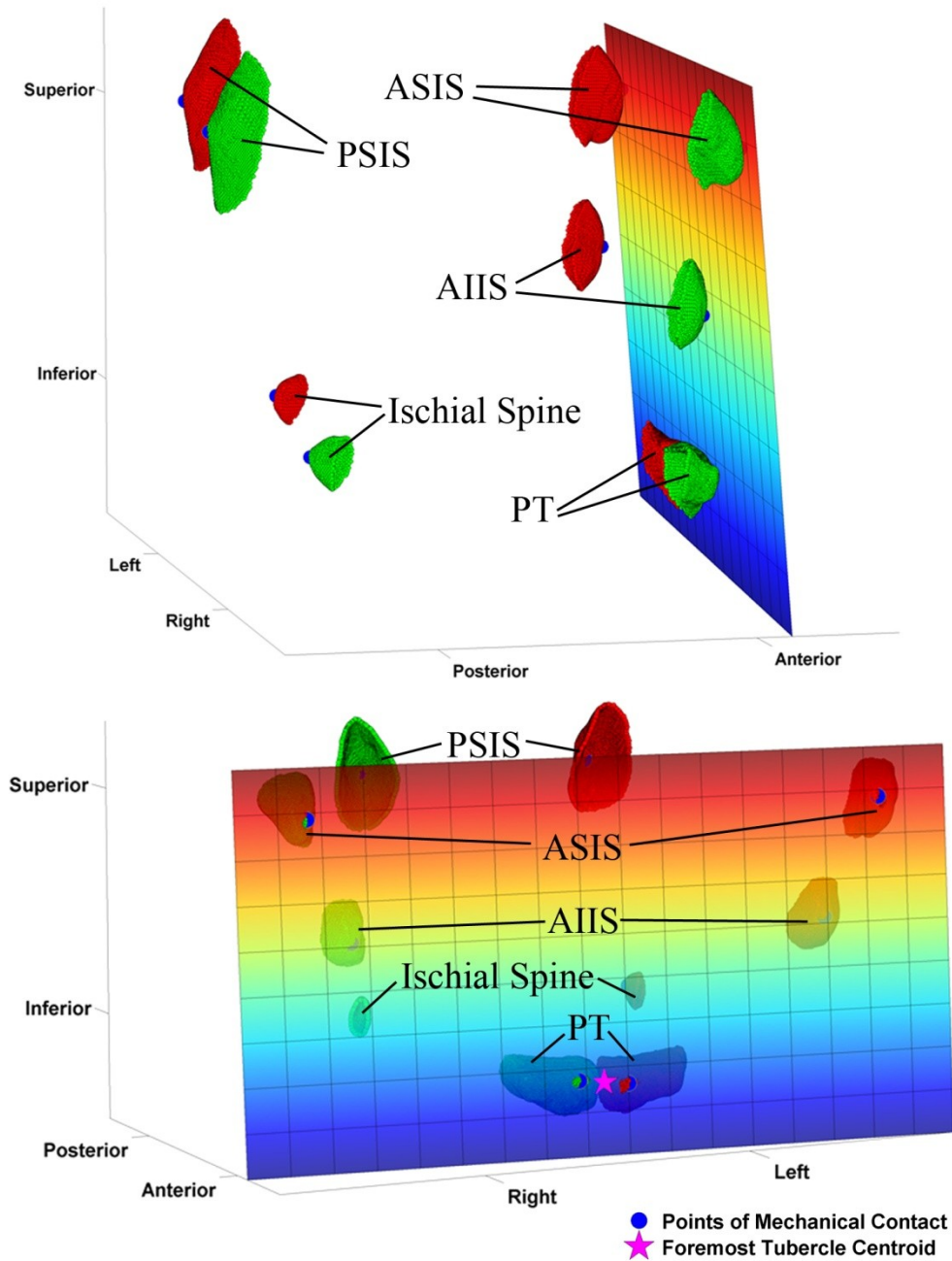


**Figure 2.17-** Acetabulator output plots of automatically generated C.S.. Oblique lateral (*top*) and frontal (*bottom*) views showing APP (*multicolor*) contacting the foremost surfaces of the ASIS and PT. Automatically located points for both the full and hemipelvis shown (*blue*).





dimensionally "boxed" in. The SPP was used to locate the most posterior points on the bilateral ischial spines using the same convention.

The true and false pelvic regions, along with the hemi-pelvis C.S., were established using all of the points previously located on each innominate bone. The reference frame was constructed around an initial sagittal plane. This sagittal plane used the points of the ischial spine, PSIS, and a point at the center of the pubic tubercle's flat interior face where it joins at the pubic symphysis. The coronal plane was normal to the sagittal plane and contained the points of the ASIS and foremost PT. The axial plane was normal to both sagittal and coronal planes (Figure 2.19). Because the hemi-pelvis C.S. was constructed exclusively from unilateral points, it does not directly correspond to the reference frames of either the body or the pelvis. However, establishing reference planes that have orientations unaffected by size or normal anatomic variability is the most important factor to be considered when devising a C.S.. The arrangement described above forms planes with consistent orientations that can be reliably reproduced on both male and female anatomy independent of the specimen's size. This is because the even physeal growth of the innominate bone primarily changes the span points within their respective planes and leaves their relative orientation to one another unchanged. The arrangement of points used to establish the sagittal plane was also chosen because each point resides on a separate region of the innominate bone. Namely, the PSIS belongs to the ilium, the ischial spine to the ischium, and the point on the tubercle face resides on the pubis.

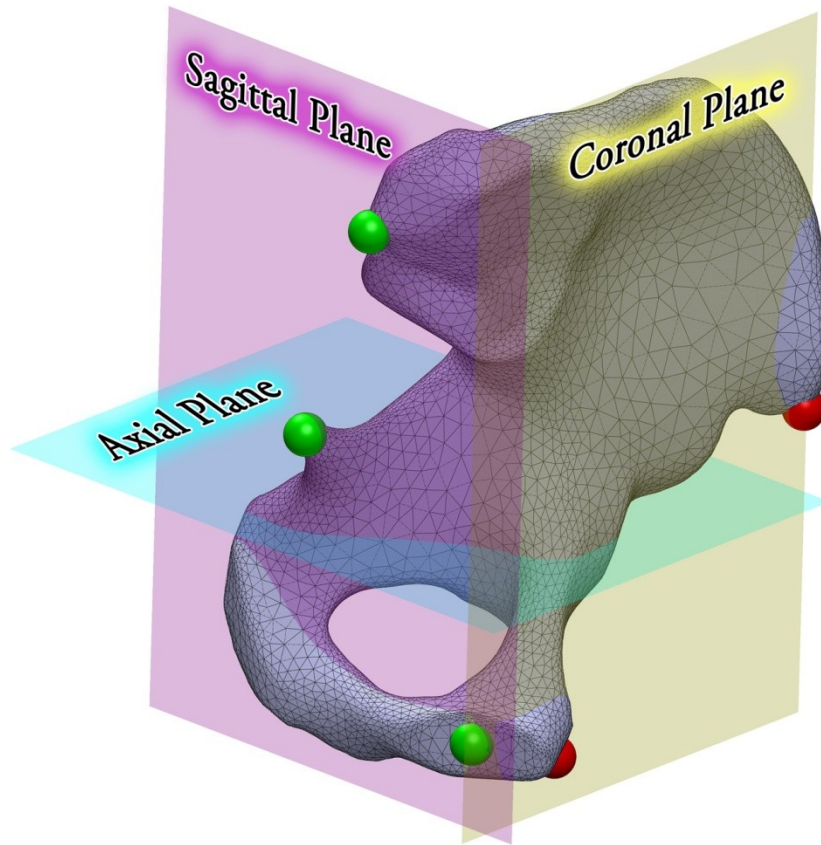


**Figure 2.19-** Hemi-pelvis C.S. shown on left innominate bone. Sagittal Plane (*pink*): Ipsilateral points of the PSIS, ischial spine, and center of the pubic tubercle's interior face (*green*). Coronal Plane (*yellow*): Containing the points of the PT and ASIS (*red*) and normal to the sagittal plane. Axial Plane (*blue*): Normal to both coronal and sagittal planes.

It is worth noting that other configurations were explored for constructing the hemi-pelvis C.S.. One established the sagittal plane using the ischial spine, PSIS, and a point located where the insertion of the inguinal ligament forms a distinguishable prominence on the PT. It was found that the location where the inguinal ligament inserts varies widely, shifting medially or laterally along the superior ramus. In females, the insertion point was shifted laterally, and in males the location tended to be more medial. These variations appeared to be independent of the innominate bone's size. This directly affected the sagittal plane's orientation and therefore made it unacceptable to use as a reference plane. Another arrangement that was explored utilized the flat interior face of the pubic tubercle to form a sagittal plane. A point cloud was captured on the flat surface and its nodes were used to fit a least-squares plane that closely corresponded to the

sagittal planes of the both the body and the pelvis. However, a wide range of morphology was observed in this region as well. In some cases, this face was irregular and in other instances there was not a distinct flat face at the symphyseal union of the tubercles. Thus, normal anatomic variability made using this surface unsuitable for consistently forming a reference plane.

Because the point cloud data of the tubercle already existed from the previous C.S. investigated, it was used to determine its center point of the interior face. Due to their physical arrangement, almost any point along the short axis of the interior face of the tubercle would have sufficed to form an equivalent sagittal plane. This is because the tubercle's short axis is relatively small and the sagittal plane intersected it at an acute angle. Theoretically, any point on the face parallel to the line connecting the ischial spine and PSIS would have formed the *exact* same plane. A shift along the long axis of the tubercle's face would have caused the largest possible change in the sagittal plane's orientation (Figure 2.20).

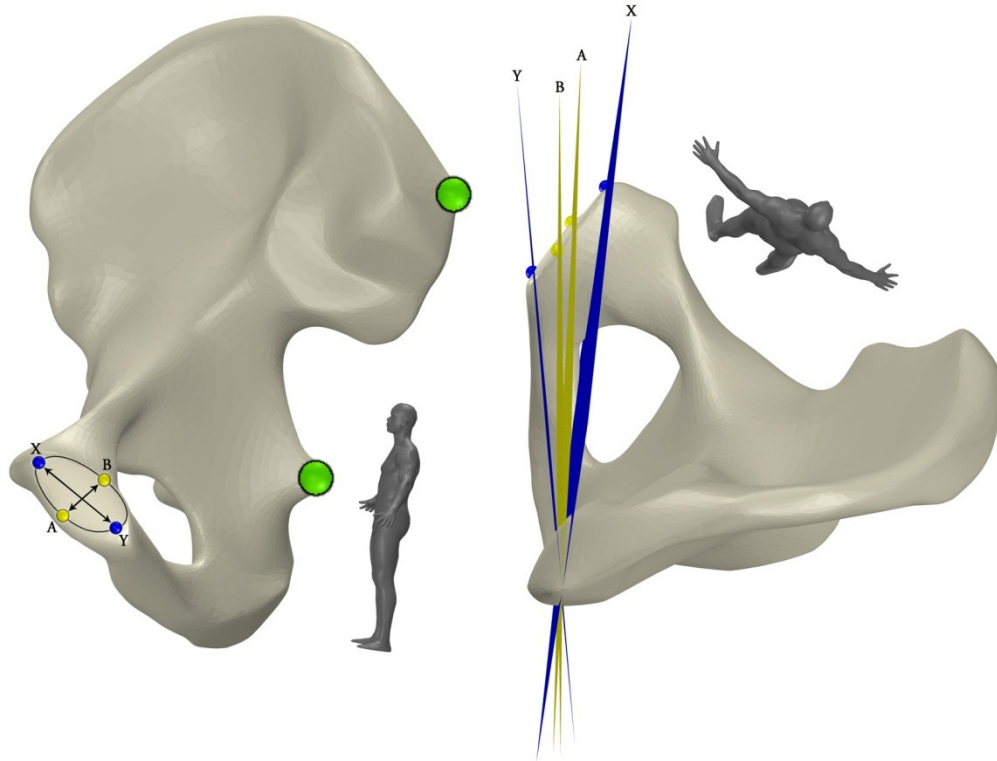


**Figure 2.20-** Variable orientation of the hemi-pelvis sagittal plane. Interior-lateral view of long (X-Y) and short (A-B) axes of the tubercle face (*left*). Craniocaudal view of plane orientation range resulting from selecting points at the extrema of the tubercle face (*right*). The selection variability along the short axis (*yellow*) has less impact as selection along the long axis (*blue*).

### 2.3.3 AR Point Selection & Plane Fitting

Subject specific parameters were used to select the points on each AR. These parameters were determined from both the size of the AR and resolution of the scan from which it originated. In general, it is appropriate to select *either* a point directly visible on a tomogram, *or* an interpolated point between two neighboring slices. Using *both* an interpolated point and the points from which it was directly attained is inappropriate because it is in-fact creating data that does not exist. This limits the amounts of "unique" data points that can be yielded from any single scan. To maintain the integrity of the data, two criteria were adhered to when selecting data points from the 3-D renderings. Firstly, points needed to be sufficiently spaced to assure that they were unique. Every facet on the surface produces three points, which all have locations driven by its orientation. If points were selected in close proximity to one another, than two non-

unique points from single facet could have been selected. Therefore, any two consecutive points selected on a surface (in this case the AR) were separated by at least one discrete facet.

Secondly, the number of points selected on any surface should have never exceeded the data available from its originating scan. Specifically, the number of points should not have exceeded the total number of times each tomogram intersected a margin of the AR (Figure 2.21). For example, if a very coarse scan only intersected the AR three times on both the anterior and posterior margins, only six unique points could be selected. Thus, the number of points selected on *any* surface was driven by both the size of the anatomic feature and the resolution of the scan. All of the scans used in this study were attained using 1mm slice increments, however the Acetabulator has established parameters that can be adjusted for scans as coarse as 4mm using the GUI controls.

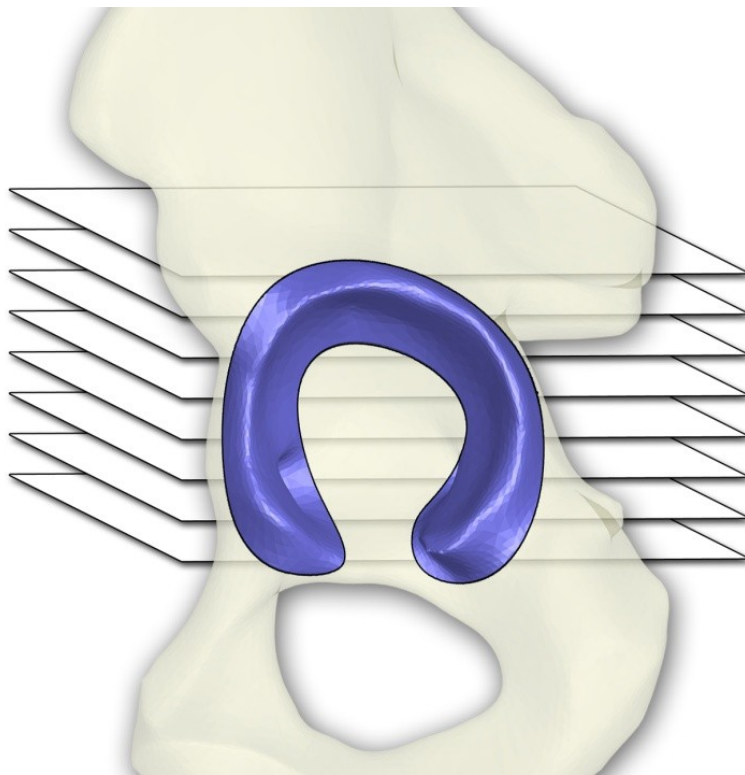


**Figure 2.21-** Depiction of tomograms slicing the surface of the AR. Each margin of the AR intersected by a slice can produce a unique data point.

If the circumference of the AR was divided up into equal sections for locating points, the theoretical upper limit of points available for selection would be limited by the scan resolution and acetabular diameter. However, the faceted surface creates another limitation that needed to be accounted for in smaller adult acetabuli (~45mm diameter).[195] The minimum spacing is a set value that was only dependent upon the facet size, which was driven by the curvature of the surface and smoothing applied. Therefore, as the diameter of the acetabulum decreases, so does the remaining portion of the AR available for point selection. If the range available to locate a single point becomes too small, the density of nodes may not provide an appropriate point on the *most* distal lateral ridge of the AR. Therefore, a balance needed to be established between the number of points selected, the range allotted to locate them (search window), and the minimum spacing separating them. A subset of four subjects (eight acetabulums) was used to empirically determine the best settings to achieve this balance. The parameters controlling the size of the search window and minimum spacing were adjusted so that an increasing number of reasonably spaced points were selected on each AR. A least-squares plane was fit to the selected points on the AR for each iteration. The orientation of this plane stabilized around a constant position as more points were selected on the AR. Akin to a spinning coin coming to rest on a flat table, convergence was assessed by measuring plane's change in orientation as more points were selected. The point locations were visually inspected using interactive 3-D plots to assure the most distal lateral ridge was selected. From observing the results shown in Figure 2.22 it was determined that a lower limit of ~17 points (ideally >20) are needed to assure a plane fit to the AR will reliably represent its orientation.

### Points Selected vs. Orientation Change

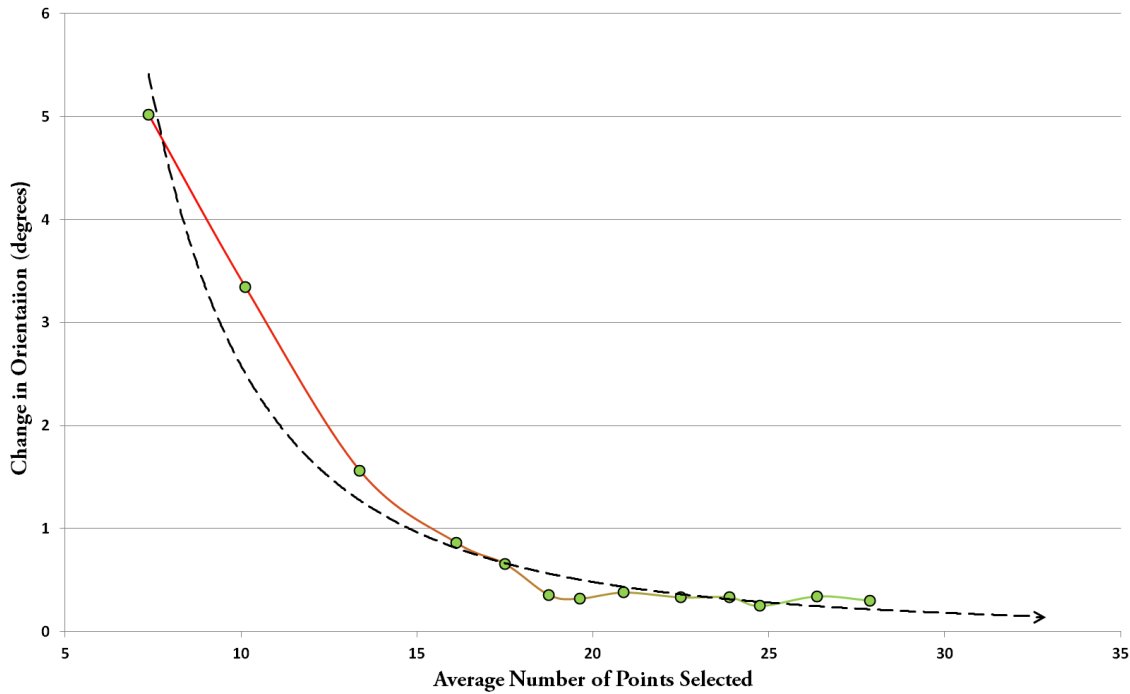


**Figure 2.22-** Plot displaying the average change in orientation of the plane fit to  $n=8$  acetabuli by increasing the number of points selected on the AR.

Because the facet edge lengths form short linear spans over curved surfaces, the minimum spacing and search windows size were calculated in terms of arc length. For scans with 1mm slice increments, it was determined that a search window of 3mm, with a minimum spacing of 1.5mm, produced ideally located points on the distal lateral AR. With the surface rendering and smoothing settings used, the typical facet edge length on the AR was  $\sim 0.75$ mm, and was never observed to exceed 1.3mm. Thus, a spacing of 1.5mm assured that a unique node would be selected for every point. In addition, these settings accommodated smaller acetabuli while still selecting a sufficient number of points to form a representative plane. Because each acetabulum has a slightly different size, dividing them evenly into perfectly sized search windows with minimum spacing (search increments) would have been highly unlikely. To accommodate for this anatomic variability, the number of search increments was rounded down to the nearest whole number and the search windows were enlarged slightly to fill the remainder space. By



allowing selection of any single point over a range (i.e.- a window), instead of forcing equal spacing, allowed for points on most distal lateral ridge to be selected. These points best represented the aperture of the bony acetabulum.

The three points located on the AR were also used to form a circle which provided an approximation of the aperture's center and diameter. The C.S. was rotated into a position at the circle's center where the z-axis was normal to the estimate plane. An initial distal lateral point was selected from the AR point cloud to replace the manually located estimate point on the posteroinferior side of the notch. This point was automatically selected from within an angular window extending  $1.25^\circ$  to each side of the estimate point. The Cartesian coordinates of the AR point cloud were converted to polar, with zero radians aligned with the new posterior point (Figure 2.23). The diameter of the circle was used to convert the arc length based search increments to radians. The arc length between zero radians and the anterior AR point was divided up to form a series of evenly adjusted search increments. This produced subject specific parameters so that more points were selected on larger acetabulums. The final search window was centered on the anterior AR point so that it could also be replaced by an automatically selected point. Thus, no manually selected points were ever used in subsequent calculations. At this stage, the AR point cloud was ready for the initial point selection routine (Figure 2.24).

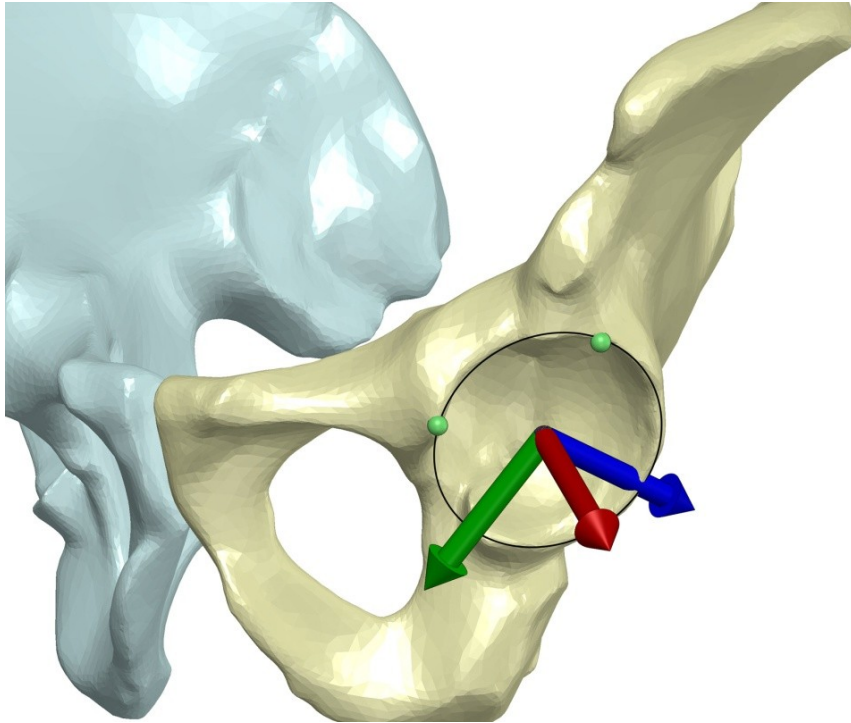


**Figure 2.23-** C.S. orientation for initial point selection routine on the AR. Z-axis (*red*) is normal to the estimate plane and the y-axis (*green*) is aligned to the new posterior AR point.

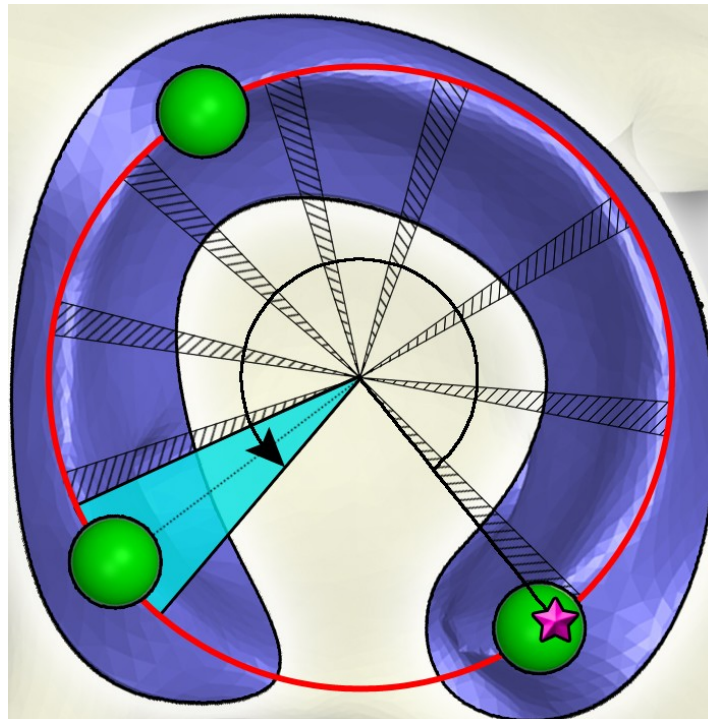


**Figure 2.24-** Minimum separation (*crosshatched*) and search windows (*coarser than actual*) determined from the estimated AR diameter (*red*). Start point located on posterior AR (*pink star*) and the last search window centered on the anterior point (*teal*).

Point selection is simplified in that, the most distal lateral point on the AR will have a maximal (or minimal) distance along the z-axis oriented normal to the estimate plane. Because the AR forms a fairly distinct ridge, selection of points using a maximum z-coordinate value will always yield the most distal lateral point(s) through a generous range of estimate plane orientations. Points with a maximum z-coordinate were selected in each of the search windows. As previously mentioned, points selected around the AIIS-to-AR margin are checked to assure that they were on the rim and had not strayed up the anterior column. To perform this check, a second degree polynomial curve was fit to the points located within 45° of either side of the AIIS in the estimate plane. The SD of the distances between the fit polynomial and the points (variance) was calculated. From visually observing points selected on plots of previous versions of the Acetabulator, the empirically derived cutoff line =  $0.91 \times SD + 0.92$  was used to determine if points were out-of-bounds (Figure 2.25). It was also determined that points at risk for straying up the anterior column were typically located at 7.5° anterior and 25° posterior to the AIIS. If the 2-D distance between any point and the polynomial within this range exceeded the limit set by the cutoff line, they were excluded (Figure 2.26). A least-squares plane was fit to the checked points on the AR. The C.S. was rotated so that the z-axis was aligned to the vector normal of the fit plane. This process was repeated until the plane converged upon the most distal lateral points of the AR. The acetabular axis (AX) was defined as the vector normal to the converged plane which best represented the aperture of the acetabulum (Figure 2.27).

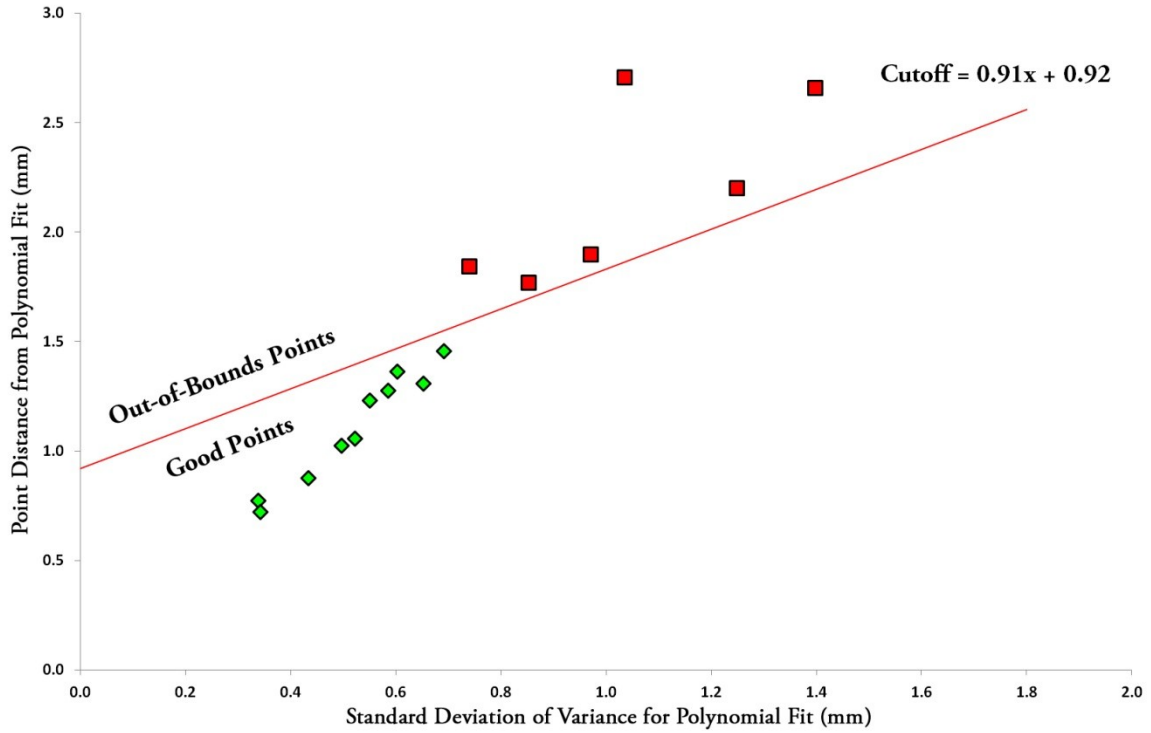


Figure 2.25- Empirically derived relationship determining out-of-bounds points straying up the anterior column.

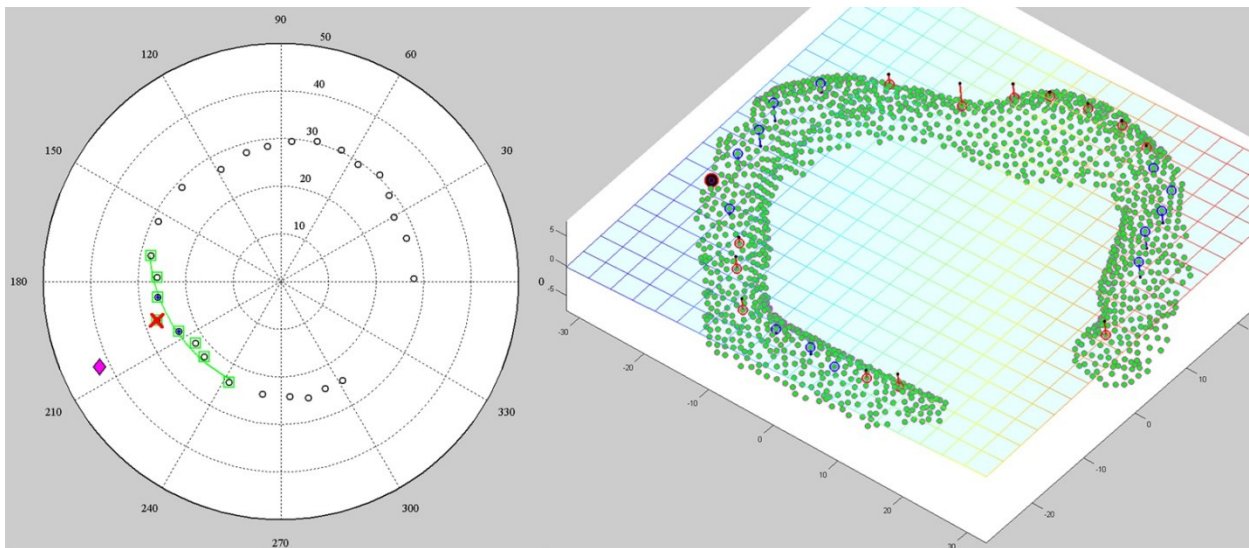
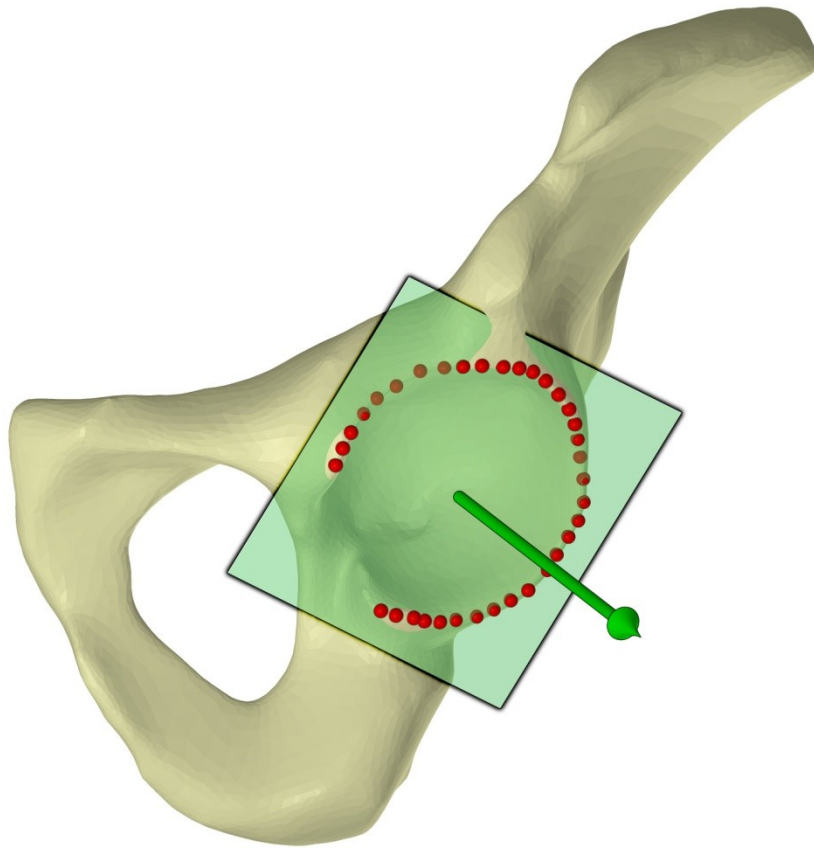


Figure 2.26- Acetabulator output plots showing out-of-bounds point. Polynomial fit (green curve) around the AIIS (pink diamond) with excluded point (red x) in the estimate plane (left). 3-D view of AR point cloud (green points) showing selected points above (blue) and below (red) the fit plane with excluded point (black).



**Figure 2.27-** Left innominate bone showing converged points that are automatically selected on AR (*red*) with the least-squares plane used to establish the AX (*green*).

### 2.3.4 True & False Pelvic Regions

Planes exclusive to the true and false pelvic regions were created to explore how the structure of the innominate bone is arranged. These regions were separated by the superoinferior division of the triradiate cartilage. The false pelvic region was described using points located only on the ilium. These points were located on the PSIS, ASIS, and AIIS which were used to form the false pelvic plane (FPP). The interior frame around the inlet of the obturator foramen was used to describe the true pelvic region. The obturator conveniently spans both the pubis and ischium and is evenly split by the growth plates separating the bones (Figure 1.3). Twelve points were automatically located on the interior most ridge formed around the inferior, medial, and

lateral margins of the obturator. The superior region of the obturator's interior frame was excluded because it forms an irregular and convoluted helical ridge which is often indistinguishable. A least-squares method was used to fit the false pelvic plane (FPP) to the 12 selected points on the obturator. Normal vectors to both the TPP and FPP were used to relate the orientation of the acetabulum to the true and false pelvic regions in subsequent calculations (Figure 2.28).

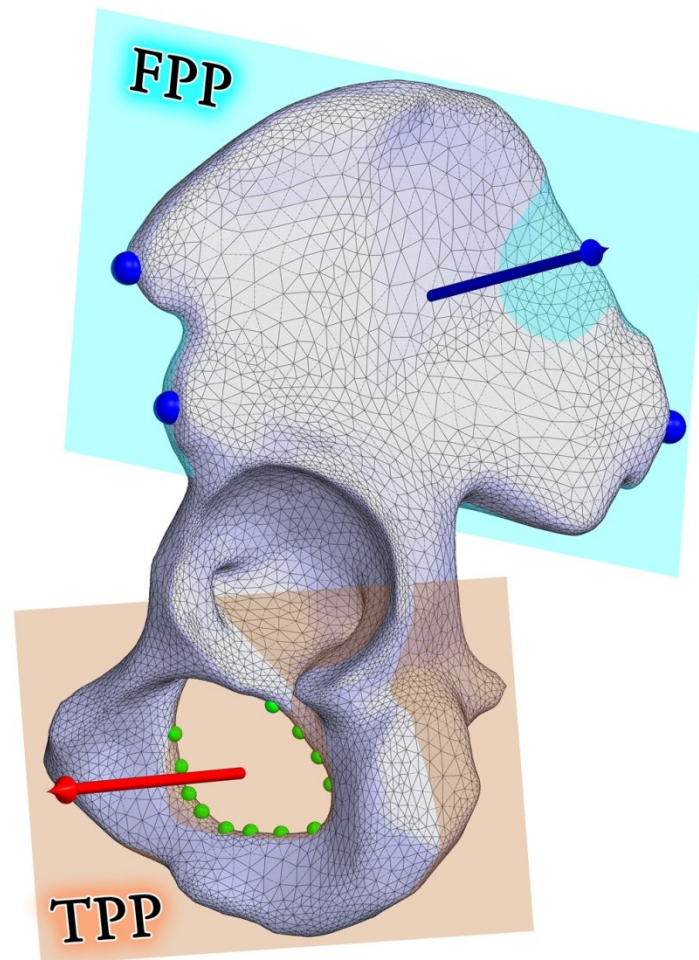


**Figure 2.28-** The normal vectors of the true (*red*) and false (*blue*) pelvic regions shown on a left innominate bone. FPP (*cyan*): Points of the PSIS, ASIS, and AIIS (*blue*). TPP (*orange*): Least-squares fit to 12 points selected obturator interior frame (*green*).

Selection of points along the interior frame of the obturator presented different challenges than that of the acetabulum. While both were used to describe the orientation of their respective

apertures, the primary difference was in how the points were selected on the bony ridges of the different structures. The most distal lateral points on the acetabulum's irregular topology were selected along a relatively uniform circular perimeter. Whereas the most interior points were selected on the obturator's more uniform topology along an irregular shaped perimeter. The interior most perimeter of the obturator's frame is apparent from any view that is approximately perpendicular to its aperture. This allows for the selection of points along the innermost ridge of the obturator by projecting the point cloud's vertices onto a plane that is relatively parallel to its aperture. The points of the ASIS, AIIS, and PT were used to form a plane that is functionally parallel to the opening of the obturator (Figure 2.29).

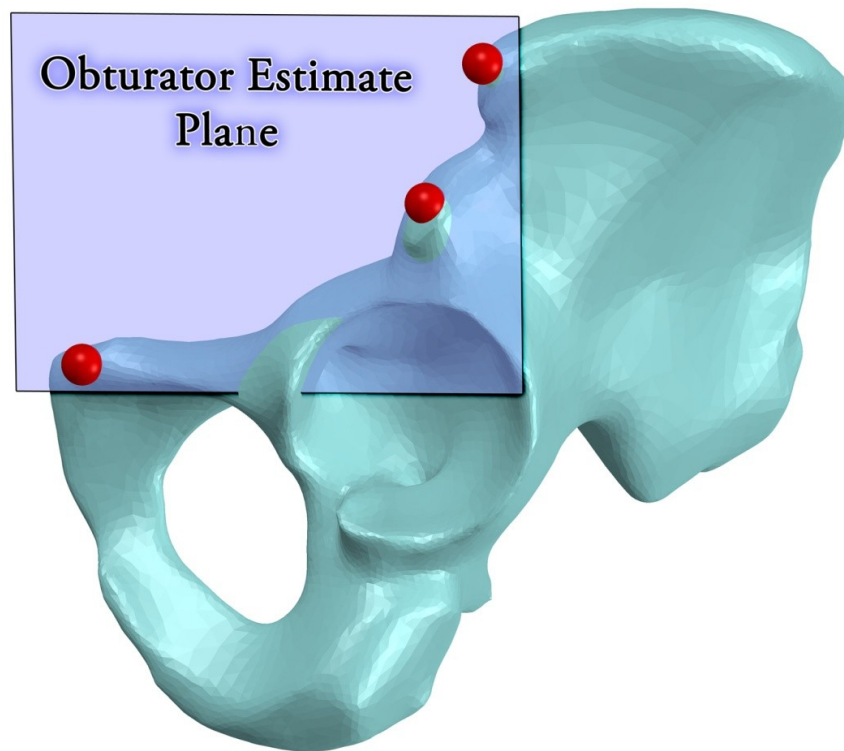


**Figure 2.29-** The points of the ASIS, AIIS, and PSIS form a plane that is approximately parallel to the aperture of the obturator.

Exclusion of the obturator's convoluted region was achieved using the posterior point selected on the AR and the foremost point located on the pubic tubercle. Conveniently, the

anatomic arrangement between these two points reliably form a line that intersects the superior region of the obturator's window when projected onto the estimate plane. This line was used to establish a cutoff vector, where all points superior to its projection were excluded (Figure 2.30). Because the interior frame still formed an irregular shape when the point cloud was projected onto the plane, its perimeter could not be divided into even angular divisions as was done for the acetabulum. To account for this, the radius from the approximated center of the obturator, to its interior bony ridge was determined around the perimeter in 6° increments. The average radius between sequential points was used to divide the irregular perimeter up into small spans of circular arcs. These estimates were used to create a normalized profile of the interior frame based on the typical arc length around the perimeter (Figure 2.31). All of the points in the obturator point cloud were then assigned a corresponding arc length value (more detail can found in Appendix A: Acetabulator- Detailed Flow Chart and Appendix B: Acetabulator- Graphical Flow Montage). A study similar to the one performed for the acetabulum was used to set the parameters for selecting points on the obturator. It was determined that 12 points with a minimum spacing of 4mm would reliably form a plane fit to the interior frame of the obturator (Figure 2.28). These settings also accommodated smaller obturators without violating any of the previously mentions criteria for selecting data points from 3-D renderings.



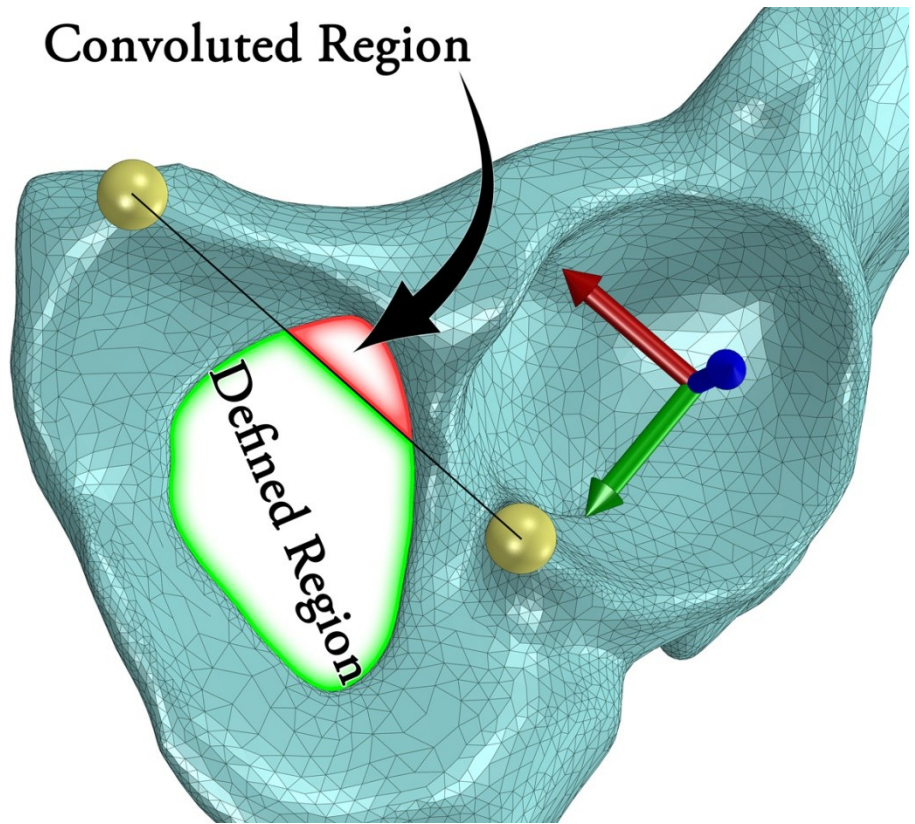


**Figure 2.30-** Points of the posterior AR and PT (*gold*) used to form the cutoff vector (*black*) separating the convoluted (*red*) and well defined (*green*) regions of the OF frame.

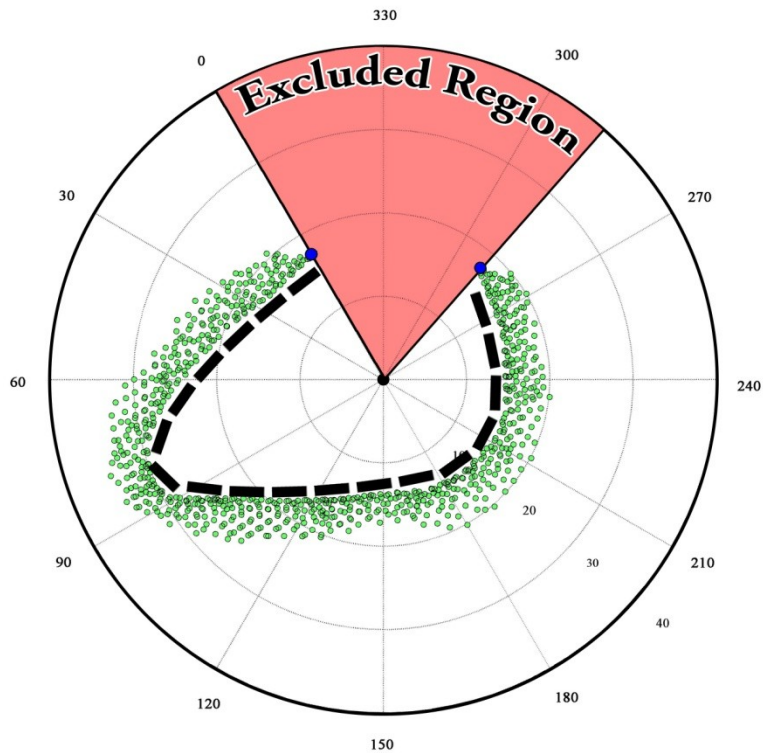


**Figure 2.31-** The obturator point cloud (*green*) projected onto the estimate plane with the interior frame normalized using typical radius for equally spaced segments (*black*).

## **2.4 CALCULATED OUTPUTS**

The Acetabulator automatically calculated the measures of interest for both the full and hemi-pelvis based analyses. The outputs were automatically written into an Excel<sup>®</sup> 2007 spreadsheet (Microsoft<sup>®</sup> Corporation, Redmond, WA) at the end of every analysis. To assure that no systematic error was produced by the Acetabulator's algorithm, two pelvic models were repeatedly crosschecked by manually recreating the same measures in a popular commercial CAD software package, SolidWorks<sup>®</sup> 2010 (Dassault Systèmes SolidWorks Corp, Waltham, MA). All measurements were consistently in agreement between the MATLAB and SolidWorks platforms.

### **2.4.1 Full Pelvis Measures**

For the full pelvis analysis, angular measures of acetabular orientation were calculated relative to the APP based C.S.. The commonly used compositions of inclination (or abduction) and anteversion were used to locate the AX in 3-D space. Previously established definitions of anatomic, radiographic, and operative angles were used to perform calculations (Figure 2.32).[214] Each measurement scheme uses a paired set of angles that are readily attainable in different applications. The definitions used for inclination and anteversion for each measurement scheme are given in Table 2.1.

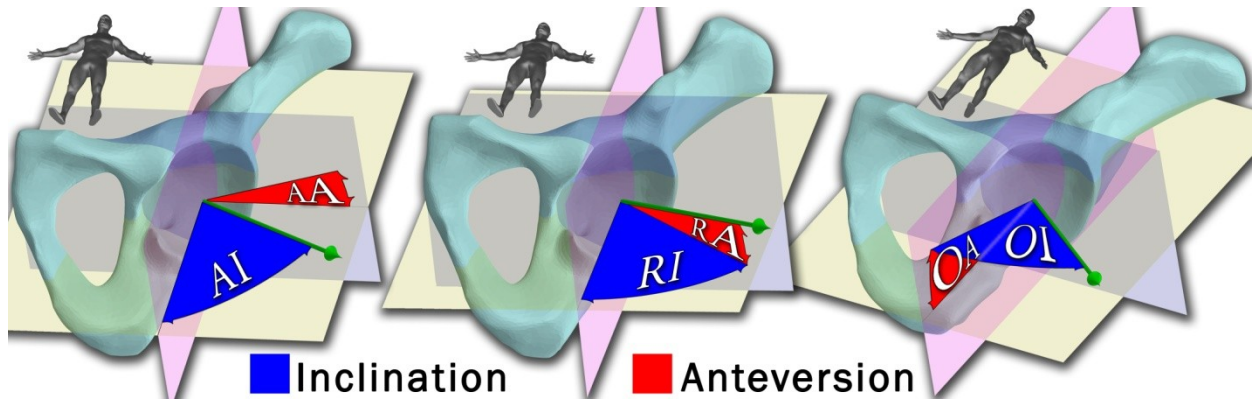


**Figure 2.32-** Left innominate bone showing standard measures of inclination (*blue*) and anteversion (*red*). Anatomic inclination (AI) and anteversion (AA) (*left*). Radiographic measures of inclination (RI) and anteversion (RA) (*center*). Operative measures of inclination (OI) and anteversion (OA) (*right*).

**Table 2.1- Definitions of Full Pelvis Acetabular Measures**

<b>Angle</b>	<b>Description of Angular Measure</b>
Anatomic Anteversion (AA)	The angle formed between the coronal plane and the projection of the AX onto transverse plane
Anatomic Inclination (AI)	The angle between the AX and the long axis of the body (line of intersection between sagittal and coronal planes)
Radiographic Anteversion (RA)	The angle formed between the AX and the coronal plane
Radiographic Inclination (RI)	The angle formed between projection of the AX onto the coronal plane and the sagittal plane
Operative Anteversion (OA)	The angle between the AX projected onto the sagittal plane and the coronal plane
Operative Inclination (OI)	The angle formed between the AX and the sagittal plane

### 2.4.2 Hemi-Pelvis Measures

For the hemi-pelvis analysis, new angular measures of acetabular and innominate orientation were calculated within the hemi-pelvis C.S.. The first set of angles measured the global orientation of the acetabulum relative to the hemi-pelvis reference frame. Version and inclination were measured by adopting the same definitions used in the radiographic scheme (Figure 2.33 & Table 2.2). The other measures related the acetabulum to the true and false pelvic regions of each innominate bone. These angles were measured between the AX and the normal

vectors of the TPP and FPP. Angles of inclination were measured between the projection of the vectors onto the coronal plane. Angles of version were measured between the same projections onto the axial plane (Figure 2.34 & Table 2.3). Positive angles indicated that the vectors formed an opening angle as they extended away from the body and each other. Negative angles indicated that the vectors formed a closing angle, crossing each other, as they extended outwards.

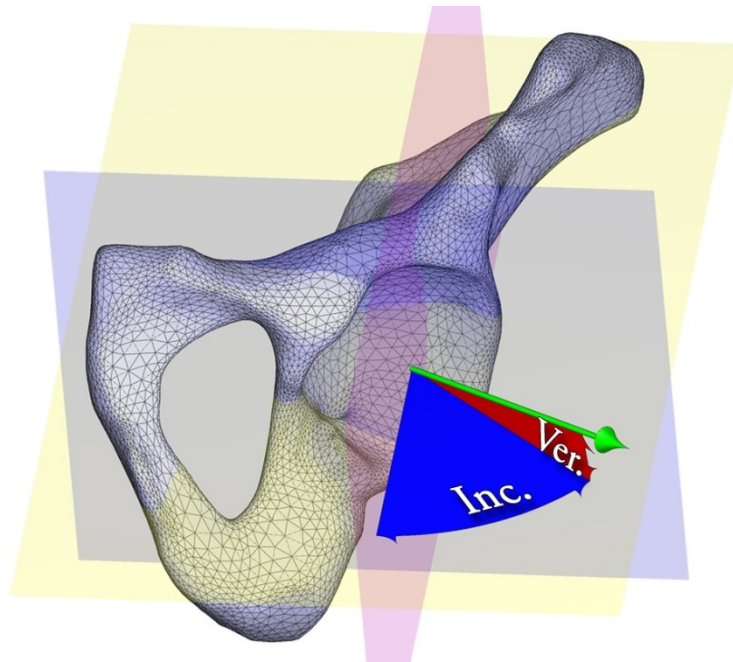


**Figure 2.33-** Measures of acetabular inclination (*blue*) and version (*red*) used for the hemi-pelvis analysis.

**Table 2.2- Definitions of Hemi-Pelvis Acetabular Measures**

Angle	Description of Angular Measure
Version (Ver.)	The angle formed between the AX and the coronal plane
Inclination (Inc.)	The angle formed between the AX's projection onto the coronal plane, and the sagittal plane

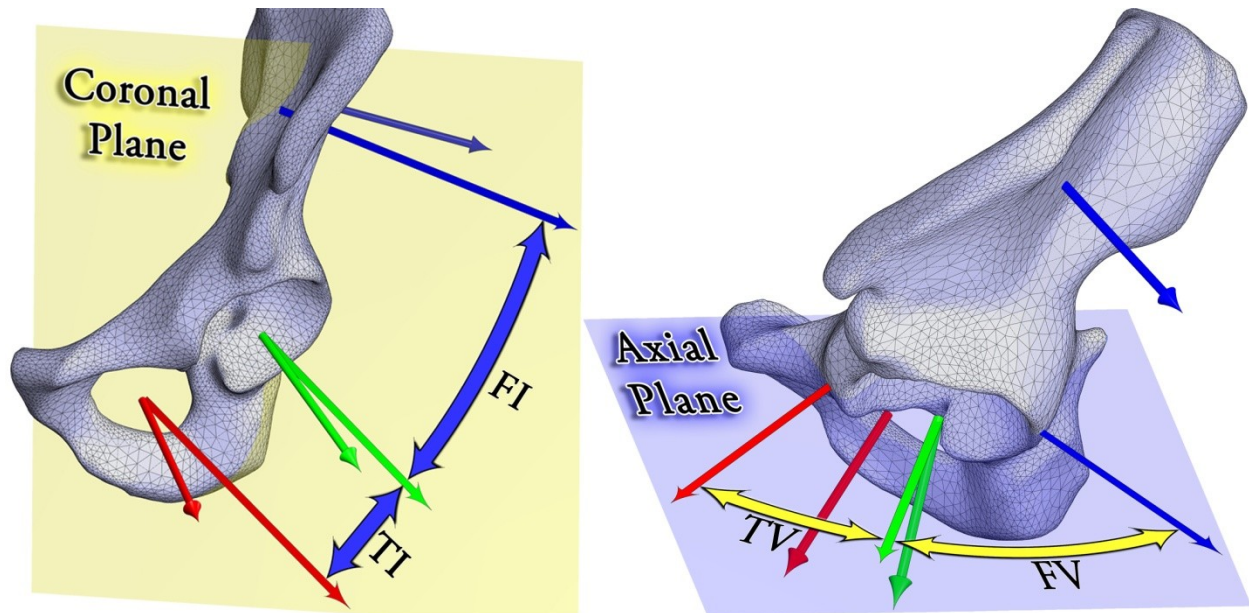


**Figure 2.34-** Hemi-pelvis measures relating acetabular orientation to the true and false pelvic regions. Measures of inclination between the true (TI) and false (FI) pelvis (*left*). Measures of version between the true (TV) and false (FV) pelvis (*right*).

**Table 2.3- Definitions of Hemi-Pelvis Innominate Measures**

Angle	Description of Angular Measure
False Inclination (FI)	The angle formed in the coronal plane between projections of the AX and vector normal of the FPP
True Inclination (TI)	The angle formed in the coronal plane between projections of the AX and vector normal of the TPP (can be negative)
False Version (FV)	The angle formed in the axial plane between projections of the AX and vector normal of the FPP
True Version (TV)	The angle formed in the axial plane between projections of the AX and vector normal of the TPP

## 2.5 STATISTICAL METHODS

### 2.5.1 Reliability Analysis

It is essentially impossible to devise a clinical measurement that is “perfectly” reliable. All instruments, their users (or raters), and in some cases the patients themselves produce some inherent level of inconsistency when attaining measurements. Consistency and reliability are governed by both the design of the system that attains measurements and the variability of the operators that use the measurement system.[185] A method of measurement is established by

training qualified users how to effectively apply a tool for attaining measures using a specific system (software and/or physical device). Ideally, any established method of measurement will provide readings that contain both the true value and some amount error due to variability contributed from the system and its users. Specific to this research, the method was comprised of the measurement system of the Acetabulator program and its users that collected its input. Variability arose from the users when extracting data from the CT scans during the masking, segmentation, and point selection on the AR (human error). Because the Acetabulator performs operations programmatically, it will have negligible levels of inconsistency in calculating measurements. One of the primary goals sought in the design intent of the Acetabulator's programming was to minimize sources of human error. Major sources of variability were eliminated by the program's ability to automatically locate bony landmarks used to establish the C.S. and select a patient specific set of points on the AR used to establish a best-fit plane.

To evaluate accuracy and reliability, a statistical analysis that estimated the amount of error attributed to our method was required. The term "accuracy" indicates how close measurements are to the actual target value. The Acetabulator provides a series of output plots displaying all automatically selected points. These plots are used to assure accuracy by visually inspecting if the foremost points were selected on the ASIS and PT to establish the APP C.S., and that the most distal lateral points on the AR were selected to establish the AX. The term "reliability" is used in statistical measures to describe how much of a measurement is a correct reading (the true value) and how much is attributed to error.[182,185,215] Reliability measures indicate the ability to detect true differences in measurements. The intraclass correlation coefficient (ICC) is widely accepted as a universal reliability index.[181,184] There are various forms of the ICC which can be used as a powerful form of evaluation in that it can reflect both

the degree of *consistency* as well as *agreement* among ratings and raters. Application of the ICC avoids a common shortcoming of other methods when assessing reliability. This pitfall occurs when a method of measurement produces results that are highly correlated, thus appearing reliable, but the measurements are not actually in agreement.[180,182,184,185,216]. Since the *exact* value of a measure can never be truly attained, the ICC serves as a means for estimating the reliability of measures (or ratings) in terms of the estimated variance inherent to the components associated with measuring the metric of interest.[180,182,184,185,217] In this case, the measures of interest are the angular outputs of the Acetabulator program, and the components contributing to the total variance are the differences arising from human error. For this application there is expected *random* variation between subjects (typical of any patient population), between raters, and within raters. As previously mentioned, crosschecking measures produced by the Acetabulator's algorithm using CAD software assured that no *systematic* error was being introduced by the program.

To qualify the method as reliable, a test-retest approach was employed. For assessing the reliability among multiple potential users, a group of targets needed to be measured by a sample of qualified users. To assess the ability of individuals to reliably and consistently reproduce measures using the method, the same users needed to repeat measurements on the same targets. The two measures of reliability required two separate ICC calculations: (1) The *intraobserver* ICC which measured reliability by estimating the variation within a typical single rater; (2) The *interobserver* ICC which measured reliability by estimating the variation amongst multiple different raters. It was of interest to assess the method for use as a universally applicable and effective tool. Therefore, it was assumed that the three raters used in this study (SH, ES, and RB) were selected from a larger population of any possible qualified users.[182] The application of a

two-way analysis of variance (ANOVA) model that accounted for *random* effects of both different users and subjects was appropriate to assess the reliability for a group of users in the calculation of the interobserver ICC.[177,180,181,217,218] To appropriately assess the ability of individual users to reliably produce (or reproduce) consistent results, the intraobserver ICC required a two-way *mixed* effects ANOVA model that treated the raters as fixed and the subjects as random effects.[180,182,184,218] The improper application of a one-way ANOVA model is commonly seen in the literature for the calculation of the intraobserver ICC.[184] All ICC calculations were made using commercially available software SPSS Statistics version 20.0.0 (IBM<sup>®</sup> Corp, Armonk, NY).

It is important to note that most reliability studies in the field of medicine use categorical data in the form of scores or classifications. In the case of categorical data, the appropriate statistical coefficient for the ICC would be the Kappa. The Kappa statistic has a much more liberal range of what is considered “in agreement” (e.g.- almost perfect  $\approx 0.81-1.00$ ).[179] This is because raters are forced to choose between two discrete levels of measurement (i.e.- categories) when borderline observations occur. Whereas for this study, the angular measurements were continuous and can hypothetically assume any fractional value between the degree increments. The appropriate statistical coefficient for the ICC in a study such as this is Cronbach’s alpha. Because the ratings are continuous, the interpretation of the ICC is more stringent (e.g.- almost perfect  $\approx 0.90-1.00$ ).[187] Because each application is different, there are no specific guidelines as to what indicates acceptable levels of agreement. Methods that use modern programmatic methods should probably be held to a higher standard.

There is no way to disentangle the sources of variation attributable to the masking, segmentation, and AR point selection process between various users. With no way to separate



these sources of variation, the random differences in angles produced by various raters are considered as relevant sources of error. The resulting ICCs can therefore be interpreted as measures of *absolute* agreement (not *just* correlation).[180,218,219] This agreement is representative of a single rating, or in this case an individual paired set of angular measures (e.g. radiographic).[218] Therefore, the intraobserver ICC can be viewed as a measure of the method's ability to reliability produce consistent results within a *single* typical user. The interobserver ICC can be interpreted as the method's ability to reliably produce absolute agreement amongst *multiple* users. Both ICCs are reliability indexes that can be interpreted as a ratio of the true measurement variance to the observed measurement variance (equation 2.1). [215]

$$Reliability (ICC) = \frac{True\ Variance}{True\ Variance + Error\ Variance} = \frac{True\ Variance}{Total\ Variance} \quad (2.1)$$

Thus, perfect agreement would yield an ICC=1, and poor agreement due to excessive variance attributable to error results in ICC values closer to zero. For this application, higher ICC values resulted from a combination of three factors: (1) Consistent masking and segmentation; (2) Consistent selection of points on the AR; (3) The impact that the Acetabulator's programmatic method has on minimizing variation via automated point selection.

By observing inter-and intraobserver ICCs yielded from a related study, a reasonable estimate ICC of 0.9 was made for planning our study.[172] This estimate assumed that the method of automatic point selection would be similar to, or better than, other methods that manually selected points on the AR. Our planned ICC estimate of 0.9 allowed the selection of an appropriate sample size of thirteen subjects ( $n=13$ ) using three raters ( $k=3$ ) for a desired 95% confidence interval ( $\alpha=0.05$ ) with a width of  $0.2^\circ$ . [177] The thirteen subjects were randomly selected from the main data set. The two trials were spaced at least two weeks apart and were

performed by three raters (SH, ES and RB) on all subjects. While each subject had two separate sets of angles for the left and right hips, they are not independent in the case of the full pelvis analysis. This is because both sets of measurements were based on the bilateral landmarks used to define the APP and establish the complete reference frame. Dependence of bilateral features made the selection of thirteen *subjects*, not thirteen *hips*, appropriate for the full pelvis reliability analysis. For the hemi-pelvis analyses, this resulted in a total of 26 independent measurement sets produced by each rater, for each of the trials. This was more than required but there was no extra “cost” to include all the resulting measurements because all calculations were made automatically using the Acetabulator. The two trials performed by the same users were used to calculate three intraobserver ICCs (one for each user). Both trials of all three users were used to calculate two interobserver ICCs (one for each trial). For evaluating the absolute agreement associated with the full pelvis analysis, inclination and anteversion were grouped by method and presented as overall ICCs for anatomic, radiographic and operative measures. Measures for the hemi-pelvis analysis were evaluated by their individual angular components.

Following previously suggested recommendations, an additional measure was also calculated in conjunction with the ICCs to give a “true” picture of the reliability.[185–187] For this specific application, the standard error of measurement (SEM) was used to compliment the ICC indices.[184,186,215,219] SEM uses the same units as the measurement to which it is applied (e.g.- degrees) and is intimately related to the unitless ICC. This made application of the SEM well suited to further clarify the results of this reliability analysis.[186,187,220] The interpretation of SEM depends on the type of reliability coefficient that is used in its computation. For the intraobserver ICC (test-retest), the SEM is indicative of the range of scores than can be expected on retesting. For the interobserver ICC, the SEM reflects the extent of

expected error in different raters' scores.[184] In general, the ICC is reflective of the ability for a testing method to reliably differentiate between measures, whereas the SEM quantifies the precision of the individual measures produced.[186,219] SEM is related to the ICC according to the following relationship:

$$SEM = SD_{measure}\sqrt{(1 - ICC)} \quad (2.2)$$

Typically the standard deviation ( $SD_{measure}$ ) is of the measure of interest that is being tested in the sample population. In this case, the measures were singular or paired angles of inclination and version describing the orientation of the acetabulum.

For this study, the performance of the instrument (overall method) was a combination of both the users whom collected the raw data and the Acetabulator which processed it. The Acetabulator's programmatic contribution to the "instrument" was its ability to calculate angles without bias or variability. As previously determined, the Acetabulator is not subject to random or systematic variability and will calculate angles of any magnitude over any possible range of values without bias. The users who directly extracted data from the CT scans did create sources of variability which would have appeared in the measurement outputs of the Acetabulator. Essentially, the SEM is an index that estimates the spacing needed between separate measurements to be considered *real* differences.[219] An estimated confidence interval can be created using the SEM for determining the minimum detectable difference (MDD) with a specified level of confidence. Using the SEM, a 95% CI was constructed using the following relationship:

$$MDD_{95} = 1.96 \times SEM \times \sqrt{n} \quad (2.3)$$

The multiplier of 1.96 is simply the  $z$ -score for a 95% CI of a normal distribution (which could be substituted to attain different CIs). The  $\sqrt{n}$  multiplier accounts for the additional uncertainty introduced by using  $n$  user's measurements or  $n$  trials.[186,187,215,220]

It was assumed that multiple users contributed *random* variance in measurement that was centered, and evenly distributed, around the true value. This held true even if a user, or users, produced some *systematic* variance. In other words, if an increasing number of measurements were made from an increasing population of users, it would be expected that the mean value for a single target would approach the *true* value. Therefore, if a reasonable estimate of an error interval was applied to the difference of two separate measures, it would be expected that zero would be within this interval (95% of the time). When the error interval contains the value zero, the difference between two measurements could be induced by error alone.[220]

For the full pelvis analysis, a single MDD for each measurement scheme was calculated as done with the ICC. Because inclination and anteversion have different expected values, the SD for inclination and version needed to be separated in each scheme. If not this would have incorrectly shown an increase in SD. The design of the test-retest experiment had three users test the same targets two times. Therefore, the SD of measures produced in both trial 1 and trial 2 for a single user were used in the calculation of the SEM for the intraobserver MDD according to the following equation:

$$SEM_{intra} = \frac{\frac{1}{2}(SD_{ver1} + SD_{ver2}) + \frac{1}{2}(SD_{inc1} + SD_{inc2})}{2} \times \sqrt{(1 - ICC_{intra})} \quad (2.4)$$

In equation 2.4 the SDs for version and inclination were calculated for each trial. For the interobserver MDD, the SEM was calculated in a similar fashion:

$$SEM_{inter} = \frac{\frac{1}{3}(SD_{ver1} + SD_{ver2} + SD_{ver2}) + \frac{1}{3}(SD_{inc1} + SD_{inc2} + +SD_{inc3})}{2} \times \sqrt{(1 - ICC_{inter})} \quad (2.5)$$

The SEM calculated in equation 2.4 for the intraobserver ICC was used to calculate the corresponding MDD using the equation:

$$MDD_{95} = 1.96 \times SEM_{intra} \times \sqrt{2} \quad (2.6)$$

The  $\sqrt{2}$  accounted for the additional uncertainty introduced by using two trials. The MDD for the interobserver ICC was attained according to the following calculation:

$$MDD_{95} = 1.96 \times SEM_{inter} \times \sqrt{3} \quad (2.7)$$

In the case of equation 2.7, the  $\sqrt{3}$  accounted for the additional uncertainty introduced by using three user's measurements.

Equations 2.6 and 2.7 can be explained in the context of a relevant example: Comparing pre-and post-op measures of acetabular orientation when performing a reorientational osteotomy procedure that did *not* affect the foremost locations of the PT and ASIS. If the calculated  $MDD_{95}$  was  $2^\circ$ , we could be 95% confident that an observed change of  $2^\circ$  (or larger) would be an actual difference in orientation and not a result of measurement error. The SEM and MDD calculations resulting from intraobserver analysis were indicators of the reliability achievable by individual users. Conversely, the calculations resulting from interobserver analysis were indicators of the reliability achievable by multiple users. The results for all measurement schemes were averaged between all three raters in the intraobserver study, and for both trials in the interobserver study. Both results are reflective of the method's overall level of reliability. However, because the method was evaluated as a tool, the least reliable indice was the performance limiting factor for any measurement scheme. In other words, if the interobserver MDD was lower than that of the intraobserver, it could only be stated that the actual MDD is that of the interobserver for that

particular measurement scheme. All SEM and MDD<sub>95</sub> calculations were made using Excel<sup>®</sup> 2007 (Microsoft<sup>®</sup> Corporation, Redmond, WA).

### **2.5.2 Population Data Testing**

Unpaired t-tests ( $\alpha=0.05$ ) were used to evaluate the differences between male ( $n=176$  hips) and female ( $n=224$  hips) for all measures of inclination and version. All t-tests were performed using JMP<sup>®</sup> Pro 10.0.0 (SAS<sup>®</sup> Institute Inc, Cary, NC) statistical software. Typically, any measure of acetabular orientation outside of two SD from population mean is considered either questionable or abnormal.[10,41,43,44,64,110,119] Accordingly, the results for all measures were shown with any readings falling outside of two SD noted. Because anatomic anteversion and radiographic inclination are respectively measured in axial and frontal planes (pure abduction and anteversion), the subjects displaying the largest and smallest values for both were highlighted. Comparisons between the full and hemi-pelvis analyses were made using radiographic measures because the same measurement scheme was used. The difference between the orientation of the left and right acetabulum was also examined. It was expected that in a large patient population the overall difference between any bilateral measures would be insignificant.[90,96,198] Therefore, the inpatient bilateral differences were described by plotting by the frequency of measurable discrepancies using histograms. Any difference larger than one SD from the population mean was reported.

### **3 RESULTS**

An average of 31 points were selected on each AR (*range- 25 to 40 points*). A total of 18 points, on 18 different acetabulums, were detected as out-of-bounds at the AIIS-to-AR margin and dropped. The average R-squared value for the least-squares plane fit to the AR was 0.956. This R-squared value reflects the normal curvature of the AR and should not be interpreted as a typical goodness of fit indicator. A total of 58 acetabulums had either an osteophyte or an ossified section of labrum that needed to be manually removed. Three of these appeared to be minor forms OS acetabuli, where a small fragment detached at the anterior column.

#### **3.1 RELIABILITY STUDY RESULTS**

##### **3.1.1 Full Pelvis**

By using programmatic methods to automatically select points establishing the C.S. and AX, the results for both the inter-and intraobserver analysis yielded nearly perfect agreement (i.e.- ICC = 1) for the full pelvis measures (Table 3.1 & Table 3.2). This can be attributed to the removal of the major sources of human error arising from manual point selection. Although minute, the majority of the observed error that remained was from the two points flanking the notch. A slight amount of AR was either included or excluded depending on the locations of these manually selected points. This occasionally resulted in a different number of points being selected on the same AR. As observed in Figure 2.22, the addition or subtraction of a single point will cause an expected commensurate change in AX orientation of approximately 0.25°. This observation agrees with the results of the reliability study. For all 26 acetabulums measured twice, the average number of points selected on each AR for rater SH yielded 30.4 points, 30.7 points for rater ES, and 29.7 points for RB. The average linear variation in distance between all

three raters for point locations selected on the AR was 5.6mm for the superior point (*max- 15.7mm*), 3.2mm for the posterior point (*max- 10.1mm*), and 2.0mm for the anterior point (*max- 9.8mm*). On average, the selection of points was within the expected and acceptable range.

**Table 3.1- Full Pelvis Interobserver Reliability**

Measure	Anatomic	Radiographic	Operative
<b>Trial 1</b>	0.9998 [95% CI=0.9996, 0.9999]	0.9998 [95% CI=0.9997, 0.9999]	0.9995 [95% CI=0.9991, 0.9997]
<b>Trial 2</b>	0.9998 [95% CI=0.9997, 0.9999]	0.9998 [95% CI=0.9998, 0.9999]	0.9996 [95% CI=0.9992, 0.9998]

*\* All results for the estimated reliability of a single measurement*

**Table 3.2- Full Pelvis Intraobserver Reliability**

Measure	Anatomic	Radiographic	Operative
<b>SH</b>	0.9999 [95% CI=0.9998, 0.9999]	0.9999 [95% CI=0.9998, 0.9999]	0.9996 [95% CI=0.9994, 0.9998]
<b>ES</b>	0.9999 [95% CI=0.9999, 1.0000]	0.9999 [95% CI=0.9999, 1.0000]	0.9998 [95% CI=0.9996, 0.9999]
<b>RB</b>	0.9999 [95% CI=0.9998, 1.0000]	0.9998 [95% CI=0.9996, 0.9999]	0.9997 [95% CI=0.9995, 0.9998]

*\* All results for the estimated reliability of a single measurement*

The MDD was used to determine the least accurate indice, which was the performance limiting factor. Because the MDD is directly related to the ICC, the results from Table 3.1 and Table 3.2 respectively correspond with Table 3.3 and Table 3.4. Therefore, the interobserver variability from different users was the performance limiting factor for all measurement schemes. Because the desired points/targets were known (e.g.- distal lateral points on the AR), and were observed to be consistently selected on all output plots, it was established that the Acetabulator was *both* reliable and accurate. The highest level of accuracy that could be achieved when using the Acetabulator with the data collection method was 0.29° for anatomic measures, 0.26° for radiographic, and 0.55° for operative. To update the previous example of pre-and post-op measures of acetabular orientation when performing a reorientational osteotomy: If one were to measure acetabular orientation using this method, they could be 95% confident that an observed change of 0.26° (or larger) would be an actual difference in orientation using radiographic angles and not a result of measurement error. This again assumes that the foremost



locations of the PT and ASIS were unchanged (e.g.- spherical type osteotomy). The results for all three measurement schemes displayed high levels of reliability with marked improvement compared to previously mentioned 2-D measures (Table 1.7 & Table 1.8).[95,112,126,165,167] Because the automatically selected points/features were visually inspected on a series of plots, it was also confirmed that the most appropriate target points were accurately selected.

**Table 3.3- Full Pelvis Interobserver Minimum Detectable Difference**

Measure	Anatomic	Radiographic	Operative
<b>Trial 1</b>	0.31°	0.27°	0.59°
<b>Trial 2</b>	0.27°	0.24°	0.51°
<b>Average</b>	0.29°	0.26°	0.55°

*\* All results for the estimated accuracy of a single measurement*

**Table 3.4- Full Pelvis Intraobserver Minimum Detectable Difference**

Measure	Anatomic	Radiographic	Operative
<b>SH</b>	0.20°	0.18°	0.39°
<b>ES</b>	0.13°	0.12°	0.31°
<b>RB</b>	0.16°	0.24°	0.36°
<b>Average</b>	0.16°	0.18°	0.36°

*\* All results for the estimated accuracy of a single measurement*

### 3.1.2 Hemi-Pelvis

The analysis of the hemi-pelvis measures did not produce levels of reliability as high as the full pelvis (Table 3.5 & Table 3.6). However, the overall results can be considered good to excellent, on par or better than standard 2-D indices (Table 1.7 & Table 1.8), and were acceptable for performing the required analyses. It was discovered that a small fraction of the population lacked an extended ischial spine prominence. In these cases, point selection on the ischial spine was inconsistent, which directly impacted the orientation of the sagittal plane. One of the randomly selected subjects in the reliability study had a deficient ischial spine, which significantly contributed to the amount of measured variability. The lower performance can also

be partially attributed to the direct dependence of the hemi-pelvis C.S. on manually selected points. The sagittal plane was established using the centroid of the *entire* point cloud selected on the interior face of the pubic tubercle. This is essentially the same as manually selecting a point, and may have been less accurate than selecting a single point. The hemi-pelvis C.S. that was previously explored established the sagittal plane directly from the interior face of the tubercle. Therefore, the original instructions given to the raters was to select the *flat* portion of the face, and not the central region or the entire face. The other manually selected point that could have had a minor effect on the measures of the true pelvic region, was the posterior point flanking the acetabular notch (Figure 2.30). This posterior point directly formed the cutoff vector and therefore may have slightly shifted the points selected on the interior frame of the obturator.

**Table 3.5- Hemi-Pelvis Interobserver Reliability**

Measure	Acetabular Version	Acetabular Inclination	AX-to-TPP Version	AX-to-TPP Inclination	AX-to-FPP Version	AX-to-FPP Inclination
<b>Trial 1</b>	0.946 [95%CI=0.900,0.974]	0.978 [95%CI=0.959,0.990]	0.939 [95%CI=0.883,0.971]	0.965 [95%CI=0.934,0.983]	0.989 [95%CI=0.979,0.995]	0.965 [95%CI=0.934,0.983]
<b>Trial 2</b>	0.980 [95%CI=0.960,0.991]	0.992 [95%CI=0.985,0.996]	0.961 [95%CI=0.926,0.981]	0.961 [95%CI=0.927,0.981]	0.990 [95%CI=0.980,0.995]	0.948 [95%CI=0.898,0.975]

*\* All results for the estimated reliability of a single measurement*

**Table 3.6- Hemi-Pelvis Intraobserver Reliability**

Measure	Acetabular Version	Acetabular Inclination	AX-to-TPP Version	AX-to-TPP Inclination	AX-to-FPP Version	AX-to-FPP Inclination
<b>SH</b>	0.804 [95%CI=0.613,0.906]	0.924 [95%CI=0.840,0.965]	0.900 [95%CI=0.789,0.954]	0.956 [95%CI=0.905,0.980]	0.987 [95%CI=0.971,0.994]	0.982 [95%CI=0.949,0.992]
<b>ES</b>	0.937 [95%CI=0.865,0.972]	0.963 [95%CI=0.919,0.983]	0.958 [95%CI=0.910,0.981]	0.987 [95%CI=0.971,0.994]	0.988 [95%CI=0.973,0.995]	0.933 [95%CI=0.856,0.969]
<b>RB</b>	0.913 [95%CI=0.816,0.960]	0.930 [95%CI=0.850,0.968]	0.947 [95%CI=0.887,0.976]	0.979 [95%CI=0.954,0.991]	0.996 [95%CI=0.991,0.998]	0.963 [95%CI=0.919,0.983]

*\* All results for the estimated reliability of a single measurement*

It is intuitive to expect that multiple users will introduce the most variability to any repeated measure. It was therefore somewhat surprising to see that the performance limiting indices are mixed between inter-and intraobserver MDD for the hemi-pelvis (Table 3.7 & Table 3.8). This can be partially attributed to the poor internal consistency of rater SH. The accuracy

estimated for hemi-pelvis measures ranged from about 2.5 to 6 degrees, whereas the full pelvis measures all achieved levels less than a degree.

**Table 3.7- Hemi-Pelvis Interobserver Minimum Detectable Difference**

Measure	Acetabular Version	Acetabular Inclination	AX-TPP Version	AX-TPP Inclination	AX-FPP Version	AX-FPP Inclination
<b>Trial 1</b>	4.55°	2.87°	2.78°	4.73°	2.89°	5.59°
<b>Trial 2</b>	3.58°	1.82°	2.33°	5.08°	2.47°	6.86°
<b>Average</b>	4.07°	2.34°	2.56°	4.91°	2.68°	6.23°

\* All results for the estimated accuracy of a single measurement

**Table 3.8- Hemi-Pelvis Intraobserver Minimum Detectable Difference**

Measure	Acetabular Version	Acetabular Inclination	AX-TPP Version	AX-TPP Inclination	AX-FPP Version	AX-FPP Inclination
<b>SH</b>	7.73°	4.37°	2.91°	4.47°	2.22°	3.29°
<b>ES</b>	4.77°	3.14°	1.90°	2.35°	2.22°	6.58°
<b>RB</b>	5.47°	4.35°	2.25°	2.99°	1.29°	4.52°
<b>Average</b>	5.99°	3.95°	2.35°	3.27°	1.91°	4.80°

\* All results for the estimated accuracy of a single measurement

### 3.2 FULL PELVIS ANALYSIS RESULTS

Significant differences between genders were observed in anteversion for all measurement schemes ( $p < 0.0001$ ). There was also a significant difference between male and female anatomic inclination ( $p < 0.002$ ) (Table 3.9). Because significant differences were observed between genders in overall *anatomic* orientation, and because it is the proper measurement scheme for this type of study [214], graphical displays of the results for inclination and anteversion are respectively are presented in Figure 3.1 and Figure 3.2.

**Table 3.9- Results For Full Pelvis Measures**

Group	Anatomic		Radiographic		Operative	
	Anteversion <sup>†</sup>	Inclination <sup>††</sup>	Anteversion <sup>†</sup>	Inclination	Anteversion <sup>†</sup>	Inclination
<b>Male</b>	21.5°±6.1°	55.7°±3.9°	17.5°±5.0°	53.6°±4.1°	28.0°±7.6°	49.9°±4.1°
<b>Female</b>	24.7°±6.6°	57.1°±4.5°	20.5°±5.8°	54.3°±4.5°	32.6°±8.8°	49.2°±4.2°
<b>Total</b>	23.2°±6.6°	56.5°±4.3°	19.2°±5.6°	54.0°±4.3°	30.6°±8.6°	49.5°±4.2°
<b>Range</b>	2.3° to 41.0°	44.1° to 68.5°	1.8° to 34.9°	41.6° to 67.2°	3.0° to 54.2°	37.9° to 62.9°

Statistically significant differences between genders <sup>†</sup> $p < 0.0001$  and <sup>††</sup> $p < 0.002$

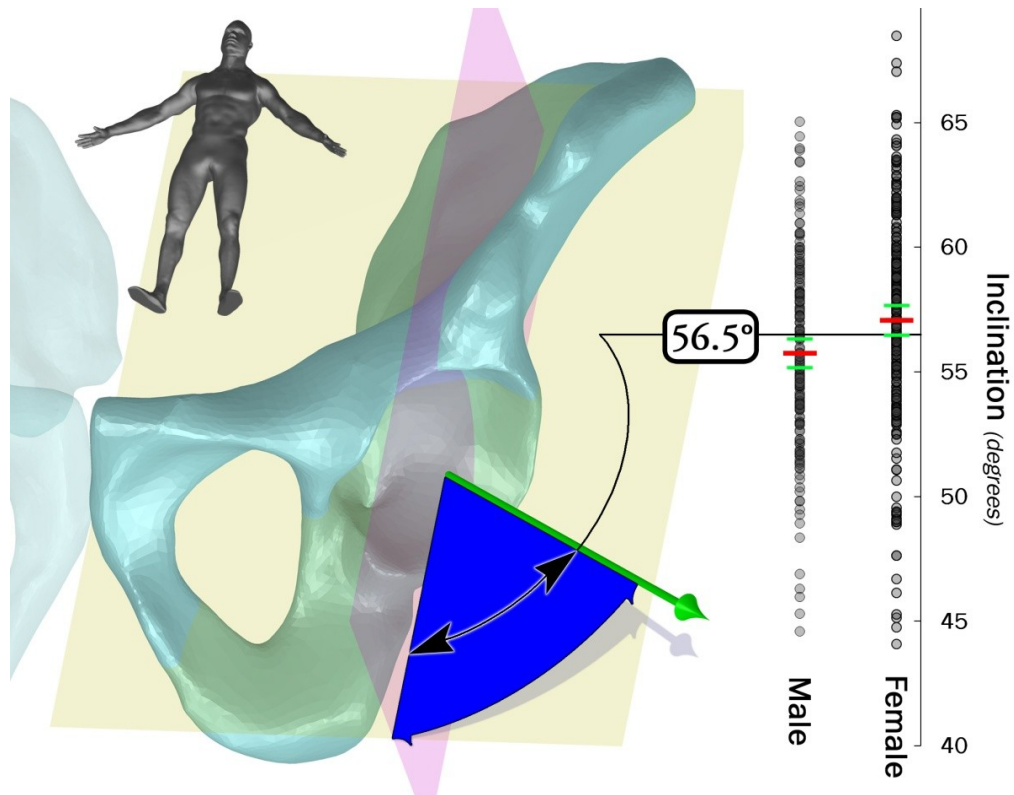


**Figure 3.1-** Mean anatomic inclination depicted on left acetabulum for entire population ( $56.5^\circ \pm 4.3^\circ$ ). Scatter plot displaying the differences between male and female mean anteversion (*red bars*) with 95% confidence interval of the mean (*green bars*).

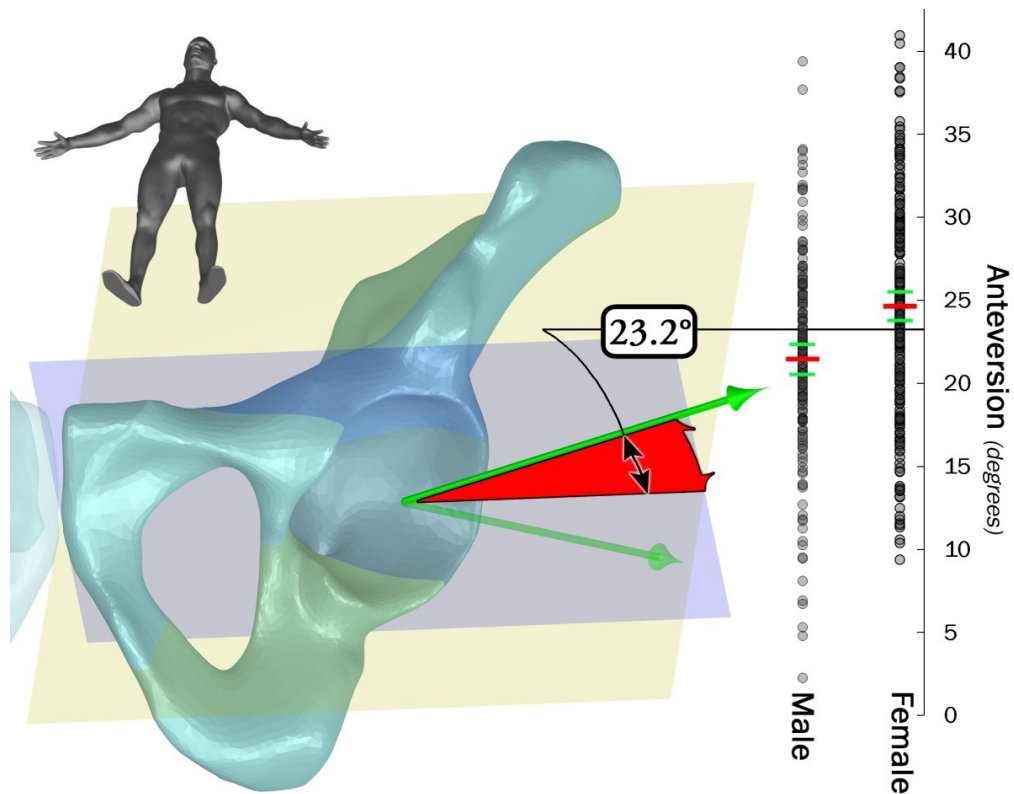


**Figure 3.2-** Mean anatomic anteversion depicted on left acetabulum for entire population ( $23.2^\circ \pm 6.6^\circ$ ). Scatter plot displaying the differences between male and female mean anteversion (*red bars*) with 95% confidence interval of the mean (*green bars*).

Inclination and anteversion for all measurement schemes were evenly distributed about their respective means. Overall, very few subjects exhibited measures outside of  $\pm 2$  SD (Figure 3.6 thru Figure 3.7). This is reflective of the normal subjects in the sample population and both the accuracy and reliability achieved in the measures. For *radiographic inclination*, 22 acetabulums (5.5%) in 18 subjects (9% of the population) were measured outside of two SD from the mean (Figure 3.3). Sixteen acetabulums in six females and six males had lower values of inclination, indicating possible excessive superolateral coverage. The remaining six acetabulums, in five females and one male, had excessive inclination angles, indicative of deficient superolateral coverage. Four (3 male/1 female) out of the twelve subjects with notably lower inclination angles had bilateral involvement. Conversely, all of the observed subjects with excessive inclination only had unilateral involvement. There were no retroverted acetabuli observed for any of the anteversion measures ( $\text{angle} < 0^\circ$ ). This again speaks to the normality of the population. Nineteen acetabulums (4.8%), in 14 subjects (7% of the population), were measured outside of two SD from the mean *anatomic anteversion* (Figure 3.6). Five males and one female had notably small anteversion angles, with three out of the five males having bilateral involvement. Interestingly, seven out of the eight subjects with notable excessive anteversion were female. Of these eight, one female and one male had excessive anteversion of both acetabulums.

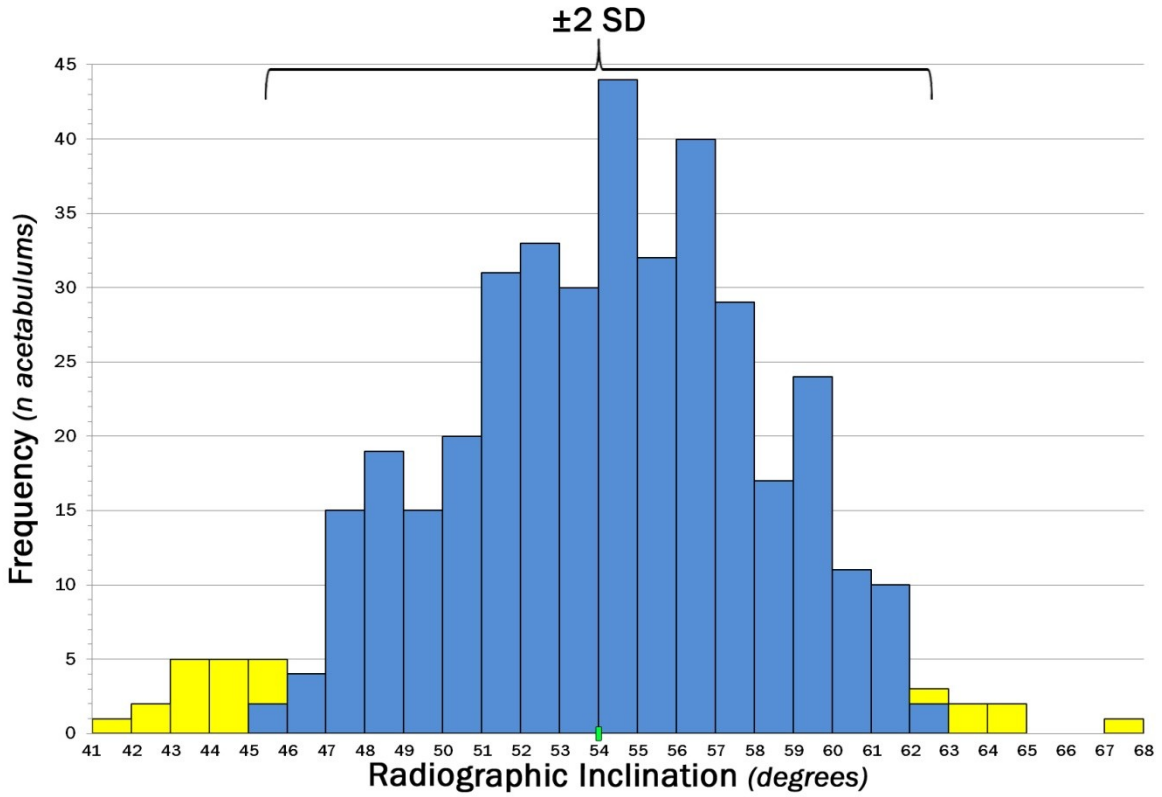


Figure 3.3- Population results for radiographic inclination, with  $n=22$  acetabulums falling outside of  $\pm 2$  SD (yellow).

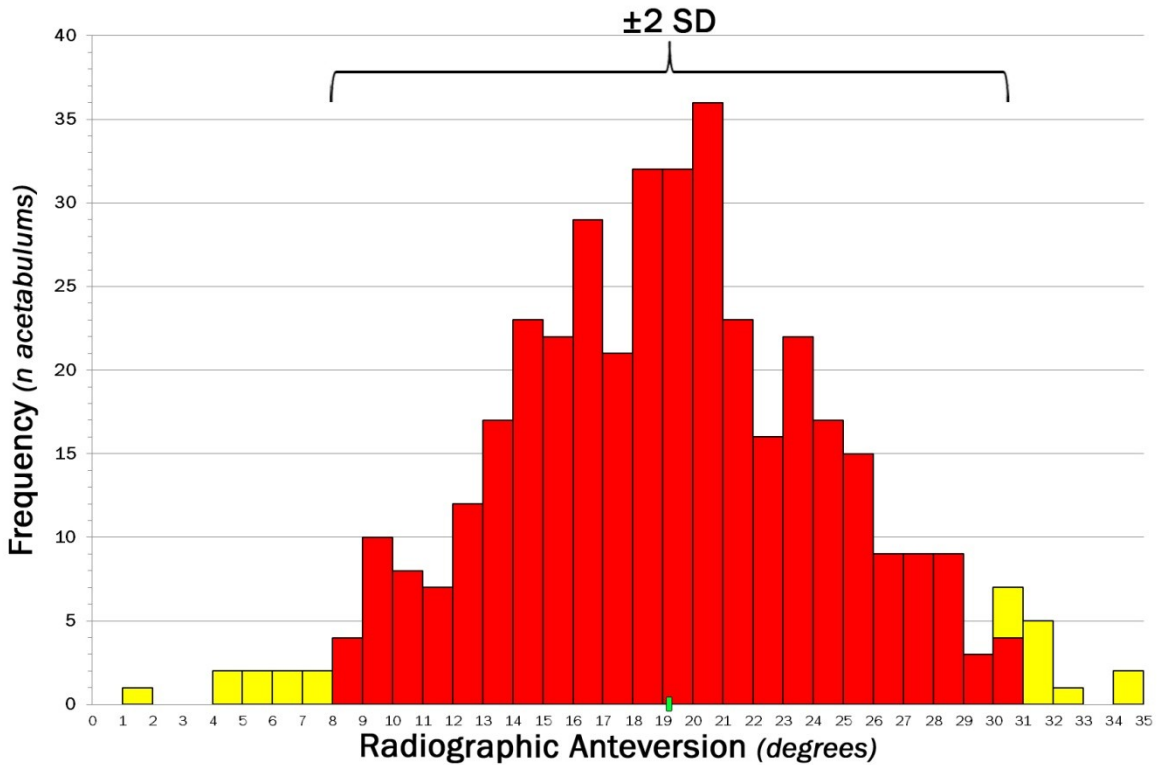


Figure 3.4- Population results for radiographic anteversion, with  $n=20$  acetabulums falling outside of  $\pm 2$  SD (yellow).

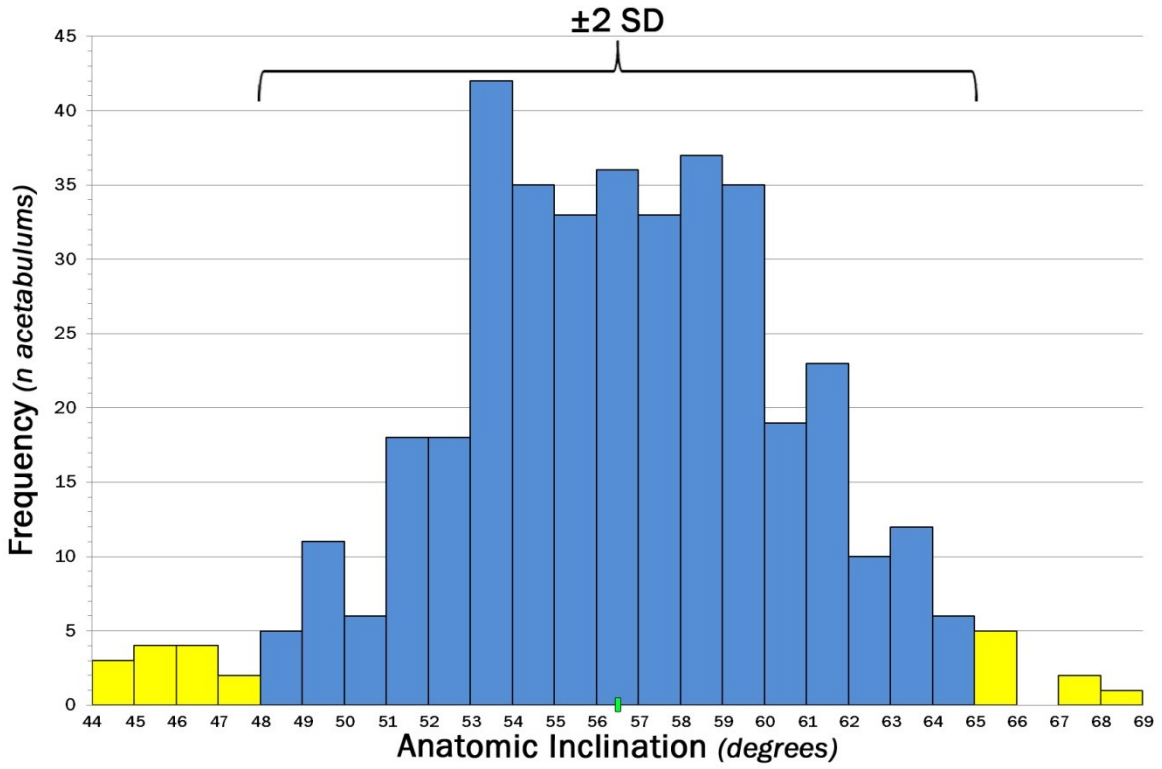


Figure 3.5- Population results for anatomic inclination, with  $n=21$  acetabulums falling outside of  $\pm 2$  SD (yellow).

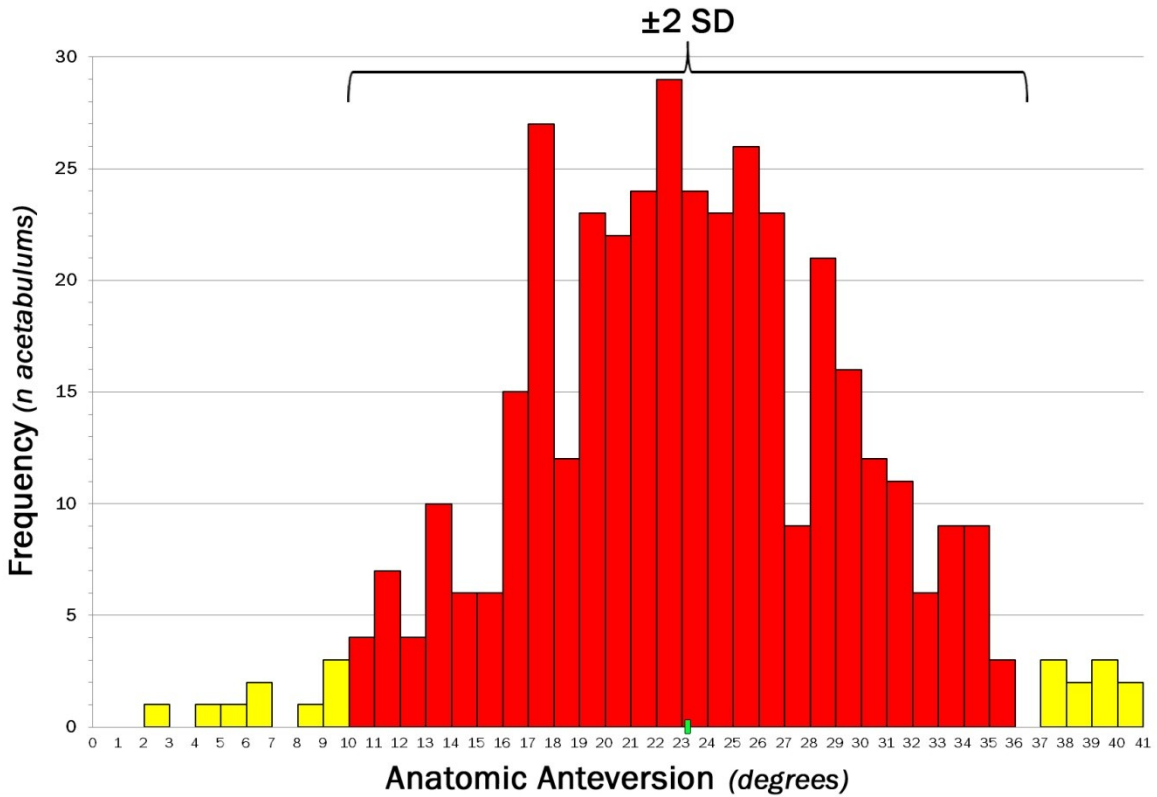


Figure 3.6- Population results for anatomic anteversion, with  $n=19$  acetabulums falling outside of  $\pm 2$  SD (yellow).

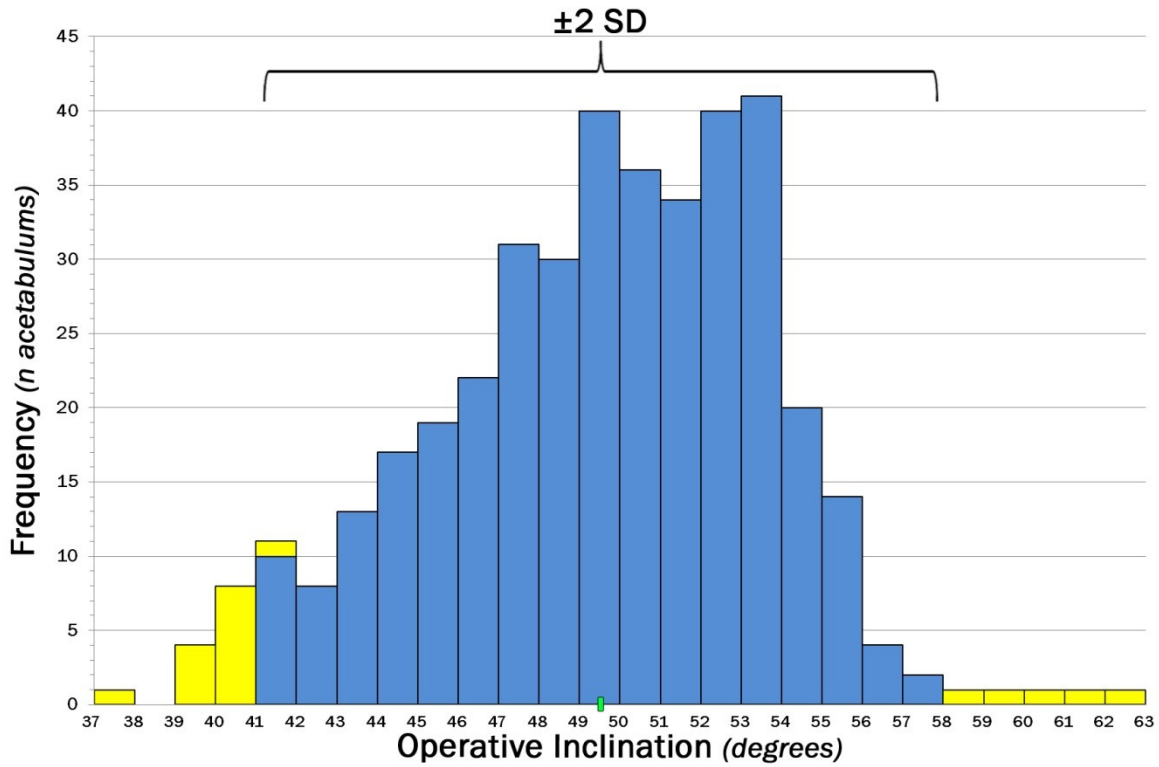


Figure 3.7- Population results for operative inclination, with  $n=19$  acetabulums falling outside of  $\pm 2$  SD (yellow).

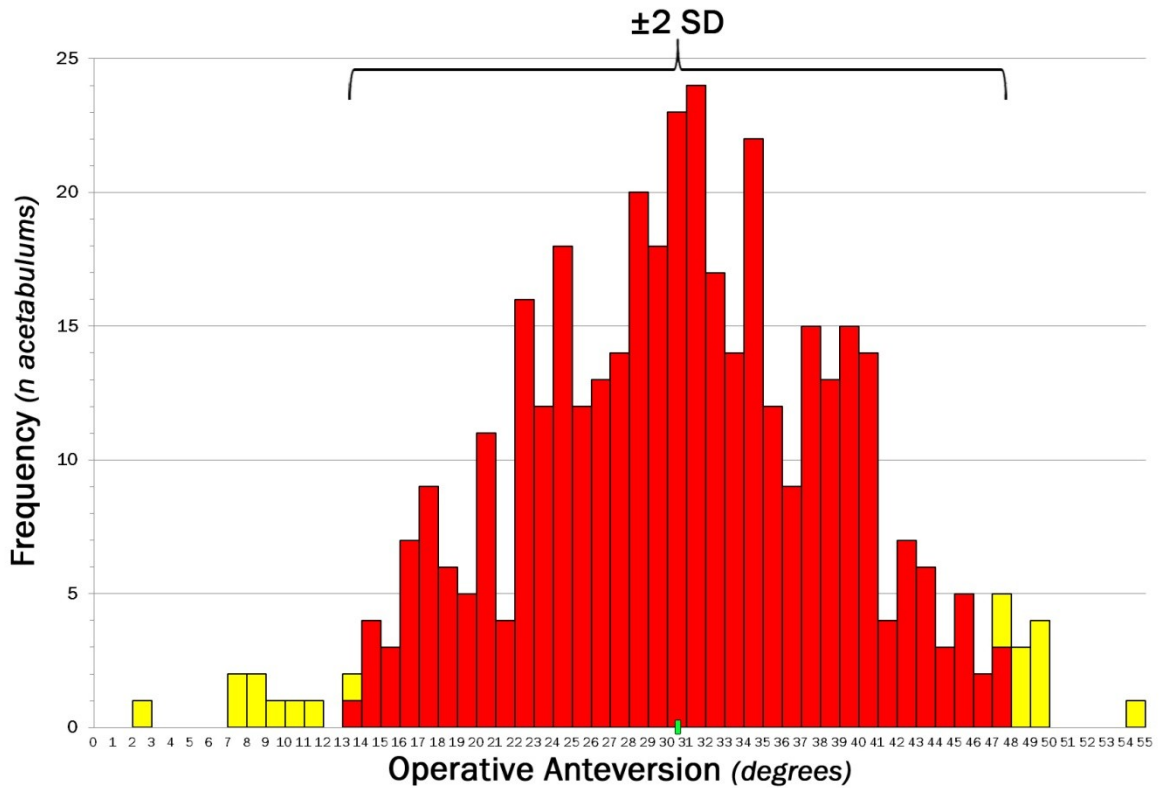
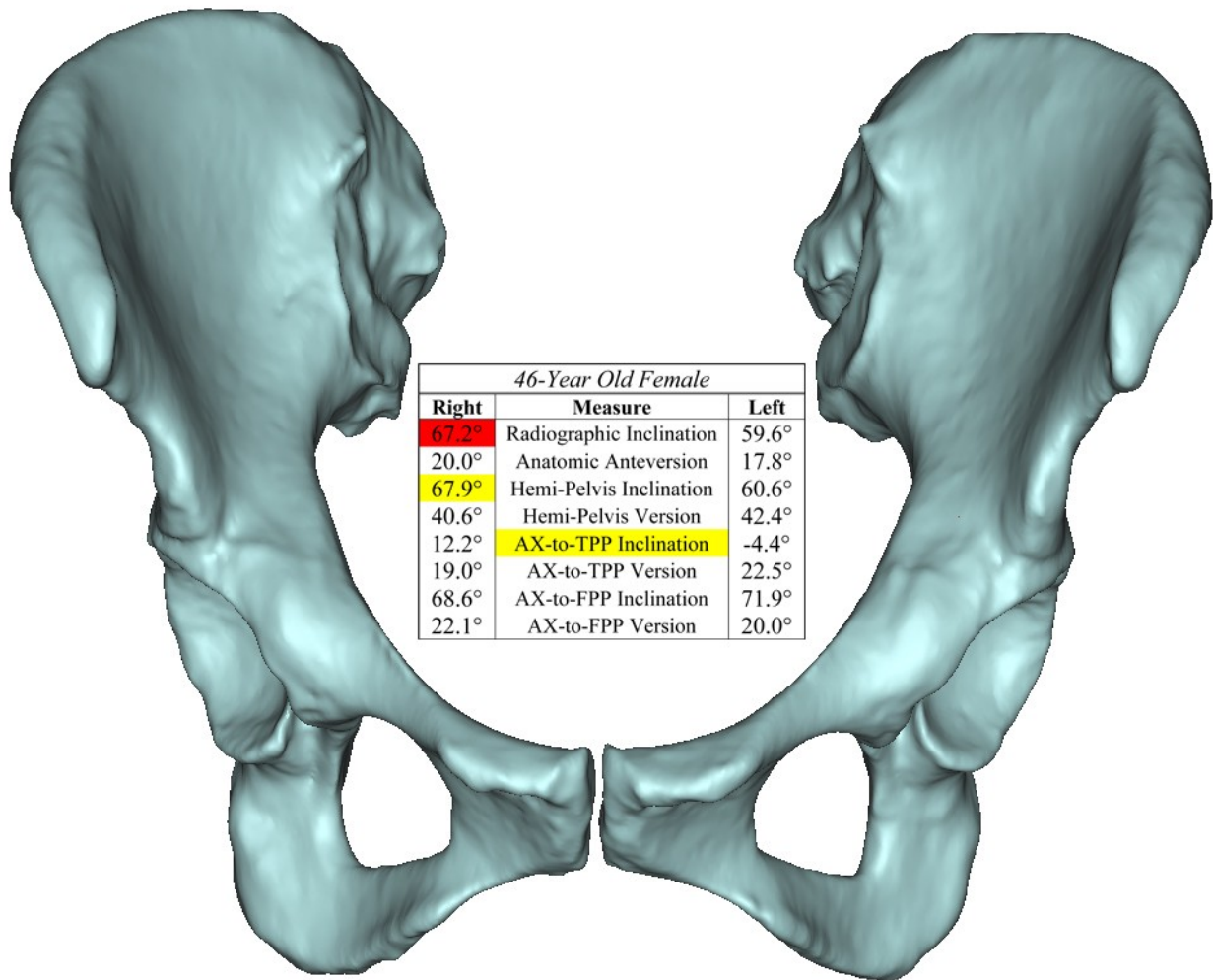


Figure 3.8- Population results for operative anteversion, with  $n=19$  acetabulums falling outside of  $\pm 2$  SD (yellow).



Two subjects were observed to have measures of both anatomic anteversion and radiographic inclination outside of the two SD limit. A 52-year old male had notably increased bilateral anteversion (*left-39.4°/right-37.7°*) and a small amount of unilateral inclination (*left-45.3°*). A 66-year old female was observed to have unilaterally small levels of both inclination (44.8°) and anteversion (9.4°) on the left side. The subjects with maximum and minimum values for anatomic anteversion and radiographic inclination were outside of 2 SD for corresponding measures in all schemes. The most inclined acetabulum was measured at 67.2° in a 46-year old female (Figure 3.9). The acetabulum with the least amount of inclination, at 41.6°, occurred in a 45-year old male, who's contralateral side was also outside of 2 SD (44.8°) (Figure 3.10). Both subjects with the most extreme values for anteversion had bilateral acetabulums outside of two SD (in the same direction). A 58-year old male had the least amount of anteversion on the left side 2.3°, and a notably small amount on the right 6.9° (Figure 3.11). The most anteverted acetabulums were both in a 52-year old female with the left side measured at 41.0°, and the right at 40.5° (Figure 3.12).

Note- When viewing the figures for the subjects interest, all measures appearing outside of the normal range are both denoted in the caption and highlighted in the table. If an observation for a measure on a single acetabulum was outside of  $\pm 2$  SD it appears highlighted in **yellow** in the column corresponding to the respective side. If an observation for a bilateral difference was outside of  $\pm 1$  SD, the center column denoting the measure is highlighted in **yellow**. If either a single measure or a bilateral difference is highlighted in **red**, they were observed to have the most maximal or minimal value(s) observed for the entire cohort.



**Figure 3.9-** 46-year old female subject of interest observed to have the most radiographic inclination on the right side. This subject also had notably large hemi-pelvis inclination on the right side and a bilateral discrepancy in AX-to-TPP inclination.

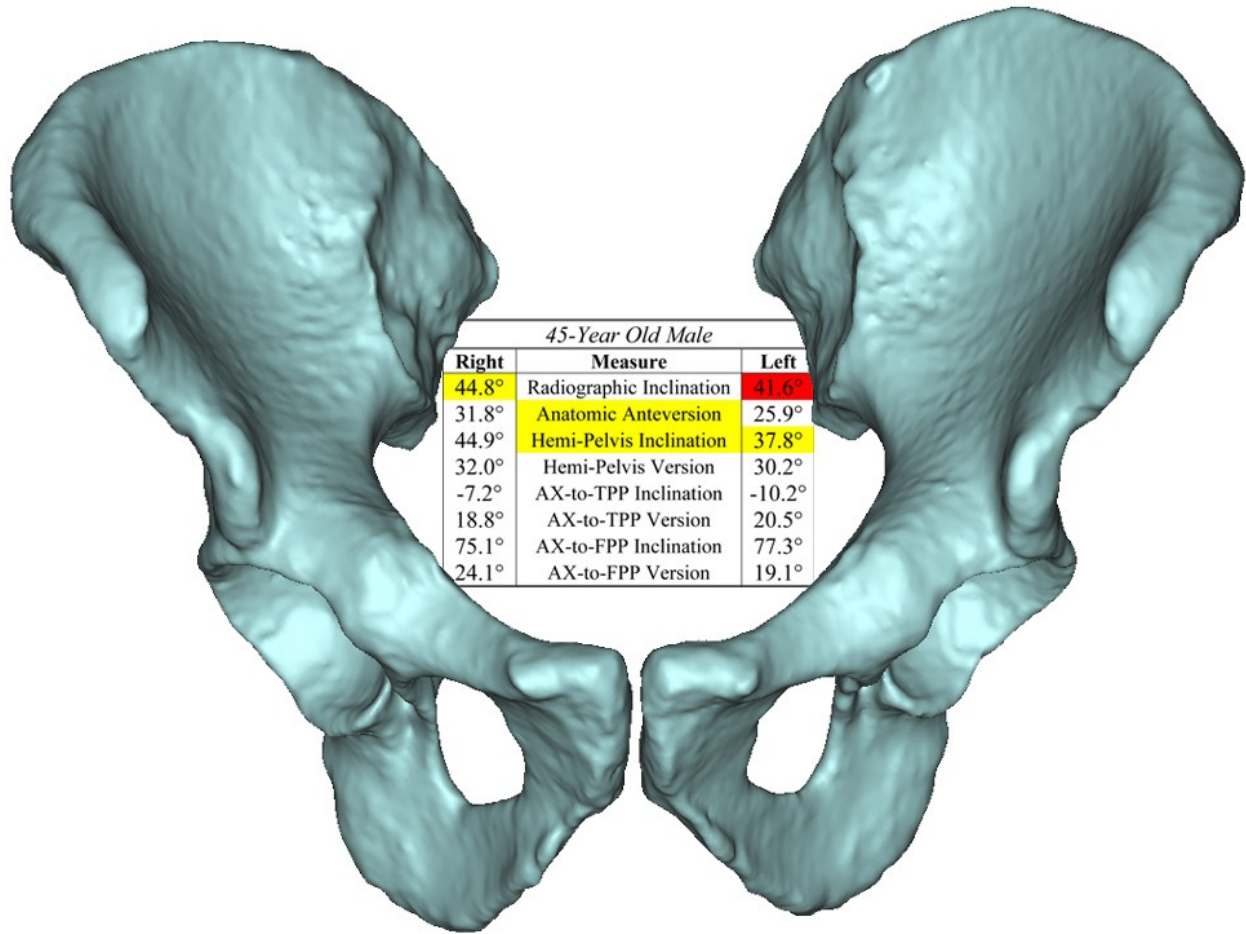


**Figure 3.10-** 45-year old male subject of interest observed to have the least radiographic inclination on the left side and a notably low reading on the right side. This subject also had a notable bilateral difference in hemi-pelvis inclination with a small value on the left side. A notable bilateral discrepancy in anatomic anteversion was also measured.

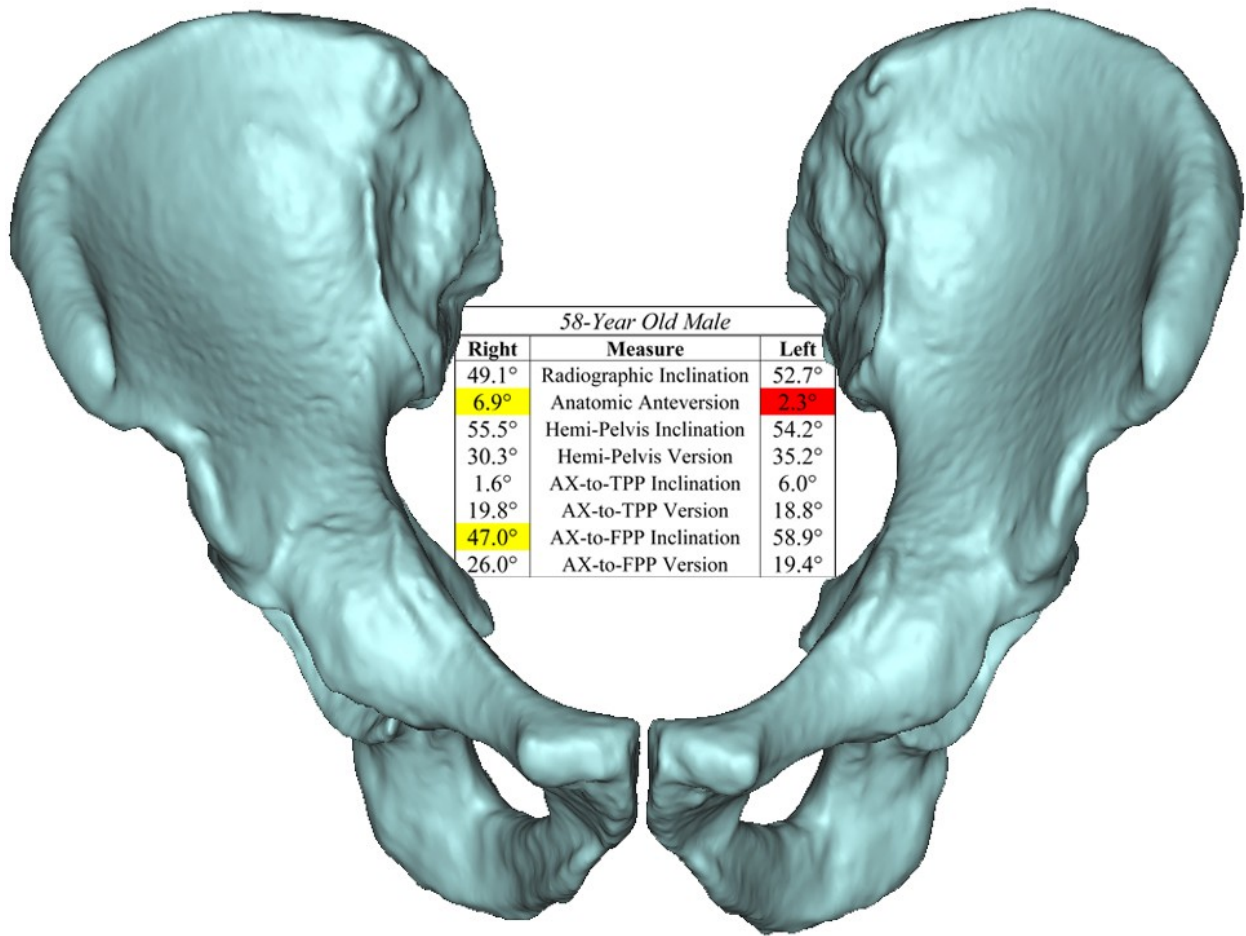


**Figure 3.11-** 58-year old male subject of interest observed to have the least anatomic anteversion on the left side and a notably low reading on the right side. This subject also had notably small hemi-pelvis inclination on the right.

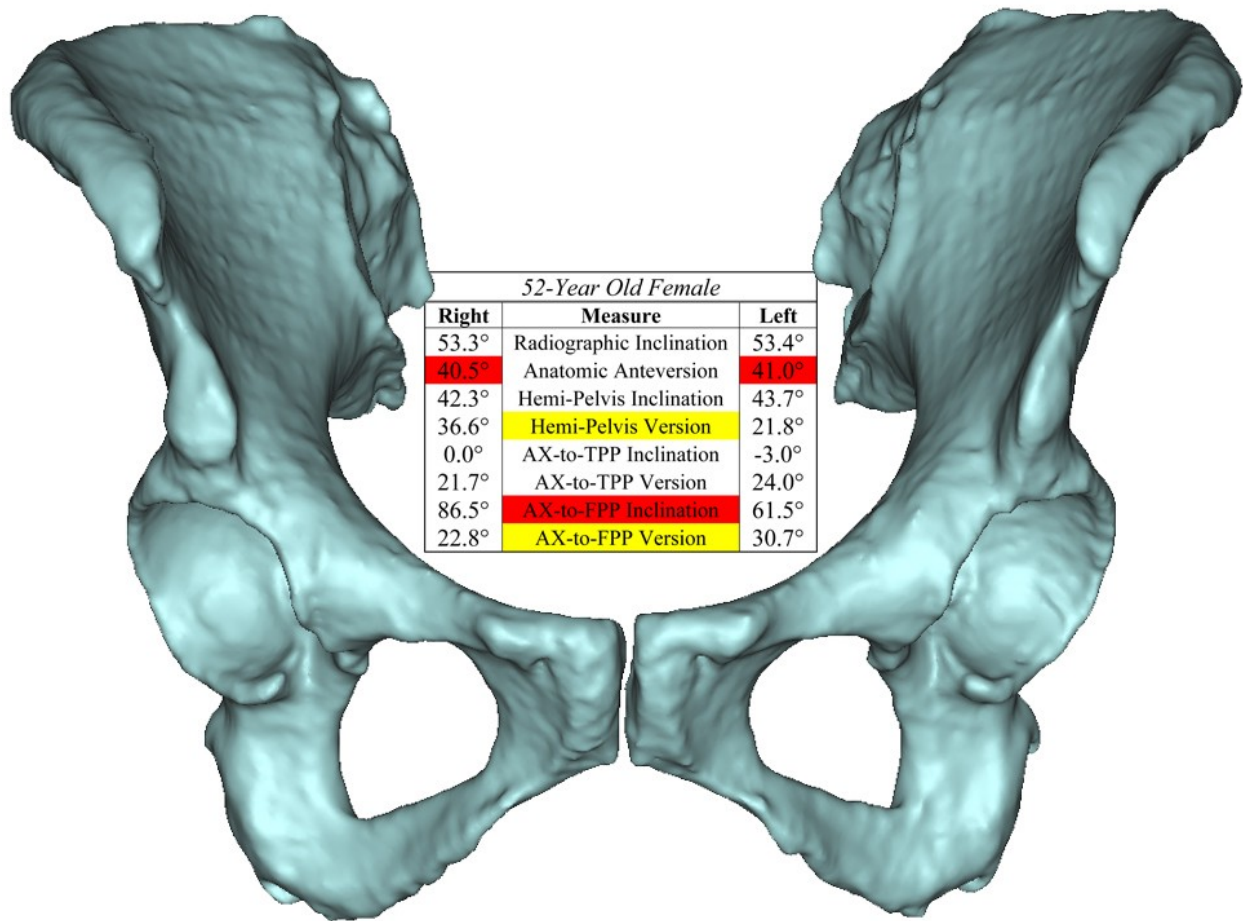


**Figure 3.12-** 52-year old female subject of interest observed to have the most anatomic anteversion on both the left and right side. This subject also had the largest bilateral discrepancy in AX-to-FPP inclination, and notable differences in hemi-pelvis version and AX-to-FPP version.

Bilateral differences for all measures of anteversion and inclination were evenly distributed around 0° (left *minus* right). The majority of subjects with bilateral discrepancies larger than one SD, displayed this difference in all measurement schemes. Radiographic inclination had 11.0% ( $n=22$ ) of the subjects with a difference larger than 4.3° ( $max=12.0^\circ$ ) (Figure 3.13). Radiographic anteversion showed that 12.0% ( $n=24$ ) of the population had bilateral differences larger than 5.6° ( $max=9.3^\circ$ ) (Figure 3.14). Discrepancies in anatomic inclination larger than 4.3° were observed 6.5% ( $n=13$ ) of the subjects ( $max=10.9^\circ$ ) (Figure

3.15). For anatomic anteversion, 12.5% ( $n=25$ ) of the population displayed differences larger than  $6.6^\circ$  ( $max=12.1^\circ$ ) (Figure 3.16). Finally, operative measures showed 6.0% ( $n=12$ ) and 20.0% ( $n=40$ ) of the population to have respective bilateral differences for inclination and anteversion larger than  $4.2^\circ$  ( $max=10.1^\circ$ ) (Figure 3.17) and  $8.6^\circ$  ( $max=13.7^\circ$ ) (Figure 3.18).

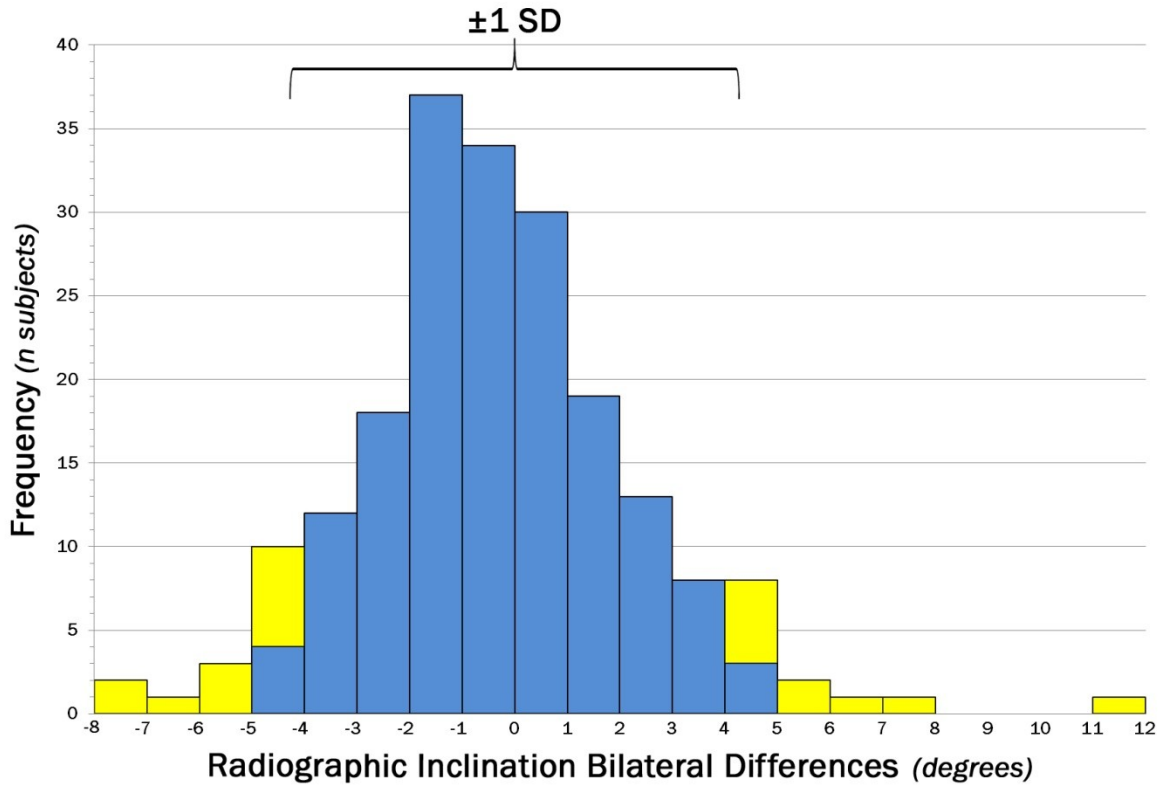


Figure 3.13- Bilateral differences in radiographic inclination,  $n=22$  subjects displayed differences larger than  $\pm 1$  SD (yellow).

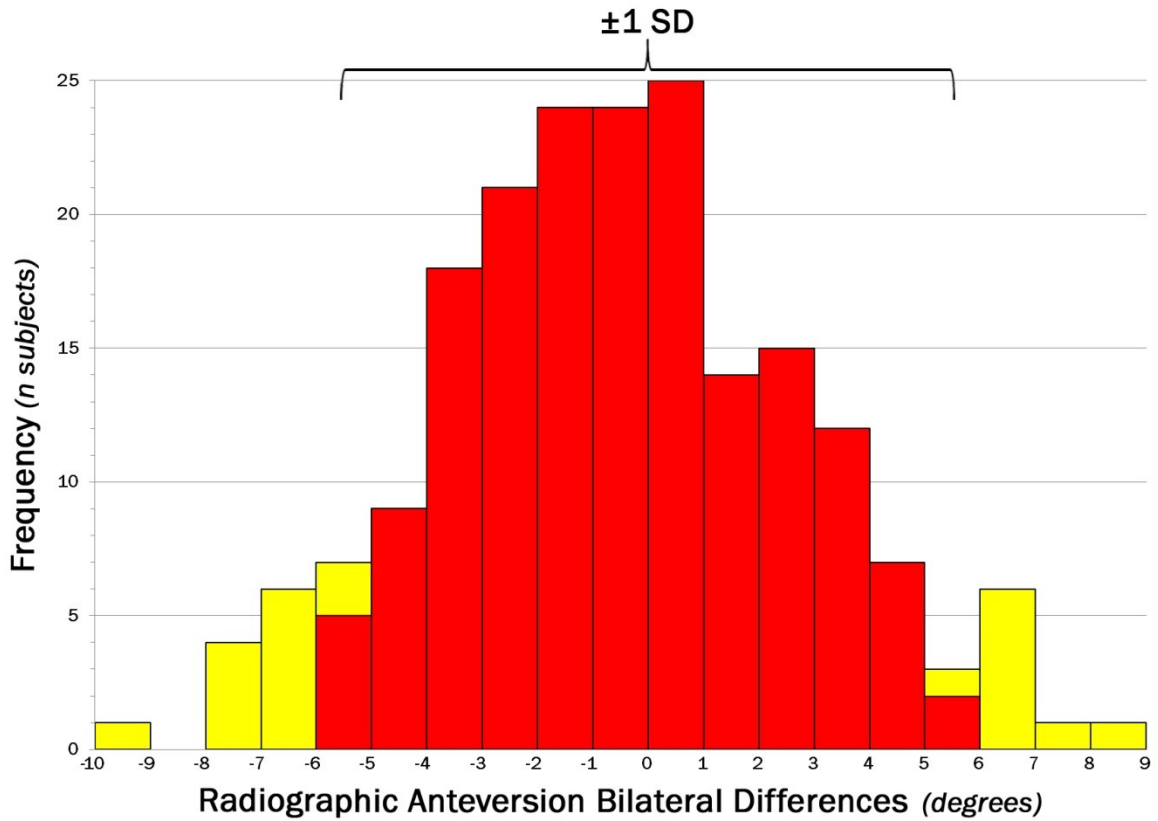


Figure 3.14- Bilateral differences in radiographic anteversion,  $n=24$  subjects displayed differences larger than  $\pm 1$  SD (yellow).

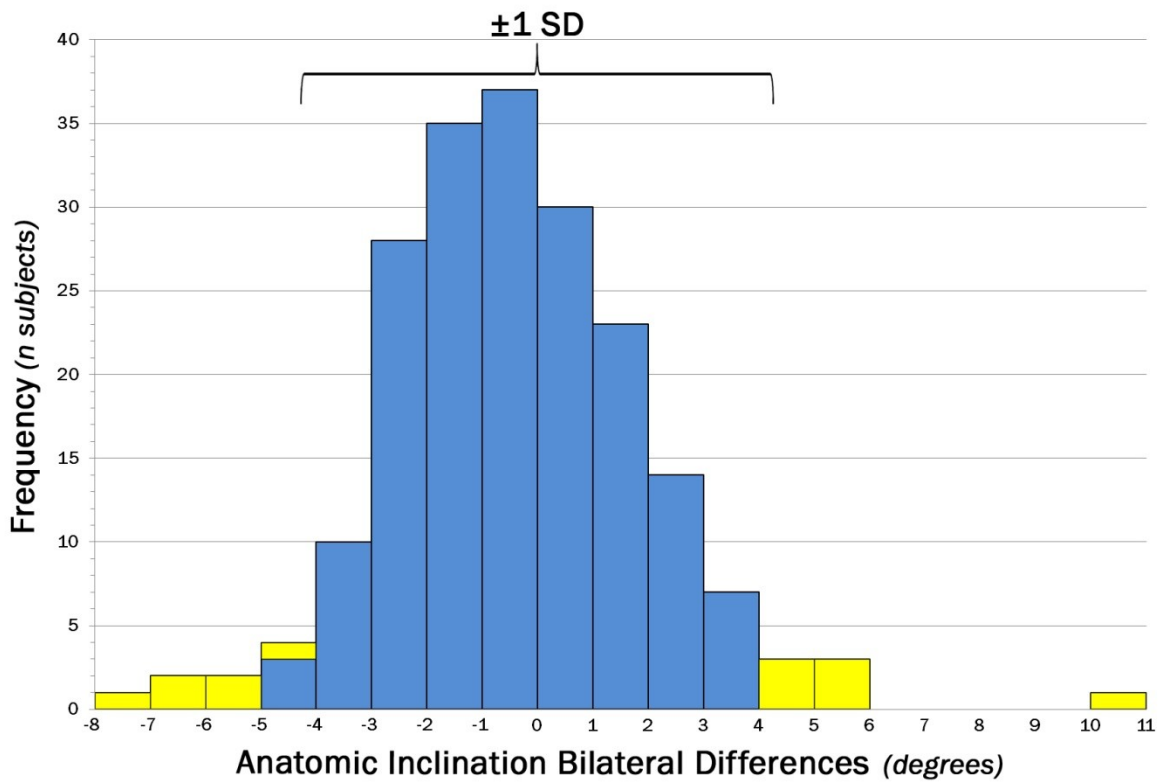


Figure 3.15- Bilateral differences in anatomic inclination,  $n=13$  subjects displayed differences larger than  $\pm 1$  SD (yellow).

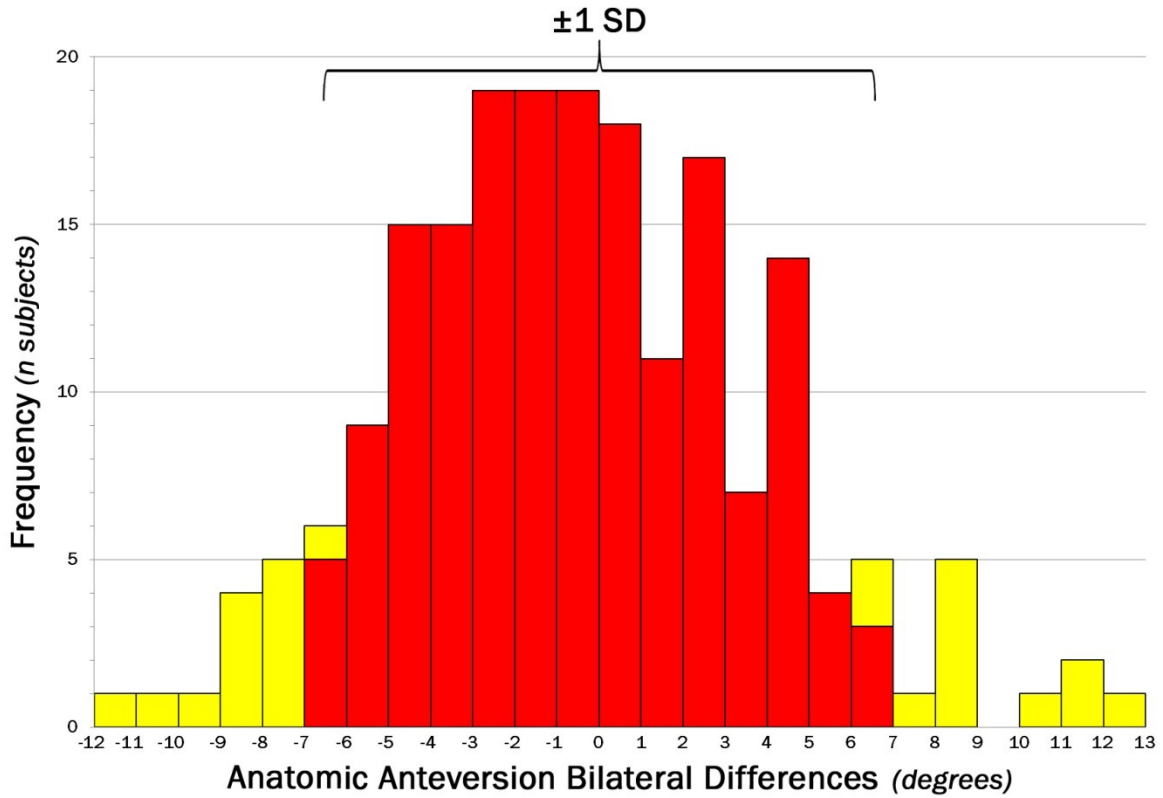


Figure 3.16- Bilateral differences in anatomic anteversion,  $n=25$  subjects displayed differences larger than  $\pm 1$  SD (yellow).

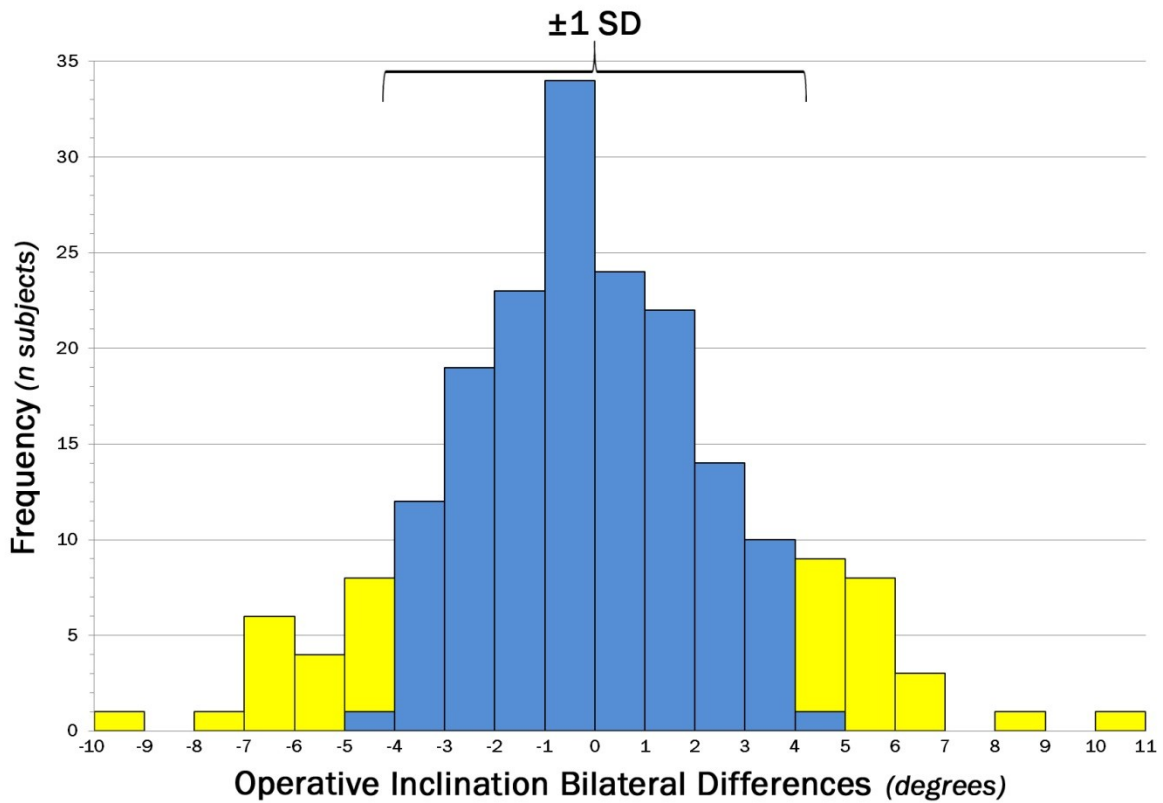


Figure 3.17- Bilateral differences in operative inclination,  $n=40$  subjects displayed differences larger than  $\pm 1$  SD (yellow).



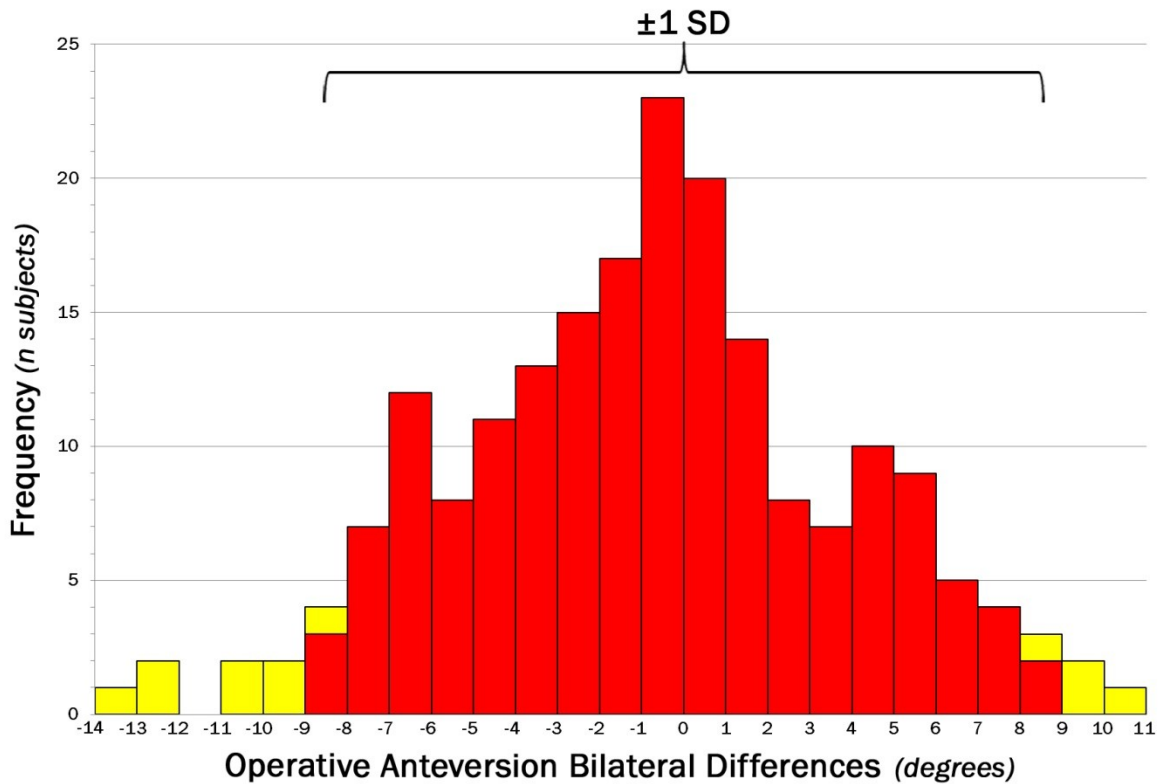


Figure 3.18- Bilateral differences in operative anteversion,  $n=12$  subjects displayed differences larger than  $\pm 1$  SD (yellow).

### 3.3 HEMI-PELVIS ANALYSIS RESULTS

Anteversion and inclination for the entire population were  $39.0^{\circ} \pm 9.0^{\circ}$  and  $53.6^{\circ} \pm 5.9^{\circ}$ , respectively. Highly significant differences between genders were observed for all measures except for the inclination between the AX and TPP (Table 3.10). Relative to the global hemipelvis C.S., male anteversion ( $33.8^{\circ} \pm 8.4^{\circ}$ ), was significantly less than that of females ( $43.1^{\circ} \pm 7.1^{\circ}$ ) ( $p < 0.0001$ ). The same was true for the inclination difference between males ( $52.0^{\circ} \pm 5.0^{\circ}$ ) and females ( $54.9^{\circ} \pm 6.2^{\circ}$ ) ( $p < 0.0001$ ). Because the hemipelvis C.S. spans the entire innominate bone, the significant differences in the orientations of the true and false pelvic regions undoubtedly affected the global orientation of the acetabulum.

**Table 3.10- Results For Hemi-Pelvis Measures**

<b>Measure</b>	<b>Acetabular Version<sup>†</sup></b>	<b>Acetabular Inclination<sup>†</sup></b>	<b>AX-TPP Version<sup>†</sup></b>	<b>AX-TPP Inclination</b>	<b>AX-FPP Version<sup>†</sup></b>	<b>AX-FPP Inclination<sup>†</sup></b>
<b>Male</b>	33.8°±8.4°	52.0±5.0°	21.4°±3.8°	-0.1°±5.3°	20.6°±7.6°	66.2°±13.0°
<b>Female</b>	43.1°±7.1°	54.9°±6.2°	17.9°±4.8°	1.2°±8.0°	17.0°±6.9°	78.2°±9.0°
<b>Total</b>	39.0°±9.0°	53.6°±5.9°	19.4°±4.7°	0.7°±6.9°	18.6°±7.5°	72.9°±12.4°
<b>Range</b>	15.3° to 62.3°	76.5° to 35.7°	3.9° to 32.6°	-20.0° to 23.9°	0.5° to 43.6°	18.8° to 90.0°

Statistically significant differences between genders <sup>†</sup>p<0.0001

The hemi-pelvis measures for global inclination and version appeared evenly distributed around their respective means (Figure 3.19 & Figure 3.20). Interestingly, all hemi-pelvises displaying small amounts of version were in males (11 acetabulums in 8 subjects), and all of the notably increased version occurred in females (8 acetabulums in 7 subjects). Measures of inclination showed a similar trend, with only male hemi-pelvises having notably low readings (3 acetabulums in 2 subjects). The 12 acetabulums with high readings of inclination occurred in nine subjects, only one of which was a male with bilaterally high levels, the remaining eight were female. The male subject with bilaterally high inclination displayed many other measures outside of two SD, but was bilaterally symmetric (Figure 3.21). There was a notable amount of overlap between the female hemi-pelvises with both increased version and inclination. Of the seven innominate bones with notably high inclination, six were also observed to have version above the 2 SD threshold (the other only ~2° away). Most interestingly, of the 15 acetabulums that measured outside of two SD for inclination (3 low/12 high), six were included in the group outside of two SD for radiographic inclination in the full pelvis (2 low/4 high). The same 45-year old male with bilaterally low inclination for full pelvis radiographic inclination (right 44.8°/left 41.6°), accounted for the only two overlapping acetabulums from the hemi-pelvis group (right 44.9°/left 37.8°) (Figure 3.10). None of the acetabulums with notable levels of APP based radiographic anteversion appeared outside of the two SD threshold for hemi-pelvis based version.

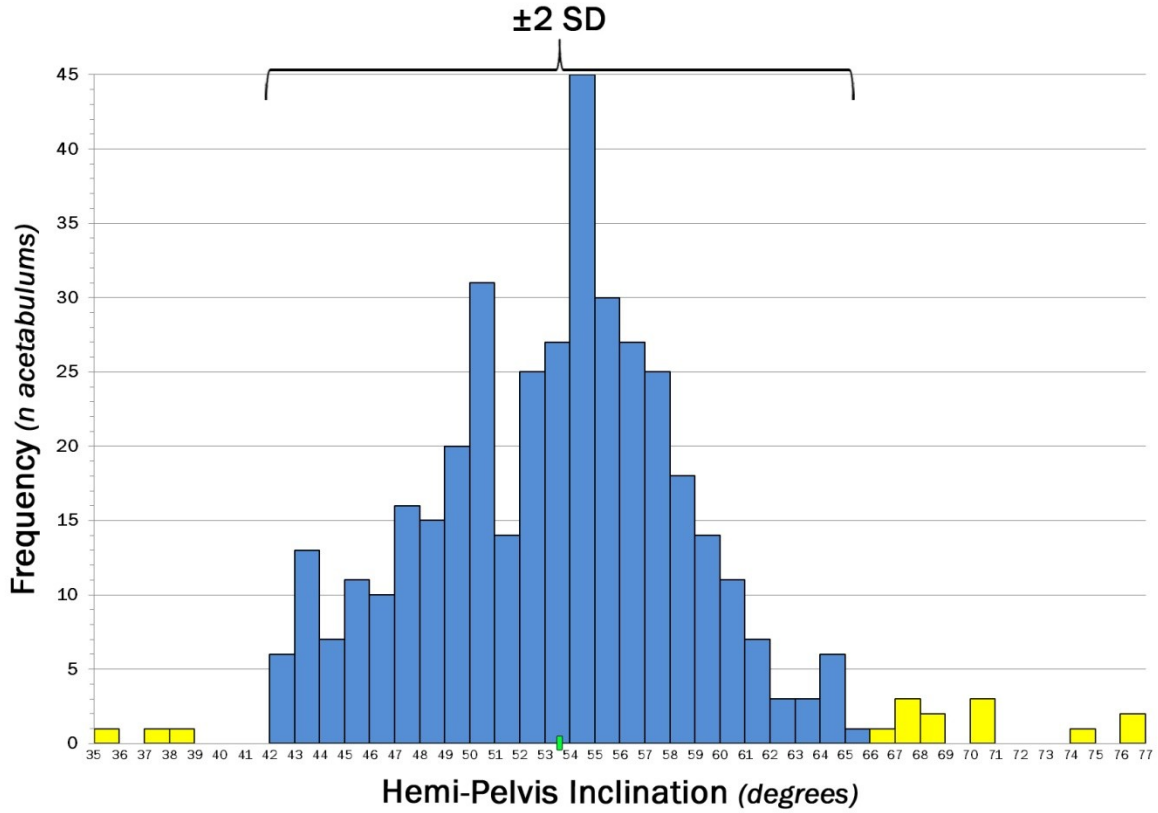


Figure 3.19- Population results for hemi-pelvic inclination, with  $n=15$  acetabulums falling outside of  $\pm 2$  SD (yellow).

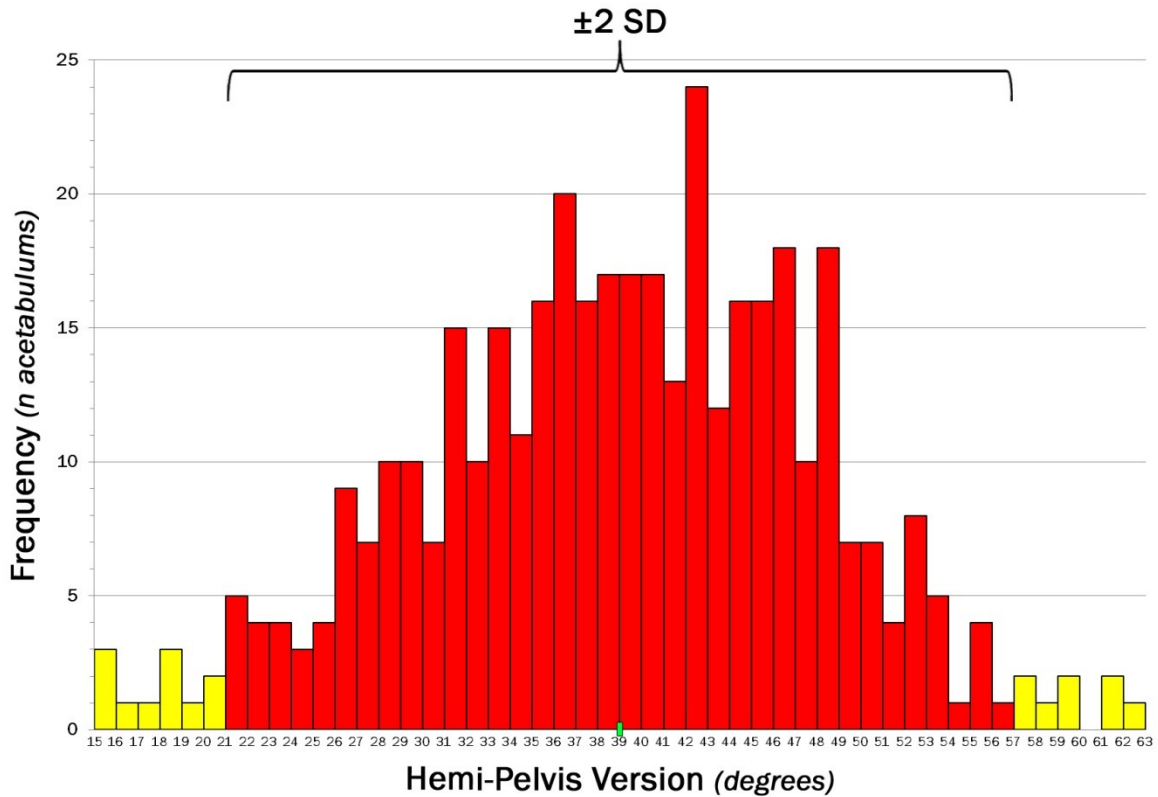
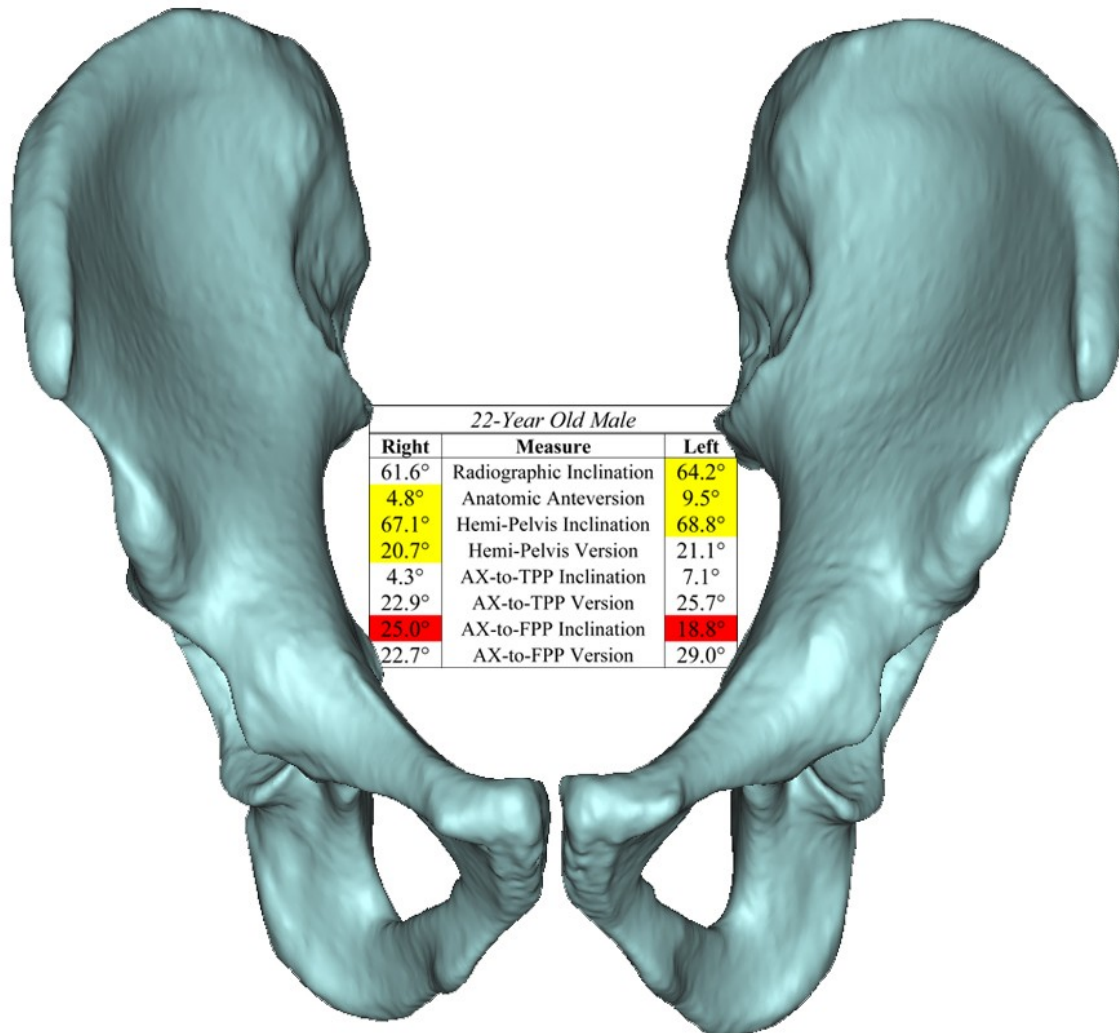


Figure 3.20- Population results for hemi-pelvic version, with  $n=19$  acetabulums falling outside of  $\pm 2$  SD (yellow).



**Figure 3.21-** 22-year old male subject of interest observed to have the least AX-to-FPP inclination on both on left and right sides. This subject showed notably low levels bilateral anatomic anteversion, notably high bilateral hemi-pelvis inclination, and on the left side for radiographic inclination.

The most inconsistent measure for the hemi-pelvis analysis was the inclination between the acetabulum and true pelvis (AX-to-TPP), where on average, the opening of the acetabulum was closely aligned with that of the obturator's. The inclined orientation of the true pelvis relative to the AX ranged over 20° in each direction, sometimes forming both closing and opening angles (i.e.- positive or negative values). An interesting phenomena was observed in the measured inclination between the acetabulum and true pelvis. The inclined orientation of the TPP appeared to have a bimodal distribution, with a split around values just above zero (Figure

3.22). No immediate explanation can be offered for this observation, but lack of intermediate values appears to be present in both males and females (Figure 3.23). The lowest values for TPP inclination occurred in four hemi-pelvises, belonging to three females. All 10 measurements of inclination in excess of the 2 SD limit were in seven females except for one.

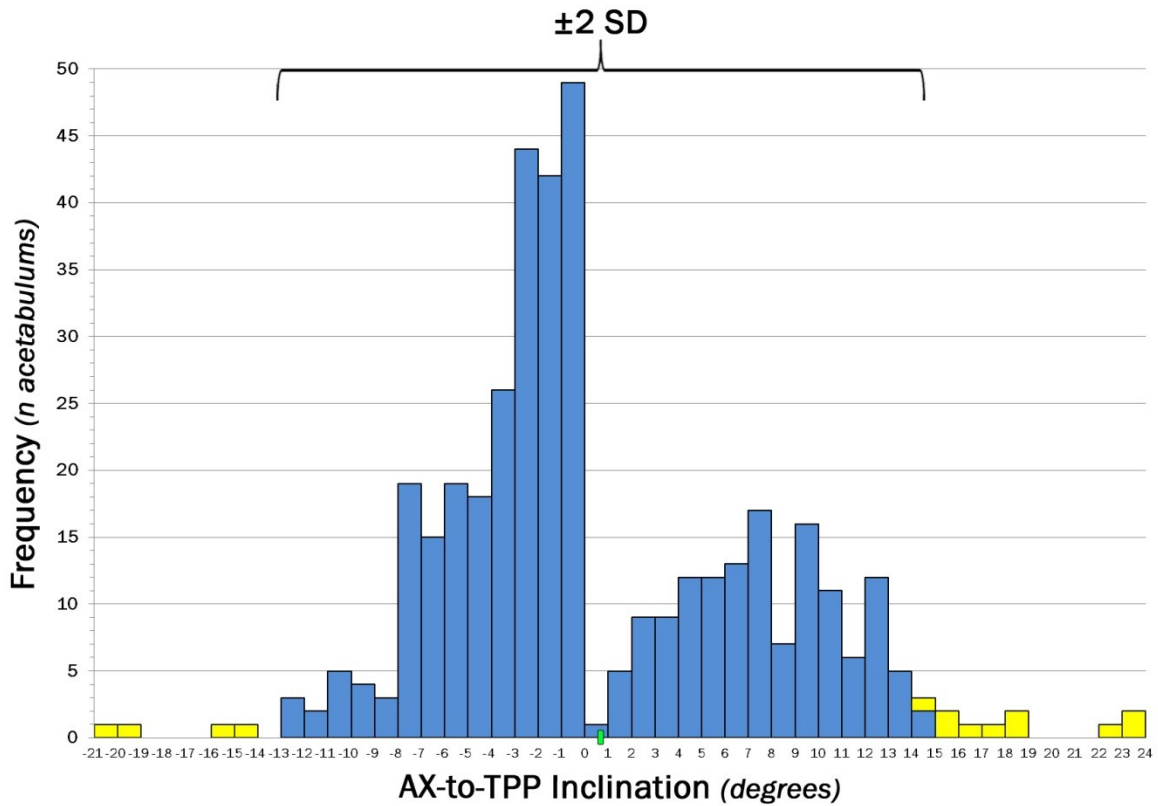


Figure 3.22- Population results for acetabulum-to-true pelvis inclination, with  $n=14$  hemi-pelvises outside of  $\pm 2$  SD (yellow). A notable lack of readings occurred around zero and slightly larger values.

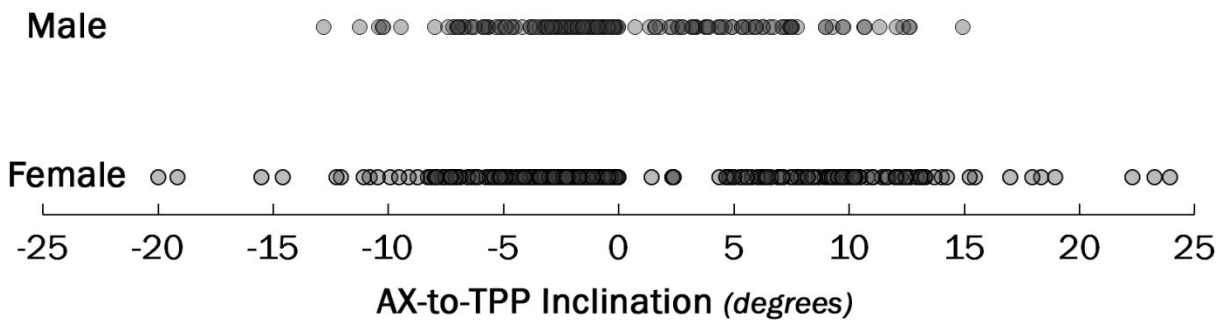
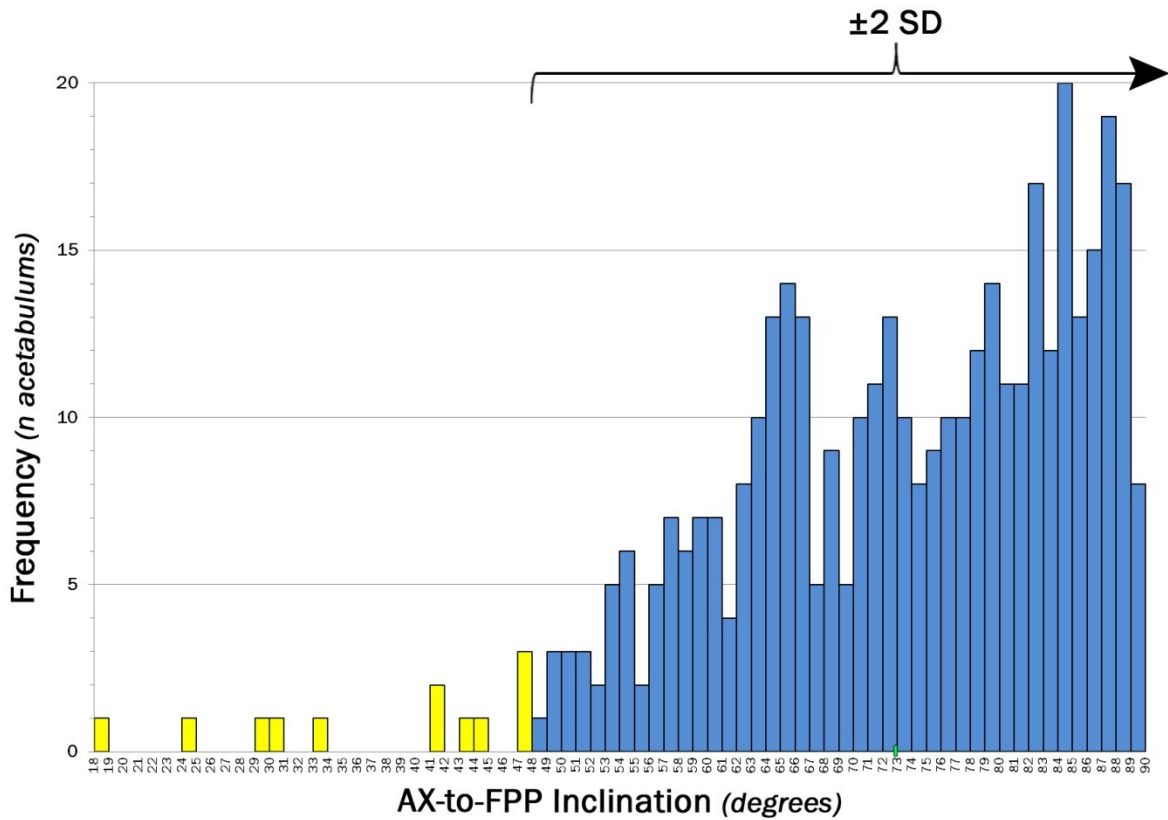


Figure 3.23- Distributions of male and female acetabulum-to-true pelvis inclination. Both genders appear to have infrequent measures just above zero degrees.

The inclination between the acetabulum and false pelvic region (AX-to-FPP) was spread over a wide range and clearly skewed towards higher values (Figure 3.24). Interestingly, the inclination of the FPP appeared to have a definitive limit of 90°. This is most likely due to the structure of the sacrum preventing further medial migration of the ilium. The only readings outside of two SD for inclination between the false pelvis and the acetabulum were low values. Of the twelve notable low measures, only one occurred in a female hemi-pelvis, the rest were in seven male subjects. The 22-year old male that had that the lowest value for AX-to-FPP inclination on the left side (18.8°), also had a notable value on the right side (25.0°). This was the same male subject was previously mentioned to have bilaterally high levels of global hemi-pelvis inclination (left 68.8°/right 67.1°) and decreased global version (left 20.7°/right 21.1°). Not surprisingly, this same individual displayed readings for version and inclination outside of the two SD limit for full pelvis based measures as well (Figure 3.21).



**Figure 3.24-** Population results for acetabulum-to-false pelvis inclination, with  $n=12$  hemi-pelvises outside of  $\pm 2$  SD (yellow). The readings are noticeably skewed towards higher values up to 90 degrees.

The version between the acetabulum and true pelvis (AX-to-TPP) was evenly distributed about the mean (Figure 3.25). In agreement with the overall full pelvis results, 14 of the 15 acetabulums with notably small readings of true pelvic version resided in nine females. Notably large values of inclination and small version occurred simultaneously in three female innominate bones, two of which were in the same subject. The version between the acetabulum and false pelvis (AX-to-FPP) was also evenly distributed around the mean (Figure 3.26). Five out of the six small measures of FPP version occurred in five different females. The large readings of FPP version were observed in nine hemi pelvises in five males and two females. Three of the males with notably increased version also had inclination outside of 2 SD, one of which occurred bilaterally.

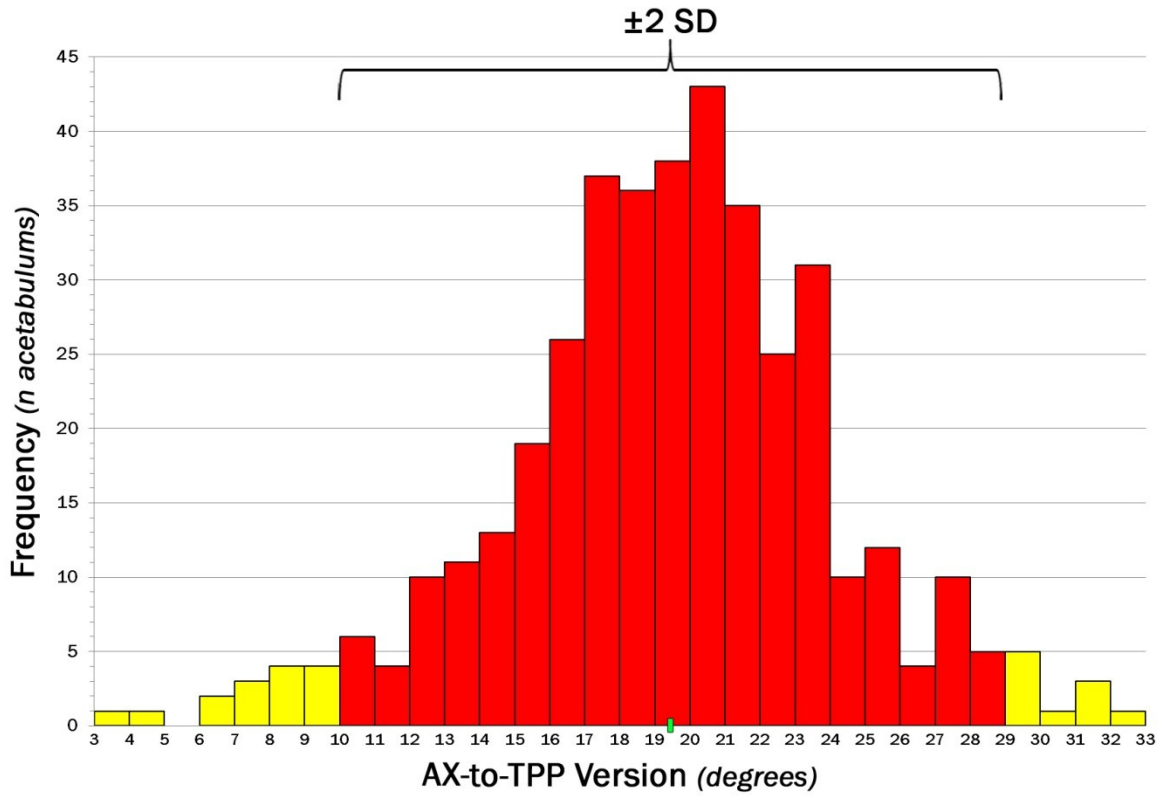


Figure 3.25- Population results for acetabulum-to-true pelvis version, with  $n=25$  hemi-pelvises outside of  $\pm 2$  SD (yellow).

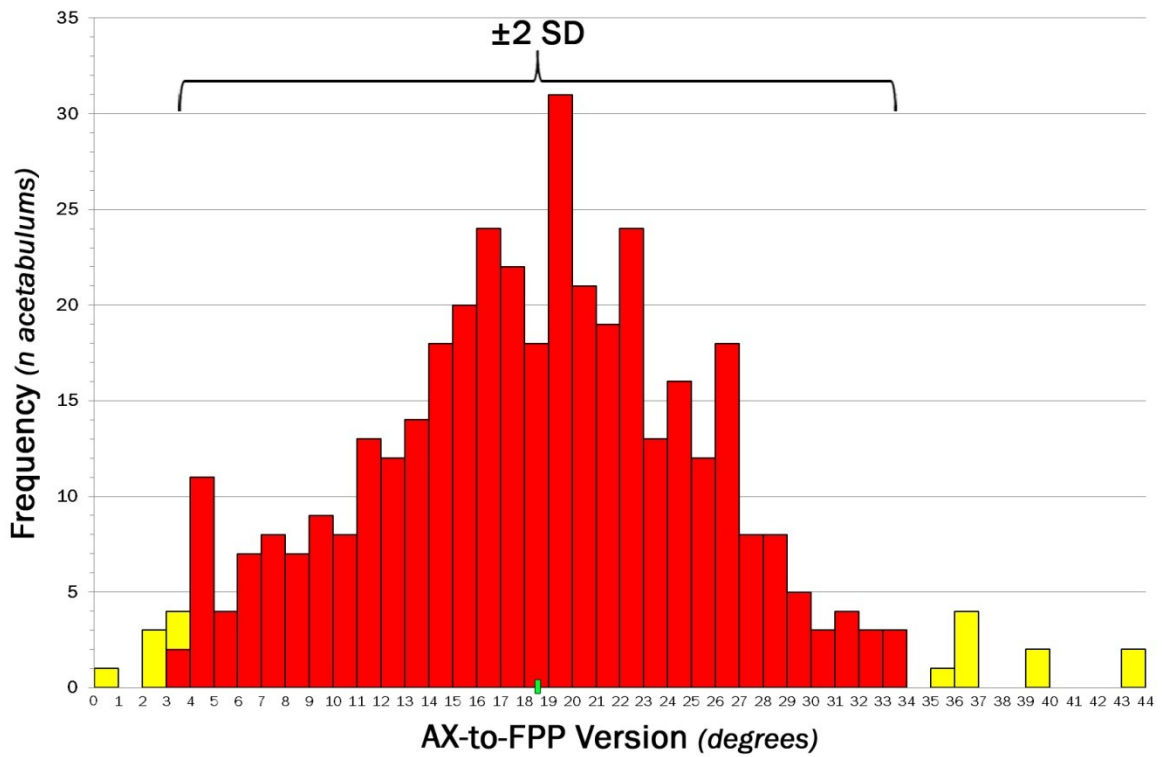
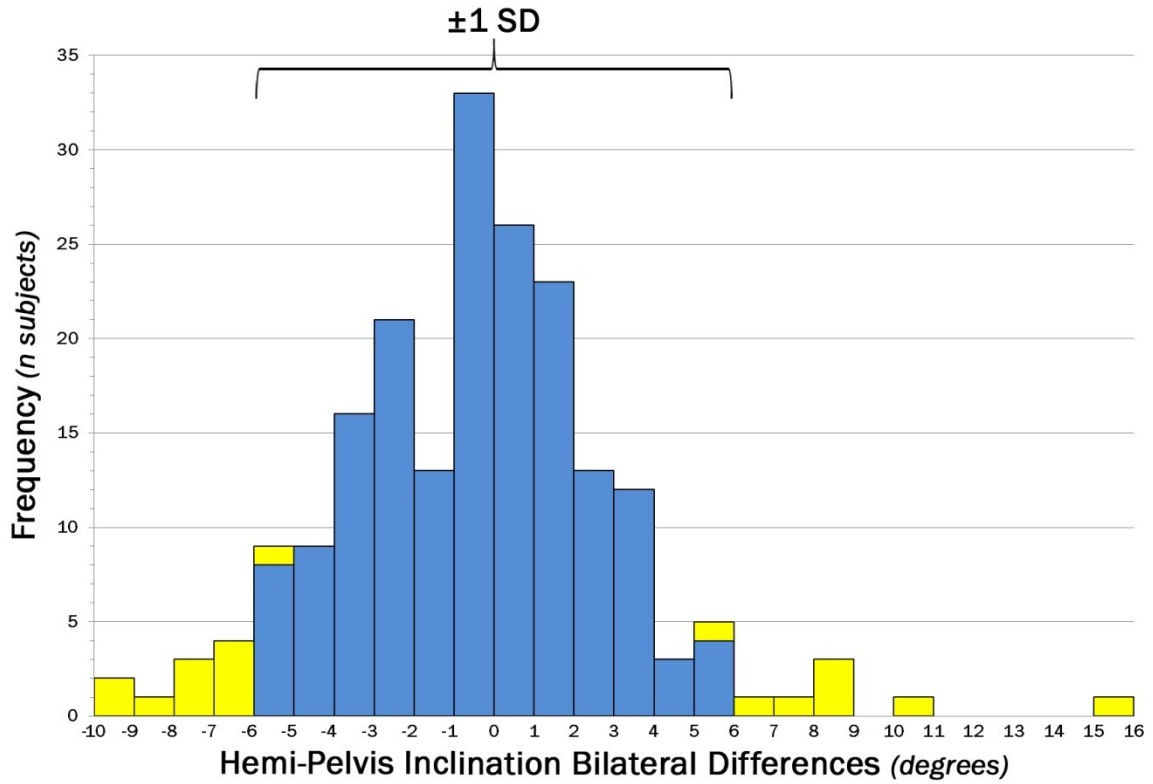


Figure 3.26- Population results for acetabulum-to-false pelvis version, with  $n=15$  hemi-pelvises outside of  $\pm 2$  SD (yellow).



The bilateral asymmetry observed in measures of the hemi-pelvis were all evenly distributed around zero. Bilateral discrepancies of global inclination and version were similar to that of full pelvic measures (Figure 3.27 & Figure 3.28). Differences within a single subject greater than one SD occurred in 9.5% ( $n=19$ ) of the population for inclination, and 8% ( $n=16$ ) for version. A considerably tighter range of version bilateral asymmetry was observed in both the true and false pelvic regions compared to that of inclination (Figure 3.29 thru Figure 3.32). However, the large bilateral discrepancies for inclination appear to be sparse outliers. This may be related to how the other regions of the innominate bone develop relative to the acetabulum in the axial plane. When viewed in the axial plane, the torsional relationship (or twisting) of the different regions may be arranged more consistently because of the unions formed at the sacrum and pubic symphysis. For the relationship between the true pelvis and acetabulum (AX-to-TPP), inpatient differences larger than one SD occurred in 13% ( $n=26$ ) of the population for inclination, and 6% ( $n=12$ ) for version. Notable bilateral differences in AX-to-TPP version seemed evenly mixed between males and females. Conversely, discrepancies in AX-to-TPP inclination larger than one SD occurred in 20 females and only 6 males. Only three individuals with large bilateral differences in AX-to-TPP version displayed notable differences in inclination (2 male/1 female). The relationship between the false pelvis and the acetabulum (AX-to-FPP) displayed inpatient differences larger than one SD in 7% ( $n=14$ ) of the population for inclination, and 8.5% ( $n=17$ ) for version. More females appeared to have notable differences in AX-to-FPP version (12 females/5 males), and discrepancies larger than one SD for inclination were mixed (9 female/5 males). Five individuals displayed notable discrepancies in both inclination and version between the false pelvis and acetabulum. The same 52-year old female

that had the two lowest readings for anatomic anteversion, also had the largest bilateral discrepancy in the inclination of the false pelvis ( $\sim 25^\circ$ ) (Figure 3.12).



**Figure 3.27-** Bilateral differences in global hemi inclination,  $n=19$  subjects displayed differences larger than  $\pm 1$  SD (yellow).

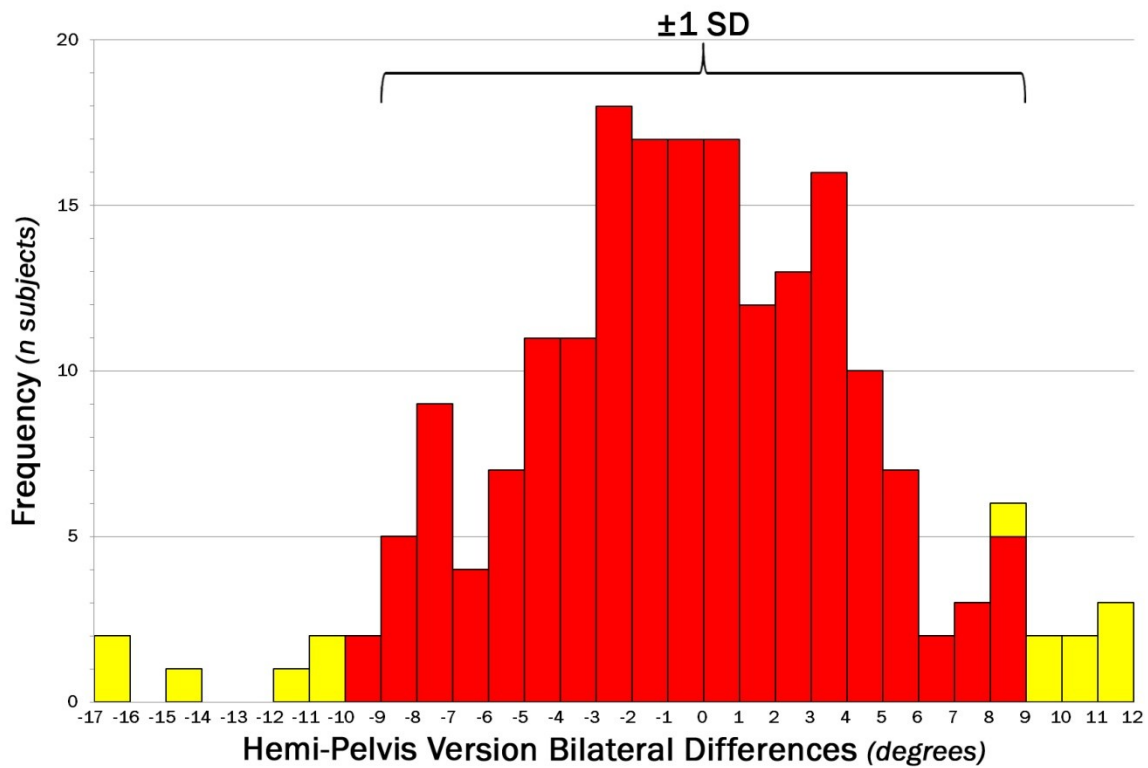


Figure 3.28- Bilateral differences in global hemi version,  $n=16$  subjects displayed differences larger than  $\pm 1$  SD (yellow).

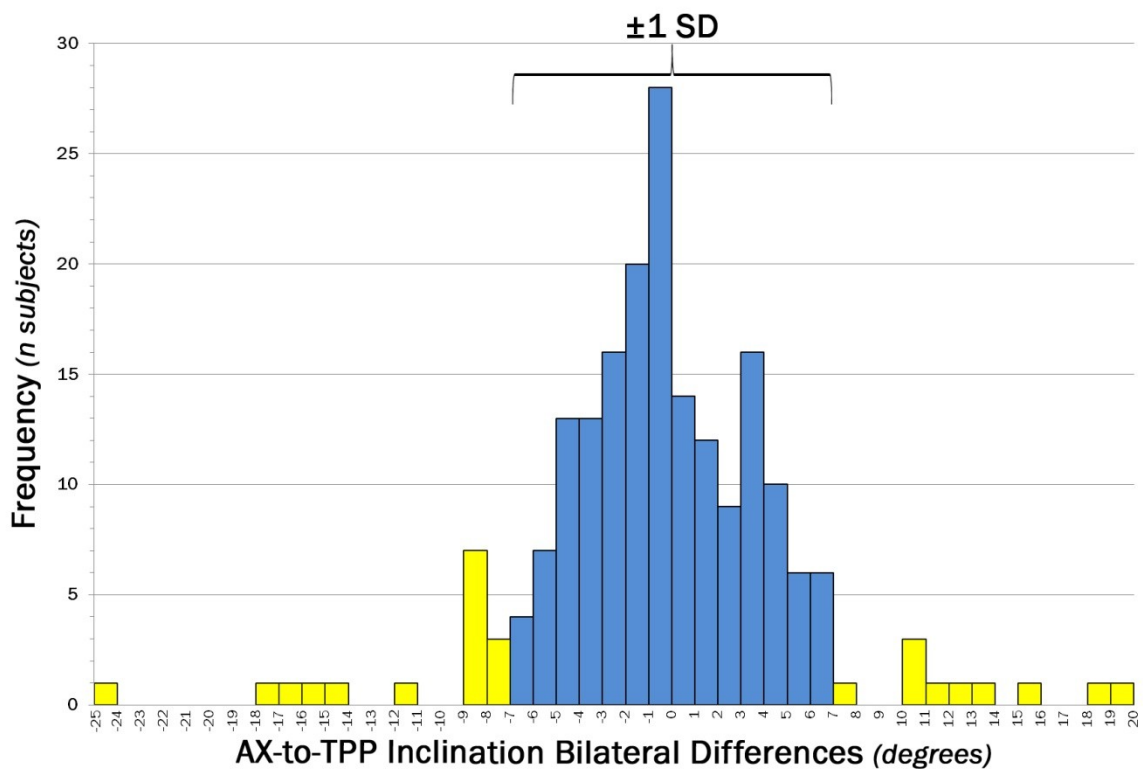


Figure 3.29- Bilateral differences in AX-to-TPP inclination,  $n=26$  subjects displayed differences larger than  $\pm 1$  SD (yellow).

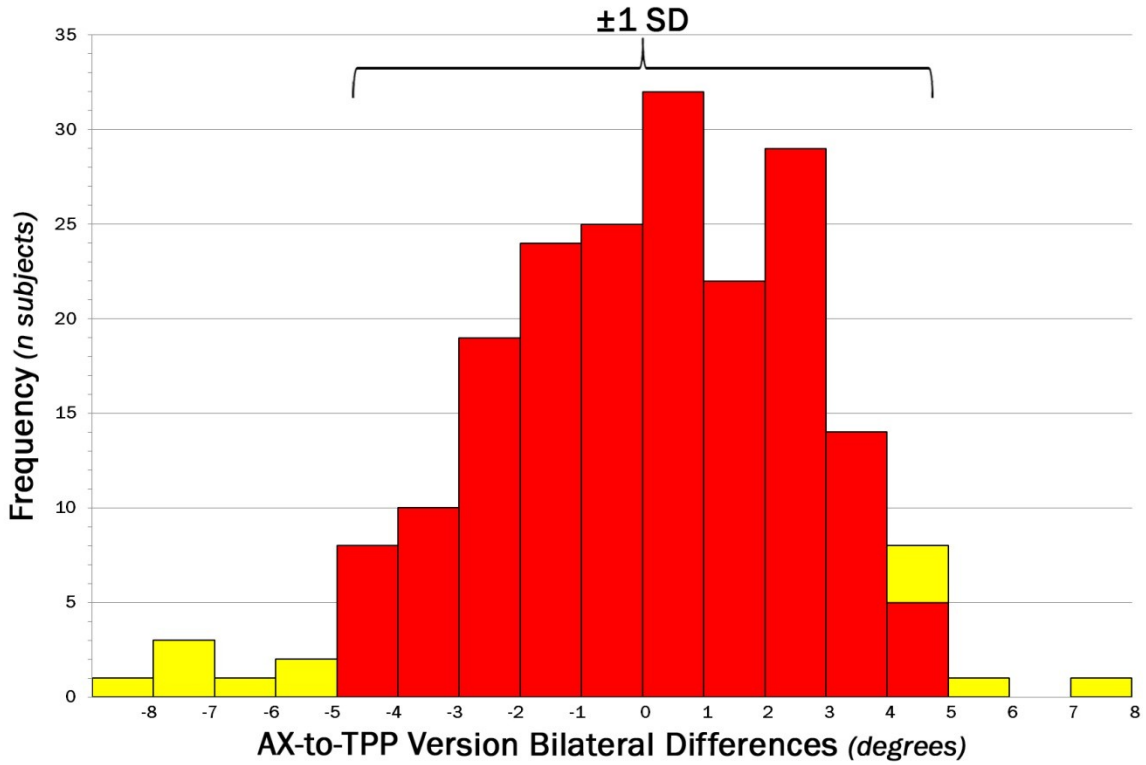


Figure 3.30- Bilateral differences in AX-to-TPP version,  $n=12$  subjects displayed differences larger than  $\pm 1$  SD (yellow).

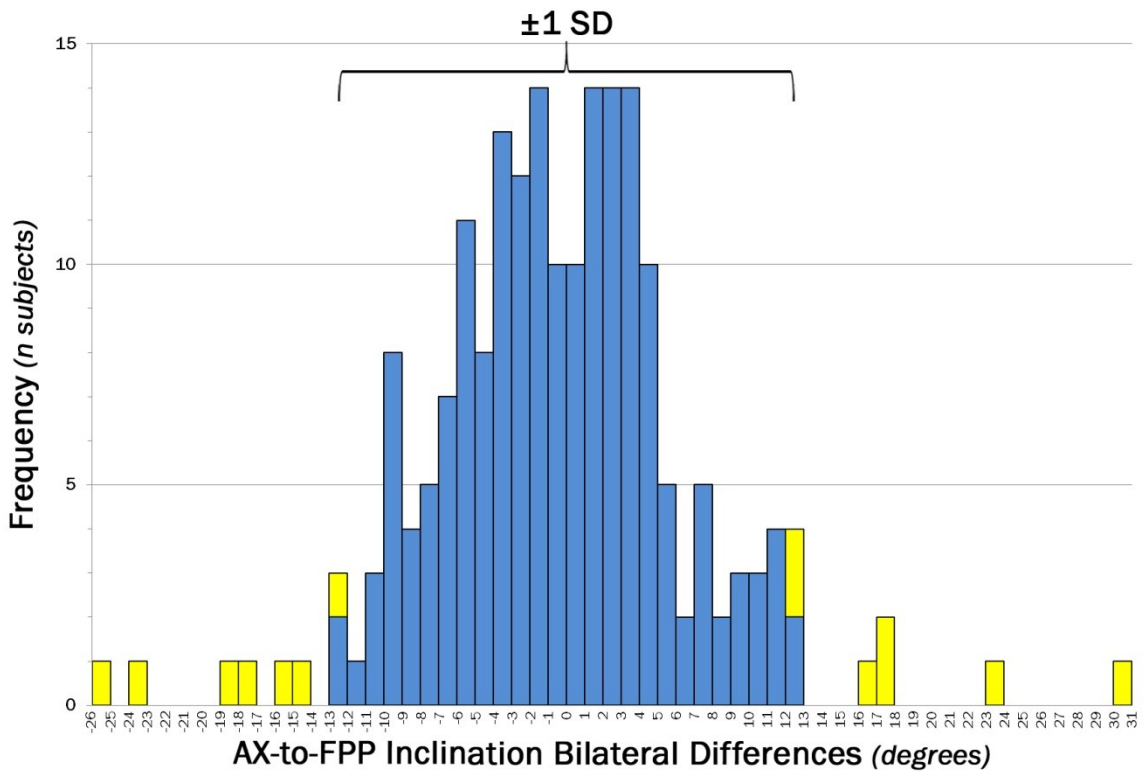
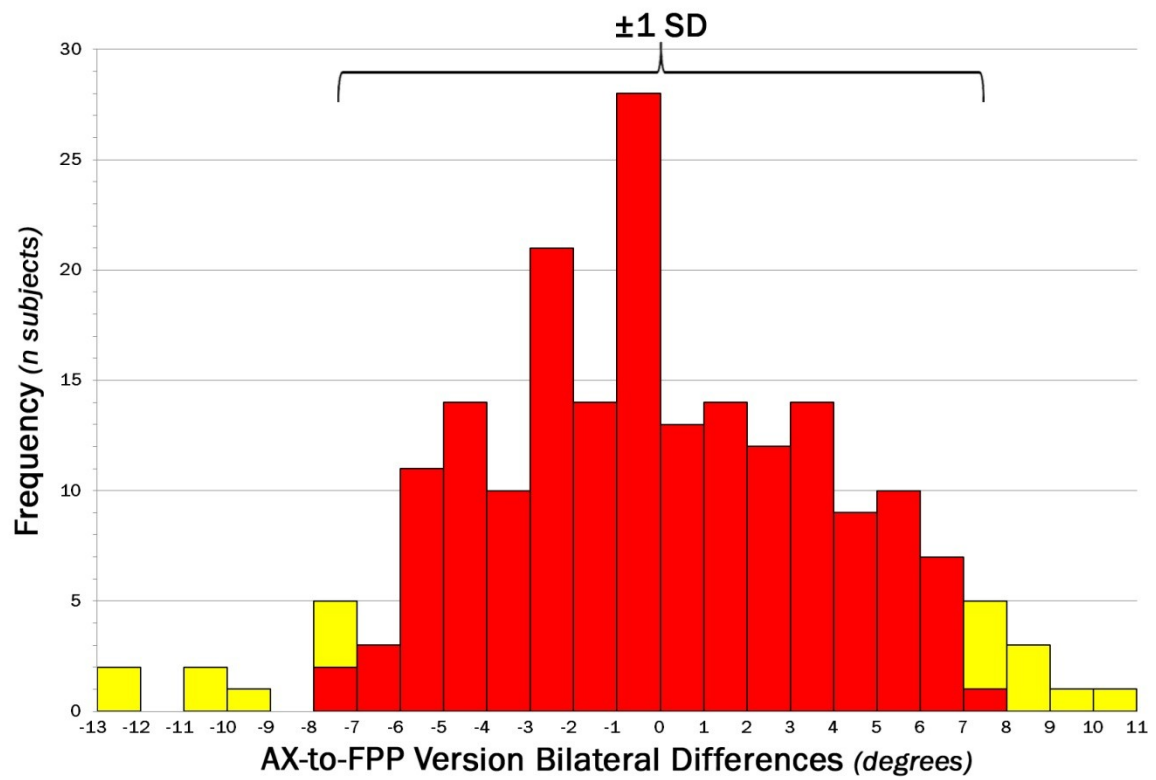


Figure 3.31- Bilateral differences in AX-to-FPP inclination,  $n=14$  subjects displayed differences larger than  $\pm 1$  SD (yellow).



**Figure 3.32-** Bilateral differences in AX-to-FPP version,  $n=17$  subjects displayed differences larger than  $\pm 1$  SD (yellow).

## **4 DISCUSSION**

While the classic biomechanical description of the hip joint simplifies it as a ball-and-socket mechanism, the actual relationship between the femoroacetabular components is considerably more complex and dynamic. The elaborate and interlinked anatomic structures determining femoroacetabular coverage, congruency, and range of motion create challenges in discerning between hips that have normal mechanics and those with a pathomechanical flaw predisposing it to OA. By their very nature, disorders and treatments of the hip joint are three-dimensional, occurring around the periphery of both the femoral and acetabular components. Therefore, the osseous structures cannot be fully appreciated or accurately evaluated using 2-D radiographic methods.[175,130,48] One of the primary benefits and goals of 3-D based pelvic studies is to correct for the variability of patient positioning. Accurate measurement techniques that can eliminate the error introduced by patient malpositioning provide a more robust diagnostic and surgical planning tool. The method of measurement developed for this study was able to correct for patient positioning by programmatically detecting the C.S.. The APP based C.S. used for the full pelvis analysis can be considered the ground truth reference frame for performing acetabular measures. To-date, no method has been presented to automatically detect the APP. This study was able to accurately and reliably capture the entire 3-D structure of the acetabulum to determine its true orientation.

### **4.1 Hemi-Pelvis**

The ability to quantify the relationship between acetabulum and the innominate bone in which it is embedded could be of great interest and utility to better understand diseases that can sometimes effect only one side of the pelvis, such as unilateral DDH.[46,55,60,97,121,221]

Knowledge of the hemi-pelvis remains sparse due to the limitations of the available methods used to study the innominate bone. The goal for the hemi-pelvis analysis was to devise a C.S. exclusive to the innominate bone that could be consistently formed within normal anatomic variation. Results from the reliability study showed more than acceptable outcomes which validated its usage for this study. Despite not achieving levels of reliability on par with the full pelvis measures, highly significant differences between genders were observed. This provides strong evidence that the entire structure of the innominate bone is oriented differently around the acetabulum for males and females. While the landmarks used for establishing the hemi-pelvis C.S. create a reference frame intrinsic to the innominate bone, they are not accessible during any surgical procedure. Therefore, the biggest strength of the hemi-pelvis analysis is also its biggest shortcoming, in that its usage as a practical reference frame is limited. It is possible to use geometrical relationships to relate the of the points on the tubercle face and ischial spine to ones that could be palpated, but it would have to be done on an individual basis making it impractical.

The results for global acetabular orientation within the hemi-pelvis C.S. were in agreement with the observations made in the APP based C.S.. On average, female acetabulums were almost  $10^{\circ}$  more anteverted (forward rotation) than that of their male counterparts. Female acetabulums were also significantly more inclined (upwards rotation) than males by approximately three degrees. The other new measures relating the orientations of both the true and false pelvic regions to the acetabulum also yielded interesting new information. In the axial plane, the female innominate bone was arranged in a torsional manner that was significantly different than that of males (Table 3.10). The female innominate bone had true and false pelvic regions that were almost evenly rotated by  $\sim 17^{\circ}$ - $18^{\circ}$ , split by the AX in the axial plane. The corresponding regions of the male innominate were also evenly split by the AX, but by slightly

larger and significant values ( $\sim 21^\circ$ ). The largest difference observed between genders was in the inclination of the false pelvic region. The wing of the ilium was tilted  $10^\circ$  more towards the acetabulum (downwards) in the frontal plane of male innominate bones.

Very few quantitative studies exist to make relevant comparisons. Only two studies could be located that observed the torsional relationship in the axial plane between the acetabulum and other regions of the innominate bone, both of which used the entire pelvis and were limited to 2-D measures only.[48,56] The observation in this study, of the ilium in female innominate bones being slightly less everted than males ( $\sim 2^\circ$ ), is in agreement with Maruyama et al.[48], and the well established anatomic understanding of gender differences between the structures of the entire pelvis.[52] The study by Maruyama et al., measured the angle formed between the APP and wing of the ilium using a line connecting the ASIS and PSIS directly measured on anatomic specimens.[48] They observed a significant difference of approximately two degrees between genders, with females having an ASIS directed more laterally and the PSIS medially (externally rotated wing in the AP direction). They also measured the anatomic anteversion of the acetabulum from the APP, which can be subtracted from the angle of the ilium to give a comparable 2-D indice similar to the AX-to-FPP angle used in this study. After subtraction, the male acetabular version relative to the iliac wing was  $40.2^\circ$  and the female was  $39.2^\circ$ . While the measures in this study are not directly comparable to ones in their study due to the differing C.S.; the direction, magnitude, and significant difference between genders are all in agreement. The second study by Fujii et al., used axial tomography to measure AcAV and the torsion of *female* innominate bones at levels of the ASIS and AIIS relative to the APP.[56] If the difference is split between the angles formed at the levels of the ASIS and AIIS, their resulting angle is similar to that of Maruyama et al.'s ( $57.9^\circ$  vs.  $60.5^\circ$ ). Interestingly, if the AcAV angle ( $18.6^\circ$ ) is subtracted



from the compound angle of the ilium, the resulting angle for females is almost exactly the same for both studies ( $\sim 39.2^\circ$ ). Fujii et al. also measured the torsion of the pelvis using superimposed levels to form a line connecting the ischial spine to the anterosuperior edge of the pubic symphysis. They showed highly significant differences in torsion at all three levels of the innominate bone between the normal and DDH group, which were also significantly correlated to the orientation of the acetabulum. In addition, they showed globally reduced coverage in hips with DDH using sector angles.[56] This study confirmed that the growth disturbances effect the entire structure of the pelvis along with the acetabulum. However, all of their indices were 2-D and depended on bilateral features of the pelvis to perform measurements. Therefore, it could be of interest to investigate this further using the independent and three-dimensionally based hemipelvis measures of the Acetabulator.

The small but significant external rotation of the anterior superior ilium observed in both this study and in Maruyama et al.'s [48], is in agreement with the conventional anatomic understanding that the distance between the ASIS in the female pelvis is relatively larger than in males.[52] However, the observed gender-based relationship between the inclination of the false pelvis and acetabulum is somewhat conflicting. It would have been expected that the superior region of the innominate bone would have been more outwardly tilted in the frontal plane in females than in males. In fact, the exact opposite was observed with females being on average  $10^\circ$  more vertical relative to the AX than males (Table 3.10). With the difference in axial torsion between genders being only a few degrees, the difference of  $10^\circ$  in inclination along the vertical length of the ilium would intuitively result in a decreased distance between ASIS points in females. However, when viewing the pelvis as a whole it appears wider in females than in males.

This indicates that the gender differences typically observed for the full pelvis are controlled a great deal by the structure of the sacrum which separates the innominate bones.

Besides the differences between genders, most of the observations for the measures and their bilateral differences were as expected, respectively distributed about the mean and zero. The only two exceptions were the inclinations of the true and false pelvis regions. While it may be of little consequence, it was interesting to observe that the inclination of the false pelvis had measures notable shifted towards the seemingly definitive limit of  $90^\circ$  (Figure 3.24). One of the most interesting observations was the lack of measurements around the average reading ( $\sim 1$  degree) of inclination in the true pelvic region (Figure 3.22 & Figure 3.23). There were only 37 subjects (17male/20 female) where the angle on one side formed an opening angle (positive) and the other formed a closing angle (negative), with no obvious bias towards the left or right side. There is no immediately apparent reason for why the readings split evenly about the mean. However, the gender differences around the structures of the pubic arch and obturator have been partially responsible. Females have wider pubic arches (angle between the bilateral inferior pubic rami in the frontal plane) with smaller obturator openings that form more triangular shapes. Males have larger, more ovular obturator openings that create a tighter angle at the pubic arch.[52,222] This may have also affected the observed measures of the true pelvic regions.

## **4.2 Full Pelvis**

Using the latest software to reconstruct 3-D models from DICOM images, in conjunction with the purpose specific Acetabulator program, the method used in this study to measure acetabular orientation was statistically shown to be both accurate and reliable. From observing the output plots, it was determined that target points were accurately identified. The thorough reliability study showed that these targets were consistently selected. Using this robust

methodology, the true 3-D orientation of the acetabulum was determined from a large sample of normal subjects. The high levels of accuracy allowed for elucidation into the subtle gender specific differences in acetabular orientation. Females were observed to have significantly more anteversion in all measurement schemes and also in anatomic inclination. To the best of this author's knowledge, there is yet to be a study showing differences in *both* inclination and anteversion between genders using 3-D measures. The larger baseline for normal female inclination may partially account for females displaying more frequent and severe signs of dysplasia than their male counterparts.[30,33,34,64,132] These findings add more impetus to the discussion of whether or not it is appropriate to account for gender specific morphology.[200,223]

Many of the criticisms pertaining to previous 3-D studies noted the loss of model accuracy due to smoothing, model control, or inadequate rendering algorithms. [50,130,175,198,200,203] These deficiencies have been addressed in the recent model rendering software used in this study, with newly implemented features such as the ability to volumetrically compensate for shrinkage when smoothing. Critical geometry of the acetabular roof that can be lost due to oblique tomograph orientation was minimized using 1mm slice increments.[130] Capturing more of the superolateral AR structure may partially account for the differences in inclination observed between males and females. The primary limitation to this investigation is that it only analyzed the acetabulum. The mechanics of the hip joint are governed by the compounding relationship between the femoral and acetabular structures, and both should be considered when analyzing the joint as a system. Additionally, complete medical histories for the patients were not available; therefore it could not be assured that all subjects were free of any

previous hip related issues. There were some osteophytes and a few minor instances of OS acetabuli noted, which are possible indicators of underlying abnormalities and/or arthritis.

The results for normal acetabular orientation in this study are in close agreement with the first reported 3-D values from Murphy & Millis et al. of  $20.4^{\circ} \pm 7.1^{\circ}$  for anteversion (anatomic) and  $53.0^{\circ} \pm 6.3^{\circ}$  for abduction (radiographic inclination).[77,201] These, and other early studies, did an exceptional job of describing 3-D coverage of normal acetabuli as a nearly perfect hemisphere with centers of acetabular and femoral head rotation closely coinciding (<1mm) showing good congruency.[77,130,200,201] With this information existing in the literature, it was expected that normal acetabuli would be both congruent and provide adequate coverage. Therefore, it was not critical to report this for the normal population used in this study. However, a measure of depth would be needed to comprehensively compare dysplastic to normal hips. Using the sparse number of studies that could be located, Table 4.1 and Table 4.2 have been assembled to provide a consensus from the literature of true 3-D acetabular orientation. All of the studies noted in the tables below used the APP to correct for positioning and reported the more common anatomic and radiographic angular schemes for normal acetabuli.

**Table 4.1- Normal Values Reported For 3-D Anteversion**

Study Information			Measure of Anteversion					
Study	n Hips	Method/ Slice Increment	Male		Female		Total	
			Radiographic	Anatomic	Radiographic	Anatomic	Radiographic	Anatomic
Murphy et al., 1990	49 (subset of 14 females)	3-D Reconstruct/ CT ?	NR	NR	15.0°±6.7°	17.7°±6.7°	16.5°±7.1°	20.4°±7.1°
Vandenbussche et al., 2007†	200 (100 male/100 female)	3-D Reconstruct/ CT 1.25mm	11.8°±4.9°	15.1°±4.9°	11.9°±4.9°	18.8°±4.9°	13.3°±5.5°	16.9°±5.5°
Vandenbussche et al., 2007	68 (26 male/42 female)	Direct Measure/ Cadaver	12.0°±8.8°	15.7°±8.8°	16.2°±7.8°	24.1°±7.8°	16.1°±9.1°	20.9°±9.1°
Nagao et al., 2008*	110 (NR)	Direct Measure/ Cadaver	NR	NR	NR	NR	16.0°±5.2°	20.8°±5.2°
Murtha et al., 2008†**	42 (20 male/22 female)	3-D Reconstruct/ CT 1-1.25mm @ cup & 5mm elsewhere	15.8°±6.9°	19.3°±6.9°	20.1°±5.8°	24.1°±5.8°	18.1°±5.8°	21.8°±6.7°
Köhnlein et al., 2009	58 (42 male/16 female)	Direct Measure/ Cadaver	20.6°±4.5°	26.8°±4.5°	22.3°±7.7°	28.2°±7.7°	21.1°±5.4°	27.3°±5.4°
Lubovsky et al., 2010***	50 (22 male/28 female)	3-D Reconstruct/ CT ~4mm	16.5°±6.0°‡	19.5°±6.0°	18.1°±5.4°‡	22.7°±5.4°	17.4°±5.6°‡	21.2°±5.6°
Lubovsky et al., 2011†	76 (44 male/32 female)	3-D Reconstruct/ CT 1.25mm	NR	NR	NR	NR	16.9°±9.2°	22.8°±9.2°
Current Study, 2012†	400 (176 male/224 female)	3-D Reconstruct/ CT 1.00mm	17.5°±5.0°	21.5°±6.1°	20.5°±5.8°	24.7°±6.6°	19.2°±5.6°	23.2°±6.6°
<b>Weighted Average</b>	1053 total (444 male/478 female)	Gender based average on: 400 male/446 female	15.8°±5.3°	19.8°±5.8°	17.9°±5.9°	23.1°±6.3°	17.2°±6.1°	21.5°±6.5°

† Statistically significant difference between genders

NR = Not reported

\* Only used 3 points to directly define opening plane

\*\* Used Data Thief to calculate SD from plot (B. Tummers, DataThief III. 2006 <<http://datathief.org/>>)

\*\*\* Calculated gender specific values from table

‡ Radiographic anteversion = 90°-reported anteversion value

XX.X° [Italics] Values calculated using conversions below from [214]- SD are "best guesses" taken from converted measurement scheme

$\tan(AA) = \tan(RA) \div \sin(RI)$ $\cos(AI) = \cos(RI) \times \cos(RA)$ $\sin(RA) = \sin(AA) \times \sin(AI)$ $\tan(RI) = \tan(AI) \times \cos(AA)$
---

AA= anatomic anteversion  
 AI=anatomic inclination  
 RA= radiographic anteversion  
 RI= radiographic inclination

**Table 4.2- Normal Values Reported For 3-D Inclination**

Study Information			Measure of Inclination					
Study	n Hips	Method/ Slice Increment	Male		Female		Total	
			Radiographic	Anatomic	Radiographic	Anatomic	Radiographic	Anatomic
Murphy et al., 1990	49 (subset of 14 females)	3-D Reconstruct/ CT ?	NR	NR	57.2°±4.3°	58.5°±4.3°	53.0°±6.3°	54.8°±6.3°
Vandenbussche et al., 2007	200 (100 male/100 female)	3-D Reconstruct/ CT 1.25mm	51.0°±4.7°‡	52.0°±4.7°	51.6°±4.8°‡	53.1°±4.8°	51.3°±4.8°‡	52.5°±4.8°
Vandenbussche et al., 2007	68 (26 male/42 female)	Direct Measure/ Cadaver	49.0°±4.8°‡	50.1°±4.8°	49.5°±4.3°‡	52.1°±4.3°	49.3°±4.4°‡	51.2°±4.4°
Nagao et al., 2008*	110 (NR)	Direct Measure/ Cadaver	NR	NR	NR	NR	49.1°±4.8°	51.0°±4.8°
Murtha et al., 2008**	42 (20 male/22 female)	3-D Reconstruct/ CT 1-1.25mm @ cup & 5mm elsewhere	53.9°±4.6°	55.5°±4.6°*	54.7°±4.2°	57.1°±4.2°*	54.2°±4.3°	56.3°±4.4°*
Köhnlein et al., 2009	58 (42 male/16 female)	Direct Measure/ Cadaver	48.1°±4.1°	51.3°±4.1°	49.8°±4.1°	53.3°±4.1°	48.3°±4.4°	51.6°±4.4°
Lubovsky et al., 2010***	50 (22 male/28 female)	3-D Reconstruct/ CT ~4mm	56.9°±5.1°	58.4°±5.1°	51.5°±6.7°	53.7°±6.7°	53.9°±6.6°	55.8°±6.6°
Lubovsky et al., 2011	76 (44 male/32 female)	3-D Reconstruct/ CT 1.25mm	NR	NR	NR	NR	46.1°±9.4°	48.4°±9.4°
Current Study, 2012†	400 (176 male/224 female)	3-D Reconstruct/ CT 1.00mm	53.6°±4.1°	55.7°±3.9°	54.3°±4.5°	57.1°±4.5°	54.0°±4.3°	56.5°±4.3°
<b>Weighted Average</b>	1053 total (444 male/478 female)	Gender based average on: 400 male/446 female	52.1°±4.4°	53.9°±4.3°	53.0°±4.7°	55.4°±4.7°	51.7°±5.0°	53.8°±5.0°

† Statistically significant difference between genders

NR = Not reported

\* Only used 3 points to directly define opening plane

\*\* Used Data Thief to calculate SD from plot (B. Tummers, DataThief III. 2006 <<http://datathief.org/>>)

\*\*\* Calculated gender specific values from table

‡ Radiographic inclination = 90°-reported inclination value

**XX.X° [Italics]** Values calculated using conversions above from [214]- SD are "best guesses" taken from converted measurement scheme

The stability of the acetabular and femoral components implanted during THA procedures is dependent on their relative positions to each other. The concept of a “safe zone” for the optimal orientation of the acetabular component to reduce the risk of dislocation has been investigated and discussed by many authors.[48,89,199,200,212,214,224–226] The safe zone first proposed by Lewinnek et al. has become the *de facto* standard that many surgeons and implant developers use as a guide to install the acetabular component.[200,212,214] In their study, Lewinnek et al. measured the radiographic orientation of the acetabular component postoperatively to see which hips appeared stable and which hips dislocated. From their observations, they determined that respective ranges for optimal radiographic inclination and anteversion were  $40^{\circ}\pm 10^{\circ}$  and  $15^{\circ}\pm 10^{\circ}$ . This recommended safe zone has been a source of controversy in the recent literature.[199,200,223–226] Murtha et al. recently compared Lewinnek et al.’s proposed safe zone for THA against the orientation of the native acetabulum using 3-D reconstructions. [200,212] The results from this study complement Murtha et al.'s findings, and the combined findings from other studies, which bring the suggested safe zone into further question (Figure 4.1, Table 4.1 & Table 4.2).[90,198,200] Whether or not the target orientation of the acetabular component should be determined by the patient's specific anatomy or by a generalized safe zone is a separate discussion.[90,227–229] Regardless of the varying perspectives on proper component placement, the results from this study clearly show that the orientation of the native acetabulum does not correspond to previously suggested orientations of cup placement.

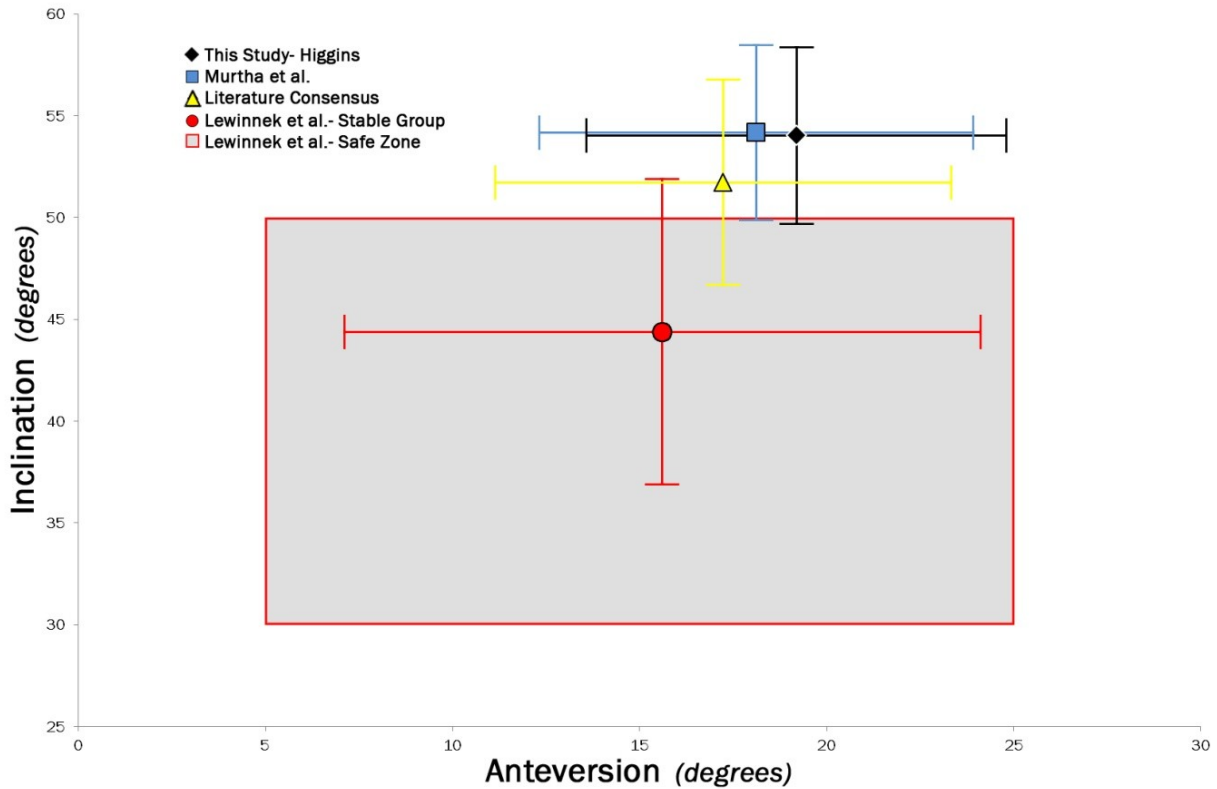


**Figure 4.1-** Comparisons of normal radiographic acetabular orientation. The shaded area shows the recommended safe zone from Lewinnek et al. (inclination-  $40^{\circ} \pm 10^{\circ}$ /anteversion-  $15^{\circ} \pm 10^{\circ}$ ), and the circle (*red*) is their mean of 122 stable hips. The square (*blue*) is the mean of 42 hips from Murtha et al. which is in close agreement with diamond (*black*) is the mean from this study. The triangle (*yellow*) shows the consensus from the literature summarized in Tables 4.1 & 4.2.

It should be understood that any proposed safe zone is also dependent on the manufactured geometries of the implant components, which have their own set of pre-designed compounding angles. Therefore, any safe zone or recommended orientation for components may be valid if it is within the intended design parameters of the manufacturer, even if it is outside of the normal anatomic range. Interestingly, a recent study from Krebs et al., funded by a major implant manufacturer, reported results for normal acetabular orientation within Lewinnek et al.'s safe zone.[209] They used the border of the acetabulum as a guide to align the largest size cup to the native, unreamed, acetabulums of 50 anatomic pelvic specimens ( $n=100$  hips). Their reported value of  $39.8^{\circ} \pm 7^{\circ}$  for radiographic inclination is in almost perfect agreement with Lewinnek et al.. While their reported anteversion of  $20.7^{\circ} \pm 3.8^{\circ}$  is more in-line with recent 3-D



studies, it still places their normal orientation within the safe zone. This may indicate that using visual clues to align the acetabular component may be complicated by the limited perspective of the surgeon's view, resulting in a skewed perception of orientation. Regardless of the possible causes for this discrepancy, it is the responsibility of designers to develop implants that best match patient anatomy. With more robust methods of performing 3-D measurements, improved implant designs can be developed which may in turn reduce dislocations, reduce wear, and increase functional longevity. For example, recent 3-D reconstructions and detailed cadaveric studies have quantified the irregular contour of the acetabulum's osseous border.[48–51] These findings have been reflected in surgical considerations for joint preserving procedures as well as the design of new acetabular cups intended to prevent iliopsoas impingement.

During the course of this research, many inconsistencies in both angular and C.S. definitions were observed in the literature. While not limited to the cases noted here, some authors inappropriately make direct comparisons between 2-D and 3-D measures.[200,224] Others go to great lengths in characterizing large patient populations but fail to mention how angles were measured.[230] While a few select studies properly compare findings, many inappropriately make direct comparisons without accounting for all the 3-D parameters. When properly accounting for parameters such as angular definitions and coordinate systems, it has been shown that some disagreements noted between comparable research regarding safe zones were actually in considerably more agreement than initially reported.[89] Murray provides excellent guidance on commonly used angular measures and their proper application.[214] Expanding upon his advocacy for proper usage of completely defined angular measures, a fully defined 3-D reference frame must also be described. Because they are dependent upon one

another, it is impossible to make accurate and direct comparisons to other studies without complete definitions needed to reconstruct both the C.S. and measurements.

As the development of new software progresses, the need to manually capture landmarks and features for performing measures will need to be reduced to make them more reliable and practical to use. The new method from Tan et al. for automatically detecting the AR shows an advantage in that it doesn't require separate software to render the 3-D surfaces (i.e.- Mimics).[203,205] However, much like this study, areas of interest still needed to be isolated to separate them from the surrounding surface to form discrete data sets. As previously noted, their method has not undergone any reported statistical qualification or reliability analysis. It also appears that the detail of the surfaces was greatly reduced to form an over simplified cup shape. It is suspected that the surface(s) needed to be idealized, by removing anatomically present features that form prominent ridgelines around the fossa/articular cartilage margins and acetabular notch, to prevent edge detection at undesired locations. The authors also noted the need to make patient specific adjustments to the algorithm's curvature based settings to detect the edge of each acetabulum. The additional operator time needed to make patient specific adjustments and idealize the surfaces would make such a method impractical for use in analyzing a sizable data set or in a clinical setting.

Even though the other recently presented method from Puls et al. is yet to be applied to actual data acquired using CT or MRI imaging [204], 3-D data can be similarly represented when attained from either a scanner or a rendering of medical images by simple post-processing to change file formats. From observing its rigorous statistical evaluation and logical programmatic approach, their method presented for detecting the profile of the acetabulum by appears that it would transfer well to bodies rendered from DICOM images. However, this is yet to be seen in

the reported literature. Their method does show an advantage in that they use a general population based estimate for the initial "best guess" of acetabular orientation. While it is unclear as to how they exclude the acetabular notch, using a similar approach could eliminate the need to manually select three points on the AR to provide an initial estimate of acetabular orientation as was done in this study. The method developed for measuring acetabular orientation in this research shows multiple advantages to both of the previously proposed methods of Tan et al. and Puls et al..[203,204] Firstly, there was no need to make patient specific adjustments for automatically detecting the AR. Furthermore, the thorough statistical evaluation showed that the AR was detected with an almost perfect level of reliability over a range of users and subjects. Most importantly, the Acetabulator automatically detected the points used to establish the APP based C.S.. No other method has been proposed to automatically detect the points for establishing the APP. From observing the results attained using previous versions of the Acetabulator (v1.0-2.2) where these points were manually selected, this greatly increased the reliability of measures performed in this study. All of these advantages make the programmatic approach of the Acetabulator a more practical solution for clinical and research based investigations of acetabular orientation.

The amount of time required to gather and process data along with the inaccuracies associated with human error arising during manual operations, are commonly noted restraints of 3-D based studies of the acetabulum and any effort made to optimize and automate this process would be highly beneficial.[85,88,167,172,198,202–204] By utilizing currently available software for surface rendering and segmentation, in conjunction with Acetabulator's programmatic routine for automatically selecting points and performing subsequent calculations, the time required to process data in this study was greatly reduced. However, due to the large

sample size and experimental nature of the Acetabulator's development, a considerable amount of time was still required to perform this study. In the future, it would be ideal to have a standalone program that could automatically generate surfaces, isolate the AR, correct for patient positioning, and perform subsequent measures of interest.

Clinically relevant levels of accuracy can be viewed in terms of how closely surgical targets can be achieved and the accuracy needed in the diagnostic measures used to set the targets and evaluate their results (i.e.- for THA component placement, reorientation osteotomies, etc.). The newest robotically assisted procedures for THA claim that component placement can be achieved within  $\pm 5^\circ$  in any direction.[231] Our method has been statistically proven to reliably achieve levels of accuracy far exceeding this mark. To-date, no published study could be found with reliability measures matching that of this study. This enabled the detection of subtle differences that would have otherwise been indistinguishable due to variation arising in measurement error. The functional orientation of the acetabulum's aperture was determined on a large population of normal subjects, where females were observed to have significantly more inclination and anteversion than males. Continuing advances will enable the progression of ever improving methods for performing clinical measures, consequently reducing the diagnostic "no man's land", ideally enabling the development of new and innovative surgical techniques to ameliorate patient outcomes.

#### **4.3 Future Research**

The possible directions for future research with new, more accurate, programmatic tools hold many exciting opportunities. Without question, the development of new measurement techniques for analyzing the hip joint have lagged behind the recent improvements made in medical imaging.[165,210] As technology progresses, the methods developed to quantitatively

diagnose patients should commensurately continue to improve. Having a more accurate and reliable platform for performing acetabular measures, such as the Acetabulator, may elucidate important relationships between normal and abnormal hip joints. Hopefully, with enhanced diagnostic and research capability will come further knowledge pertaining to various abnormalities and afflictions.

There are interesting investigations that could be performed with the currently available data that was used in this study. First, it would be of interest to see if any of the numerous parameters measured in this study were statistically correlated. There are also other parameters that could be incorporated into the Acetabulator to make its analysis more complete. Primarily, adding a measure of acetabular depth would be of interest to determine how much coverage is provided by the acetabulum. While this is not critical for normal hips, it is of great importance to evaluate acetabulums at risk for both DDH and FAI. The anatomic parameter quantifying the orientation of the acetabular notch, known as acetabular "clocking", has been rarely reported on.[51,194,232] Normalizing the orientation of the acetabulum aperture's relative to its clocked location may yield new and useful information.

Of course, utilizing the Acetabulator for investigating abnormal hips would be of great interest. Using the normal benchmarks established in this study, hips displaying symptoms and/or confirmed diagnosis of diseases such as DDH, FAI, and OA could all be accurately compared and thoroughly analyzed. The appearance of osteophytes has been linked to DDH and OA [69,96,98,121,128,233], and are a primary observation for the classic osteoarthritis classification system of Kellgren and Lawrence.[234] Osteophytes were noted and removed/excluded for this study but not analyzed in depth. The size and location of these

osteophytes could be accurately compared to the various parameters of the acetabulum to see if a relationship exists.

Most importantly, incorporating the integral femur into the analysis is critical to gaining an understanding of the hip joint as complete system. Because tomograms of the condyles were not available, this study was unable to include the femoral aspect. New software has been recently developed to analyze the 3-D range of motion in hip and further investigate FAI.[155,156,235] Preoperative knowledge of where contact/impingement is occurring can enable less invasive procedures. A similar algorithm could be developed using the preexisting Acetabulator platform to include the geometry of the femur bone. It is the theory of this author that the underlying causes of FAI, especially cam type, is a result of an underlying mechanical imbalance of the femoroacetabular components. The development of excess bony tissue that eventually causes the primary source of impingement, could be simply be the natural response of Wolff's law.[71,72] If the compounding angles and coverage of the hip joint result in high levels of stress from the loads experienced during activity, the bones will remodel to reinforce themselves in corresponding areas of high stress. Furthermore, it is hypothesized that the underlying geometric imbalance is sometimes subtle, which is why it has yet to be uncovered with current measurement techniques. This theory is supported by the fact that patients with FAI are typically young and physically active.[34,157,159,161] The persistent and increased loading of the hip joint from athletic activities, coupled with the youthful ability to regenerate tissue, could be resulting in excessive remodeling of tissue at the point of impingement. The classic stress analysis of the hip joint is limited to a simple 2-D coronal perspective.[68,70] This theory could be investigated by using an accurate method to ascertain the exact geometric structures of both the femur and acetabulum. This method could then be expanded to account for the

arrangement between the two bony structures and simulate the range of motion during normal activities. With the detailed knowledge of both the structures and their relative motion, application of modern 3-D finite element analysis could be used to confirm the theory by observing if stress concentrations corresponded to the locations of impingement.

Regardless of what direction future research takes, new programmatic methods such as the Acetabulator are going to be important in creating consistency across studies. This consistency can be realized by using software that abets operators into using the same definitions for both indices and coordinate systems while reliably and accurately performing analyses. If such a system could be used by different observers in various clinics and research settings, everyone could fully profit from reported experiences by enabling the recommendations from different studies to be directly compared.[30,89] If substantial consensus could be obtained through further improvements in 3-D software programs, this would enable new devices and treatments to be developed for improved and timely intervention.[89,161] Although the precision of any treatment or intervention may not be as accurate as the tools such as the Acetabulator that could be used for preoperative planning, it is important to have the most precise data available before undertaking any procedure.[170] In 1950, Massie and Howorth stated: "A perfect method of grading would eliminate the personal factor, both in the patient and the observer, so that the same conditions reviewed by any trained observer would receive the same grade. No such system has been found in the literature, *nor could one be devised*." [30] It would have been impossible for them to foresee what was going to be possible as the age of computers just on the horizon. The research and new methods presented herein challenges their notion of what was previously thought to be impossible.

## Literature Cited

- [1] Hilgenreiner H., 1925, "Early diagnosis and early treatment of congenital dislocation of the hip," *Med Klin*, **21**, pp. 1385–1389.
- [2] Lequesne M., 1963, "Mesure des angles fondamentaux de la hanche radiographique de l'adulte par un rapporteur combiné.," *Rev Rhum*, **30**, pp. 479–485.
- [3] Heyman C. H., and Herndon C. H., 1950, "Legg-Perthes disease: a method for the measurement of the roentgenographic result," *J Bone Joint Surg Am*, **32(A:4)**, pp. 767–778.
- [4] Wiberg G., 1939, "Studies on dysplastic acetabula and congenital subluxation of the hip joint, with special reference to the complication of osteoarthritis," *Acta Chir Scand*, **Supplementum 58**, p. 83.
- [5] Stubbs A. J., Anz A. W., Frino J., Lang J. E., Weaver A. A., and Stitzel J. D., 2011, "Classic measures of hip dysplasia do not correlate with three-dimensional computer tomographic measures and indices," *Hip Int*, **21(5)**, pp. 549–558.
- [6] Lequesne M., and de Sèze S., 1961, "Le faux profile du bassin: Nouvelle incidence radiographique pour l'étude de la hanche. Son utilité dans les dysplasies et les différentes coxopathies," *Rev Rhum Mal Osteoartic*, **28**, pp. 643–652.
- [7] Visser J. D., and Jonkers A., 1980, "A method for calculating acetabular anteversion, femur anteversion and the instability index of the hip joint," *Neth J Surg*, **32(4)**, pp. 146–149.
- [8] Anda S., Svenningsen S., Dale L. G., and Benum P., 1986, "The acetabular sector angle of the adult hip determined by computed tomography," *Acta Radiol Diagn (Stockh)*, **27(4)**, pp. 443–447.
- [9] Reikerås O., Høiseth A., Reigstad A., and Fönstelién E., 1982, "Femoral neck angles: a specimen study with special regard to bilateral differences," *Acta Orthop Scand*, **53(5)**, pp. 775–779.
- [10] Anda S., Terjesen T., Kvistad K. A., and Svenningsen S., 1991, "Acetabular angles and femoral anteversion in dysplastic hips in adults: CT investigation," *J Comput Assist Tomogr*, **15(1)**, pp. 115–120.
- [11] Rabin D. L., Barnett C. R., Arnold W. D., Freiburger R. H., and Brooks G., 1965, "Untreated congenital hip disease: a study of the epidemiology, natural history, and social



- aspects of the disease in a Navajo population,” *Am J Public Health Nations Health*, **55**, pp. SUPPL:1–44.
- [12] Tan L., Aktas S., Copuroglu C., Ozcan M., and Ture M., 2001, “Reliability of radiological parameters measured on anteroposterior pelvis radiographs of patients with developmental dysplasia of the hip,” *Acta Orthop Belg*, **67**(4), pp. 374–379.
- [13] Connolly P., and Weinstein S. L., 2007, “The natural history of acetabular development in developmental dysplasia of the hip,” *Acta Orthop Traumatol Turc*, **41 Suppl 1**, pp. 1–5.
- [14] Lee M. C., and Ebersson C. P., 2006, “Growth and development of the child’s hip,” *Orthopedic Clinics of North America*, **37**(2), pp. 119–132.
- [15] Ponseti I. V., 1978, “Growth and development of the acetabulum in the normal child. Anatomical, histological, and roentgenographic studies,” *J Bone Joint Surg Am*, **60**(5), pp. 575–585.
- [16] Polkowski G. G., and Clohisy J. C., 2010, “Hip Biomechanics,” *Sports Medicine and Arthroscopy Review*, **18**(2), pp. 56–62.
- [17] Fagerson T. L., 1998, *The Hip Handbook*, Butterworth-Heinemann.
- [18] Netter F. H., 2006, *Atlas of Human Anatomy*, 4th Edition, Saunders.
- [19] Anatomical Chart Company, 2004, *Anatomy and Injuries of the Hip Anatomical Chart*, Lippincott Williams & Wilkins.
- [20] Nordin M., and Frankel V. H., 1989, *Basic Biomechanics of the Musculoskeletal System*, Lea & Febiger.
- [21] Bergmann G., Graichen F., and Rohlmann A., 1993, “Hip joint loading during walking and running, measured in two patients,” *J Biomech*, **26**(8), pp. 969–990.
- [22] Brinckmann P., Frobin W., and Leivseth G., 2002, *Musculoskeletal biomechanics*, Thieme.
- [23] Roach K. E., and Miles T. P., 1991, “Normal hip and knee active range of motion: the relationship to age,” *Phys Ther*, **71**(9), pp. 656–665.
- [24] Cailliet R., 2004, *The Illustrated Guide to Functional Anatomy of the Musculoskeletal System*, AMA Press, Chicago.
- [25] Hughes P. E., Hsu J. C., and Matava M. J., 2002, “Hip anatomy and biomechanics in the athlete,” *Sports Medicine and Arthroscopy Review*, **10**(2), p. 103.
- [26] Stillwell W. T., 1987, *The Art of Total Hip Arthroplasty*, Grune & Stratton.

- [27] Steppacher S. D., Tannast M., Werlen S., and Siebenrock K. A., 2008, "Femoral Morphology Differs Between Deficient and Excessive Acetabular Coverage," *Clin Orthop Relat Res*, **466**(4), pp. 782–790.
- [28] Gerscovich E. O., 1997, "A radiologist's guide to the imaging in the diagnosis and treatment of developmental dysplasia of the hip," *Skeletal radiology*, **26**(7), pp. 386–397.
- [29] Delaunay S., Dussault R. G., Kaplan P. A., and Alford B. A., 1997, "Radiographic measurements of dysplastic adult hips," *Skeletal radiology*, **26**(2), pp. 75–81.
- [30] Massie W. K., and Howorth M. B., 1950, "Congenital dislocation of the hip. Part I. Method of grading results," *J Bone Joint Surg Am*, **32-A**(3), pp. 519–531.
- [31] Weinstein S. L., 1987, "Natural history of congenital hip dislocation (CDH) and hip dysplasia," *Clin. Orthop. Relat. Res.*, (225), pp. 62–76.
- [32] Balderston R., 1992, *The Hip*, Lea & Febiger, Philadelphia.
- [33] Harris W. H., 1986, "Etiology of osteoarthritis of the hip," *Clin. Orthop. Relat. Res.*, (213), pp. 20–33.
- [34] Ganz R., Leunig M., Leunig-Ganz K., and Harris W. H., 2008, "The etiology of osteoarthritis of the hip: an integrated mechanical concept," *Clin. Orthop. Relat. Res.*, **466**(2), pp. 264–272.
- [35] Stulberg S. D., Cooperman D. R., and Wallensten R., 1981, "The natural history of Legg-Calvé-Perthes disease," *J Bone Joint Surg Am*, **63**(7), pp. 1095–1108.
- [36] Kim H. K. W., 2010, "Legg-Calvé-Perthes disease," *J Am Acad Orthop Surg*, **18**(11), pp. 676–686.
- [37] Hergan K., Oser W., and Moriggl B., 2000, "Acetabular ossicles: normal variant or disease entity?," *Eur Radiol*, **10**(4), pp. 624–628.
- [38] Kim H. T., Kim J. I., and Yoo C. I., 2000, "Diagnosing childhood acetabular dysplasia using the lateral margin of the sourcil," *Journal of Pediatric Orthopaedics*, **20**(6), p. 709.
- [39] Scoles P. V., Boyd A., and Jones P. K., 1987, "Roentgenographic parameters of the normal infant hip," *J Pediatr Orthop*, **7**(6), pp. 656–663.
- [40] Than P., Sillinger T., Kráncz J., and Bellyei Á., 2004, "Radiographic parameters of the hip joint from birth to adolescence," *Pediatric Radiology*, **34**(3), pp. 237–244.
- [41] Fredensborg N., 1976, "The CE angle of normal hips," *Acta Orthopaedica*, **47**(4), pp. 403–405.

- [42] Kleinberg S., and Lieberman H. S., 1936, "The acetabular index in infants in relation to congenital dislocation of the hip," *Archives of Surgery*, **32**(6), p. 1049.
- [43] Wilkinson J., and Carter C., 1960, "Congenital dislocation of the hip: the results of conservative treatment," *Journal of Bone and Joint Surgery-British Volume*, **42**(4), p. 669.
- [44] Schwend R. M., Pratt W. B., and Fultz J., 1999, "Untreated acetabular dysplasia of the hip in the Navajo: a 34 year case series followup," *Clinical orthopaedics and related research*, **364**, p. 108.
- [45] McKibbin B., 1970, "Anatomical factors in the stability of the hip joint in the newborn," *J Bone Joint Surg Br*, **52**(1), pp. 148–159.
- [46] Bolton-Maggs B. G., and Crabtree S. D., 1983, "The opposite hip in congenital dislocation of the hip," *Journal of Bone and Joint Surgery-British Volume*, **65**(3), p. 279.
- [47] Gray H., Warren H. Lewis, edited by, 1918, *Anatomy of the Human Body*, Lea and Febiger.
- [48] Maruyama M., Feinberg J. R., Capello W. N., and D'Antonio J. A., 2001, "The Frank Stinchfield Award: Morphologic features of the acetabulum and femur: anteversion angle and implant positioning," *Clin. Orthop. Relat. Res.*, (393), pp. 52–65.
- [49] Vandenbussche E., Saffarini M., Delogé N., Moctezuma J.-L., and Nogler M., 2007, "Hemispheric cups do not reproduce acetabular rim morphology," *Acta Orthop*, **78**(3), pp. 327–332.
- [50] Vandenbussche E., Saffarini M., Taillieu F., and Mutschler C., 2008, "The asymmetric profile of the acetabulum," *Clin. Orthop. Relat. Res.*, **466**(2), pp. 417–423.
- [51] Köhnlein W., Ganz R., Impellizzeri F. M., and Leunig M., 2009, "Acetabular Morphology: Implications for Joint-preserving Surgery," *Clin Orthop Relat Res*, **467**(3), pp. 682–691.
- [52] Cunningham D. J., and Robinson A., 1922, *Cunningham's Textbook of Anatomy*, Henry Frowde.
- [53] Klaue K., Durnin C. W., and Ganz R., 1991, "The acetabular rim syndrome. A clinical presentation of dysplasia of the hip," *Journal of Bone and Joint Surgery-British Volume*, **73**(3), p. 423.
- [54] Fujii M., Nakashima Y., Yamamoto T., Mawatari T., Motomura G., Matsushita A., Matsuda S., Jingushi S., and Iwamoto Y., 2010, "Acetabular Retroversion in Developmental Dysplasia of the Hip," *The Journal of Bone and Joint Surgery*, **92**(4), pp. 895–903.

- [55] Albiñana J., Morcuende J. A., Delgado E., and Weinstein S. L., 1995, "Radiologic pelvic asymmetry in unilateral late-diagnosed developmental dysplasia of the hip," *J Pediatr Orthop*, **15**(6), pp. 753–762.
- [56] Fujii M., Nakashima Y., Sato T., Akiyama M., and Iwamoto Y., 2011, "Pelvic Deformity Influences Acetabular Version and Coverage in Hip Dysplasia," *Clin Orthop Relat Res*, **469**(6), pp. 1735–1742.
- [57] Aoki H., Nagao Y., Ishii S., Masuda T., and Beppu M., 2010, "Acetabular and proximal femoral alignment in patients with osteoarthritis of the dysplastic hip and its influence on the progression of disease," *J Bone Joint Surg Br*, **92**(12), pp. 1703–1709.
- [58] Lafferty C. M., Sartoris D. J., Tyson R., Resnick D., Kursunoglu S., Pate D., and Sutherland D., 1986, "Acetabular alterations in untreated congenital dysplasia of the hip: computed tomography with multiplanar re-formation and three-dimensional analysis," *J Comput Assist Tomogr*, **10**(1), pp. 84–91.
- [59] Kim S. S., Frick S. L., and Wenger D. R., 1999, "Anteversion of the acetabulum in developmental dysplasia of the hip: analysis with computed tomography," *J Pediatr Orthop*, **19**(4), pp. 438–442.
- [60] Jia J., Li L., Zhang L., Zhao Q., and Liu X., 2011, "Three dimensional-CT evaluation of femoral neck anteversion, acetabular anteversion and combined anteversion in unilateral DDH in an early walking age group," *International Orthopaedics*.
- [61] Millis M. B., Murphy S. B., and Poss R., 1996, "Osteotomies about the hip for the prevention and treatment of osteoarthritis," *Instr Course Lect*, **45**, pp. 209–226.
- [62] Stulberg S. D., and Harris W. H., 1974, "Acetabular dysplasia and development of osteoarthritis of the hip," *The Hip: Proceedings of the Second Open Scientific Meeting of the Hip Society*, pp. 82–93.
- [63] Ömeroğlu H., Özçelik A., Inan U., and Seber S., 2006, "Assessment of the correlation between commonly used radiographic parameters in normal, subluxated and dislocated hips," *Journal of Pediatric Orthopaedics B*, **15**(3), p. 172.
- [64] Tönnis D., 1976, "Normal values of the hip joint for the evaluation of X-rays in children and adults," *Clin. Orthop. Relat. Res.*, (119), pp. 39–47.
- [65] Coleman S. S., 1968, "Congenital dysplasia of the hip in the Navajo infant," *Clin. Orthop. Relat. Res.*, **56**, pp. 179–193.
- [66] Hasegawa Y., Iwata H., Mizuno M., Genda E., Sato S., and Miura T., 1992, "The natural course of osteoarthritis of the hip due to subluxation or acetabular dysplasia," *Archives of orthopaedic and trauma surgery*, **111**(4), pp. 187–191.

- [67] Reikerås O., Bjerkreim I., and Kolbenstvedt A., 1983, "Anteversion of the acetabulum and femoral neck in normals and in patients with osteoarthritis of the hip," *Acta Orthop Scand*, **54**(1), pp. 18–23.
- [68] Pauwels F., 1976, *Biomechanics of the Normal and Diseased Hip: Theoretical Foundation, Technique, and Results of Treatment: An Atlas*, Springer-Verlag, Berlin.
- [69] Bombelli R., Santore R. F., and Poss R., 1984, "Mechanics of the normal and osteoarthritic hip. A new perspective," *Clin. Orthop. Relat. Res.*, (182), pp. 69–78.
- [70] Bombelli R., 1993, *Structure and function in normal and abnormal hips : how to rescue mechanically jeopardized hips*, Springer-Verlag, Berlin;New York.
- [71] Fung Y. C., 1993, *Biomechanics: Mechanical Properties of Living Tissues*, Springer.
- [72] Wolff J., 1986, "Das Gesetz der Transformation der Knochen A. Hirschwald: Berlin, 1892," *The Law of Bone Remodelling*. Berlin: Springer.
- [73] Frost H. M., 2004, "A 2003 update of bone physiology and Wolff's Law for clinicians," *Angle Orthod*, **74**(1), pp. 3–15.
- [74] Jacobsen S., 2006, "Adult hip dysplasia and osteoarthritis. Studies in radiology and clinical epidemiology," *Acta Orthop Suppl*, **77**(324), pp. 1–37.
- [75] Jacobsen S., and Sonne-Holm S., 2005, "Hip dysplasia: a significant risk factor for the development of hip osteoarthritis. A cross-sectional survey," *Rheumatology*, **44**(2), p. 211.
- [76] Cooperman D. R., Wallensten R., and Stulberg S. D., 1983, "Acetabular dysplasia in the adult," *Clin. Orthop. Relat. Res.*, (175), pp. 79–85.
- [77] Murphy S. B., Kijewski P. K., Millis M. B., and Harless A., 1990, "Acetabular dysplasia in the adolescent and young adult," *Clin. Orthop. Relat. Res.*, (261), pp. 214–223.
- [78] Reikerås O., Bjerkreim I., and Kolbenstvedt A., 1982, "Anteversion of the acetabulum in patients with idiopathic increased anteversion of the femoral neck," *Acta Orthop Scand*, **53**(6), pp. 847–852.
- [79] Murphy S. B., Ganz R., and Müller M. E., 1995, "The prognosis in untreated dysplasia of the hip. A study of radiographic factors that predict the outcome," *J Bone Joint Surg Am*, **77**(7), pp. 985–989.
- [80] Dorrell J. H., and Catterall A., 1986, "The torn acetabular labrum.," *J Bone Joint Surg Br*, **68**(3), pp. 400–403.

- [81] Ömeroğlu H., Kaya A., and Güçlü B., 2007, "Evidence-based current concepts in the radiological diagnosis and follow-up of developmental dysplasia of the hip," *Acta Orthop Traumatol Turc*, **41 Suppl 1**, pp. 14–18.
- [82] Sarban S., Ozturk A., Tabur H., and Isikan U. E., 2005, "Anteversion of the acetabulum and femoral neck in early walking age patients with developmental dysplasia of the hip," *J Pediatr Orthop B*, **14(6)**, pp. 410–414.
- [83] Clohisy J. C., Carlisle J. C., Trousdale R., Kim Y.-J., Beaulé P. E., Morgan P., Steger-May K., Schoenecker P. L., and Millis M., 2009, "Radiographic evaluation of the hip has limited reliability," *Clin. Orthop. Relat. Res.*, **467(3)**, pp. 666–675.
- [84] Nelitz M., Guenther K. P., Gunkel S., and Puhl W., 1999, "Reliability of radiological measurements in the assessment of hip dysplasia in adults," *Br J Radiol*, **72(856)**, pp. 331–334.
- [85] Tannast M., Zheng G., Anderegg C., Burckhardt K., Langlotz F., Ganz R., and Siebenrock K. A., 2005, "Tilt and rotation correction of acetabular version on pelvic radiographs," *Clin. Orthop. Relat. Res.*, **438**, pp. 182–190.
- [86] Nicholls A. S., Kiran A., Pollard T. C. B., Hart D. J., Arden C. P. A., Spector T., Gill H. S., Murray D. W., Carr A. J., and Arden N. K., 2011, "The association between hip morphology parameters and nineteen-year risk of end-stage osteoarthritis of the hip: a nested case-control study," *Arthritis Rheum.*, **63(11)**, pp. 3392–3400.
- [87] Tallroth K., and Lepistö J., 2006, "Computed tomography measurement of acetabular dimensions: normal values for correction of dysplasia," *Acta Orthop*, **77(4)**, pp. 598–602.
- [88] Zheng G., Tannast M., Anderegg C., Siebenrock K. A., and Langlotz F., 2007, "Hip2Norm: an object-oriented cross-platform program for 3D analysis of hip joint morphology using 2D pelvic radiographs," *Comput Methods Programs Biomed*, **87(1)**, pp. 36–45.
- [89] Yoon Y. S., Hodgson A. J., Tonetti J., Masri B. A., and Duncan C. P., 2008, "Resolving inconsistencies in defining the target orientation for the acetabular cup angles in total hip arthroplasty," *Clinical Biomechanics*, **23(3)**, pp. 253–259.
- [90] Lubovsky O., Wright D., Hardisty M., Kiss A., Kreder H., and Whyne C., 2012, "Acetabular orientation: anatomical and functional measurement," *Int J CARS*, **7(2)**, pp. 233–240.
- [91] Severin E. A., 1941, "Contribution to the knowledge of congenital dislocation of the hip joint: late results of closed reduction and arthrographic studies of recent cases," *Acta Chir Scand*, **84(Supplementum 63)**, pp. 1–142.

- [92] Tönnis D., 1987, *Congenital dysplasia and dislocation of the hip in children and adults*, Springer-Verlag, Berlin; New York.
- [93] Zionts L. E., and MacEwen G. D., 1986, "Treatment of congenital dislocation of the hip in children between the ages of one and three years," *J Bone Joint Surg Am*, **68**(6), pp. 829–846.
- [94] Anda S., 1993, "Acetabular dysplasia in the adolescent and young adult- Letters to the Editor," *Clin Orthop Relat Res*, (286), pp. 308–310.
- [95] Jacobsen S., Sonne-Holm S., Lund B., Søballe K., Kiaer T., Røvsing H., and Monrad H., 2004, "Pelvic orientation and assessment of hip dysplasia in adults," *Acta Orthop Scand*, **75**(6), pp. 721–729.
- [96] Jacobsen S., Sonne-holm S., Søballe K., Gebuhr P., and Lund B., 2005, "Hip dysplasia and osteoarthritis," *Acta Orthopaedica*, **76**, pp. 149–158.
- [97] Jacobsen S., Rømer L., and Søballe K., 2006, "The other hip in unilateral hip dysplasia," *Clin. Orthop. Relat. Res.*, **446**, pp. 239–246.
- [98] Jacobsen S., Rømer L., and Søballe K., 2005, "Degeneration in dysplastic hips. A computer tomography study," *Skeletal Radiol.*, **34**(12), pp. 778–784.
- [99] Shenton E. W. H., 1911, *Disease in bone and its detection by the x-rays*, Macmillan.
- [100] Perkins G., 1928, "Signs by Which to Diagnose Congenital Dislocation of the Hip," *The Lancet*, **211**(5457), pp. 648–650.
- [101] Harris N. H., Lloyd-Roberts G. C., and Gallien R., 1975, "Acetabular development in congenital dislocation of the hip. With special reference to the indications for acetabuloplasty and pelvic or femoral realignment osteotomy," *J Bone Joint Surg Br*, **57**(1), pp. 46–52.
- [102] Aronsson D. D., Goldberg M. J., Kling T. F. Jr, and Roy D. R., 1994, "Developmental dysplasia of the hip," *Pediatrics*, **94**(2 Pt 1), pp. 201–208.
- [103] Jones D. H. A., 2010, "Shenton's line," *J Bone Joint Surg Br*, **92**(9), pp. 1312–1315.
- [104] Guevara C. J., Pietrobon R., Carothers J. T., Olson S. A., and Vail T. P., 2006, "Comprehensive Morphologic Evaluation of the Hip in Patients with Symptomatic Labral Tear," *Clinical Orthopaedics and Related Research*, **453**, pp. 277–285.
- [105] Rhee P. C., Woodcock J. A., Clohisy J. C., Millis M., Sucato D. J., Beaulé P. E., Trousdale R. T., and Sierra R. J., 2011, "The Shenton line in the diagnosis of acetabular dysplasia in the skeletally mature patient," *J Bone Joint Surg Am*, **93 Suppl 2**, pp. 35–39.

- [106] Perkins G., 1992, "Signs by which to diagnose congenital dislocation of the hip. 1928.," *Clin Orthop Relat Res*, (274), pp. 3–5.
- [107] Boniforti F., Fujii G., Angliss R., and Benson M., 1997, "The reliability of measurements of pelvic radiographs in infants," *Journal of Bone and Joint Surgery-British Volume*, **79**(4), p. 570.
- [108] Putti V., 1934, "Risultati Della Cura Incruenta Della Lussazione Congenita dell'anca- 523 casi riesaminati dopo un minimo di 4 anni ad un massimo di 27 anni.," *Chir. d. Org. di Movimento*, (20), pp. 93–112.
- [109] Tönnis D., 1962, "Über Änderungen des Pfannendachwinkels der Hüftgelenke bei Dreh- und Kippstellung des kindlichen Beckens," *Z Orthop*, **96**, pp. 462–478.
- [110] Nakamura S., Ninomiya S., and Nakamura T., 1989, "Primary osteoarthritis of the hip joint in Japan," *Clin. Orthop. Relat. Res.*, (241), pp. 190–196.
- [111] Nagao Y., Aoki H., Ishii S.-J., Masuda T., and Beppu M., 2008, "Radiographic method to measure the inclination angle of the acetabulum," *J Orthop Sci*, **13**(1), pp. 62–71.
- [112] Mast N. H., Impellizzeri F., Keller S., and Leunig M., 2011, "Reliability and agreement of measures used in radiographic evaluation of the adult hip," *Clin. Orthop. Relat. Res.*, **469**(1), pp. 188–199.
- [113] Werner C. M. L., Copeland C. E., Ruckstuhl T., Stromberg J., Turen C. H., and Bouaicha S., 2011, "Relationship between Wiberg's lateral center edge angle, Lequesne's acetabular index, and medial acetabular bone stock," *Skeletal Radiol.*, **40**(11), pp. 1435–1439.
- [114] Werner C. M. L., Ramseier L. E., Ruckstuhl T., Stromberg J., Copeland C. E., Turen C. H., Rufibach K., and Bouaicha S., 2012, "Normal values of Wiberg's lateral center-edge angle and Lequesne's acetabular index-a coxometric update," *Skeletal radiology*.
- [115] Lequesne M., Malghem J., and Dion E., 2004, "The normal hip joint space: variations in width, shape, and architecture on 223 pelvic radiographs," *Ann. Rheum. Dis.*, **63**(9), pp. 1145–1151.
- [116] Mast J. W., Brunner R. L., and Zebrack J., 2004, "Recognizing acetabular version in the radiographic presentation of hip dysplasia," *Clin. Orthop. Relat. Res.*, (418), pp. 48–53.
- [117] Carlisle J. C., Zebala L. P., Shia D. S., Hunt D., Morgan P. M., Prather H., Wright R. W., Steger-May K., and Clohisy J. C., 2011, "Reliability of various observers in determining common radiographic parameters of adult hip structural anatomy," *Iowa Orthop J*, **31**, pp. 52–58.
- [118] Dickens D. R., and Menelaus M. B., 1978, "The assessment of prognosis in Perthes' disease," *J Bone Joint Surg Br*, **60-B**(2), pp. 189–194.



- [119] Wiig O., Terjesen T., and Svenningsen S., 2002, "Inter-observer reliability of radiographic classifications and measurements in the assessment of Perthes' disease," *Acta Orthop Scand*, **73**(5), pp. 523–530.
- [120] Engesæter I. O., Laborie L. B., Lehmann T. G., Sera F., Fevang J., Pedersen D., Morcuende J., Lie S. A., Engesæter L. B., and Rosendahl K., 2012, "Radiological findings for hip dysplasia at skeletal maturity. Validation of digital and manual measurement techniques," *Skeletal Radiol.*, **41**(7), pp. 775–785.
- [121] Okano K., Takaki M., Okazaki N., and Shindo H., 2008, "Bilateral incidence and severity of acetabular dysplasia of the hip," *J Orthop Sci*, **13**(5), pp. 401–404.
- [122] Tannast M., Siebenrock K. A., and Anderson S. E., 2007, "Femoroacetabular impingement: radiographic diagnosis--what the radiologist should know," *AJR Am J Roentgenol*, **188**(6), pp. 1540–1552.
- [123] Broughton N. S., Brougham D. I., Cole W. G., and Menelaus M. B., 1989, "Reliability of radiological measurements in the assessment of the child's hip," *J Bone Joint Surg Br*, **71**(1), pp. 6–8.
- [124] Sallis J. G., and Smith R. G., 1965, "A study of the development of the acetabular roof in congenital dislocation of the hip," *Br J Surg*, **52**, pp. 44–46.
- [125] Dandachli W., Kannan V., Richards R., Shah Z., Hall-Craggs M., and Witt J., 2008, "Analysis of cover of the femoral head in normal and dysplastic hips: new CT-based technique," *J Bone Joint Surg Br*, **90**(11), pp. 1428–1434.
- [126] Anda S., Svenningsen S., Grontvedt T., and Benum P., 1990, "Pelvic inclination and spatial orientation of the acetabulum. A radiographic, computed tomographic and clinical investigation," *Acta Radiol*, **31**(4), pp. 389–394.
- [127] Anderson L. A., Gililand J., Pelt C., Linford S., Stoddard G. J., and Peters C. L., 2011, "Center edge angle measurement for hip preservation surgery: technique and caveats," *Orthopedics*, **34**(2), p. 86.
- [128] Murray R. O., 1965, "The aetiology of primary osteoarthritis of the hip," *Br J Radiol*, **38**(455), pp. 810–824.
- [129] Zingg P. O., Werner C. M. L., Sukthankar A., Zanetti M., Seifert B., and Dora C., 2009, "The anterior center edge angle in Lequesne's false profile view: interrater correlation, dependence on pelvic tilt and correlation to anterior acetabular coverage in the sagittal plane. A cadaver study," *Arch Orthop Trauma Surg*, **129**(6), pp. 787–791.
- [130] Klaue K., Wallin A., and Ganz R., 1988, "CT evaluation of coverage and congruency of the hip prior to osteotomy," *Clin. Orthop. Relat. Res.*, (232), pp. 15–25.

- [131] Tönnis D., and Heinecke A., 1999, "Acetabular and Femoral Anteversion: Relationship with Osteoarthritis of the Hip," *The Journal of Bone and Joint Surgery*, **81**(12), p. 1747.
- [132] Sharp I. K., 1961, "ACETABULAR DYSPLASIA: The Acetabular Angle," *J Bone Joint Surg Br*, **43-B**(2), pp. 268–272.
- [133] Crowe J. F., Mani V. J., and Ranawat C. S., 1979, "Total hip replacement in congenital dislocation and dysplasia of the hip," *J Bone Joint Surg Am*, **61**(1), pp. 15–23.
- [134] Ullmann K., 1939, "Zur Frage der röntgenologischen Beurteilung des Pfannendaches. Verh Dtsch Ges Orthop, 33. Kongr.," *Z Orthop Ihre Grenzgeb*, **69**, pp. 268–271.
- [135] Tönnis D., Behrens K., and Tucharani F., 1981, "A modified technique of the triple pelvic osteotomy: early results," *J Pediatr Orthop*, **1**(3), pp. 241–249.
- [136] Vare V. B. Jr, 1952, "The anatomy of the pelvic tear figure," *J Bone Joint Surg Am*, **34-A**(1), pp. 167–169.
- [137] Katz J. F., 1969, "Identification of the 'teardrop' figure and acetabular margins on the roentgenogram," *Clin. Orthop. Relat. Res.*, **62**, pp. 232–239.
- [138] Katz J. F., 1979, "Precise identification of radiographic acetabular landmarks," *Clin. Orthop. Relat. Res.*, (141), pp. 166–168.
- [139] Armbuster T. G., Guerra J. Jr, Resnick D., Goergen T. G., Feingold M. L., Niwayama G., and Danzig L. A., 1978, "The adult hip: an anatomic study. Part I: the bony landmarks," *Radiology*, **128**(1), pp. 1–10.
- [140] Lee Y.-K., Chung C. Y., Koo K.-H., Lee K. M., Kwon D. G., and Park M. S., 2011, "Measuring acetabular dysplasia in plain radiographs," *Arch Orthop Trauma Surg*, **131**(9), pp. 1219–1226.
- [141] Idelberger K., and Frank A., 1952, "A new method for determination of the angle of the pelvic acetabulum in child and in adult [German]," *Z Orthop Ihre Grenzgeb*, **82**(4), pp. 571–577.
- [142] Fuchs-Winkelmann S., Peterlein C.-D., Tibesku C. O., and Weinstein S. L., 2008, "Comparison of pelvic radiographs in weightbearing and supine positions," *Clin. Orthop. Relat. Res.*, **466**(4), pp. 809–812.
- [143] Visser J. D., Jonkers A., and Hillen B., 1982, "Hip joint measurements with computerized tomography," *J Pediatr Orthop*, **2**(2), pp. 143–146.
- [144] LeDamany P., 1908, "Die angeborene Hüftgelenksverrenkung," *Zeitschrift für orthopädische Chirurgie*, **21**, pp. 129–169.

- [145] Anda S., Svenningsen S., Slørdahl J., and Benum P., 1986, "Voluntary hip subluxation examined by computed tomography," *Acta Orthop Scand*, **57**(1), pp. 94–95.
- [146] Anda S., Terjesen T., and Kvistad K. A., 1991, "Computed tomography measurements of the acetabulum in adult dysplastic hips: which level is appropriate?," *Skeletal Radiol.*, **20**(4), pp. 267–271.
- [147] Anda S., and Amdal I. K., 1993, "Simple mathematical relations between the acetabular anteversion and sector angles," *Acta Radiol*, **34**(1), pp. 99–100.
- [148] Høiseth A., Reikerås O., and Fønstelien E., 1989, "Lack of correlation between femoral neck anteversion and acetabular orientation. Radiography and computed tomography in cadavers and in vivo," *Acta Orthop Scand*, **60**(1), pp. 93–96.
- [149] Toogood P. A., Skalak A., and Cooperman D. R., 2009, "Proximal femoral anatomy in the normal human population," *Clin. Orthop. Relat. Res.*, **467**(4), pp. 876–885.
- [150] Hoaglund F. T., and Low W. D., 1980, "Anatomy of the femoral neck and head, with comparative data from Caucasians and Hong Kong Chinese," *Clin. Orthop. Relat. Res.*, (152), pp. 10–16.
- [151] Jamali A. A., Mladenov K., Meyer D. C., Martinez A., Beck M., Ganz R., and Leunig M., 2007, "Anteroposterior pelvic radiographs to assess acetabular retroversion: high validity of the 'cross-over-sign'," *J. Orthop. Res.*, **25**(6), pp. 758–765.
- [152] Weil U., 1978, *Acetabular dysplasia Skeletal dysplasias in childhood*, Springer-Verlag, Berlin; New York.
- [153] Murphy S. B., Simon S. R., Kijewski P. K., Wilkinson R. H., and Griscom N. T., 1987, "Femoral anteversion," *J Bone Joint Surg Am*, **69**(8), pp. 1169–1176.
- [154] Ito K., Minka M. A. 2nd, Leunig M., Werlen S., and Ganz R., 2001, "Femoroacetabular impingement and the cam-effect. A MRI-based quantitative anatomical study of the femoral head-neck offset," *J Bone Joint Surg Br*, **83**(2), pp. 171–176.
- [155] Kubiak-Langer M., Tannast M., Murphy S. B., Siebenrock K. A., and Langlotz F., 2007, "Range of motion in anterior femoroacetabular impingement," *Clin. Orthop. Relat. Res.*, **458**, pp. 117–124.
- [156] Tannast M., Kubiak-Langer M., Langlotz F., Puls M., Murphy S. B., and Siebenrock K. A., 2007, "Noninvasive three-dimensional assessment of femoroacetabular impingement," *J. Orthop. Res.*, **25**(1), pp. 122–131.
- [157] Bredella M., 2005, "MR Imaging of Femoroacetabular Impingement," *Magnetic Resonance Imaging Clinics of North America*, **13**(4), pp. 653–664.

- [158] Beck M., Kalthor M., Leunig M., and Ganz R., 2005, "Hip morphology influences the pattern of damage to the acetabular cartilage: femoroacetabular impingement as a cause of early osteoarthritis of the hip," *J Bone Joint Surg Br*, **87**(7), pp. 1012–1018.
- [159] Ganz R., Parvizi J., Beck M., Leunig M., Nötzli H., and Siebenrock K. A., 2003, "Femoroacetabular impingement: a cause for osteoarthritis of the hip," *Clin. Orthop. Relat. Res.*, (417), pp. 112–120.
- [160] Beaulé P. E., Zaragoza E., Motamedi K., Copelan N., and Dorey F. J., 2005, "Three-dimensional computed tomography of the hip in the assessment of femoroacetabular impingement," *J. Orthop. Res.*, **23**(6), pp. 1286–1292.
- [161] Kavanagh E. C., Read P., Carty F., Zoga A. C., Parvizi J., and Morrison W. B., 2011, "Three-dimensional magnetic resonance imaging analysis of hip morphology in the assessment of femoral acetabular impingement," *Clinical Radiology*, **66**(8), pp. 742–747.
- [162] Kim W. Y., Hutchinson C. E., Andrew J. G., and Allen P. D., 2006, "The relationship between acetabular retroversion and osteoarthritis of the hip," *Journal of Bone and Joint Surgery-British Volume*, **88**(6), p. 727.
- [163] Ecker T. M., Tannast M., Puls M., Siebenrock K. A., and Murphy S. B., 2007, "Pathomorphologic alterations predict presence or absence of hip osteoarthritis," *Clin. Orthop. Relat. Res.*, **465**, pp. 46–52.
- [164] Carroll K. L., Murray K. A., MacLeod L. M., Hennessey T. A., Woiczik M. R., and Roach J. W., 2011, "Measurement of the center edge angle and determination of the Severin classification using digital radiography, computer-assisted measurement tools, and a Severin algorithm: intraobserver and interobserver reliability revisited," *J Pediatr Orthop*, **31**(4), pp. e30–35.
- [165] Pedersen D. R., Lamb C. A., Dolan L. A., Ralston H. M., Weinstein S. L., and Morcuende J. A., 2004, "Radiographic measurements in developmental dysplasia of the hip: reliability and validity of a digitizing program," *J Pediatr Orthop*, **24**(2), pp. 156–160.
- [166] Ward W. T., Vogt M., Grudziak J. S., Tümer Y., Cook P. C., and Fitch R. D., 1997, "Severin classification system for evaluation of the results of operative treatment of congenital dislocation of the hip. A study of intraobserver and interobserver reliability," *J Bone Joint Surg Am*, **79**(5), pp. 656–663.
- [167] Tannast M., Mistry S., Steppacher S. D., Reichenbach S., Langlotz F., Siebenrock K. A., and Zheng G., 2008, "Radiographic analysis of femoroacetabular impingement with Hip2Norm-reliable and validated," *J. Orthop. Res.*, **26**(9), pp. 1199–1205.
- [168] Ball F., and Kommenda K., 1968, "Sources of error in the roentgen evaluation of the hip in infancy," *Ann Radiol (Paris)*, **11**(5), pp. 298–303.

- [169] Tannast M., Langlotz U., Siebenrock K.-A., Wiese M., Bernsmann K., and Langlotz F., 2005, "Anatomic referencing of cup orientation in total hip arthroplasty," *Clin. Orthop. Relat. Res.*, (436), pp. 144–150.
- [170] van Bosse H. J. P., Lee D., Henderson E. R., Sala D. A., and Feldman D. S., 2011, "Pelvic positioning creates error in CT acetabular measurements," *Clin. Orthop. Relat. Res.*, **469**(6), pp. 1683–1691.
- [171] Siebenrock K. A., Kalbermatten D. F., and Ganz R., 2003, "Effect of pelvic tilt on acetabular retroversion: a study of pelves from cadavers," *Clin. Orthop. Relat. Res.*, (407), pp. 241–248.
- [172] Perreira A. C., Hunter J. C., Laird T., and Jamali A. A., 2010, "Multilevel Measurement of Acetabular Version Using 3-D CT-generated Models: Implications for Hip Preservation Surgery," *Clin Orthop Relat Res*, **469**(2), pp. 552–561.
- [173] PALMEN K., 1961, "Preluxation of the hip joint. Diagnosis and treatment in the newborn and the diagnosis of congenital dislocation of the hip joint in Sweden during the years 1948-1960," *Acta Paediatr Suppl*, **50**(Suppl 129), pp. 1–71.
- [174] Kutty S., Schneider P., Faris P., Kiefer G., Frizzell B., Park R., and Powell J. N., 2011, "Reliability and predictability of the centre-edge angle in the assessment of pincer femoroacetabular impingement," *International Orthopaedics*.
- [175] Murphy S. B., Kijewski P. K., Simon S. R., Chandler H. P., Griffin P. P., Reilly D. T., Penenberg B. L., and Landy M. M., 1986, "Computer-aided simulation, analysis, and design in orthopedic surgery," *Orthop. Clin. North Am.*, **17**(4), pp. 637–649.
- [176] Möller T. B., and Reif E., 1997, *Pocket atlas of radiographic positioning*, Thieme.
- [177] Bonett D. G., 2002, "Sample size requirements for estimating intraclass correlations with desired precision," *Statist. Med.*, **21**(9), pp. 1331–1335.
- [178] Haber M., Barnhart H. X., Song J., and Gruden J., 2005, "Observer variability: a new approach in evaluating interobserver agreement," *Journal of Data Science*, **3**, pp. 69–83.
- [179] Landis J. R., and Koch G. G., 1977, "The measurement of observer agreement for categorical data," *Biometrics*, **33**(1), pp. 159–174.
- [180] McGraw K. O., and Wong S. P., 1996, "Forming inferences about some intraclass correlation coefficients," *Psychological methods*, **1**(1), p. 30.
- [181] Shoukri M. M., 2004, *Measures of interobserver agreement*, CRC Press.

- [182] Shrout P. E., and Fleiss J. L., 1979, "Intraclass correlations: uses in assessing rater reliability.," *Psychological bulletin*, **86**(2), p. 420.
- [183] Walter S. D., Eliasziw M., and Donner A., 1998, "Sample size and optimal designs for reliability studies," *Stat Med*, **17**(1), pp. 101–110.
- [184] Portney L. G., and Watkins M. P., 2009, *Foundations of clinical research: applications to practice*, Pearson/Prentice Hall.
- [185] Bruton A., Conway J. H., and Holgate S. T., 2000, "Reliability: What is it, and how is it measured?," *Physiotherapy*, **86**(2), pp. 94–99.
- [186] Fritz S. L., Blanton S., Uswatte G., Taub E., and Wolf S. L., 2009, "Minimal detectable change scores for the Wolf Motor Function Test," *Neurorehabil Neural Repair*, **23**(7), pp. 662–667.
- [187] Steffen T., and Seney M., 2008, "Test-retest reliability and minimal detectable change on balance and ambulation tests, the 36-item short-form health survey, and the unified Parkinson disease rating scale in people with parkinsonism," *Phys Ther*, **88**(6), pp. 733–746.
- [188] Kalberer F., Sierra R. J., Madan S. S., Ganz R., and Leunig M., 2008, "Ischial spine projection into the pelvis : a new sign for acetabular retroversion," *Clin. Orthop. Relat. Res.*, **466**(3), pp. 677–683.
- [189] Ball F., 1979, "Possibilities of error in the radiological diagnosis of hip dysplasia," *Rontgenpraxis*, **32**(3), pp. 58–74.
- [190] Konishi N., and Mieno T., 1993, "Determination of acetabular coverage of the femoral head with use of a single anteroposterior radiograph. A new computerized technique," *J Bone Joint Surg Am*, **75**(9), pp. 1318–1333.
- [191] Janzen D. L., Aippersbach S. E., Munk P. L., Sallomi D. F., Garbuz D., Werier J., and Duncan C. P., 1998, "Three-dimensional CT measurement of adult acetabular dysplasia: technique, preliminary results in normal subjects, and potential applications," *Skeletal Radiol.*, **27**(7), pp. 352–358.
- [192] Abel M. F., Sutherland D. H., Wenger D. R., and Mubarak S. J., 1994, "Evaluation of CT scans and 3-D reformatted images for quantitative assessment of the hip," *J Pediatr Orthop*, **14**(1), pp. 48–53.
- [193] Zilber S., Lazennec J. Y., Gorin M., and Saillant G., 2004, "Variations of caudal, central, and cranial acetabular anteversion according to the tilt of the pelvis," *Surg Radiol Anat*, **26**(6), pp. 462–465.

- [194] Lazennec J.-Y., Charlot N., Gorin M., Roger B., Arafati N., Bissery A., and Saillant G., 2004, "Hip-spine relationship: a radio-anatomical study for optimization in acetabular cup positioning," *Surg Radiol Anat*, **26**(2), pp. 136–144.
- [195] Govsa F., Ozer M. A., and Ozgur Z., 2005, "Morphologic features of the acetabulum," *Arch Orthop Trauma Surg*, **125**(7), pp. 453–461.
- [196] Urban J. E., Weaver A. A., Theivendran K., and Stitzel J. D., 2011, "Acetabular rim profile measurement in femoroacetabular impingement patients - biomed 2011," *Biomed Sci Instrum*, **47**, pp. 118–123.
- [197] Azuma H., Taneda H., and Igarashi H., 1991, "Evaluation of acetabular coverage: three-dimensional CT imaging and modified pelvic inlet view," *J Pediatr Orthop*, **11**(6), pp. 765–769.
- [198] Lubovsky O., Peleg E., Joskowicz L., Liebergall M., and Khoury A., 2010, "Acetabular orientation variability and symmetry based on CT scans of adults," *Int J CARS*, **5**(5), pp. 449–454.
- [199] Wan Z., Malik A., Jaramaz B., Chao L., and Dorr L. D., 2008, "Imaging and Navigation Measurement of Acetabular Component Position in THA," *Clin Orthop Relat Res*, **467**(1), pp. 32–42.
- [200] Murtha P. E., Hafez M. A., Jaramaz B., and DiGioia A. M. 3rd, 2008, "Variations in acetabular anatomy with reference to total hip replacement," *J Bone Joint Surg Br*, **90**(3), pp. 308–313.
- [201] Millis M. B., and Murphy S. B., 1992, "Use of computed tomographic reconstruction in planning osteotomies of the hip," *Clin Orthop*, **274**(154), p. 9.
- [202] Arenson R. L., Andriole K. P., Avrin D. E., and Gould R. G., 2000, "Computers in imaging and health care: now and in the future," *J Digit Imaging*, **13**(4), pp. 145–156.
- [203] Tan S., Yao J., Yao L., Summers R. M., and Ward M. M., 2008, "Acetabular rim and surface segmentation for hip surgery planning and dysplasia evaluation," *SPIE*, p. 69181N–69181N–10.
- [204] Puls M., Ecker T. M., Steppacher S. D., Tannast M., Siebenrock K. A., and Kowal J. H., 2011, "Automated detection of the osseous acetabular rim using three-dimensional models of the pelvis," *Comput. Biol. Med.*, **41**(5), pp. 285–291.
- [205] Tan S., Yao J., Ward M. M., Yao L., and Summers R. M., 2007, "Level sets on non-planar manifolds for ridge detection on isosurfaces," *SPIE*, pp. 651230–651230–12.

- [206] Boulay C., Tardieu C., Bénaim C., Hecquet J., Marty C., Prat-Pradal D., Legaye J., Duval-Beaupère G., and Pélissier J., 2006, "Three-dimensional study of pelvic asymmetry on anatomical specimens and its clinical perspectives," *J. Anat.*, **208**(1), pp. 21–33.
- [207] Badii M., Shin S., Torreggiani W. C., Jankovic B., Gustafson P., Munk P. L., and Esdaile J. M., 2003, "Pelvic Bone Asymmetry in 323 Study Participants Receiving Abdominal CT Scans," *Spine*, **28**(12), pp. 1335–1339.
- [208] Tague R. G., 1989, "Variation in pelvic size between males and females," *Am. J. Phys. Anthropol.*, **80**(1), pp. 59–71.
- [209] Krebs V., Incavo S. J., and Shields W. H., 2009, "The anatomy of the acetabulum: what is normal?," *Clin. Orthop. Relat. Res.*, **467**(4), pp. 868–875.
- [210] Kuszyk B. S., Heath D. G., Bliss D. F., and Fishman E. K., 1996, "Skeletal 3-D CT: advantages of volume rendering over surface rendering," *Skeletal Radiol.*, **25**(3), pp. 207–214.
- [211] Delp S. L., Taylor C., and Wells W. M., 1998, *Medical Image Computing and Computer-assisted Intervention: International Conference*, Springer, Cambridge, MA, USA.
- [212] Lewinnek G. E., Lewis J. L., Tarr R., Compere C. L., and Zimmerman J. R., 1978, "Dislocations after total hip-replacement arthroplasties," *J Bone Joint Surg Am*, **60**(2), p. 217.
- [213] DiGioia A. M., Jaramaz B., Blackwell M., Simon D. A., Morgan F., Moody J. E., Nikou C., Colgan B. D., Aston C. A., Labarca R. S., Kischell E., and Kanade T., 1998, "The Otto Aufranc Award. Image guided navigation system to measure intraoperatively acetabular implant alignment," *Clin. Orthop. Relat. Res.*, (355), pp. 8–22.
- [214] Murray D. W., 1993, "The definition and measurement of acetabular orientation," *Journal of Bone and Joint Surgery-British Volume*, **75**(2), p. 228.
- [215] Harvill L. M., 1991, "Standard error of measurement," *Educational Measurement: Issues and Practice*, **10**(2), pp. 33–41.
- [216] Bland J. M., and Altman D. G., 1986, "Statistical methods for assessing agreement between two methods of clinical measurement," *Lancet*, **1**(8476), pp. 307–310.
- [217] Bartko J. J., 1966, "The intraclass correlation coefficient as a measure of reliability," *Psychol Rep*, **19**(1), pp. 3–11.
- [218] Nichols D. P., 1998, "Choosing an intraclass correlation coefficient," *From SPSS Keywords*, (Number 67).



- [219] Weir J. P., 2005, "Quantifying test-retest reliability using the intraclass correlation coefficient and the SEM," *J Strength Cond Res*, **19**(1), pp. 231–240.
- [220] Beckerman H., Roebroek M. E., Lankhorst G. J., Becher J. G., Bezemer P. D., and Verbeek A. L., 2001, "Smallest real difference, a link between reproducibility and responsiveness," *Qual Life Res*, **10**(7), pp. 571–578.
- [221] Kobayashi D., Satsuma S., Kuroda R., and Kurosaka M., 2010, "Acetabular development in the contralateral hip in patients with unilateral developmental dysplasia of the hip," *J Bone Joint Surg Am*, **92**(6), pp. 1390–1397.
- [222] Ridgeway B., Arias B., and Barber M., 2008, "Variation of the obturator foramen and pubic arch of the female bony pelvis," *American Journal of Obstetrics and Gynecology*, **198**(5), pp. 546.e1–546.e4.
- [223] Busch C., 2008, "Further Opinion: Variations in acetabular anatomy with reference to total hip replacement," *Journal of Bone and Joint Surgery - British Volume*, **90-B**, pp. 1–2.
- [224] Stem E. S., O'Connor M. I., Kransdorf M. J., and Crook J., 2006, "Computed tomography analysis of acetabular anteversion and abduction," *Skeletal Radiol.*, **35**(6), pp. 385–389.
- [225] Beckmann J., Lüring C., Tingart M., Anders S., Grifka J., and Köck F. X., 2009, "Cup positioning in THA: current status and pitfalls. A systematic evaluation of the literature," *Arch Orthop Trauma Surg*, **129**(7), pp. 863–872.
- [226] Hassan D. M., Johnston G. H. , Dust W. N. , Watson G., and Dolovich A. T., 1998, "Accuracy of intraoperative assessment of acetabular prosthesis placement," *The Journal of arthroplasty*, **13**(1), pp. 80–84.
- [227] DiGioia A. M. 3rd, Jaramaz B., and Colgan B. D., 1998, "Computer assisted orthopaedic surgery. Image guided and robotic assistive technologies," *Clin. Orthop. Relat. Res.*, (354), pp. 8–16.
- [228] Steppacher S. D., Kowal J. H., and Murphy S. B., 2011, "Improving cup positioning using a mechanical navigation instrument," *Clin. Orthop. Relat. Res.*, **469**(2), pp. 423–428.
- [229] Moskal J. T., and Capps S. G., 2010, "Improving the Accuracy of Acetabular Component Orientation: Avoiding Malposition," *J Am Acad Orthop Surg*, **18**(5), pp. 286–296.
- [230] Tohtz S. W., Sassy D., Matziolis G., Preininger B., Perka C., and Hasart O., 2010, "CT evaluation of native acetabular orientation and localization: Sex-specific data comparison on 336 hip joints," *Technology and Health Care*, **18**(2), pp. 129–136.
- [231] MAKO Surgical Corp, 2011, "A New Level of Precision," [www.makosurgical.com](http://www.makosurgical.com).

- [232] Fujii M., Nakashima Y., Sato T., Akiyama M., and Iwamoto Y., 2012, “Acetabular Tilt Correlates with Acetabular Version and Coverage in Hip Dysplasia,” *Clinical orthopaedics and related research*.
- [233] Jacobsen S., Sonne-Holm S., Søballe K., Gebuhr P., and Lund B., 2004, “Radiographic case definitions and prevalence of osteoarthritis of the hip: a survey of 4 151 subjects in the Osteoarthritis Substudy of the Copenhagen City Heart Study,” *Acta Orthop Scand*, **75**(6), pp. 713–720.
- [234] Kellgren J. H., and Lawrence J. S., 1957, “Radiological assessment of osteo-arthritis,” *Ann. Rheum. Dis.*, **16**(4), pp. 494–502.
- [235] Hu Q., Langlotz U., Lawrence J., Langlotz F., and Nolte L. P., 2001, “A fast impingement detection algorithm for computer-aided orthopedic surgery,” *Comput. Aided Surg.*, **6**(2), pp. 104–110.

# Appendix A: Acetabulator- Detailed Flow Chart

Acetabulator- Program Code	
Version 3.0	5/6/2012



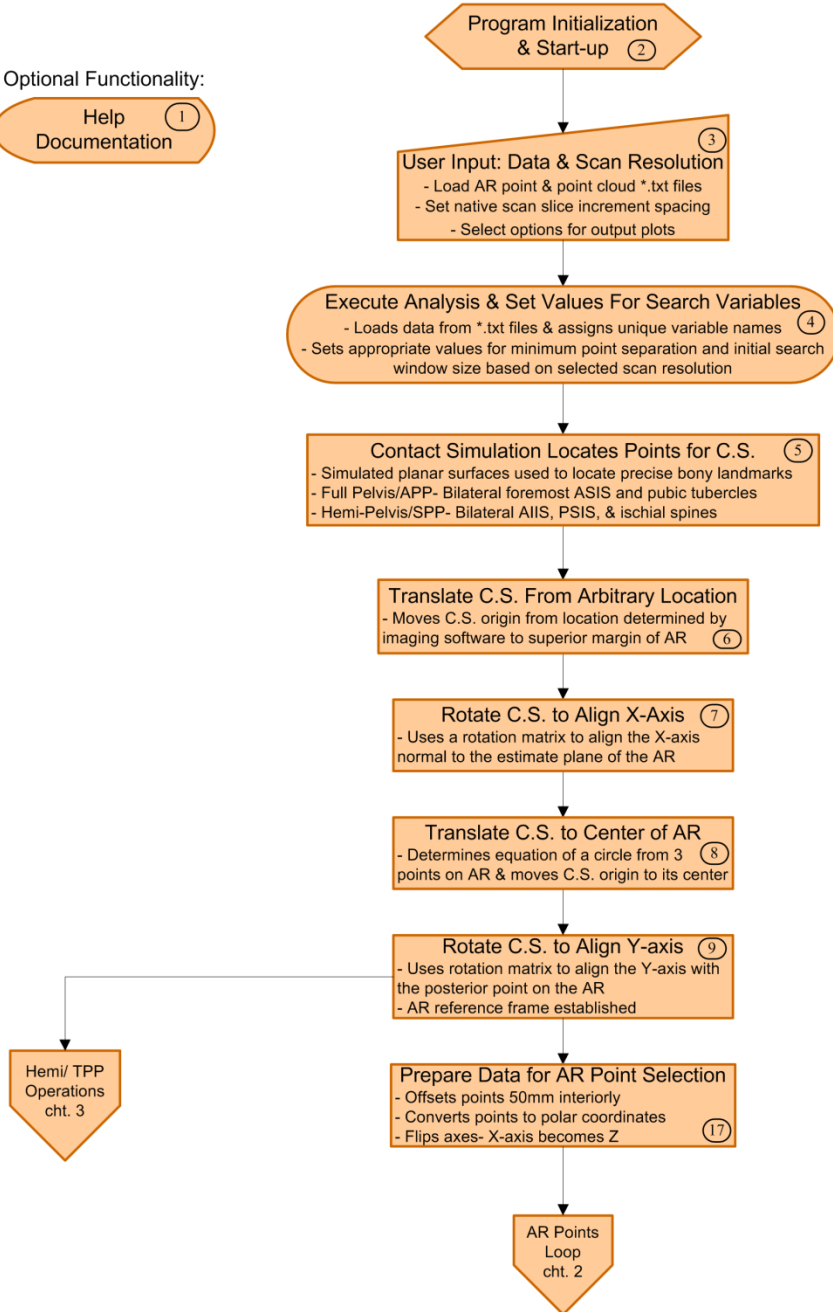
All Operation(s) Performed in MATLAB®

† Operation(s) Exclusive to True/ False Pelvis Analysis

# Corresponding Appendix B Block Section

Optional Functionality:

Help (1)  
Documentation

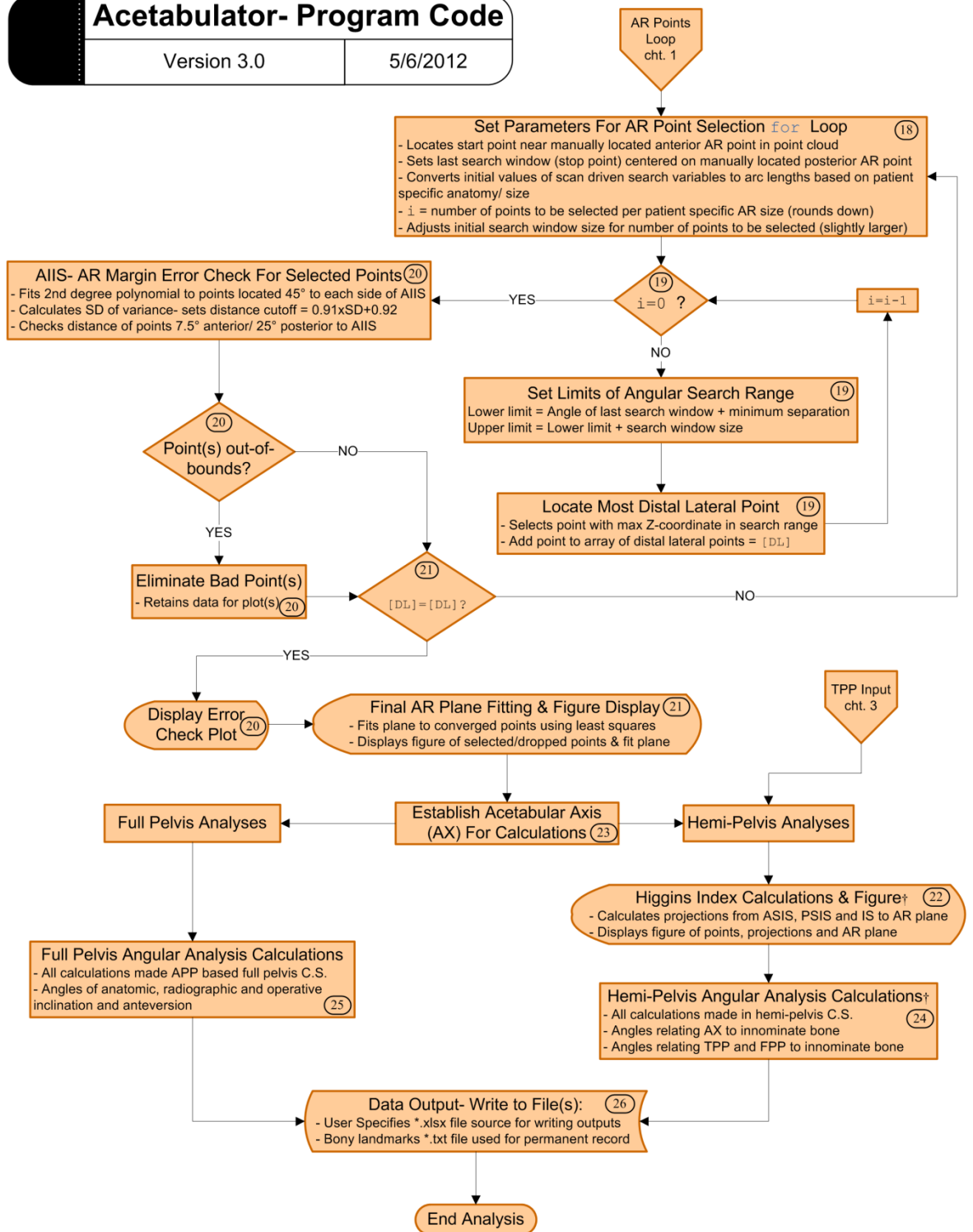


cht. 1

# Acetabulor- Program Code

Version 3.0

5/6/2012



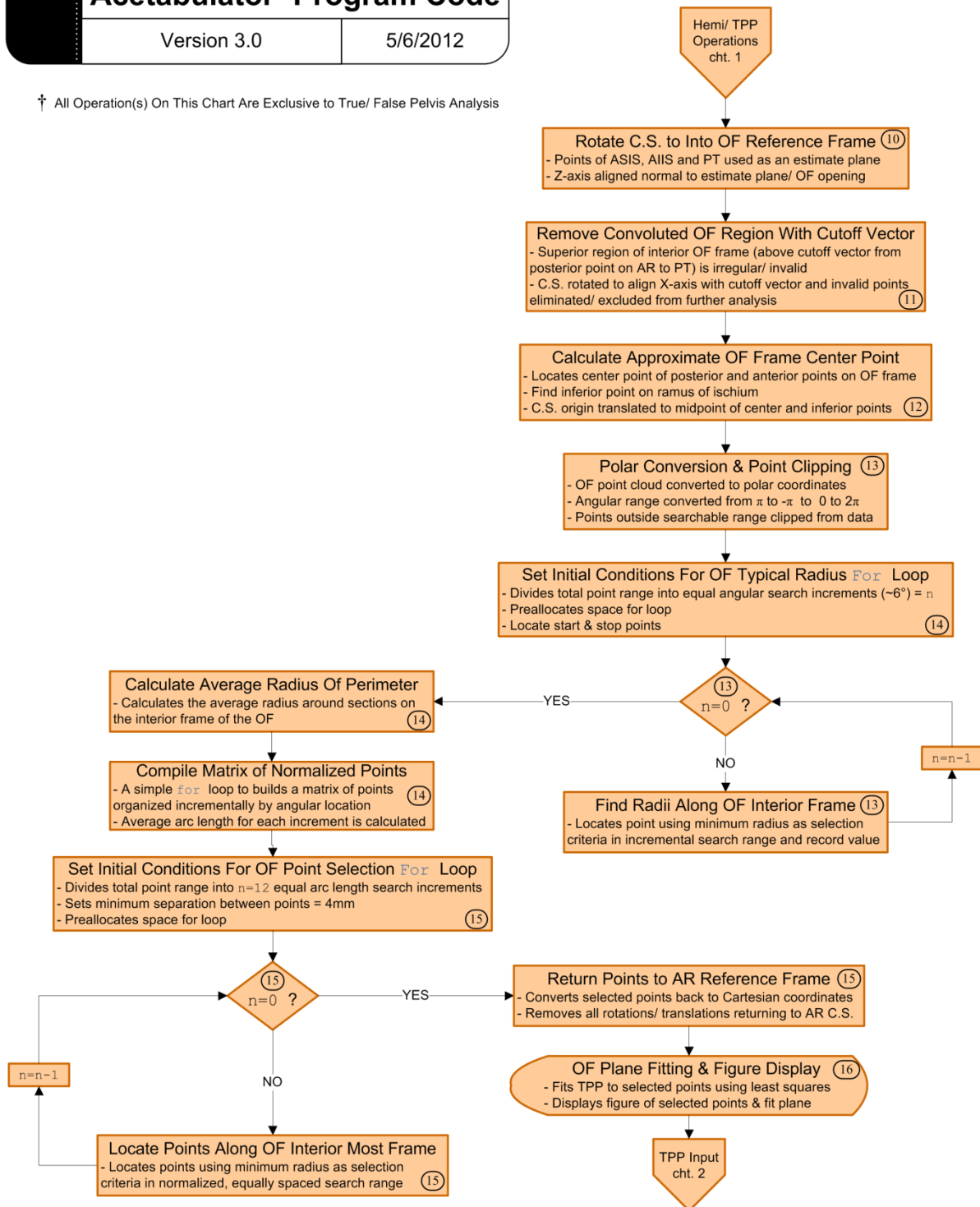
cht. 2

# Acetabulator- Program Code

Version 3.0

5/6/2012

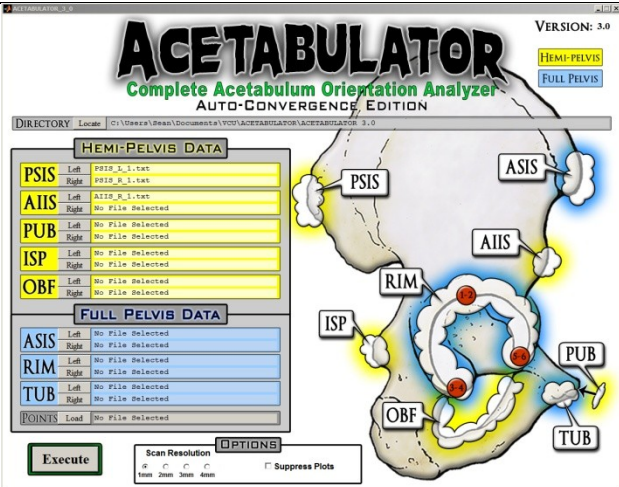
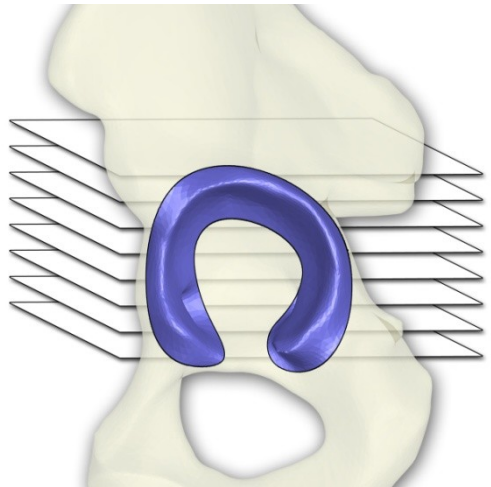
† All Operation(s) On This Chart Are Exclusive to True/ False Pelvis Analysis



cht. 3

## Appendix B: Acetabulator- Graphical Flow Montage

**Table B.1- Acetabulator Code Summary (v3.0)**

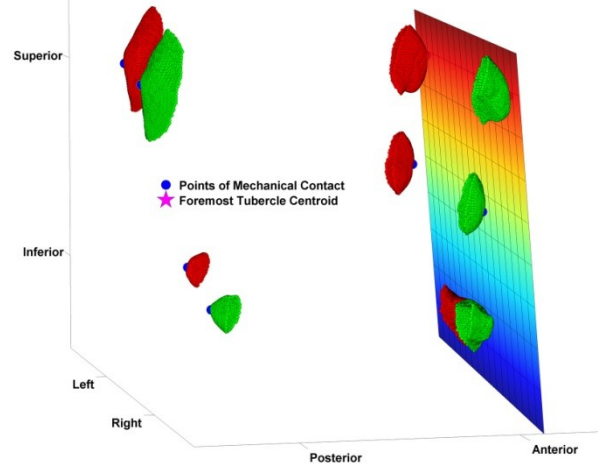
Section Summary	Code/ Figure/ Reference
<p><b>1:Version Info &amp; Help Documentation</b> Code Lines: 2-175</p> <p>This section provides information pertaining to the released version of the Acetabulator program. There is also help documentation provided that can be called on and displayed in the MATLAB® command window.</p>	<p>For help documentation the command: “help acetabulator_3_0”</p> <p>*Or other version as “acetabulator_x_x”</p>
<p><b>2:Initialization &amp; Program Start-up</b> Code Lines: 176-238</p> <p>This section contains code that initializes the program. The MATLAB® graphical user interface (GUI) platform has a structure for defining and retrieving variables referred to as a “handles structure”. The GUI background image must be in the same folder as the Acetabulator m-file (*.m).</p>	<p>Background File Name: “Acetabulator_Background.jpg”</p>
<p><b>3:File Location &amp; Input/ Output Controls</b> Code Lines: 239-557</p> <p>These lines of code create the functionality for the GUI push and radio buttons. Push buttons are used to locate the appropriate text (*.txt) files containing the bony landmarks and point cloud data. Each button opens a file browser to locate the corresponding data file and will display the path of the located file(s) in the GUI window. The radio buttons allow the user to select the source/native scan resolution. Scan resolution specific parameters are used for selecting the appropriate number of points on the AR. An option to suppress the output plots is available.</p> <p><b>Figure:</b> GUI interface with push buttons for locating/loading *.txt files.</p>	
<p><b>4: Execute- Load Data &amp; Assign Parameters</b> Code Lines: 558-766</p> <p>When the “Execute” button is depressed the files that have been previously located are opened. Each point cloud *.txt file is scanned and loaded as an <math>n \times 3</math> array containing the 3-D coordinates of all the points in a Cartesian coordinate system (C.S.) (Table B.2). Each point cloud array is assigned a unique variable name. The file containing the bony landmarks on the AR is scanned and each properly ordered point location is extracted and assigned a unique variable name. Parameters of minimum point spacing and search window size (for point selection) are set from the user specified scan resolution.</p> <p><b>Figure:</b> Depiction of CT slices intersecting AR. Every slice that intersects the AR will yield two unique points.</p>	

## 5:Contact Simulation To Locate Points

Code Lines: 767-1016

The subfunction "contact\_points" is called to locate bony landmarks on the pelvis (Table B.2). Contact is simulated using an "inside-out" method that locates distal points along the anterior direction of a vector normal to an estimate plane from inside the convex hulls of the points clouds. A while loop repeatedly reorients the estimate plane until the most distal three point are converged on. Points on the posterior are located along the vector normal of the converged plane.

**Figure:** Lateral view in output plot showing point clouds of the left (red) and right side (green). The APP (multicolor) is determined from the converged points on the ASIS and PT. The APP and SPP determine the posterior points (blue)



## 6:Translate C.S. To Superior Point on AR

Code Lines: 1017-1059

The C.S. origin is translated from an arbitrary point in space, defined by the software of the imaging equipment, to the point selected on the superior margin of the AR.

*\*All operations are performed bilaterally in the code to mirror the left and right sides.*

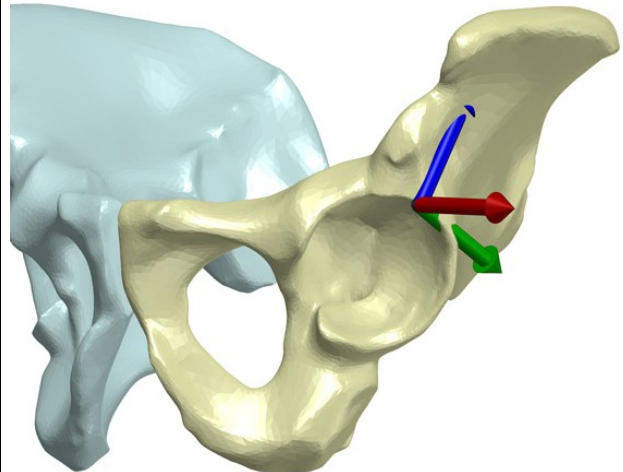
**Figure:** Left side C.S. translated to point on the top of the AR with axes still aligned to original/ equipment specified orientation.

### Axis Legend:

X-Axis- Red

Y-Axis- Green

Z- Axis- Blue

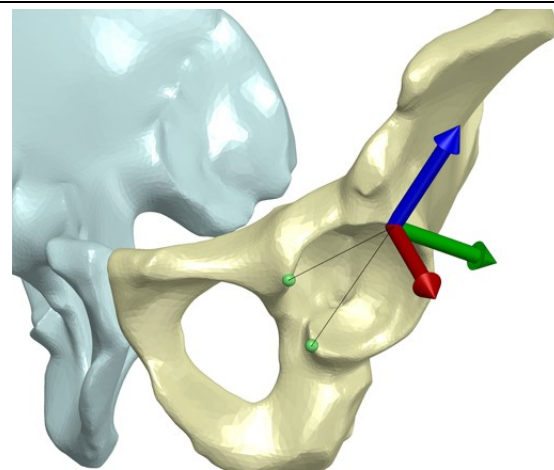


## 7:Rotate C.S. To Align X-Axis

Code Lines: 1060-1270

An estimated plane of the acetabular opening is formed using the three selected points (green & origin) on the AR. The vector normal to this plane is calculated from the cross product of two vectors originating from the top of the AR and extending to the posterior and anterior points of the AR. Euler angles about the Z and Y' axes are calculated using trigonometric relations. A rotation matrix constructed from the Euler angles is used to align the X-axis of the C.S. with the vector normal of the estimate plane.

**Figure:** Vectors used for determining the vector normal to the AR estimate plane (black). The X-axis (red) of the C.S. aligned to the vector normal of the estimate plane.

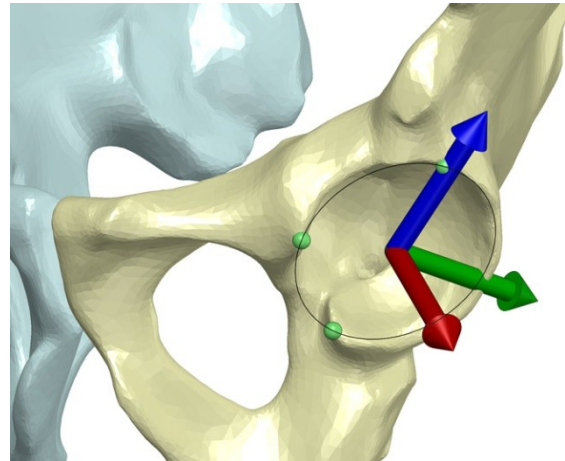


### 8: Translate C.S. To Center of Acetabulum

Code Lines: 1271-1345

Equations of two lines originating at the point on the top of the AR and terminating at the anterior and posterior points of the AR are calculated. Using the slopes of both lines and their end points, the center of a circle formed by the three points on the AR is calculated. This circle's center serves as an approximate location for the center diameter of the AR in the estimate plane. The C.S. origin is translated to the calculated circle's center point.

**Figure:** Three points (*green*) used to calculate the center of the circle (*black*) approximating the AR. The left side C.S. translated to the center point of the calculated circle.

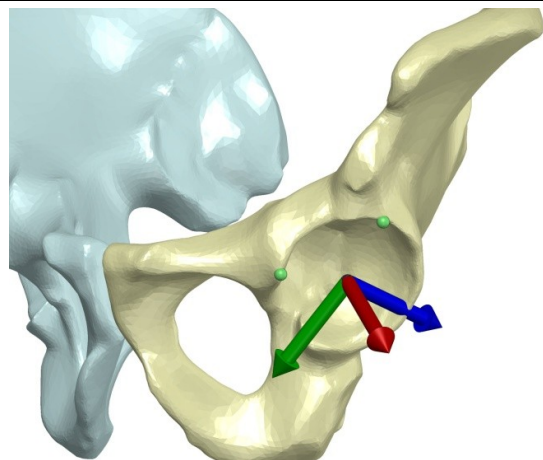


### 9: Rotate C.S. To Align Y-Axis

Code Lines: 1346-1530

Using a rotation matrix the Y-axis of the C.S. is aligned to the posterior point on the AR. This simplifies later operations by aligning all points in the AR point cloud to a functional zero start point. Most calculations and subsequent routines are performed in this reference frame, which will be referred to as the AR reference frame (or C.S.). The points of the obturator foramen (OF) point cloud are sorted by x-coordinate values in descending order for the ensuing operations.

**Figure:** The Y-axis (*green*) of the left side C.S. rotated into alignment with the posterior point of the AR.

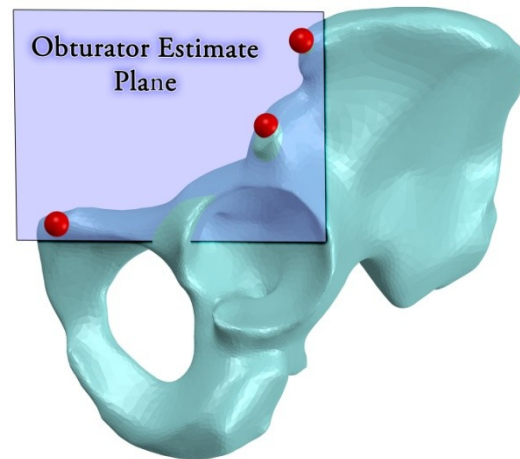


### 10: Rotate C.S. Into OF Reference Frame †

Code Lines: 1531-1605

For the hemi-pelvis analysis, the plane of the true pelvis is established using points on the bony ridge of the interior frame of the OF. The point cloud containing the OF first needs to be rotated into a C.S. facing the opening/ window of the interior frame. The points of the ASIS, AIIS and foremost point of the ipsilateral pubic tubercle (PT) create a plane that is functionally parallel to the window of the OF. Using rotations about the Z and Y' axes, the Z-axis for the OF point cloud, PT, and posterior point of the AR is aligned normal to the estimated plane.

**Figure:** Points of the ASIS, AIIS and PT (*red*) used to form a plane that faces the opening of the OF interior frame.





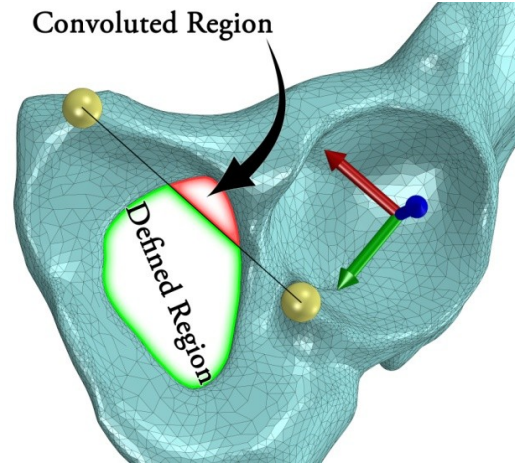
### 11: Rotate C.S. To Align X-Axis With Cutoff †

Code Lines: 1606-1642

One final rotation is applied to the OF reference frame to align the X-axis parallel to a line connecting the PT to the posterior point of the AR. A 2-D “cutoff” vector collinear to this line, in the XY plane of the current reference frame, intersects the interior frame of the OF. The intersection consistently splits OF frame into two regions. The superior region of the interior OF frame forms a convoluted helical ridge which is irregular and often indistinguishable.

**Figure:** Points of the posterior AR and PT (*gold*) used to form the cutoff vector (*black*). Convoluted (*red*) and well defined (*green*) regions of the OF frame. Final C.S. orientation for the OF reference frame as shown.

Convoluted Region

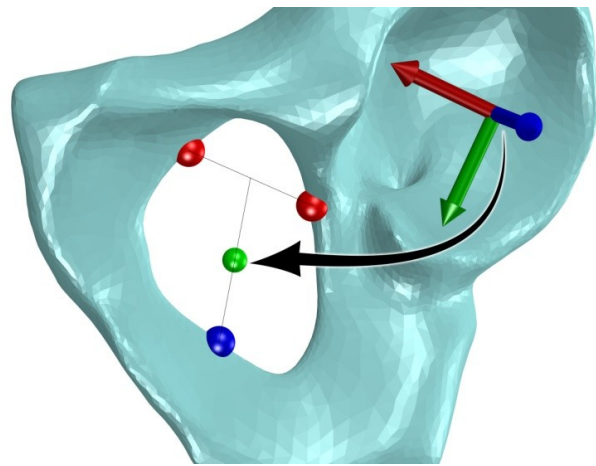


### 12: Locate Approximate OF Center Point †

Code Lines: 1643-1849

Using logic based operations; two points are selected on opposite sides of the interior OF frame within a range 1mm inferior to the cutoff vector. A point on the inferior ridge of the OF frame, on the ramus of ischium, is located along the direction of the Y-axis (*green*) which is normal to the cutoff vector. The point is located within a 1mm range, centered on the midpoint of the two points found above. The C.S. is translated to an approximated OF center point, located at the midpoint of a line between the inferior point and the midpoint of the two points below the cutoff vector.

**Figure:** Two points below cutoff vector (*red*) with inferior point on the Ischium (*blue*) locate new C.S. center (*green*).

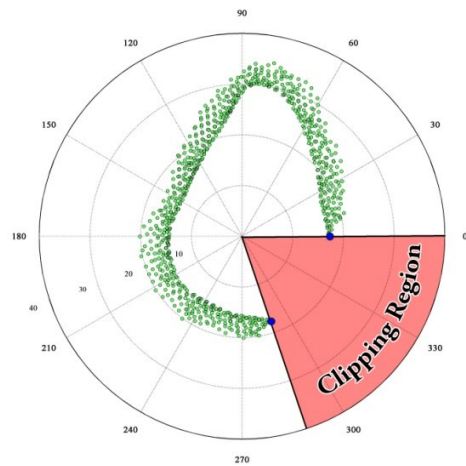


### 13: Polar Conversion/ Point Cloud Clipping †

Code Lines: 1850-1944

The points on the OF point cloud are converted to polar coordinates. Conversion to polar coordinates in MATLAB® results in an angular range of  $\pi$  to  $-\pi$  (radians). Using logical expressions, the range is converted to 0 to  $2\pi$ . The points are rotated to align 0 radians with the anterior point previously located on the OF frame (below the cutoff vector). The searchable range of points is defined from 0 radians to the angle at the posterior point on the OF frame (*blue points*). This potentially places some points outside of the searchable range which are clipped from the set.

**Figure:** Polar coordinate points of the OF point cloud (*green*) in the X-Y plane and clipping region (*red*).

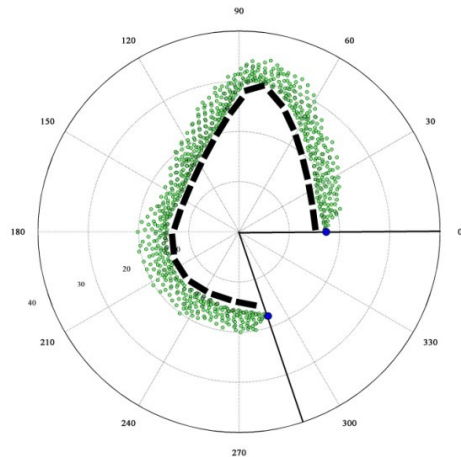


#### 14: Irregular Profile Correction Factor †

Code Lines: 1945-2216

Because the border of the OF interior frame is irregular and its center point is approximated, it cannot simply be divided into equal angular sections to select evenly spaced points. Using a `for` loop, the radius from the center to the interior bony ridge is determined in  $6^\circ$  increments. The average radius and arc length between sequential points is calculated to create a normalized profile of the interior frame based on arc length. All of the points in the OF point cloud are assigned an arc length value in the  $6^\circ$  increments.

**Figure:** Interior profile of the OF frame normalized and divided into equally spaced segments (*black*) based on average arc length between points.

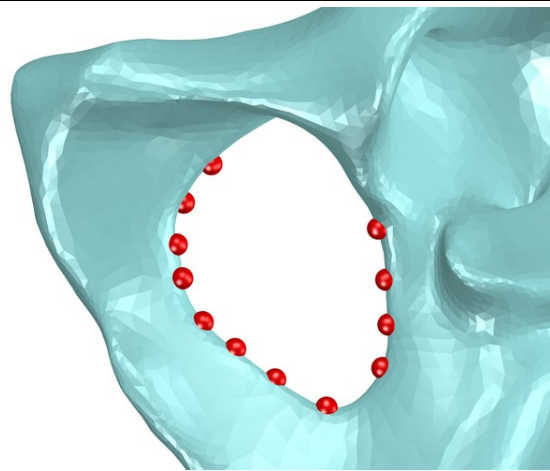


#### 15: Locate Points On The OF Interior Frame †

Code Lines: 2217-2368

The entire searchable range of points is divided into equal sized search windows based on arc length. Using a `for` loop, 12 properly spaced points along the bony ridge of the interior OF frame are located. The points are separated by a minimum of 4mm which assures that they are both unique and do not exceed the resolution of the scan data (1-4mm slice thickness). Points are selected based on minimum radius values which indicate that a point is located on the interior most edge of the bony ridge. Selected points are converted back to Cartesian coordinates and all rotations/translations are reverted back to the AR reference frame.

**Figure:** Selected points on the interior OF frame (*red*).

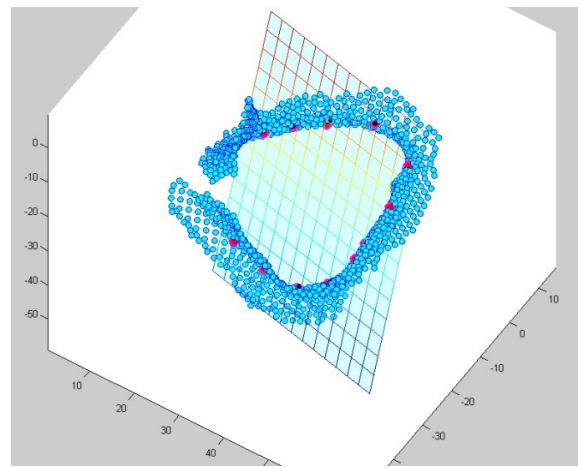


#### 16: OF Plane Fitting & Figure Generation †

Code Lines: 2369-2592

A plane is fit to the selected points on the OF frame using a least squares method. The sum of the squared residuals determined from the fit is used to calculate an  $R^2$  value which is reported in the output to describe the plane's goodness of the fit. The vector normal to the plane is established for later calculations. An interactive 3-D plot is generated which highlights the selected points and fit plane. To assure the routine selected appropriate points, the plot view can be dynamically rotated and manipulated.

**Figure:** OF figure rotated in oblique superoinferior view. Display of selected points (*red*), fit plane (*multicolor*), OF point cloud (*blue points*) and residuals (*black lines*).

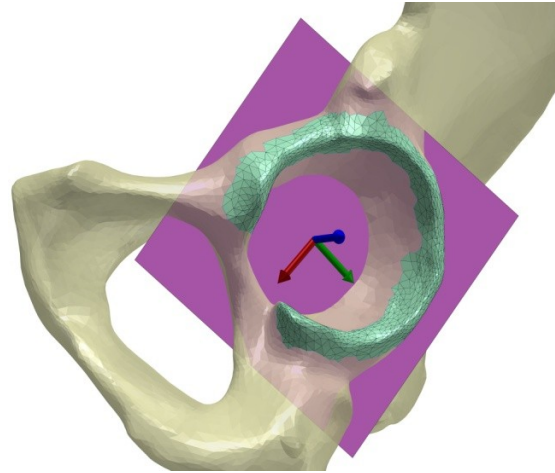


### 17:AR Point Selection Preparation

Code Lines: 2593-2700

In the current AR reference frame (Block 9), the level of the Y-Z plane has some portions of the AR residing on each side of it. The C.S. of the AR point cloud is offset 50mm interiorly to assure all points on the bony ridge of the rim reside to the exterior of the plane. To simplify coding operations the axes are changed as follows: X-axis to Z-axis, Y-axis to X-axis, and Z-axis to Y-axis. The points of the anterior AR and AR point cloud are converted to polar coordinates. The angular range is again converted to positive values 0 to  $2\pi$  using logic based operations.

**Figure:** Left AR with offset plane (*pink*), surface comprising the point cloud (*teal*), and switched C.S. axes.

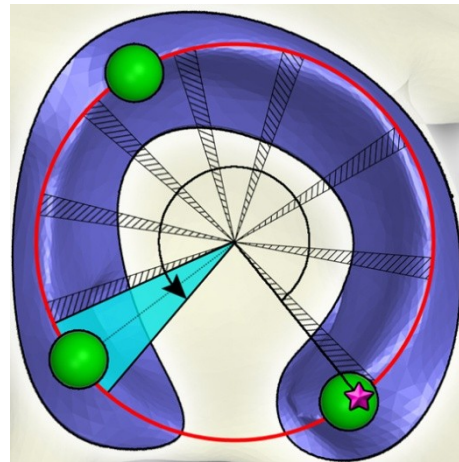


### 18:Initialize Patient Driven Search Parameters

Code Lines: 2701-2811

Start point located in the AR point cloud within  $\pm 1.25^\circ$  of the posterior AR point. The last search window is centered on the anterior AR point. The three points previously located on the AR provide an estimate of diameter used to determine the arc length (search range) between the start and stop. The scan resolution search parameters are converted to arc length and search window size is increased slightly to find an exact number of points per patient specific AR diameter.

**Figure:** Minimum separation (*crosshatched*) and search windows (*coarser than actual*). Estimated diameter of AR (*red*). Start point located on posterior AR point (*pink star*). Last search window centered on the anterior point (*teal*).

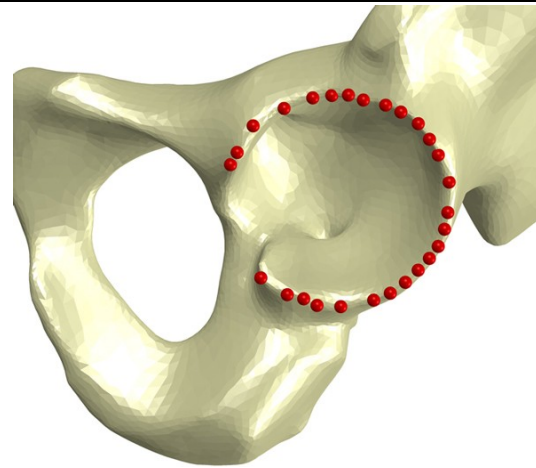


### 19:Locate Points On Distal Lateral AR

Code Lines: 2812-2956

A `for` loop is used to locate distal lateral points with maximal values along the direction of the X-axis (normal to the estimate plane). Points are separated by a minimum amount to assure that they are unique and do not exceed the scan data. The rim is divided into arc length increments of minimum separation + search window according to its size. Therefore, the larger the AR, the more slices will intersect its borders (unique points) and thus more points will be selected. Typical number of points selected/ search windows  $\approx 31$ / per AR.

**Figure:** Selected points on the distal lateral AR ridge (*red*).

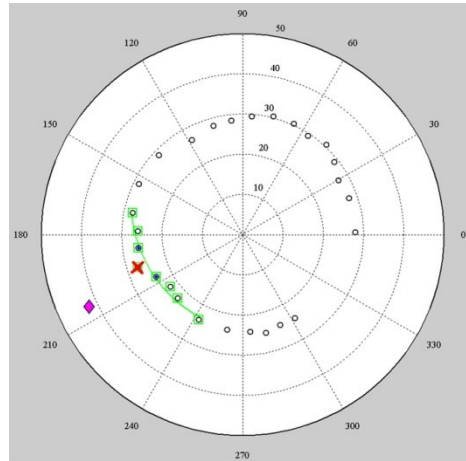


## 20: AIIS-AR Margin Error Check

Code Lines: 2957-3022

If the margin between the AR and AIIS lacks a distinct border, points not on the actual AR ridge could be errantly selected. A check is made to fully assure only befitting points are selected. A second degree polynomial is fit to selected points located  $45^\circ$  to each side of the AIIS and the SD of their variance calculated. The distance from the polynomial fit of points  $7.5^\circ$  anterior and  $25^\circ$  posterior to the AIIS (margin location) are checked. If they are above the line  $= 0.91 \times SD + 0.92$ , they are dropped and reported.

**Figure:** Plot showing AIIS (pink diamond), polynomial fit (green line/boxes), points checked (blue fills), and out-of-bounds point (red X) to be dropped.

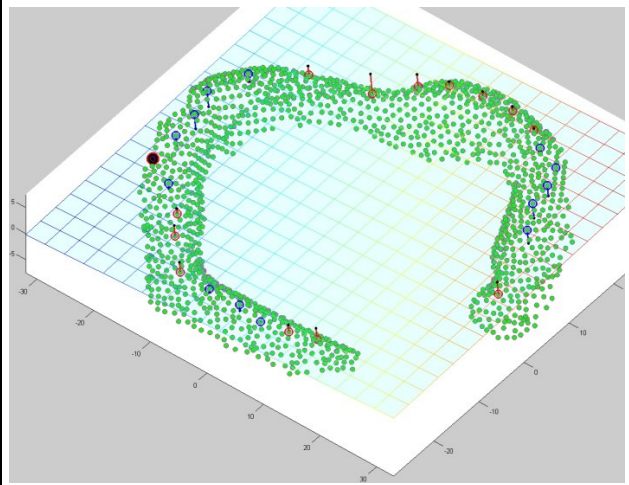


## 21: AR Convergence & Figure Generation

Code Lines: 3023-3942

The plane that defined the direction for maximal point selection (Z-axis) is replaced with least squares plane fit to selected points on the AR. The code in blocks 18-21 are nested within a `while` loop, and these processes repeat until the most distal lateral points are converged on. The 50mm offset is removed and points are converted back to Cartesian coordinates. A 3-D interactive plot is generated to visually assure only appropriate points on the most distal lateral ridge of the AR have been selected.

**Figure:** Oblique inferosuperior view of AR plot showing all points of the point cloud (green), the fit plane (multicolor), selected points lateral (blue) and medial (red) to the plane, and a point dropped on the AIIS-AR margin (black).

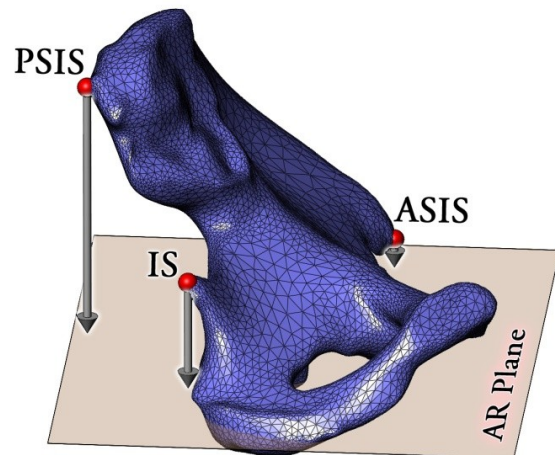


## 22: Higgins Index Projection Analysis & Figure†

Code Lines: 3943-4131

Projections from the points of the ASIS, PSIS and IS to the AR plane are calculated. These points span the majority of the innominate bone and can be used to describe its orientation relative to the opening of the acetabulum. By using ratios of the projections, indices can be measured independent of anatomical size. Ratios of PSIS:ASIS and IS:ASIS can be used to describe version of the innominate bone relative to the acetabulum. Similarly the ratios of IS:PSIS and IS:ASIS can be used to describe inclination of the innominate bone. *\*These values were not reported on.*

**Figure:** Left innominate bone and calculated projections (grey arrows) to the least squares fit AR plane.

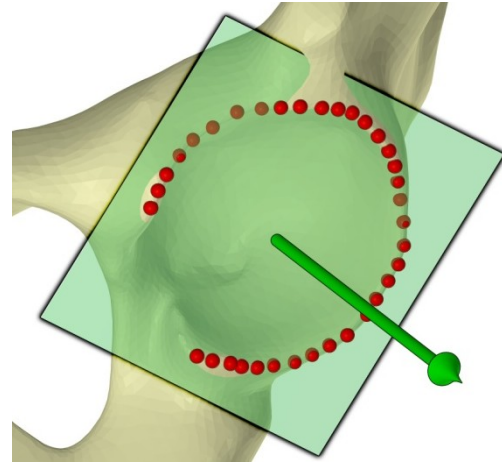


### 23: Establish Acetabular Axis for Calculations

Code Lines: 4132-4139

The acetabular axis (AX) is established as the normal vector of the final/converged least-squares plane fit of the points selected on the AR (Block 21). The AX best represents the opening direction of the acetabulum's aperture. The AX is used in all subsequent calculations to determine various measures of acetabular orientation.

**Figure:** Left innominate bone displaying automatically selected/converged points (red). The least-squares plane fit to the points best representing the aperture of the AR establish the AX (green).

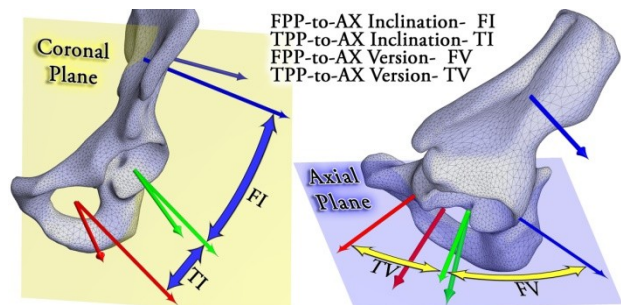


### 24: Hemi-Pelvis Angular Analysis Calculations†

Code Lines: 4140-4563

A vector normal to the false pelvic plane (FPP) is calculated using points of the PSIS, AIIS and ASIS. The previously determined plane and vector normal to OF is used to represent the true pelvic plane (TPP). Angles of inclination in the hemi-frontal plane, and version angles in the hemi-axial plane, are calculated.

**Figure:** Angles between AX (green) and normal vectors of the TPP (red) and FPP (blue). \*Global measures not shown.

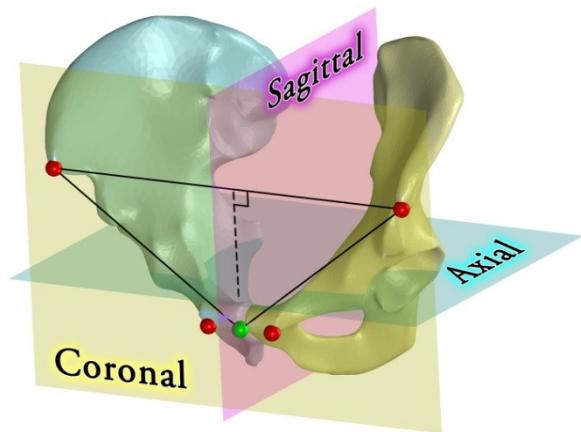


### 25: Full Pelvis Analysis Calculations

Code Lines: 4564-4706

Vectors used for determining angular measurements in the APP based full pelvis C.S. are calculated. Sets of two Euler angles can be used to fully describe the orientation of the acetabular opening in 3-D space within the pelvic reference frame. The commonly reported Euler angle sets of anteversion and inclination for anatomic, radiographic and operative measurement schemes are calculated using trigonometric relationships.

**Figure:** Three anatomic planes defining the APP based full pelvic reference frame. Automatically located points of the bilateral ASIS and PT (red). Midpoint between PT points (green) used to calculate the APP with the ASIS points.



### 26: Data Output & Write Options

Code Lines: 4707-4887

If the analysis completed without error, a dialog appears with options to record the results of the analysis. prompting the user to locate a properly formatted MS Excel® spreadsheet (\*.xlsx) for writing all outputs to. For a permanent, the outputs are also automatically appended to the end of the text file (\*.txt) which contains the bony landmarks.

**Figure:** Successful analysis dialog and output file location.

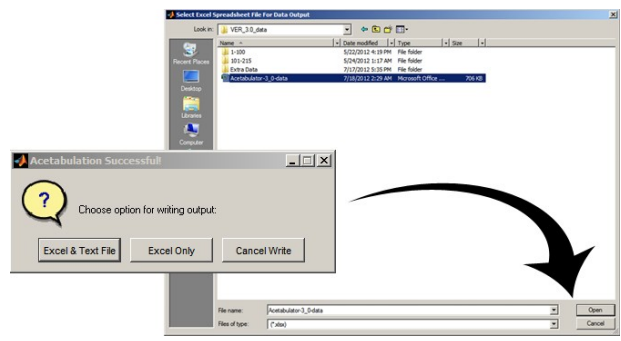


**Table B.2- Point Clouds & Located Points**

<b>Analysis</b>	<b>Point Cloud Name</b>	<b>Anatomic Landmark/Points Located</b>
Hemi-Pelvis	PSIS	Left/right posterior superior iliac spine
Hemi-Pelvis	AIIS	Left/right anterior inferior iliac spine
Hemi-Pelvis	PUB	Left/right center of interior pubic tubercle face
Hemi-Pelvis	ISP	Left/right ischial spine
Hemi-Pelvis	OFB	Left/right obturator foramen interior frame points
Full Pelvis	ASIS	Left/right foremost anterior superior iliac spine
Full Pelvis	RIM	Left/right distal lateral acetabular rim points
Full Pelvis	TUB	Left/right anterior pubic tubercle points

## **Vita**

Sean William Higgins was born and raised in the wonderful state of Maine. He graduated from Yarmouth High School in May of 1998. After high school, he thoroughly enjoyed attending Virginia Polytechnic Institute and State University (Virginia Tech) in Blacksburg Virginia. During his time at Virginia Tech, he was involved with an orthopaedic related design project which peaked his interest in medical devices. Sean graduated in May of 2004 with a Bachelor of Science degree in mechanical engineering. During the first few years of his professional career, he worked for an orthopaedic power instrument company as a design and project engineer. Sean started his own company, Titanium Surgical Technologies, which was incorporated in May of 2007. Since then he has both designed and provided consultation on the development of medical devices ranging from complex powered gastrointestinal staplers to simple instrumentation. In the fall of 2009, he enrolled in the Biomedical Engineering, Master of Science program at Virginia Commonwealth University. During the course of this research, portions of the work were presented at the 2012 annual meeting of the Orthopaedic Research Society. After graduation, Sean plans on continuing his entrepreneurial career in the orthopaedic industry.